ELECTRON SPIN RESONANCE OF TRANSITION METAL COMPLEXES

B. A. Goodman and J. B. Raynor

Department of Chemistry, University of Leicester, Leicester, England

I. Introduction

There have been many reviews and books on electron spin resonance (ESR) and several on transition metal ions. Many of these publications have been written by physicists or theoreticians and are very comprehensive. This review is aimed at inorganic chemists who have had no experience relating to electron spin resonance and who are becoming more and more likely either to use the technique or to need to appreciate the significance of the information available from the technique.

The first part of the review gives an elementary account of the relevant theory. There are many good books for further reading (*25*, *44*, *46*, *78*, *118*, *121*, *122*, *457*, *458*, *542*, *551*, *562*, *591*, *629*, *650*) for the inorganic chemist who wishes to go deeper into the subject. The second part of the review is a comprehensive survey of the results of ESR studies on compounds of transition elements. Inevitably there has had to be some selection of material, and the criteria for inclusion or rejection has been based upon the likely interest an inorganic chemist might have in the species. This is particularly so in areas where there is a lot of related work, e.g., the Mn^{2+} host–lattice data. In the case of copper d^9 complexes, there has been much duplication of work and papers devoted to the spectra of complexes where a minor substitutive change has been made to a bulky organic ligand. In general, data have been rejected from the tables where hyperfine structure has not been observed because of measurements on undiluted samples. Less emphasis is, in general, placed on ions stabilized by diamagnetic host lattices, e.g., Mn^{2+} in NaF. This latter type of study is nevertheless of great importance to the inorganic chemist since unstable complex ions can be studied. In the case just described, the environment is such that the $[MnF_6]^{4-}$ ion can be readily studied.

There have been recent reviews on transition metal ESR by McGarvey (*504*), König (*409*), Kokoszka and Gordon (*400*), and Fujiwara (*226*). Another review, by Kuska and Rogers (*428*), is the more complete, but it covers only the first row of the transition elements. ESR is reviewed in *Annual Reports on the Progress of Chemistry* (Chemical Society, London), *Annual Reviews of Physical Chemistry, Analytical Chemistry, Spectroscopic Properties of Inorganic and Organometallic Compounds* (Chemical Society, London), and *Reports of Progress in Physics,* the earlier volumes of which have good reviews on the theory (in particular, Volumes 16, 18, and 22).

This review covers all ions which might be described by a nominal electron configuration ranging from d^1 to d^9. The lanthanide and actinide elements are, however, excluded.

In the tables of experimental data, hyperfine coupling are given in units of 10^{-4} cm^{-1} except where the authors quoted their data in gauss, in which case the symbol G is used after the value.

II. Principles of Electron Spin Resonance

A. ELECTRON SPIN LEVELS: ONE ELECTRON CASE

The electron has associated with it a magnetic moment so it may be treated as a tiny bar magnet with magnetic moment μ_e given by

$$\mu_e = -g\beta_e S \text{ (erg/gauss)} \tag{1}$$

where β_e is called the Bohr magneton and equals $eh/4\pi mc = 0.92731 \times 10^{-20}$ erg/gauss, and S is the spin quantum number of the electron, e and m are the charge and mass of the electron. Free electrons (in the absence of a crystal or magnetic field) are aligned at random, but in the presence of an external magnetic field, the lower energy state occurs when the electrons are lined up with the magnetic field. A higher energy state occurs when the electrons line up in opposition to the magnetic field. This is sometimes called the electronic Zeeman effect, or the first-order Zeeman effect. The difference in energy between these two states is proportional to the applied field H_0. Thus

$$\Delta E \propto \beta_e H_0 \tag{2}$$

or

$$\Delta E = g\beta_e H_0 \tag{3}$$

The constant of proportionality g equals 2.0023 for a free electron and is called the spectroscopic splitting factor, or just the g factor. It is equivalent to the Lande g factor of atomic spectroscopy.

In quantum mechanical terms, the allowable electron spin states are quantized, and the component m_s of the electron spin vector in any given direction can only take one set of discrete values which are $+s$ or $-s$, i.e., $m_s = +\frac{1}{2}$ (sometimes referred to as $\uparrow$ or α spin) and $-\frac{1}{2}$ ($\downarrow$ or β spin). Electrons in the lower state, $m_s = -\frac{1}{2}$, can now be excited to the upper state, $m_s = +\frac{1}{2}$ (Fig. 1) and for a given applied field H_0 (gauss), the energy ΔE(ergs) required for the transition will be

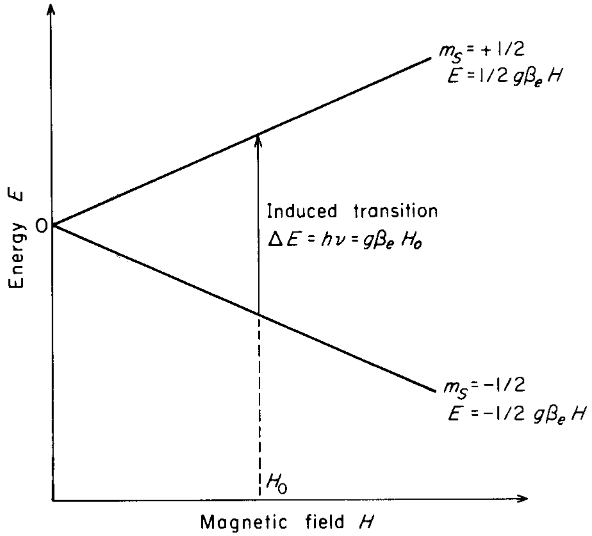

FIG. 1. Effect of an external magnetic field upon the energy levels of an electron and the transition induced by an electromagnetic field.

$$\Delta E = h\nu = g\beta_e H_0 \text{ (ergs)} \tag{4}$$

where ν is the frequency of the applied radiation (cycles/sec or Hz). Since the energy gap is very small, the most convenient radiation frequencies occur when the magnetic field is about 3000 gauss and ν then lies in the microwave region of the electromagnetic spectrum (~9000 MHz). Field strengths are usually measured in gauss and frequency in MHz. The constant g varies from 2.0023 when the unpaired electron is no longer free, i.e., when it is in a molecule. The significance of these variations will be discussed in Section IV.

An ESR spectrometer thus measures the energy required to reverse the spin of an electron in an external magnetic field. Experimentally, this is performed by placing the substance containing unpaired electrons in an absorption cell in the form of a resonance cavity. The sample is adjusted within the cavity in such a way that the microwave magnetic field is at its maximum and the electric field is at its minimum. The cavity is placed between the poles of the magnet. The microwave energy is modulated and the absorption measured by detector coils, amplified and ultimately displayed on a chart recorder as the first derivative of the absorption. Since it is easier to vary the magnetic field rather than the frequency, the resonance condition $h\nu = g\beta_e H_0$ is observed at constant frequency and the magnetic field varied so that an absorption may be observed. Care must be taken not to saturate the system, i.e., raise too many electrons to the upper level so that there are as many there as in the lower level. From the Boltzmann distribution law, the excess of electrons in the lower level for a separation of 1 gauss is about one for every million in the upper level.

B. Spectrum Display and Intensity

The intensity, or area beneath the ESR absorption curve, is proportional to the number of unpaired spins in the sample, but since it is

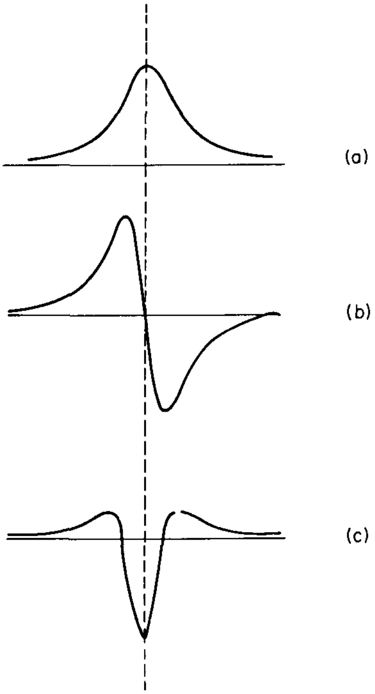

Fig. 2. Lorentzian line shapes: (a) zero, (b) first, and (c) second derivatives.

usually the desire of the ESR spectroscopist to study his compound in a nonmagnetic environment (i.e., in dilute solution or diluted in a diamagnetic isomorphous crystal or powder) the concentration of radicals is seldom of any concern except when it is too low for the spectrum to be seen easily, or too high so that magnetic interactions between different paramagnetic ions occur.

For instrumental purposes and for improved resolution, an ESR spectrum is usually recorded as the first derivative of the absorption spectrum instead of the absorption itself. This means that the point where the derivative crosses the base line corresponds to the peak of the absorption. In poorly resolved spectra, it often helps to record the second derivative spectrum, the peak of which is at the same position as the original absorption peak (Fig. 2). An analysis of the line shapes has been given by Petrakis (*558*).

C. NUCLEAR SPIN LEVELS

The nucleus also has associated with it the property of spin. This is given by the nuclear spin quantum number I which may have values 0, $\frac{1}{2}$, 1, $\frac{3}{2}$, 2, etc. Nuclei having an even number of protons and an even number of neutrons have $I = 0$; nuclei having an odd number of protons and an odd number of neutrons have $I =$ an integer, 1, 2, 3, ... Nuclei with an even number of protons and an odd number of neutrons (or vice

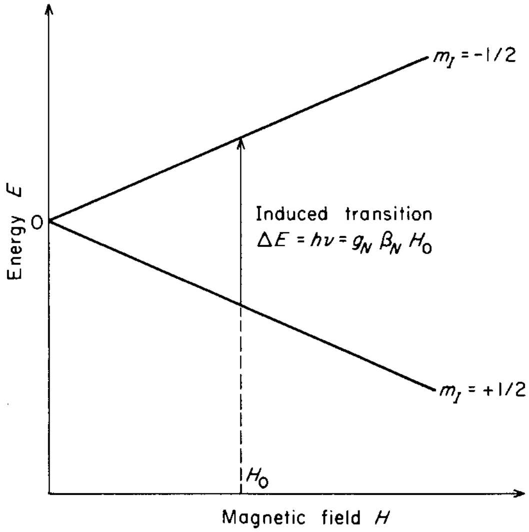

FIG. 3. The NMR experiment. The effect of an external magnetic field upon the energy of a nucleus with spin $I = \frac{1}{2}$.

versa) have half-integral nuclear spin $I = \frac{1}{2}, \frac{3}{2}, \frac{5}{2}$, etc. The magnetic moment of the nucleus μ_N is given by

$$\mu_N = g_N \beta_N I \text{ (erg/gauss)} \tag{5}$$

where β_N is the nuclear magneton $(eh/4\pi Mc)$ and equals 0.50505×10^{-23} erg/gauss. Table I gives the magnetic properties of all stable nuclei. In the presence of a magnetic field, the nuclear spin states are quantized and the component m_I of the nuclear spin vector may take up the following values,

$$I, (I-1), (I-2), (I-3) \ldots -I \tag{6}$$

Thus, for $I = \frac{1}{2}$, the energy levels are represented in Fig. 3. This is the nuclear Zeeman effect and is the basis of nuclear magnetic resonance.

For a field of 3000 gauss, the NMR resonance of a proton ($I = \frac{1}{2}$) occurs at about 12.673 MHz. This may be compared with the ESR resonance of a free electron which would occur at 8408 MHz at the same

TABLE I

MAGNETIC PROPERTIES OF NUCLEI

Isotope	Natural abundance (%)	Magnetic moment μ_N in multiples of the nuclear magneton $(eh/4\pi Mc)$	Spin I in multiples of $h/2\pi$
^{1}H	99.9844	2.79268	$\frac{1}{2}$
^{2}H	1.56×10^{-2}	0.857386	1
^{3}He	10^{-5}–10^{-7}	−2.1274	$\frac{1}{2}$
^{6}Li	7.43	0.82192	1
^{7}Li	92.57	3.2560	$\frac{3}{2}$
^{9}Be	100	−1.1773	$\frac{3}{2}$
^{10}B	18.83	1.8005	3
^{11}B	81.17	2.6880	$\frac{3}{2}$
^{13}C	1.108	0.70220	$\frac{1}{2}$
^{14}N	99.635	0.40358	1
^{15}N	0.365	−0.28304	$\frac{1}{2}$
^{17}O	3.7×10^{-2}	−1.8930	$\frac{5}{2}$
^{19}F	100	2.6273	$\frac{1}{2}$
^{21}Ne	0.257	−0.66176	$\frac{3}{2}$
^{23}Na	100	2.2161	$\frac{3}{2}$
^{25}Mg	10.05	−0.85471	$\frac{5}{2}$

TABLE I—*cont.*

MAGNETIC PROPERTIES OF NUCLEI

Isotope	Natural abundance (%)	Magnetic moment μ_N in multiples of the nuclear magneton ($eh/4\pi Mc$)	Spin I in multiples of $h/2\pi$
^{27}Al	100	3.6385	$\frac{5}{2}$
^{29}Si	4.70	–0.55477	$\frac{1}{2}$
^{31}P	100	1.1305	$\frac{1}{2}$
^{33}S	0.74	0.64274	$\frac{3}{2}$
^{35}Cl	75.4	0.82091	$\frac{3}{2}$
^{37}Cl	24.6	0.68330	$\frac{3}{2}$
^{39}K	93.08	0.39094	$\frac{3}{2}$
^{41}K	6.91	0.21488	$\frac{3}{2}$
^{43}Ca	0.13	–1.3153	$\frac{7}{2}$
^{45}Sc	100	4.7492	$\frac{7}{2}$
^{47}Ti	7.75	–0.78711	$\frac{5}{2}$
^{49}Ti	5.51	–1.1022	$\frac{7}{2}$
^{50}V	0.24	3.3413	6
^{51}V	99.76	5.1392	$\frac{7}{2}$
^{53}Cr	9.54	–0.47354	$\frac{3}{2}$
^{55}Mn	100	3.4611	$\frac{5}{2}$
^{57}Fe	2.245	0.0903	$\frac{1}{2}$
^{59}Co	100	4.6388	$\frac{7}{2}$
^{61}Ni	1.25	0.746	$\frac{3}{2}$
^{63}Cu	69.09	2.2206	$\frac{3}{2}$
^{65}Cu	30.91	2.3790	$\frac{3}{2}$
^{67}Zn	4.12	0.87354	$\frac{5}{2}$
^{69}Ga	60.2	2.0108	$\frac{3}{2}$
^{71}Ga	39.8	2.5549	$\frac{3}{2}$
^{73}Ge	7.61	–0.87677	$\frac{9}{2}$
^{75}As	100	1.4349	$\frac{3}{2}$
^{77}Se	7.50	0.5325	$\frac{1}{2}$
^{79}Br	50.57	2.0991	$\frac{3}{2}$
^{81}Br	49.43	2.2626	$\frac{3}{2}$
^{83}Kr	11.55	–0.96705	$\frac{9}{2}$
^{85}Rb	72.8	1.3482	$\frac{5}{2}$
^{87}Rb	27.2	2.7414	$\frac{3}{2}$
^{87}Sr	7.02	–1.0893	$\frac{9}{2}$
^{89}Y	100	–0.13682	$\frac{1}{2}$

TABLE I—*cont.*

MAGNETIC PROPERTIES OF NUCLEI

Isotope	Natural abundance (%)	Magnetic moment μ_N in multiples of the nuclear magneton $(eh/4\pi Mc)$	Spin I in multiples of $h/2\pi$
^{91}Zr	11.23	−1.298	$\frac{5}{2}$
^{93}Nb	100	6.1435	$\frac{9}{2}$
^{95}Mo	15.78	−0.9099	$\frac{5}{2}$
^{97}Mo	9.60	−0.9290	$\frac{5}{2}$
^{99}Tc[a]	—	5.6572	$\frac{9}{2}$
^{99}Ru	12.81	−0.63	$\frac{5}{2}$
^{101}Ru	16.98	−0.69	$\frac{5}{2}$
^{103}Rh	100	−0.0879	$\frac{1}{2}$
^{105}Pd	22.23	−0.57	$\frac{5}{2}$
^{107}Ag	51.35	−0.1130	$\frac{1}{2}$
^{109}Ag	48.65	−0.1299	$\frac{1}{2}$
^{111}Cd	12.86	−0.5922	$\frac{1}{2}$
^{113}Cd	12.34	−0.6195	$\frac{1}{2}$
^{113}In	4.16	5.4960	$\frac{9}{2}$
^{115}In	95.84	5.5073	$\frac{9}{2}$
^{115}Sn	0.35	−0.9132	$\frac{1}{2}$
^{117}Sn	7.67	−0.9949	$\frac{1}{2}$
^{119}Sn	8.68	−1.0409	$\frac{1}{2}$
^{121}Sb	57.25	3.3417	$\frac{5}{2}$
^{123}Sb	42.75	2.5334	$\frac{7}{2}$
^{123}Te	0.89	−0.7319	$\frac{1}{2}$
^{125}Te	7.03	−0.8824	$\frac{1}{2}$
^{127}I	100	2.7937	$\frac{5}{2}$
^{129}Xe	26.24	−0.77255	$\frac{1}{2}$
^{131}Xe	21.24	0.68680	$\frac{3}{2}$
^{133}Cs	100	2.5642	$\frac{7}{2}$
^{135}Ba	6.59	0.83229	$\frac{3}{2}$
^{137}Ba	11.32	0.93107	$\frac{3}{2}$
^{139}La	99.911	2.7615	$\frac{7}{2}$
^{141}Pr	100	3.92	$\frac{5}{2}$
^{143}Nd	12.20	−1.25	$\frac{7}{2}$
^{145}Nd	8.30	−0.78	$\frac{7}{2}$
^{147}Sm	15.07	−0.68	$\frac{7}{2}$
^{149}Sm	13.84	−0.55	$\frac{7}{2}$

TABLE I—*cont.*

MAGNETIC PROPERTIES OF NUCLEI

Isotope	Natural abundance (%)	Magnetic moment μ_N in multiples of the nuclear magneton ($eh/4\pi Mc$)	Spin I in multiples of $h/2\pi$
^{151}Eu	47.77	3.441	$\frac{5}{2}$
^{153}Eu	52.23	1.521	$\frac{5}{2}$
^{155}Gd	14.68	−0.25	$\frac{3}{2}$
^{157}Gd	15.64	−0.34	$\frac{3}{2}$
^{159}Tb	100	1.52	$\frac{3}{2}$
^{161}Dy	18.73	−0.38	$\frac{5}{2}$
^{163}Dy	24.97	−0.53	$\frac{5}{2}$
^{165}Ho	100	3.31	$\frac{7}{2}$
^{167}Er	22.82	0.48	$\frac{7}{2}$
^{169}Tm	100	−0.229	$\frac{1}{2}$
^{171}Yb	14.27	0.4926	$\frac{1}{2}$
^{173}Yb	16.08	−0.677	$\frac{5}{2}$
^{175}Lu	97.40	2.230	$\frac{7}{2}$
^{176}Lu[a]	2.60	4.2	6
^{177}Hf	18.39	0.61	$\frac{7}{2}$
^{179}Hf	13.78	−0.47	$\frac{9}{2}$
^{181}Ta	100	2.340	$\frac{7}{2}$
^{183}W	14.28	0.115	$\frac{1}{2}$
^{185}Re	37.07	3.1437	$\frac{5}{2}$
^{187}Re	62.93	3.1760	$\frac{5}{2}$
^{187}Os	1.64	0.12	$\frac{1}{2}$
^{189}Os	16.1	0.6507	$\frac{3}{2}$
^{191}Ir	38.5	0.16	$\frac{3}{2}$
^{193}Ir	61.5	0.17	$\frac{3}{2}$
^{195}Pt	33.7	0.6004	$\frac{1}{2}$
^{197}Au	100	0.1439	$\frac{3}{2}$
^{199}Hg	16.86	0.4979	$\frac{1}{2}$
^{201}Hg	13.24	−0.5513	$\frac{3}{2}$
^{203}Tl	29.52	1.5960	$\frac{1}{2}$
^{205}Tl	70.48	1.6115	$\frac{1}{2}$
^{207}Pb	21.11	0.5837	$\frac{1}{2}$
^{209}Bi	100	4.0389	$\frac{9}{2}$
^{209}Po[a]	—	—	$\frac{1}{2}$
^{227}Ac[a]	—	1.1	$\frac{3}{2}$

TABLE I—*cont.*

MAGNETIC PROPERTIES OF NUCLEI

Isotope	Natural abundance (%)	Magnetic moment μ_N in multiples of the nuclear magneton $(eh/4\pi Mc)$	Spin I in multiples of $h/2\pi$
^{231}Pa[a]	—	1.96	$\frac{3}{2}$
^{233}U[a]	—	0.54	$\frac{5}{2}$
^{235}U[a]	0.71	0.35	$\frac{7}{2}$
^{237}Np[a]	—	2.5	$\frac{5}{2}$
^{239}Np[a]	—	—	$\frac{1}{2}$
^{239}Pu[a]	—	0.4	$\frac{1}{2}$
^{241}Pu[a]	—	1.4	$\frac{5}{2}$
^{241}Am[a]	—	1.4	$\frac{5}{2}$
^{243}Am[a]	—	1.4	$\frac{5}{2}$
^{244}Cm[a]	—	—	$\frac{7}{2}$

[a] Radioactive.

magnetic field. Thus the resonance frequency in ESR, and therefore the energy of the absorptions is about 700 times larger than for the NMR transitions.

D. ELECTRON SPIN–NUCLEAR SPIN INTERACTIONS: HYPERFINE STRUCTURE

In an atom subjected to an external magnetic field, the electron spin and nuclear spin will interact. All combinations of electron and nuclear spin are allowed, thus for $S = \frac{1}{2}$ and $I = \frac{1}{2}$,

$$\begin{aligned} m_s &= -\tfrac{1}{2} \qquad m_I = \pm\tfrac{1}{2} \\ m_s &= +\tfrac{1}{2} \qquad m_I = \pm\tfrac{1}{2} \end{aligned} \tag{7}$$

The relative energies of these levels are shown in Fig. 4.

At low magnetic fields, the energy levels are no longer parallel to one another for each electron spin case. This is because even at zero magnetic field, the orbital angular momentum of the nucleus spin (I) and the electron spin (S) can interact. For most ESR experiments, the magnetic field is large and this effect can be neglected. Since $g_e\beta_e$ is much larger than $g_N\beta_N$, it is usual to draw only the central portion of the energy levels where to a good approximation the m_I levels are parallel to each

TABLE II

LINE INTENSITIES FOR n EQUIVALENT NUCLEI OF SPIN I

I	n	Line intensities
$I = \frac{1}{2}$[a]	$n = 1$	1 1
	2	1 2 1
	3	1 3 3 1
	4	1 4 6 4 1
	5	1 5 10 10 5 1
	6	1 6 15 20 15 6 1
	7	1 7 21 35 35 21 7 1
	8	1 8 28 56 70 56 28 8 1
$I = 1$	$n = 1$	1 1 1
	2	1 2 3 2 1
	3	1 3 6 7 6 3 1
	4	1 4 10 16 19 16 10 4 1
	5	1 5 15 30 45 51 45 30 15 5 1
	6	1 6 21 50 90 126 141 126 90 50 21 6 1
$I = \frac{3}{2}$	$n = 1$	1 1 1 1
	2	1 2 3 4 3 2 1
	3	1 3 6 10 12 12 10 6 3 1
	4	1 4 10 20 31 40 44 40 31 20 10 4 1
$I = 2$	$n = 1$	1 1 1 1 1
	2	1 2 3 4 5 4 3 2 1
	3	1 3 6 10 15 18 19 18 15 10 6 3 1
	4	1 4 10 20 35 52 68 80 85 80 68 52 35 20 10 4

---

[a] In this case, the relative intensities are equal to the coefficients of the binomial expansion of $(1 + x)^n$.

other. At constant frequency, the transitions are as shown. Only transitions between the same m_I states are allowed. The selection rules for ESR transitions are

$$m_s = \pm 1 \qquad \text{and} \qquad m_I = 0 \tag{8}$$

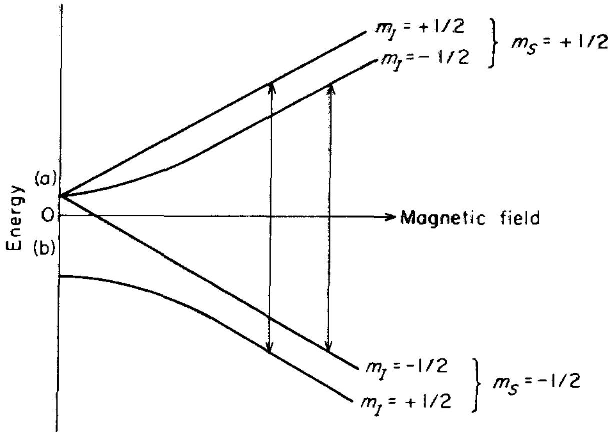

FIG. 4. Effect of an external magnetic field upon the energy levels of an electron interacting with a nucleus with $I = \frac{1}{2}$, showing the two transitions. Energy at (a) $= g\beta A/4$; and at (b) $E = -3g\beta A$.

Breakdown of these rules can occur sometimes with the result of "forbidden" lines in the spectrum. This is described in Section VII,C,4.

Interactions of the electron spin with the nucleus of spin I yields $2I + 1$ transitions which are, to a first approximation, equally separated with a spacing A. If there are n equivalent nuclei of nuclear spin I, then each line is further split. The relative intensities of these lines is given in Table II. Any number, e.g., that arrowed in the table, is the sum of the $2I + 1$ numbers encircled immediately above it. Hyperfine couplings are measured in gauss and often converted to cm^{-1}. The choice of units and their conversion factors are discussed in Section VII,E. The energy separation between the absorptions is referred to as the hyperfine coupling and in the displayed spectrum such absorptions are referred to as hyperfine structure.

E. HAMILTONIANS

A Hamiltonian is an operator which operates upon a wave function. When it is applied to the wave function of a particular system, it gives the permitted energy levels of that system. A simple form of the general Hamiltonian for an ion in a crystalline environment and with an applied magnetic field may be written as

$$\begin{aligned}\mathscr{H} = \mathscr{H}_V + \mathscr{H}_{LF} + \mathscr{H}_{LS} + \mathscr{H}_{SS} + \mathscr{H}_{IH} + \mathscr{H}_Q \\ + \mathscr{H}_{SH} + \mathscr{H}_{LH} + \mathscr{H}_{SI} + \mathscr{H}_{LI}\end{aligned} \tag{9}$$

TABLE III

HAMILTONIAN OPERATORS IN ORDER OF APPROXIMATE DECREASING MAGNITUDE[a]

Hamiltonian	Interaction	Magnitude (cm^{-1})	Expanded form
$\mathscr{H}_V$	Electron–electron	10^5	$\sum_{k>j=1}^{n} \frac{e^2}{r_{kj}}$
$\mathscr{H}_{LF}$	Ligand field	10^4	$\sum_k - eV(x_k, y_k, z_k)$
$\mathscr{H}_{LS}$	Spin–orbit	10^2–10^3	$\lambda \hat{L}\cdot\hat{S}$
$\mathscr{H}_{SS}$	Electron–electron dipole	10^{-1}–1	$\beta_e{}^2 r_{12}^{-3}\left[\hat{s}_1\cdot\hat{s}_2 - \frac{3(\hat{s}_1\cdot\hat{r}_{12})(\hat{s}_2\cdot\hat{r}_{12})}{r_{12}^2}\right]$
$\mathscr{H}_{IH}$	Nuclear Zeeman	10^{-1}–10^{-3}	$-g_N\beta_N\hat{H}\cdot\hat{I}$
$\mathscr{H}_Q$	Nuclear quadrupole	10^{-3}	$Q'[I_z{}^2 - \frac{1}{3}I(I+1)]$ where $Q' = \frac{3eQ}{4I(2I-1)}\cdot\frac{\partial^2 V}{\partial z^2}$
$\mathscr{H}_{SH}$	Electron Zeeman	—	$\left.\begin{matrix} g\beta_e\hat{H}\cdot\hat{S} \\ \beta_e\hat{L}\cdot\hat{H} \end{matrix}\right\}$ often combined as $\beta_e(\hat{L}+g\hat{S})\hat{H}$
$\mathscr{H}_{SI}$	Electron spin–nuclear spin Anisotropic part	10^{-2}–10^{-4}	$-g\beta_e g_N\beta_N\left[\frac{3(\hat{I}\cdot\hat{r})(\hat{S}\cdot\hat{r})}{r^5} - \frac{\hat{I}\cdot\hat{S}}{r^3}\right]$ or $g\beta_e g_N\beta_N\left\langle\frac{3\cos^2\alpha - 1}{r^3}\right\rangle\cdot\hat{I}\cdot\hat{S}$ or $A\cdot\hat{I}\cdot\hat{S}$
	Isotropic part	10^{-2}–10^{-4}	$\frac{8\pi}{3}g\beta_e g_N\beta_N\lvert\psi_0\rvert^2$
$\mathscr{H}_{LI}$	Nuclear–spin orbit	—	$g\beta_e g_N\beta_N\langle r^{-3}\rangle\hat{L}\cdot\hat{I}$

[a] $-e$, charge on electron; r_{kj}, distance between the kth and jth electron; V, electric field potential; x_k, y_k, z_k, coordinates of the kth electron; λ, spin–orbit coupling constant; $\hat{L}$, total orbital angular memontum operator; $\hat{S}$, total electron spin operator; ; $\hat{s}_i$, electron spin operator of electron i; and Q, quadrupole moment.

Each term may be treated as a perturbation of the previous ones, and hence they are treated in order of decreasing energy. The form of these operators is summarized in Table III.

F. Tensors

The part of the general Hamiltonian incorporating (in particular) the g and A factors needs to be explained in more detail, i.e.,

$$\mathscr{H} = \beta_e \hat{H}\cdot g\cdot \hat{S} + \hat{I}\cdot A\cdot \hat{S} \tag{10}$$

$\hat{H}$, $\hat{S}$, and $\hat{I}$ are vectors, whereas g and A are tensors. Each expression, when written in full, has the form

$$[H_x, H_y, H_z]\begin{bmatrix} g_{xx} & g_{yx} & g_{zx} \\ g_{xy} & g_{yy} & g_{zy} \\ g_{xz} & g_{yz} & g_{zz} \end{bmatrix}\begin{bmatrix} S_x \\ S_y \\ S_z \end{bmatrix} \tag{11}$$

where H_x, S_x, etc., are the scalar components of the vectors in the Cartesian coordinate scheme x, y, and z fixed in the molecule. (The axis of highest symmetry in the molecule is conventionally taken as the z axis.) The g and A tensors are almost always symmetrical with, for example, $g_{yx} = g_{xy}$. The tensor is thus capable of being diagonalized, i.e., transformed to a new set of Cartesian axes such that the off-diagonal terms are zero. The resulting values of g_{xx}, g_{yy}, and g_{zz} are referred to as the principal values of the g tensor and relate to the directions of the principal axes. The average g value is equal to one-third of the trace of the tensor, i.e., $\frac{1}{3}(g_{xx} + g_{yy} + g_{zz})$. Only this value will be obtained from the spectra of complexes in fluid solution.

The principal values and directions of the g and A tensors are of vital importance in ESR and the determination and practical significance of these terms as far as transition metal complexes are concerned will be the subject of the remainder of this review.

III. Hyperfine Coupling

A. Components of the Hyperfine Coupling Tensor

The nuclear hyperfine coupling is the field at the electron due to the nucleus and its magnitude depends on whether the electron which is interacting with the nucleus is in an s or a p or d orbital. Since s orbitals have high electron density at the nucleus, the hyperfine coupling constant will be large and since s orbitals are symmetrical, it will be independent of direction. This interaction is called the isotropic hyperfine coupling (A_{iso}) or the Fermi contact interaction. In p or d orbitals, where there is no electron density at the nucleus, the electron is to be found some distance away from the nucleus. The interaction between it and the nucleus will be as two magnetic dipoles and consequently the interaction will be small and dependent on the direction of the orbital with respect to the applied magnetic field as well as to their separation. This interaction is called the anisotropic hyperfine coupling (A_{aniso}) and may be resolved into unique directions (x, y, and z). When integrated over all directions, the magnitude of this hyperfine coupling becomes zero, i.e., $A_x + A_y + A_z = 0$.

Since any orbital may be considered as a hybrid of suitable combinations of s, p, or d orbitals, so also may a hyperfine coupling be divided into a contribution due to p or d orbitals and that due to s orbitals. In a fluid solution anisotropic coupling is averaged to zero and the only observed interaction is the isotropic coupling A_{iso}. In a frozen solution or any other solid matrix, e.g., single crystal, however, the observed interaction will be the sum of the anisotropic and the isotropic interactions. The anisotropic contribution is calculated from the coupling along the three principal directions x, y, and z, after the isotropic contribution has been subtracted. Thus from a spectrum obtained using fluid and rigid solutions (or single crystal), A_{iso} and A_{aniso} may be computed and consequently the unpaired electron population in s and p/d orbitals calculated. From the ratio of these numbers, the hybridization of the orbital under consideration may be estimated.

B. ANISOTROPIC HYPERFINE COUPLING

1. *Dipolar Coupling*

In a strong magnetic field, the electron and nuclear spin vectors, $\hat{I}$ and $\hat{S}$ are fully decoupled and each have their axis parallel to the applied field. If θ is the angle between the axis of the dipoles (Fig. 5) and the line joining them, and r is their separation, then the Hamiltonian representing the energy of dipolar interaction is

$$\mathscr{H} = -g\beta_e g_N \beta_N \left[\frac{\hat{I}\cdot\hat{S}}{r^3} - \frac{3(\hat{I}\cdot r)(\hat{S}\cdot r)}{r^5}\right] \tag{12}$$

or

$$\mathscr{H} = g\beta_e g_N \beta_N \frac{(3\cos^2\theta - 1)}{r^3} \cdot \hat{I}\cdot\hat{S} \tag{13}$$

When Eq. 13 is applied to the electron wave function by substituting M_I for $\hat{I}$ and M_S for $\hat{S}$, the energies of the levels M_I, M_S are given by

$$E_{M_I, M_S} = g\beta_e g_N \beta_N M_I M_S \frac{3\cos^2\theta - 1}{\langle r^3\rangle} \text{ (ergs)} \tag{14}$$

For an electron in an orbital centered on the nucleus in question (Fig. 6), the anisotropic hyperfine coupling follows from Eq. 14, but having in addition a term $\langle 3\cos^2\alpha - 1\rangle$ which represents the average direction of the electron spin vector within the orbital. The anisotropic hyperfine splitting can now be defined as the separation between adjacent energy levels, viz. M_S, M_I and M_S, M_{I-1}, and equals

$$A_{aniso} = \frac{g\beta_e g_N \beta_N}{2} \cdot \frac{3\cos^2\theta - 1}{\langle r^3\rangle} \cdot \langle 3\cos^2\alpha - 1\rangle \text{ (ergs)} \qquad (15)$$

where α is the angle between r and the principal axis of the orbital, and θ is the angle between the principal axis of the orbital and the direction of the nuclear magnetic moment vector. $\langle\ \rangle$ indicates the average value.

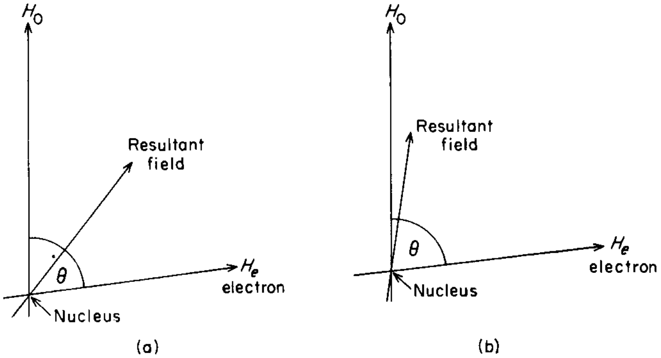

FIG. 5. (a) The weak field case, $H_0 < H_e$. (b) The strong field case, $H_0 > H_e$.

For any p orbital $\langle 3\cos^2\alpha - 1\rangle$ is equal to $+\frac{4}{5}$. By setting $P = g\beta_e g_N \beta_N / \langle r^3\rangle$, A_{aniso} becomes $\frac{2}{5}P(3\cos^2\theta - 1)$ for an electron in a p orbital.

When $\theta = 0$, the orbital is parallel to the nuclear magnetic moment which itself will be parallel to the external magnetic field if the latter field is much stronger than the field at the nucleus due to the electron (see Fig. 6). This is referred to as the strong-field approximation and it follows that for a p orbital, A_{aniso} $(A_{zz}) = \frac{4}{5}P$ and when $\theta = 90°$, A_{aniso} $(A_{xx,yy}) = -\frac{2}{5}P$. The tensor thus has the form $|\frac{4}{5}P, -\frac{2}{5}P, -\frac{2}{5}P|$, the principal value being positive.

In the above description, it was assumed that the nucleus lines up with the applied field in all orientations of the orbital, i.e., the applied field H_0 is much stronger than the field due to the electron at the nucleus, H_e. In practice, however, this strong field approximation is only a good one when (*a*) the applied field H_0 is large (e.g., at Q-band frequencies); (*b*) the anisotropic hyperfine coupling is small (and so the field at the nucleus is still relatively small); and (*c*) the isotropic hyperfine coupling is large (since the field due to the electron at the nucleus reinforces the applied field). Often when electrons are confined to p or d orbitals, the effective field at the nucleus due to the electron is larger than the applied field. This is because the field at the nucleus due to the electron is very many times greater than the field at the electron due to the nucleus. Thus, a 15-gauss ^1H anisotropic hyperfine coupling is equivalent to about a 5000-gauss field at the nucleus and thus is close to the external field at X-band frequencies. The resultant field may then have a significantly different direction than the applied field. Instead of the dipolar interaction varying as $(3\cos^2\theta - 1)$, it may be shown in the weaker field case that the interaction varies as $(3\cos^2\theta + 1)^{1/2}$. Plots of the variation of hyperfine splitting for an electron in a p orbital as a function of orientation within one plane for the two extreme cases are given in Fig. 7.

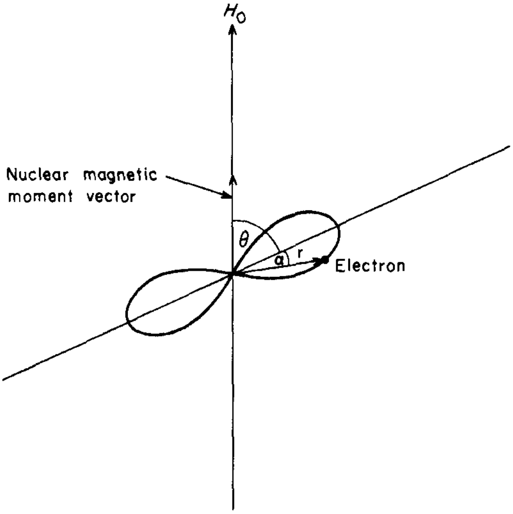

FIG. 6. The strong field approximation. The resultant field lies close to the applied field.

The numerical value of the anisotropic hyperfine coupling at the turning points of the curve (and hence the values computed from a powder spectrum—*vide supra*) are the same whichever formula is used, i.e., $\frac{4}{5}P$ and $-\frac{2}{5}P$ for $(3\cos^2\theta - 1)$ and $\frac{4}{5}P$ and $\frac{2}{5}P$ for $(3\cos^2\theta + 1)^{1/2}$. Only the signs are different and it is only when a single crystal study is undertaken that the difference manifests itself and then only in the improbable case of a very small isotropic hyperfine coupling. In practice, the situation is intermediate between the two extremes.

An alternative expression for the variation of the anisotropic hyperfine coupling with the angle is

$$A^2 = A_{\parallel}{}^2 \cos^2\theta + A_{\perp}{}^2 \sin^2\theta \qquad (16)$$

where the parameters have the same meaning as before.

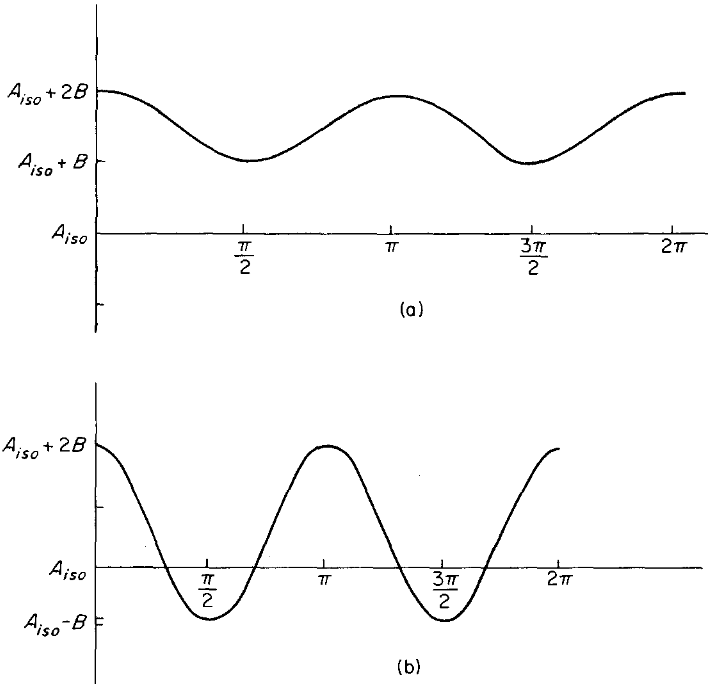

FIG. 7. Plot of variation of hyperfine coupling during a rotation for (a) low-field case $(3\cos^2\theta + 1)^{1/2}$, taking the positive root, (b) high-field case.

For an unpaired electron in a d orbital, the value of $\langle 3\cos^2\alpha - 1\rangle$ depends on the magnetic quantum number

$$\text{For } d_{z^2}, \text{ the value is } +\tfrac{4}{7} \qquad (17)$$

$$d_{xz,\,yz}, \text{ the value is } +\tfrac{2}{7} \qquad (18)$$

$$d_{x^2-y^2,\,xy}, \text{ the value is } -\tfrac{4}{7} \qquad (19)$$

The principal value of A_{aniso} (A_{zz}) is given for each d orbital when $\theta = 0$ (since the principal axis for each d orbital is the z axis), and so the tensor for, e.g., $d_{x^2-y^2}$ or d_{xy} is

$$\begin{array}{ccc} z & x & y \\ \left|-\tfrac{4}{7}P\right. & \tfrac{2}{7}P & \left.\tfrac{2}{7}P\right| \end{array} \qquad (20)$$

i.e., the principal value is negative.

This is in contrast to the d_{z^2} tensor, where the principal value is positive. In Table IV, calculated values are given of the principal value of A_{aniso} (A_{zz}) for an electron in a p orbital for nontransition ions or the $d_{x^2-y^2}$ or d_{xy} orbitals for transition element ions, assuming the orbital contribution is fully quenched. The same problem concerning the use of $(3\cos^2\theta - 1)$ and $(3\cos^2\theta + 1)^{1/2}$ occurs, as it did for the p orbitals, but the magnitude of the principle values are unaffected.

2. *Secondary Effects*

a. The Quadrupole Interaction The interaction of the nuclear electric quadrupole moment with the gradient of the electric field at the nucleus results in a mixing of nuclear spin states. This results in a second-order shift in energy levels and may make a normally forbidden transition become weakly allowed with both electron and nuclear spins changing simultaneously. The quadrupole interaction results in a shift in the energies of the different m_I energy levels relative to one another (Fig 8).

When the magnetic field is applied parallel to the symmetry axis of the crystal the shift due to the quadrupole interaction is independent of m_s and does not result in any change in the position of the resonance

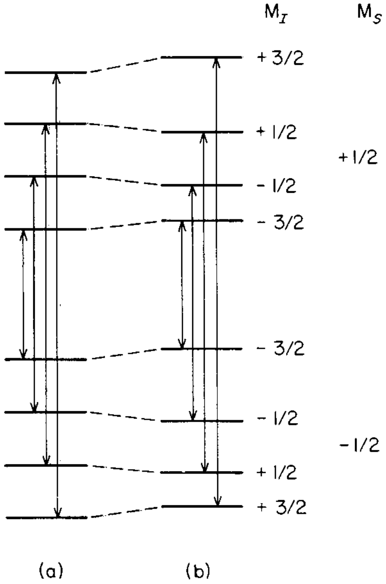

FIG. 8. Effect of electric quadruple interaction (b) upon the energy levels of a $S = \frac{1}{2}$, $I = \frac{3}{2}$ system (a).

lines. When the magnetic field is not parallel to the z axis, however, second-order effects cause a change in the shift for each level, and the resulting nuclear hyperfine lines are unequally spaced. The quadrupole term can be differentiated from other second-order effects since it does not vanish in strong fields and the separation of successive hyperfine lines is greatest in the middle or at the ends, instead of showing a progressive increase or decrease.

b. The Nuclear Zeeman Interaction The nuclear Zeeman term represents the direct interaction between the external magnetic field and the nuclear magnetic moment. This is usually neglected since it cancels for transitions between states with identical values of m_I. When "forbidden transitions" are being considered, however, it is sometimes necessary to take account of this effect. It is applicable to both anisotropic and isotropic spectra.

C. ISOTROPIC HYPERFINE COUPLING

The isotropic hyperfine coupling is made up of contributions from several effects Direct unpaired electron spin density at the nucleus occurs when the electron is in an s orbital Indirect contributions arise when the electron is in a p or d orbital and from other effects These will be treated in turn.

1. The Fermi Contact Term

The isotropic coupling A_{iso} is related to the electron spin density at the interacting nucleus, and is also related to the magnetic moment of the nucleus. The full expression is

$$A_{iso} = \frac{8\pi}{3} g_N \beta_N |\psi_0|^2 \text{ (gauss)} \tag{21}$$

and such values are positive. $|\psi_0|^2$ is the probability of finding the electron in a unit volume at the nucleus The units for such probabilities are electrons/unit volume. Values for A_0 (the hyperfine coupling for an electron localized in a pure s orbital) and $|\psi_0|^2$ are given in Table IV for different nuclei.

Calculated values rely on having accurate equations for the wave function The values given in Table IV make use of the best wave function available at the time of writing The wave function for the

TABLE IV

CALCULATED VALUES OF ANISOTROPIC AND ISOTROPIC COUPLINGS FOR FREE IONS[a]

Ion	Electronic configuration	$\langle r^{-3}\rangle$ (a.u.)	Principal value of A_{aniso}[b] (gauss)	$\lvert\psi_0\rvert^2$ (a.u.)	A_{iso} (gauss)	Reference
$^{1}H^{0}$	$1s^1$	—	—	0.318	508	*(506a)*
$^{2}H^{0}$	$1s^1$	—	—	0.318	78	*(506a)*
$^{3}He^{0}$	$1s^2$	—	—	1.798	−2192	*(506a)*
$^{6}Li^{0}$	$2s^1$	—	—	0.166	39	*(506a)*
$^{7}Li^{0}$	$2s^1$	—	—	0.166	103	*(506a)*
$^{9}Be^{0}$	$2s^2$	—	—	0.569	−128	*(506a)*
$^{10}B^{0}$	$2p^1$	0.7756	17.3	1.408	242	*(506a)*
$^{11}B^{0}$	$2p^1$	0.7756	38.1	1.408	723	*(506a)*
$^{13}C^{0}$	$2p^2$	1.6618	63.8	2.785	1119	*(506a)*
$^{14}N^{0}$	$2p^3$	3.0205	33.5	4.814	557	*(506a)*
$^{15}N^{0}$	$2p^3$	3.0205	−46.6	4.814	−781	*(506a)*
$^{17}O^{0}$	$2p^4$	4.9490	−102	7.646	−1659	*(506a)*
$^{19}F^{0}$	$2p^5$	7.5451	1085	11.378	17160	*(506a)*
$^{21}Ne^{0}$	$2p^6$	10.906	−132	16.232	−9886	*(506a)*
$^{23}Na^{0}$	$3s^1$	17.004	687	0.530	224	*(506a)*
$^{25}Mg^{0}$	$3s^2$	24.919	−233	1.217	−119	*(506a)*
$^{27}Al^{0}$	$3p^1$	1.088	43.2	2.355	983	*(506a)*
$^{29}Si^{0}$	$3p^2$	2.027	−61.5	3.827	−1218	*(506a)*
$^{31}P^{0}$	$3p^3$	3.266	202	5.673	3676	*(506a)*
$^{33}S^{0}$	$3p^4$	4.8364	56.6	7.941	975	*(506a)*
$^{35}Cl^{0}$	$3p^5$	6.7688	102	10.662	1672	*(506a)*
$^{37}Cl^{0}$	$3p^5$	6.7688	84.8	10.662	1391	*(506a)*
$^{39}K^{0}$	$4s^1$	8.9747	64.1	0.695	51.9	*(506a)*
$^{41}K^{0}$	$4s^1$	8.9747	35.2	0.695	28.6	*(506a)*
$^{43}Ca^{0}$	$4s^2$	17.7403	−182	1.384	−150	*(506a)*
$^{45}Sc^{-1}$	$3d^2\,4s^2$	1.0585	−27.97	0.7122	276	*(139a)*
$^{45}Sc^{0}$	$3d^4$	0.7647	−20.21	—	—	*(220)*
$^{45}Sc^{0}$	$3d^1\,4s^2$	1.4279	−37.74	1.6883	654.1	*(139b)*
$^{45}Sc^{+1}$	$3d^2$	1.1891	−31.43	—	—	*(139c)*
$^{45}Sc^{+2}$	$3d^1$	1.5755	−41.65	—	—	*(139c, 220)*
$^{47,49}Ti^{-1}$	$3d^3\,4s^2$	1.6236	9.96	0.779	−70.06	*(139a)*
$^{47,49}Ti^{0}$	$3d^4$	1.2658	7.76	—	—	*(220)*
$^{47,49}Ti^{0}$	$3d^2\,4s^2$	2.0148	12.36	1.964	−175.7	*(139b)*
$^{47,49}Ti^{+1}$	$3d^3$	1.7169	10.53	—	—	*(139c)*
$^{47,49}Ti^{+2}$	$3d^2$	2.1368	13.08	—	—	*(139c, 220)*
$^{47,49}Ti^{+3}$	$3d^1$	2.5433	15.60	—	—	*(139c)*
$^{51}V^{-1}$	$3d^4\,4s^2$	2.2250	−63.23	0.869	364.3	*(139a)*
$^{51}V^{0}$	$3d^5$	1.8355	−52.53	—	—	*(220)*

[a] Deduced from the wave function given in the reference. A partial list of data is given in references *(44, 46, 282, 506a)*.

[b] A_{zz} for p or $d_{x_2-y_2,xy}$ orbitals.

TABLE IV—*cont.*

CALCULATED VALUES OF ANISOTROPIC AND ISOTROPIC COUPLINGS FOR FREE IONS

Ion	Electronic configuration	$\langle r^{-3} \rangle$ (a.u.)	Principal value of $A_{aniso}{}^b$ (gauss)	$\|\psi_0\|^2$ (a.u.)	A_{iso} (gauss)	Reference
$^{51}V^0$	$3d^3\ 4s^2$	2.6434	−75.60	2.224	932.3	(*139b*)
$^{51}V^{+1}$	$3d^4$	2.2936	−65.67	—	—	(*139c, 220*)
$^{51}V^{+2}$	$3d^3$	2.7539	−78.77	—	—	(*139c, 220*)
$^{51}V^{+3}$	$3d^2$	3.2209	−92.11	—	—	(*139c*)
$^{51}V^{+4}$	$3d^1$	3.6765	−105.18	—	—	(*139a, 139c, 220*)
$^{53}Cr^{-1}$	$3d^5\ 4s^2$	2.9077	17.88	0.949	−85.5	(*139a*)
$^{53}Cr^0$	$3d^6$	2.4255	14.89	—	—	(*220*)
$^{53}Cr^0$	$3d^4\ 4s^2$	3.3466	20.58	2.495	−224.9	(*139b*)
$^{53}Cr^{+1}$	$3d^5$	2.9740	18.29	—	—	(*139c, 652*)
$^{53}Cr^{+2}$	$3d^4$	3.4528	21.23	—	—	(*139c, 220, 652*)
$^{53}Cr^{+3}$	$3d^3$	3.9614	24.36	—	—	(*139c, 220, 652*)
$^{53}Cr^{+4}$	$3d^2$	4.4820	27.56	—	—	(*139c, 220, 652*)
$^{53}Cr^{+5}$	$3d^1$	4.9925	30.66	—	—	(*139c, 652*)
$^{55}Mn^{-1}$	$3d^6\ 4s^2$	3.6143	−97.45	1.097	433.8	(*139a*)
$^{55}Mn^0$	$3d^7$	3.1215	−84.15	—	—	(*220*)
$^{55}Mn^0$	$3d^5\ 4s^2$	4.1524	−112.0	2.765	1093	(*139b*)
$^{55}Mn^{+1}$	$3d^6$	3.6754	−99.13	—	—	(*139c, 220*)
$^{55}Mn^{+2}$	$3d^5$	4.2546	−114.6	—	—	(*139c, 220*)
$^{55}Mn^{+3}$	$3d^4$	4.7915	−129.2	—	—	(*139c, 220*)
$^{55}Mn^{+4}$	$3d^3$	5.3598	−144.5	—	—	(*139c*)
$^{55}Mn^{+5}$	$3d^2$	5.9438	−160.3	—	—	(*139c*)
$^{55}Mn^{+6}$	$3d^1$	6.5138	−175.6	—	—	(*139c*)
$^{57}Fe^{-1}$	$3d^7\ 4s^2$	4.4277	−15.57	1.225	63.2	(*139a*)
$^{57}Fe^0$	$3d^8$	3.8822	−14.34	—	—	(*220*)
$^{57}Fe^0$	$3d^6\ 4s^2$	4.9769	−17.51	3.113	160.5	(*139b*)
$^{57}Fe^{+1}$	$3d^7$	4.4897	−15.79	—	—	(*139c*)
$^{57}Fe^{+2}$	$3d^6$	5.0839	−17.88	—	—	(*139c, 220*)
$^{57}Fe^{+3}$	$3d^5$	5.7260	−20.14	—	—	(*139c, 220*)
$^{59}Co^{-1}$	$3d^8\ 4s^2$	5.3443	−138.0	1.225	519.6	(*139a*)
$^{59}Co^0$	$3d^9$	4.7877	−123.7	—	—	(*220*)
$^{59}Co^0$	$3d^7\ 4s^2$	5.9261	−153.0	3.455	1308	(*139b*)
$^{59}Co^{+1}$	$3d^8$	5.3985	−139.4	—	—	(*139c*)
$^{59}Co^{+2}$	$3d^7$	6.0376	−155.8	—	—	(*139c, 220*)
$^{59}Co^{+3}$	$3d^6$	6.7011	−172.9	—	—	(*139c, 220*)
$^{61}Ni^{-1}$	$3d^9\ 4s^2$	6.3613	−61.58	1.529	216.9	(*139a*)
$^{61}Ni^0$	$3d^{10}$	5.7251	−55.41	—	—	(*220*)
$^{61}Ni^0$	$3d^8\ 4s^2$	6.9825	−67.59	3.803	539.7	(*139b*)
$^{61}Ni^{+1}$	$3d^9$	6.4216	−62.16	—	—	(*139c*)
$^{61}Ni^{+2}$	$3d^8$	7.0963	−68.69	—	—	(*139c, 220*)
$^{61}Ni^{+3}$	$3d^7$	7.7974	−75.47	—	—	(*139c, 220*)

TABLE IV—*cont.*

CALCULATED VALUES OF ANISOTROPIC AND ISOTROPIC COUPLINGS FOR FREE IONS

Ion	Electronic configuration	$\langle r^{-3}\rangle$ (a.u.)	Principal value of A_{aniso}[b] (gauss)	$\lvert\psi_0\rvert^2$ (a.u.)	A_{iso} (gauss)	Reference
^{63}Cu^{-1}	$3d^{10}\ 4s^2$	7.4902	–216.0	1.643	694.5	(*139a*)
^{63}Cu^{0}	$3d^{10}\ 4s^1$	7.5072	–216.5	—	—	(*139a*)
^{63}Cu^{0}	$3d^{9}\ 4s^2$	8.1511	–235.0	4.180	1767	(*139b*)
^{63}Cu^{+1}	$3d^{10}$	7.5407	–217.4	—	—	(*139c, 220*)
^{63}Cu^{+2}	$3d^{9}$	8.2580	–238.1	—	—	(*139c, 220*)
^{65}Cu^{-1}	$3d^{10}\ 4s^2$	7.4902	–231.4	1.643	744.0	(*139a*)
^{65}Cu^{0}	$3d^{10}\ 4s^1$	7.5072	–216.5	—	—	(*139a*)
^{65}Cu^{0}	$3d^{9}\ 4s^2$	8.1511	–251.8	4.180	1893	(*139b*)
^{65}Cu^{+1}	$3d^{10}$	7.5407	–232.9	—	—	(*139c, 220*)
^{65}Cu^{+2}	$3d^{9}$	8.2580	–250.1	—	—	(*139c, 220*)
^{67}Zn^{0}	$3d^{10}$	9.450	64.5	4.535	454	(*506a*)
^{69}Ga^{0}	$4p^1$	2.8908	106	6.946	2667	(*506a*)
^{71}Ga^{0}	$4p^1$	2.8908	135	6.946	3389	(*506a*)
^{73}Ge^{0}	$4p^2$	4.7334	–25.2	9.549	–535	(*506a*)
^{75}As^{0}	$4p^3$	6.8542	179	12.493	3431	(*506a*)
^{77}Se^{0}	$4p^4$	9.2715	270	15.754	4816	(*506a*)
^{79}Br^{0}	$4p^5$	11.9994	459	19.335	7764	(*506a*)
^{81}Br^{0}	$4p^5$	11.9994	495	19.335	8370	(*506a*)
^{83}Kr^{0}	$4p^6$	14.8867	–87.2	23.313	–1439	(*506a*)
^{85}Rb^{0}	$5s^1$	20.097	297	1.297	200	(*506a*)
^{87}Rb^{0}	$5s^1$	20.097	1005	1.297	678	(*506a*)
^{87}Sr^{0}	$5s^2$	25.8947	–1715	2.387	–1656	(*506a*)
^{89}Y^{0}	$4d^1\ 5s^2$	1.7117	9.1	2.992	–235	(*506a*)
^{89}Y^{+1}	$4d^2$	1.5898	7.81	—	—	(*220*)
^{89}Y^{+2}	$4d^1$	2.0336	9.98	—	—	(*220*)
^{91}Zr^{0}	$4d^2\ 5s^2$	2.3974	24.3	3.509	–522	(*506a*)
^{91}Zr^{+1}	$4d^1\ 5s^1\ 5p^1$	—	—	10.443	–1548	(*59a*)
^{91}Zr^{+1}	$4d^3$	1.9845	19.70	—	—	(*59a*)
^{91}Zr^{+2}	$4d^2$	2.7057	26.86	—	—	(*220*)
^{91}Zr^{+3}	$4d^1$	3.1600	31.37	—	—	(*220*)
^{93}Nb^{0}	$4d^3\ 5s^2$	3.1220	–83.3	3.978	1556	(*506a*)
^{93}Nb^{+1}	$4d^2\ 5s^1\ 5p^1$	—	—	11.740	4577	(*59a*)
^{93}Nb^{+1}	$4d^4$	2.5334	–67.36	—	—	(*59a*)
^{93}Nb^{+2}	$4d^3$	3.4141	–90.80	—	—	(*220*)
^{93}Nb^{+3}	$4d^2$	3.9134	–104.1	—	—	(*220*)
^{95}Mo^{0}	$4d^4\ 5s^2$	3.9001	27.8	4.424	–462	(*506a*)
^{95}Mo^{+1}	$4d^3\ 5s^1\ 5p^1$	—	—	12.110	–1259	(*59a*)
^{95}Mo^{+1}	$4d^5$	3.6623	25.96	—	—	(*220*)
^{95}Mo^{+2}	$4d^4$	4.1745	29.60	—	—	(*220*)
^{95}Mo^{+3}	$4d^3$	4.7066	33.37	—	—	(*220*)
^{97}Mo^{0}	$4d^4\ 5s^2$	3.9001	28.4	4.424	–471	(*506a*)

TABLE IV—*cont.*

CALCULATED VALUES OF ANISOTROPIC AND ISOTROPIC COUPLINGS FOR FREE IONS

Ion	Electronic configuration	$\langle r^{-3} \rangle$ (a.u.)	Principal value of $A_{aniso}{}^{b}$ (gauss)	$\|\psi_0\|^2$ (a.u.)	A_{iso} (gauss)	Reference
$^{97}\mathrm{Mo}^{+1}$	$4d^3\ 5s^1\ 5p^1$	—	—	12.110	−1285	*(59a)*
$^{97}\mathrm{Mo}^{+1}$	$4d^5$	3.6623	26.51	—	—	*(220)*
$^{97}\mathrm{Mo}^{+2}$	$4d^4$	4.1745	30.22	—	—	*(220)*
$^{97}\mathrm{Mo}^{+3}$	$4d^3$	4.7066	34.06	—	—	*(220)*
$^{99}\mathrm{Tc}^{0}$	$4d^5\ 5s^2$	4.7390	−116	4.855	1749	*(506a)*
$^{99}\mathrm{Tc}^{+1}$	$4d^4\ 5s^1\ 5p^1$	—	—	14.380	5162	*(59a)*
$^{99}\mathrm{Ru}^{0}$	$4d^6\ 5s^2$	5.6438	27.4	5.267	−376	*(506a)*
$^{99}\mathrm{Ru}^{+1}$	$4d^5\ 5s^1\ 5p^1$	—	—	15.682	−1129	*(59a)*
$^{99}\mathrm{Ru}^{+1}$	$4d^6$	4.8792	23.95	—	—	*(59a)*
$^{99}\mathrm{Ru}^{+2}$	$4d^5$	5.8582	28.76	—	—	*(220)*
$^{99}\mathrm{Ru}^{+3}$	$4d^4$	6.4961	31.84	—	—	*(220)*
$^{101}\mathrm{Ru}^{0}$	$4d^6\ 5s^2$	5.6438	30.4	5.267	−416	*(506a)*
$^{101}\mathrm{Ru}^{+1}$	$4d^5\ 5s^1\ 5p^1$	—	—	15.682	−1236	*(59a)*
$^{101}\mathrm{Ru}^{+1}$	$4d^7$	4.8792	26.23	—	—	*(59a)*
$^{101}\mathrm{Ru}^{+2}$	$4d^6$	5.8582	31.50	—	—	*(220)*
$^{101}\mathrm{Ru}^{+3}$	$4d^5$	6.4961	34.92	—	—	*(220)*
$^{103}\mathrm{Rh}^{0}$	$4d^7\ 5s^2$	6.6185	22.7	5.673	−286	*(506a)*
$^{103}\mathrm{Rh}^{+1}$	$4d^6\ 5s^1\ 5p^1$	—	—	16.901	−849	*(59a)*
$^{103}\mathrm{Rh}^{+1}$	$4d^8$	5.7243	19.60	—	—	*(59a)*
$^{103}\mathrm{Rh}^{+2}$	$4d^7$	6.8040	23.85	—	—	*(220)*
$^{103}\mathrm{Rh}^{+3}$	$4d^6$	7.4467	26.10	—	—	*(220)*
$^{105}\mathrm{Pd}^{0}$	$4d^8\ 5s^2$	7.6666	34.1	6.071	−397	*(506a)*
$^{105}\mathrm{Pd}^{+1}$	$4d^7\ 5s^1\ 5p^1$	—	—	18.238	−1187	*(59a)*
$^{105}\mathrm{Pd}^{+1}$	$4d^9$	6.7609	30.02	—	—	*(59a)*
$^{105}\mathrm{Pd}^{+2}$	$4d^8$	7.8144	34.70	—	—	*(220)*
$^{105}\mathrm{Pd}^{+3}$	$4d^7$	8.4871	37.69	—	—	*(220)*
$^{107}\mathrm{Ag}^{0}$	$4d^9\ 5s^2$	8.7911	38.8	6.469	−419	*(506a)*
$^{107}\mathrm{Ag}^{+1}$	$4d^8\ 5s^1\ 5p^1$	—	—	19.455	−1256	*(59a)*
$^{107}\mathrm{Ag}^{+1}$	$4d^{10}$	8.2232	36.21	—	—	*(220)*
$^{107}\mathrm{Ag}^{+2}$	$4d^9$	8.9054	39.20	—	—	*(220)*
$^{107}\mathrm{Ag}^{+3}$	$4d^8$	9.6110	42.31	—	—	*(220)*
$^{109}\mathrm{Ag}^{0}$	$4d^9\ 5s^2$	8.7911	44.5	6.469	−482	*(506a)*
$^{109}\mathrm{Ag}^{+1}$	$4d^8\ 5s^1\ 5p^1$	—	—	19.455	−1443	*(59a)*
$^{109}\mathrm{Ag}^{+1}$	$4d^{10}$	8.2232	41.62	—	—	*(220)*
$^{109}\mathrm{Ag}^{+2}$	$4d^9$	8.9054	45.06	—	—	*(220)*
$^{109}\mathrm{Ag}^{+3}$	$4d^8$	9.6110	48.63	—	—	*(220)*
$^{111}\mathrm{Cd}^{0}$	$4d^{10}\ 5s^2$	9.9041	−229	6.851	−2326	*(506a)*
$^{113}\mathrm{Cd}^{0}$	$4d^{10}\ 5s^2$	9.9041	−240	6.851	−2433	*(506a)*
$^{113/115}\mathrm{In}^{0}$	$5p^1$	4.4572	149	9.787	3417	*(506a)*
$^{115}\mathrm{Sn}^{0}$	$5p^2$	6.7468	−335	12.731	−6669	*(506a)*
$^{117}\mathrm{Sn}^{0}$	$5p^2$	6.7468	−367	12.731	−7268	*(506a)*

TABLE IV—*cont.*

CALCULATED VALUES OF ANISOTROPIC AND ISOTROPIC COUPLINGS FOR FREE IONS

Ion	Electronic configuration	$\langle r^{-3} \rangle$ (a.u.)	Principal value of A_{aniso}[b] (gauss)	$\lvert\psi_0\rvert^2$ (a.u.)	A_{iso} (gauss)	Reference
$^{119}Sn^0$	$5p^2$	6.7468	–385	12.731	–7603	*(506a)*
$^{121}Sb^0$	$5p^3$	9.2313	338	15.913	6089	*(506a)*
$^{123}Sb^0$	$5p^3$	9.2313	183	15.913	3297	*(506a)*
$^{123}Te^0$	$5p^4$	11.9366	–478	19.255	–8081	*(506a)*
$^{125}Te^0$	$5p^4$	11.9366	–576	19.255	–9738	*(506a)*
$^{127}I^0$	$5p^5$	14.8724	455	22.836	7320	*(506a)*
$^{129}Xe^0$	$5p^6$	17.8266	–754	26.735	–11827	*(506a)*
$^{131}Xe^0$	$5p^6$	17.8266	223	26.735	3504	*(506a)*
$^{133}Cs^0$	$6s^1$	23.2545	466	1.671	351	*(506a)*
$^{135}Ba^0$	$6s^2$	29.0659	442	2.968	472	*(506a)*
$^{137}Ba^0$	$6s^2$	29.0659	494	2.968	527	*(506a)*
$^{177}Hf^0$	$5d^2\ 6s^2$	4.4934	–14.9	6.596	322	*(506a)*
$^{177}Hf^+$	$5d^1\ 6s^1\ 6p^1$	—	—	19.385	965	*(59a)*
	$5d^3$	3.3165	–11.26	—	—	*(59a)*
$^{179}Hf^0$	$5d^2\ 6s^2$	4.4934	9.2	6.596	–199	*(506a)*
$^{179}Hf^+$	$5d^1\ 6s^1\ 6p^1$	—	—	19.385	–578	*(59a)*
	$5d^3$	3.3165	6.74	—	—	*(59a)*
$^{181}Ta^0$	$5d^3\ 6s^2$	5.6057	–73.1	7.399	1416	*(506a)*
$^{181}Ta^+$	$5d^2\ 6s^1\ 6p^1$	—	—	21.821	4166	*(59a)*
	$5d^4$	4.3162	–56.21	—	—	*(59a)*
$^{183}W^0$	$5d^4\ 6s^2$	6.7504	–30.3	8.148	536	*(506a)*
$^{183}W^+$	$5d^3\ 6s^1\ 6p^1$	—	—	23.760	1561	*(59a)*
	$5d^5$	5.2496	–23.51	—	—	*(59a)*
$^{185}Re^0$	$5d^5\ 6s^2$	7.9414	–195	8.832	3188	*(506a)*
$^{185}Re^+$	$5d^4\ 6s^1\ 6p^1$	—	—	25.827	9274	*(59a)*
	$5d^6$	6.3217	–154.8	—	—	*(59a)*
$^{187}Re^0$	$5d^5\ 6s^2$	7.9414	–197	8.832	3221	*(506a)*
$^{187}Re^+$	$5d^4\ 6s^1\ 6p^1$	—	—	25.827	9269	*(59a)*
	$5d^6$	6.3217	–156.4	—	—	*(59a)*
$^{189}Os^0$	$5d^6\ 6s^2$	9.1859	–77.7	9.548	1183	*(506a)*
$^{189}Os^+$	$5d^5\ 6s^1\ 6p^1$	—	—	27.664	3427	*(59a)*
	$5d^1$	7.3769	–62.33	—	—	*(59a)*
$^{191}Ir^0$	$5d^7\ 6s^2$	10.4886	–21.9	10.185	396	*(506a)*
$^{191}Ir^+$	$5d^6\ 6s^1\ 6p^1$	—	—	29.581	901	*(59a)*
	$5d^8$	8.4802	–17.62	—	—	*(59a)*
$^{193}Ir^0$	$5d^7\ 6s^2$	10.4886	–23.1	10.185	419	*(506a)*
$^{193}Ir^+$	$5d^6\ 6s^1\ 6p^1$	—	—	29.581	957	*(59a)*
	$5d^8$	8.4802	–18.71	—	—	*(59a)*
$^{195}Pt^0$	$5d^8\ 6s^2$	11.8527	–278	10.742	3709	*(506a)*
$^{195}Pt^+$	$5d^7\ 6s^1\ 6p^1$	—	—	31.612	10840	*(59a)*
	$5d^9$	9.6486	–225.7	—	—	*(59a)*

TABLE IV—*cont.*

CALCULATED VALUES OF ANISOTROPIC AND ISOTROPIC COUPLINGS FOR FREE IONS

Ion	Electronic configuration	$\langle r^{-3} \rangle$ (a.u.)	Principal value of $A_{aniso}{}^{b}$ (gauss)	$\lvert\psi_0\rvert^2$ (a.u.)	A_{iso} (gauss)	Reference
$^{197}Au^0$	$5d^9\ 6s^2$	13.2809	−25.0	11.378	313	(*506a*)
$^{197}Au^+$	$5d^8\ 6s^1\ 6p^1$	—	—	33.324	913	(*59a*)
	$5d^{10}$	10.8361	−20.24	—	—	(*59a*)
$^{199}Hg^0$	$5d^{10}\ 6s^2$	14.6560	−286	11.935	3416	(*506a*)
$^{199}Hg^+$	$5d^9\ 6s^1\ 6p^1$	—	—	35.064	9606	(*59a*)
	$5d^{10}\ 6s^1$	12.8704	−249.6	—	—	(*59a*)
$^{201}Hg^0$	$5d^{10}\ 6s^2$	14.6560	105	11.935	−1258	(*506a*)
$^{201}Hg^+$	$5d^9\ 6s^1\ 6p^1$	—	—	35.064	−3680	(*59a*)
	$5d^{10}\ 6s^1$	12.8704	92.12	—	—	(*59a*)
$^{203}Tl^0$	$6p^1$	7.5553	660	16.311	14893	(*506a*)
$^{205}Tl^0$	$6p^1$	7.5553	666	16.311	15040	(*506a*)
$^{207}Pb^0$	$6p^2$	10.9883	351	20.528	6868	(*506a*)
$^{209}Bi^0$	$6p^3$	14.5706	358	24.825	6394	(*506a*)

hydrogen atom is accurately known and its use in the calculation of A_0 is given below. The 1s electron wave function ψ is

$$\psi = \frac{1}{\sqrt{\pi a_0{}^3}}\, e^{-r/a_0} \tag{22}$$

where a_0 is the Bohr radius (0.52918×10^{-8} cm). The value of ψ at the nucleus is ψ_0 and is obtained from Eq (22) by putting $r = 0$, ψ_0 thus equals $1/\sqrt{\pi a_0{}^3}$. The isotropic coupling to hydrogen is then

$$\begin{aligned} A_{iso} &= \frac{8\pi}{3} \times 5.5854 \times 0.50504 \times 10^{-23} \times \frac{1}{\pi(0.52918 \times 10^{-8})^3} \\ &= 507.8 \text{ gauss} \end{aligned} \tag{23}$$

Refinements to the theory give a value of 506.82 gauss.

2. *Polarization of Inner Shell* s *Electrons*

Since isotropic coupling is associated with unpaired electron spin density at the nucleus, then transition metal ions with unpaired electrons in d orbitals would not be expected to exhibit any isotropic coupling. However, appreciable isotropic coupling is always observed, e.g., vanadyl complexes have values of A_{iso} (^{51}V) up to nearly 120 gauss.

Early suggestions that the apparent s character arose from spin–orbit coupling between the 3d and the 4s orbitals (*12*) or the excitation of a $3s^2$

electron to a 4*s* level (*11*) have since been shown to be inadequate for most compounds. It is probably better (*331*, *715*) to consider an exchange interaction between the unpaired *d* electrons and the paired *s* electrons in the core ($1s^2$, $2s^2$, $3s^2$, etc) which is dependent on spin orientation. In other words, there is a polarization of the ns^2 configuration which can then produce a magnetic field at the nucleus. Freeman and Watson (*220*) have suggested that the unpaired electron may be considered as attracting electrons of the same spin (by Hund's rule) and repelling those of opposite spin. Thus the nucleus feels the influence of one of the *s* electrons (α) more than the other (β) and so there is apparent unpaired α-spin density at the nucleus (Fig. 9). This will be of opposite sign to the unpaired *d* electron.

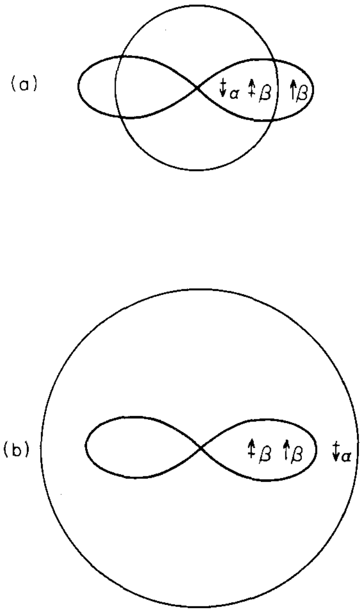

FIG. 9. Polarization of *s* electrons ↕ by a *p* or a *d* electron ↑ of β spin. (a) Inner *s*-orbitals and (b) outer *s* orbitals.

If the radial distributions of the inner *s* orbitals are now compared with those for the 3*d* orbital (Fig 10), it is seen that the 1*s* and 2*s* orbitals lie almost entirely inside the 3*d* orbital and polarization will produce a negative spin density at the nucleus In contrast, the 3*s* orbital is slightly more diffuse than the 3*d*, thus producing a positive spin density at the nucleus, i.e., it polarizes the electron nearer the nucleus thus giving it the same spin as itself. The net effect is the sum of these

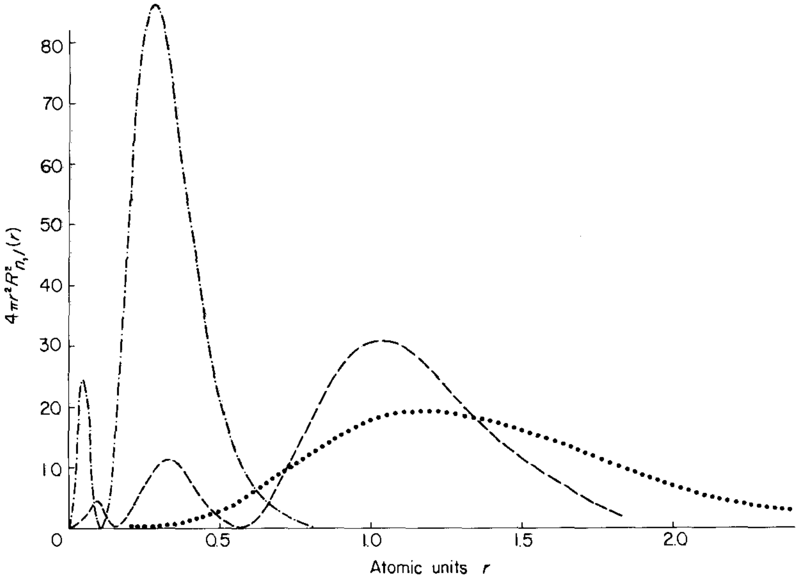

FIG. 10. Radial distribution of 2*s*, 3*s*, and 3*d* orbitals in the Ti^{3+} ion, calculated using hydrogenlike wave functions and Burns' rules for estimating the screening constants (*115*). —·—·, 2*s*; – – – –, 3*s*; and ······, 3*d*.

contributions and is illustrated for some metal ions of the first transition series in Table V. The values given are the theoretical contact term χ

TABLE V

THEORETICAL CONTACT TERMS χ, A_{iso} AND THE THEORETICAL A_0 (3*s*) FOR SOME TRANSITION METAL IONS[a]

	Mn^{2+}, d^5	Fe^{3+}, d^5	Fe^{2+}, d^6
Field at nucleus due to electron			
1*s* contribution	−6,730 (−0.16)	−10,500 (−0.25)	−8,840 (−0.21)
2*s* contribution	−283,300 (−6.73)	−358,300 (−8.51)	−328,400 (−7.80)
3*s* contribution	149,500 (+3.55)	242,900 (+5.77)	198,700 (+4.72)
Net theoretical contact term, per electron, χ	−140,500 (−3.34)	−125,900 (−3.00)	−138,700 (−3.29)
Hyperfine coupling A_{iso}	−106	−12.4	−13.6
Theoretical coupling for 3*s* electron, A_0	23,120	3,549	3,492

[a] Data in gauss, with atomic units in parentheses (*220*).

(field felt at the nucleus due to the unpaired electron) for the polarization of the *ns* orbital by *each* unpaired 3*d* electron in the free ion. These values are reduced in complexes because of the delocalization of the 3*d* electrons and there is a good correlation with the covalency of the metal-to-ligand bond. For comparison, the A_0 value for a single 3*s* electron is also given. This shows that the effect of polarization of inner *s* electrons by the 3*d* electrons is only about 0.5% of the coupling of an electron in the 3*s* orbital.

The theoretical contact term per electron χ for some ions has been calculated (*219*, *220*, *331*). The theoretical contact term resulting from polarization of *s* electrons by all unpaired *d* electrons is H_c and equals $2S\chi$. The field felt by the electron due to this field at the nucleus, A_{iso}, and the field at the nucleus are related as follows

$$\chi = \frac{\mu_e}{\mu_N} \cdot A_{iso}$$

Hence

$$\chi = \frac{g_e \beta_e}{g_N \beta_N} \hat{s}_z \cdot A_{iso} = \frac{\beta_e}{g_N \beta_N} \cdot A_{iso} \tag{24}$$

where χ and A_{iso} are given in gauss, or

$$\chi = \frac{3hca_0{}^3 A_{iso}}{2g_e \beta_e g_N \beta_N} \tag{25}$$

where χ is in atomic units and A_{iso} in cm^{-1}. (It is convenient to note that $\beta_e/\beta_N = 1836.12$.)

Because of the cancellation of very large terms of opposing signs, it is surprising that the calculations give not only the sign of χ correctly, but numerical values that are so realistic. Subtle changes in covalency between the metal and ligand atoms, and the accompanying changes in radial distribution of the *d* electrons influence the amount of polarization of the inner *s* orbitals in varying ways. A very slight change in the radial distribution of the *s* electron has a very large effect on the density at the nucleus, and hence upon A_{iso}. Whereas increasing covalency expands the *d* orbital and lowers the effective charge on the metal ion with a resultant increase in $|A_{iso}|$ (*276*), associated slight orbital expansion of inner *s* orbitals reduces the electron density at the nucleus and hence decreases $|A_{iso}|$ to a much greater extent, so that in general the net result is a decrease in $|A_{iso}|$ as covalency increases.

McGarvey (*505*) has shown that there is a close correlation between χ and $(X_A - X_C)$, the electronegativity difference between the anion and cation in the host lattice. This is similar to our correlations of A_{iso}

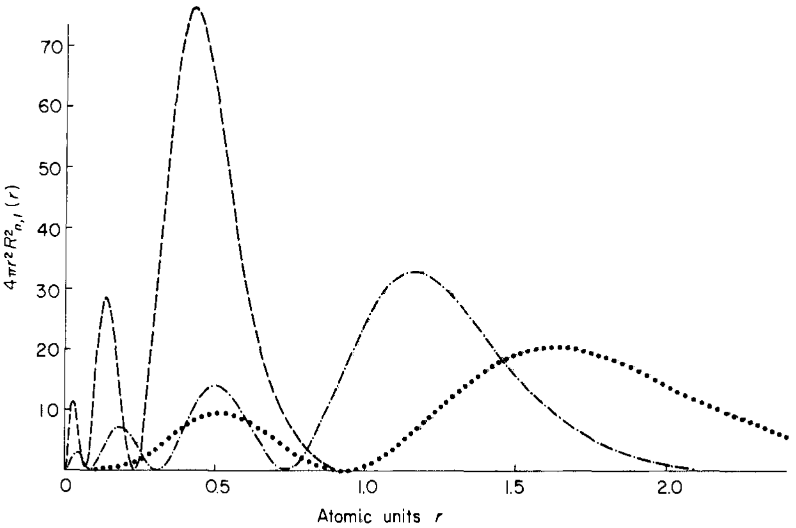

FIG. 11. Radial distribution of the 3*s*, 4*s*, and 4*d* orbitals in the Nb^{4+} ion, calculated using hydrogenlike wave functions and Burns' rules for estimating the screening constants (*115*). ----, 3*s*; –·–·–, 4*s*; and ······, 4*d*.

against g_{av} for metal ions in complexes of the same symmetries (see Figs. 38, 40, and 46).

Calculation of χ for some ions of the second transition series (*698*) show that again the resulting values are negative and about three times the magnitude of their 3*d* counterparts. The net value of χ is roughly constant and independent of ionic change (see Table VI).

TABLE VI

χ AND A_{iso} FOR SECOND TRANSITION SERIES IONS[a]

Ion	χ	A_{iso}	Ion	χ	A_{iso}
Y^{2+}	−335,100	49.9	Tc^{2+}	−371,000	−254
Zr^{2+}	−354,500	100	Ru^{3+}	−361,200	54.3
Nb^{2+}	−362,000	−269	Pd^{2+}	−374,700	46.5
Nb^{3+}	−352;000	−262	Pd^{3+}	−362,900	45.1
Mo^{+}	−368,400	73.0			

[a] Data in gauss.

An analysis of the individual shell contributions to χ has shown that $\chi(3s)$ is positive and the $\chi(1s)$, $\chi(2s)$, and $\chi(4s)$ are negative. The dominant contributions arise from $\chi(2s)$ and $\chi(4s)$ because of the different spatial relationship between the s-electron wave functions and the different parts of the $4d$ wave function. The $1s$ and $2s$ contributions are negative due to the inner lobes of $4d$, the $3s$ contribution is positive but greatly reduced compared with the $3d$ case, and the $4s$ contribution is negative and large (see Fig. 11). No calculations have been made on the sign and magnitude of any $\chi(5s)$ contribution, but it might be expected that this will be positive and large.

D. FACTORS AFFECTING THE MAGNITUDE OF METAL ISOTROPIC AND ANISOTROPIC HYPERFINE COUPLING

1. *Mixing of Other Metal Orbitals with the Orbital Formally Containing the Unpaired Electron*

a. Isotropic Coupling. When the unpaired electron is in a molecular orbital whose symmetry is such that it allows a contribution from s-atomic orbitals, then there is a Fermi contact contribution to the measured A_{iso}. This occurs in cobalt phthalocyanin (*41*) which has D_{4h} symmetry and the unpaired electron is in the a_{1g} molecular orbital. This orbital is a mixture of $3d_{z^2}$ and $4s$ and the contribution to A_{iso} is positive and of opposite sign to the contribution from the inner shell polarization. Since a small amount of unpaired electron spin density in the $4s$ orbital produces a large coupling (Table VII), the absolute magnitude of A_{iso} will be decreased and may be either negative or positive. Another example

TABLE VII

CONTRIBUTIONS TO A_{iso} FOR ONE UNPAIRED ELECTRON IN $4s$ ORBITAL FOR SOME NEUTRAL METAL IONS[a]

Ion	A_{iso}	Ion	A_{iso}
^{47,49}Ti	−175.7	^{59}Co	+1307.6
^{51}V	+932.3	^{61}Ni	+539.7
^{53}Cr	−224.9	^{63}Cu	+1766.9
^{55}Mn	+1093.2	^{65}Cu	+1892.2
^{57}Fe	+160.5		

[a] Data in gauss. The negative signs for ^{47}Ti, ^{49}Ti, and ^{53}Cr are a consequence of the negative nuclear magnetic moments of these nuclei, which changes the signs of all their coupling constants.

TABLE VIII

CALCULATED VALUES OF A_{aniso} FOR ELECTRONS IN $3p$ AND $4p$ ORBITALS FOR SOME NEUTRAL METAL IONS

Orbital	$3p^a$	$4p^b$	$4p^c$
^{47}Ti, ^{49}Ti	–146	–0.56	–2.09
^{51}V	829	2.43	10.62
^{53}Cr	–215	–0.50	–2.48
^{55}Mn	1120	2.14	10.68
^{57}Fe	172	0.26	1.37
^{59}Co	1478	2.10	10.92
^{61}Ni	643	0.85	4.65
^{63}Cu	2206	0.91	15.62
^{65}Cu	2363	0.97	16.73

[a] $3d^n$ configuration.

[b] $3d^{n-1}4p$ configuration.

[c] $3d^{n-2}4p^2$ configuration.

is $V(S_2C_2H_2)_3$, which has D_{3h} symmetry, where the unpaired electron is thought to be in the a_1' molecular orbital (*167*, *168*).

b. Anisotropic Coupling. The effect described above will decrease the anisotropic hyperfine coupling simply because the d-electron density is decreased. The effect on A_{aniso}, however, is much more marked if there is mixing of the metal d orbital with one or more of the metal p orbitals. Since the sign of the principal value of the anisotropic hyperfine tensor is negative for d_{xy}, d_{xz}, d_{yz}, and $d_{x^2-y^2}$ (Group A) and positive for d_{z^2},

TABLE IX

SUMMARY OF THE SIGNS OF METAL HYPERFINE TENSORS, ASSUMING A POSITIVE NUCLEAR MOMENT

Metal orbital containing unpaired electron	A_{iso}	A_{aniso}	$A_{pseudoiso}{}^b$
s	Very large +ve	Zero	Small +ve
p	Small, usually –ve^a	+ve	Small +ve
$3d$ and $4d$ except d_{z^2}	Small, usually –ve^a	–ve	Small +ve
$d_{z^2}{}^c$	Small, ±ve^a	+ve	Small +ve

[a] Polarization of inner shell s electrons.

[b] To be subtracted from A_{iso} (experimental).

[c] Since d_{z^2} and s orbitals may mix in all symmetries except T_d, O_h, and I_h, the resultant A_{iso} may be ±ve. In practice it is almost always negative.

p_x, p_y, and p_z (Group B), a mixing of a Group A orbital with a Group B orbital will result in a decrease in the magnitude of the resulting hyperfine interaction. The contributions to A_{aniso} of one electron in the $3p$ or $4p$ orbital for first-row transition metal atoms are given in Table VIII. A summary of the signs of the metal hyperfine tensors is given in Table IX.

An example of the application of this effect occurs in Cs_2CuCl_4 (*613*), which is discussed in more detail in Section VIII,K,4.

2. *The Nature of the Metal–Ligand Bonds*

The formation of a molecular orbital between the metal orbital containing the unpaired electron and atomic orbitals on the ligand nuclei results in a transfer of some of the unpaired electron density from the metal to the ligands. If the molecular orbital containing the unpaired electron is represented as

$$\Psi = \alpha\psi_M + (1 - \alpha^2)^{1/2} \sum_i \psi_i \tag{26}$$

the spin density on the metal becomes α^2 instead of unity. To a rough approximation, the anisotropic hyperfine interaction, will be proportional to α^2. For highly covalent compounds this picture will be complicated by the dipolar interaction between the metal nucleus and the unpaired ligand electron density. A number of authors have made attempts to rationalize ligands according to the influence they have upon the hyperfine coupling. Van Wieringen (*680*) listed ligands in the order of the influence they had upon the magnitude of the isotropic coupling of the central metal ion. He found that the magnitudes of A_{iso} were in the order $H_2O \sim F^- > CO_3^{2-} > O^{2-} > S^{2-} > Se^{2-} > Te^{2-}$. Title (*662*) obtained a correlation between A_{iso} and the percentage ionicity of the host lattice for high spin Mn^{2+} compounds. McGarvey (*505*) plotted χ (the field at the nucleus per unpaired electron) against the electronegativity difference between the anion and cation in the host lattice and obtained fairly good linear relationships for d^3, d^5, and d^7 ions, but obtained an almost random distribution of points in his plots for d^1 and d^9 ions. Two criticisms which may be levelled at these attempted correlations are, first, for transition metal compounds, A_{iso} or χ is not a good reflection of the d-electron density on the metal, and, second, the metal will be influenced more by its nearest neighbors than by its next nearest neighbors. Thus the electronegativity difference between the anion and the cation in the host or the degree of ionicity of the host is not a good parameter against which to plot the metal hyperfine coupling.

3. *Influence of Charge on the Metal*

For a free ion, one might expect an increase in magnitude of both A_{iso} and A_{aniso} as the charge on the metal is increased since the electrons are more firmly held. Calculations show that A_{aniso}, in particular, exhibits a marked dependence on charge. This is illustrated in Fig. 12 which shows some results calculated using the wave functions of Synek and Stungis (*652*).

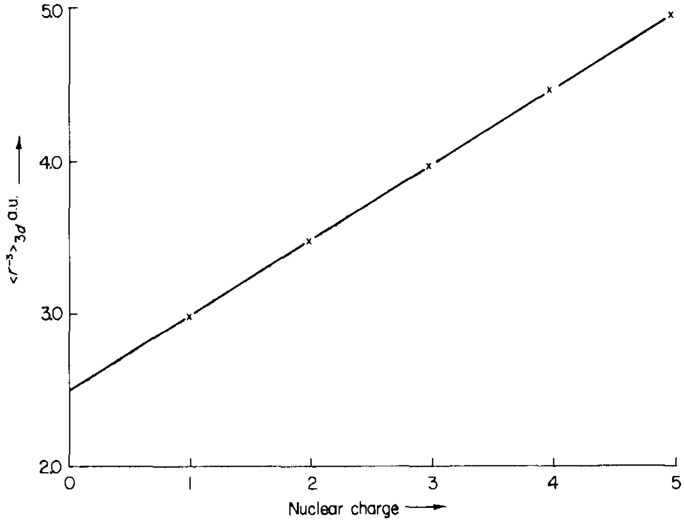

FIG. 12. Influence of nuclear charge on $\langle r^{-3}\rangle$ for Cr (*652*).

Since the above plot does not distinguish between the dependence of $\langle r^{-3}\rangle$ on (*i*) charge and (*ii*) the number of *d* electrons, a similar plot was made of $\langle r^{-3}\rangle$ against nuclear charge for a number of d^5 ions (see Fig. 13).

Gerschwind (*262*) and McGarvey (*505*) have observed a steady increase in χ as the number of *d* electrons of ions in a host lattice is increased (see Table X).

TABLE X

AVERAGE VALUE OF χ IN OXIDE LATTICES[a]

d^1	d^2	d^3	d^4	d^5	d^7	d^8	d^9
−84,000	−88,000	−96,000	−105,000	−113,000	−126,000	−135,000	−143,000

[a] Data in gauss (*505*).

4. Libration

If the molecule, or part of the molecule is vibrating in a nonquantum mechanical way, then the magnitude of the anisotropic hyperfine tensor is reduced. If the libration is about one of the principal directions, then the effective value of the coupling in that direction will be the coupling appropriate to the mean angle of deviation from the principle direction.

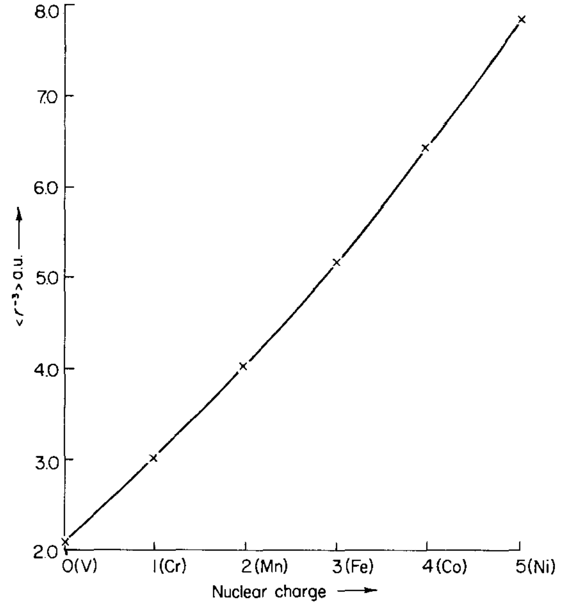

FIG. 13. Influence of nuclear charge on $\langle r^{-3}\rangle$ for d^5 ions (*652*).

E. SUPERHYPERFINE COUPLING TO LIGANDS

A superhyperfine coupling may sometimes be observed when there are ligands or other atoms in the molecule whose nuclei have magnetic moments. If the unpaired electron is located entirely in an atomic orbital on the metal and the ligands are held entirely by crystal field forces, then the only interaction between a ligand nucleus and the unpaired electron is dipolar. This is inversely proportional to the mean cube of the distance of the electron from the ligand nucleus. As was the case for the dipolar interaction between the electron and its own nucleus, this interaction is anisotropic and vanishes when the molecule is tumbling rapidly. It is usual, however, for a small amount of the unpaired electron to be delocalized onto the ligands as a result of the formation of molecular orbitals. Contributions from other terms are also probable. The measured superhyperfine coupling to a ligand nucleus along the three principal directions will be made up of

$$A_{expt} = A_{aniso} + A_{dipolar} + A_{iso} + \text{smaller terms}$$

Since A_{iso} may be obtained from the measurements in fluid solution and $A_{dipolar}$ may be calculated, A_{aniso} is readily obtained. From the computed values of A_{aniso} and A_{iso}, and assuming the other terms are small, the *p* or *d* and *s* character of the orbital on the ligand with which the unpaired electron is interacting may be deduced, i.e., the hybridization is found.

1. *Dipolar Coupling*

An estimation of the contribution to the anisotropic hyperfine coupling of a ligand nucleus due to dipolar coupling may be calculated in several ways depending on the accuracy required and the separation between the metal and ligand nuclei.

a. Point-Dipole Approximation. The average position of the unpaired electron is considered to be located at the metal nucleus which is at a distance r(cm) from the ligand. Use is made of the general classical formula for the field at the electron due to the nucleus, namely,

$$A = g\beta_e g_N \beta_N \frac{(3\cos^2\theta - 1)}{r^3} \text{ (ergs)} \tag{27}$$

where g_N and β_N refer to the ligand nucleus. If the field is parallel to the metal–ligand bond, $\theta = 0$ and

$$A = A_\parallel = \frac{2g\beta_e g_N \beta_N}{r^3} \text{ (ergs)} \tag{28}$$

and

$$A_\perp = \frac{-g\beta_e g_N \beta_N}{r^3} \text{ (ergs)} \tag{29}$$

The calculation of $g_N\beta_N$ is as follows.

Since

$$\mu_N = g_N \beta_N I \text{ (erg/gauss)} \tag{30}$$

$$g_N \beta_N = \frac{\mu_N}{I} \qquad \text{(erg/gauss)} \tag{31}$$

The magnetic moment of the nucleus, however, is usually expressed in multiples of nuclear magnetons β_N and such numbers are obtained from the tables (e.g., Table I). This numerical value has to be multiplied by β_N for substitution in Eq. (31).

This method is not suitable for metal–ligand distances below about 2 Å (*496*).

b. Separate Dipoles Approximation. A refinement to the above approach is to consider a fraction of the electron in each lobe of the metal orbital. There are three different orientations of *d* orbitals to consider, and these are illustrated in Fig. 14.

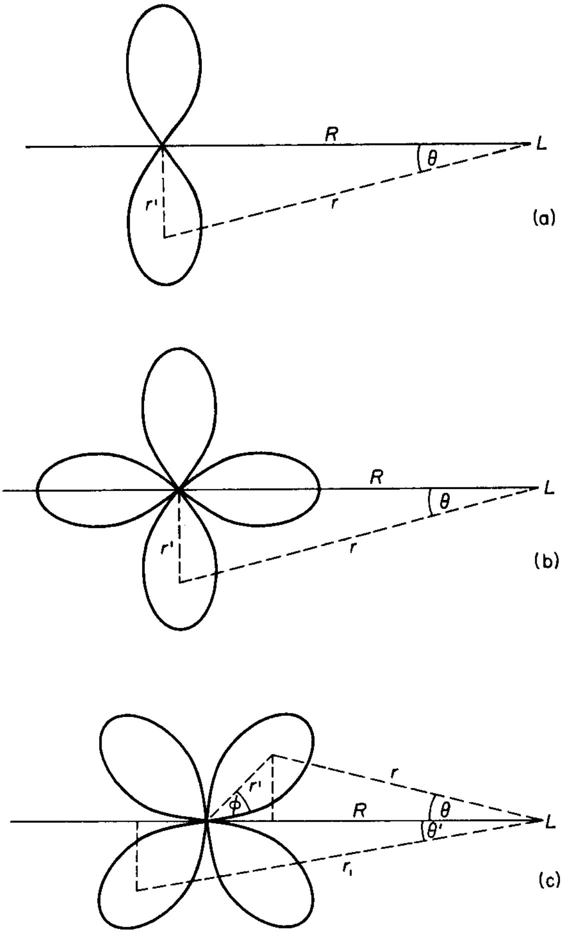

FIG. 14. Dipolar interaction of an unpaired electron in a *d* orbital with a ligand (a) orbital perpendicular, (b) one lobe parallel, and (c) all lobes at 45° to the metal–ligand bond.

(*i*) *The orbital perpendicular to the metal–ligand bond.* For the applied field parallel to the metal–ligand bond,

$$A_{\parallel} = \frac{g\beta_e g_N \beta_N (2R^2 - r'^2)}{(R^2 + r'^2)^{5/2}} \text{ (ergs)} \qquad (32)$$

If $R \gg r'$, then r'^2 may be ignored and Eq. (32) reduces to the point-dipole approximation [Eq. (28)].

(*ii*) *One lobe parallel to the metal–ligand bond.* For the applied field parallel to one lobe of the d orbital

$$A_{\parallel} = g\beta_e g_N \beta_N \frac{2R - r'^2}{2(R + r'^2)^{5/2}} + \frac{(R - r')^3 + (R + r')^3}{2(R + r')^3\,(R - r')^3} \text{ (ergs)} \tag{33}$$

If $R \gg r'$, then r'^2 may be ignored and Eq. (33) reduces to the point-dipole approximation [Eq. (28)].

(*iii*) *All lobes at 45° to the metal–ligand bond.* For the applied field passing through the dihedral angle for a d orbital

$$A_{\parallel} = g\beta_e g_N \beta_N \left\{ \frac{2(R - r'/\sqrt{2}) - r'^2/2}{2[(R - r'/\sqrt{2})^2 + r'^2/2]^{5/2}} + \frac{2(R + r'/\sqrt{2}) - r'^2/2}{2[(R + r'/\sqrt{2})^2 + r'^2/2]^{5/2}} \right\} \tag{34}$$

If $R \gg r'$, then r'^2 may be ignored and Eq. (34) reduces to the point-dipole approximation [Eq. (28)].

The difficulty with this approach is estimation of r'. The mean value can be obtained from wave functions calculated from free atoms and ions, but this is not completely satisfactory since the interaction is proportional to r'^3. This approach, however, gives more realistic values than the point-dipole approximation when the metal–ligand bond distances are less than 2 Å.

When dealing with the d_{z^2} orbital, it may be treated as the sum of $d_{z^2-x^2}$ and $d_{z^2-y^2}$.

c. Semiclassical Quantum Mechanical Approach. Both of the previous approximations break down for very small metal–ligand bond lengths. In such a case, it is necessary to solve

$$\langle \psi | \mathscr{H}_{dipolar} | \psi \rangle \tag{35}$$

where the dipolar Hamiltonian is given by

$$\mathscr{H}_{dipolar} = \frac{\hat{\mu}_N \hat{\mu}_e}{|\bar{r}|^3} - \frac{3(\hat{\mu}_N \bar{r})(\hat{\mu}_e \bar{r})}{|\bar{r}|^5} \tag{36}$$

$\bar{r}$ is the radius vector connecting the nucleus in question with the electron, μ_e and μ_N are the electron and nuclear magnetic moment operators, respectively, and ψ is the Slater wave function of the orbital containing the unpaired electron.

The method is only advantageous for small nuclear separations, i.e., 1 Å.

2. *Ligand Contact Interaction*

As pointed out in Section III,D,2, the formation of molecular orbitals may result in the orbital containing the unpaired electron being partially delocalized onto some or all of the ligands. If, as previously, the molecular orbital containing the unpaired electron is represented as

$$\Psi = \alpha\psi_M + (1 - \alpha^2)^{1/2} \sum_i \psi_i \qquad (37)$$

the total ligand spin density is $(1 - \alpha^2)$. By obtaining spectra in fluid and solid states one is able to estimate the *s*- and *p*- or *d*-electron density on the ligands from the isotropic and anisotropic superhyperfine coupling constants in exactly the same way as for the central metal atom.

3. *Spin Polarization of Molecular Orbitals* (*Configuration Interaction*)

In addition to real electron density, ligand superhyperfine coupling may result from spin polarization of filled molecular orbitals having appreciable ligand character by an exchange mechanism analogous to the core polarization on the central metal atom. This may also be imagined as a mixing-in of excited states. The effect is greater, the closer the interacting energy levels are (*391*).

It is often not possible to distinguish between the effects of spin polarization and direct electron density on the ligands, although the latter mechanism may sometimes be eliminated if the molecular orbital containing the unpaired electron does not possess ligand orbitals capable of producing the observed ligand spin density, e.g., in $[Cr(CN)_5NO]^{3-}$ the unpaired electron is in the molecular orbital which has no nitrosyl character. The ^{14}N superhyperfine coupling, however, indicates either 15% $p\pi(N)$ or 7.5% $p\pi(N)$ character. It is thus necessary to invoke spin polarization of the *e*-molecular orbital which contains metal d_{xz}, d_{yz}, and nitrosyl π and π^* orbitals as a means of obtaining the nitrogen electron density (*216*, *279*).

4. *Spin–Orbit Coupling*

Spin–orbit coupling may produce an orbital magnetic moment on the ligands. This leads to a modification of the main spin-dipole term by a small correction term proportional to $(g - 2)$.

The presence of this unquenched orbital magnetic moment on the ligands, however, may lead to appreciable direct interaction with the ligand nucleus in some cases. An estimation of the magnitude of this term by Marshall (*458*) has shown that in the cases of Ni^{2+} and Cr^{3+} ions it may account for 30% of the observed ligand hyperfine interaction.

The effect of spin–orbit coupling upon the hyperfine coupling is to add another term to expressions for $A_{\parallel}$ and $A_{\perp}$ such that

$$A_{\parallel} = A_{iso} - B + \frac{n_1 \lambda}{\Delta_1} \cdot \frac{B}{2} \tag{38}$$

$$A_{\perp} = A_{iso} + \frac{B}{2} + \frac{n_2 \lambda}{\Delta_2} \cdot \frac{B}{2} \tag{39}$$

where λ is the spin–orbit coupling constant, Δ is the energy separation between the orbital containing the unpaired electron and the orbital into which it may mix by spin–orbit coupling, B is part of the anisotropic hyperfine tensor which is of the form $|-B, +B/2, +B/2|$, and the coefficient n may be deduced from the magic pentagon below, n being the number on the line linking the d orbitals under consideration.

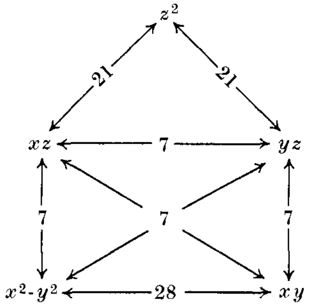

λ/Δ is calculated from a knowledge of Δg (see Section IV,D) and substituted back into the above equations.

From Eqs. (38) and (39)

$$A_{av} = A_{iso} + \frac{1}{3}\left(\frac{n_1 \lambda}{\Delta_1} \cdot \frac{B}{2} + \frac{2n_2 \lambda}{\Delta_2} \cdot \frac{B}{2}\right) \tag{40}$$

The additional term in parentheses is the pseudocontact term and is always a positive quantity.

A number of other small contributions to the ligand hyperfine interaction have been discussed by Marshall (*458*, *487*). These are, however, usually very small, and any estimated contributions from such terms are generally no larger than the errors in the hyperfine coupling itself.

A complete treatment of spin–orbit coupling is given by Griffiths in his book (*298*).

F. THE ANISOTROPIC HYPERFINE TENSOR

The hyperfine tensor for an axially symmetric molecule is obtained from the measured $A_{\parallel}$, $A_{\perp}$, and A_{iso} values. Since in fluid solution the anisotropy is averaged to zero, the average value of $A_{\parallel}$ and $A_{\perp}$ will be A_{iso}, i.e.,

$$\tfrac{1}{3}(A_{\parallel} + 2A_{\perp}) = A_{iso} \tag{41}$$

since there are two mutually independent perpendicular directions. The anisotropic hyperfine tensor for the metal is readily computed by subtracting the A_{iso} value from the $A_{\parallel}$ and $A_{\perp}$ values. The tensor is thus

$$\begin{array}{ccc} |A_{\parallel} - A_{iso}, & A_{\perp} - A_{iso}, & A_{\perp} - A_{iso}| \\ z & x & y \end{array} \tag{42}$$

and has the units of A.

TABLE XI

SUMMARY TABLE GIVING THE SIGNS OF THE LIGAND HYPERFINE TENSOR WHEN THE UNPAIRED ELECTRON IS IN A METAL ORBITAL[a]

Metal orbital containing electron	Direct delocalization (contact interaction)		Spin polarization (configuration interaction)	
	A_{iso}	A_{aniso}[b]	A_{iso}	A_{aniso}
p_z, d_{z^2}	$+(\sigma)$	$+(\sigma)$	$-(\pi)$[c]	$-(\pi)$[c]
p_x, p_y	—	—	$-(\sigma)$	$-(\sigma)$[d]
d_{xy}, $d_{x^2-y^2}$	—	—	$-(\pi)$	$-(\pi)$[d]
d_{xz}, d_{yz}	$+(\pi)$	$+(\pi)$	$-(\sigma)$[e]	$-(\sigma)$[e]
s	$+(\sigma)$	$+(\sigma)$	$-(\pi)$[c]	$-(\pi)$[c]

[a] σ and π refer to whether the effect operates via the σ or π metal-to-ligand bond.

[b] Dipolar coupling, which is always positive, must be subtracted from A_{aniso}.

[c] If via M–L σ bond, the value would be very small compared with direct delocalization.

[d] The sign would be +, and the magnitude cut by one-half if these were two degenerate π orbitals on the ligand, since the tensor would be made up of two, one containing half an electron along the x axis and another containing half an electron along the y axis, the z axis being the M–L axis, i.e.,

$$\begin{array}{ccc} x & y & z \\ -B & +B/2 & +B/2 \\ +B/2 & -B & +B/2 \\ \hline -B/2 & -B/2 & +B \end{array}$$

[e] If via M–L π bond, the value would be very small compared with direct delocalization.

The tensor for the ligands is worked out in a similar manner, but the dipolar and other contributions to this must be subtracted to give the real anisotropic hyperfine tensor. The large term in the tensor A_{aniso} is related to the p- or d-electron spin density in the appropriate orbital. Values for $A_{p/d}$ may be used which give the coupling to an electron which is entirely in the p or d orbital (Table IV). The ratio of the measured A_{aniso} to $A_{p/d}$ gives the spin density in the orbital under consideration. Such spin populations refer to any one ligand nucleus under consideration. If there are n equivalent ligands, then the total spin delocalization is multiplied by n.

It should be emphasized that the sign of all values in a hyperfine tensor are reversed in cases where the nucleus involved has a negative nuclear magnetic moment. Table XI summarizes the signs of the ligand hyperfine tensor when the unpaired electron is in a metal orbital.

1. *Orbital Hybridization*

From the s- and p-electron density on an atom, the hybridization sp^n may readily be deduced. Care must be taken to realize that these figures are deduced from the unpaired electron density and are not necessarily related to the bonding electrons involved with a particular ligand atom. Where it is certain that the hybridization so deduced is meaningful, then it is possible to calculate the bond angles in such ligands as —OH_2 or —NH_3 from the hybridization of the ligand orbital involved

TABLE XII

VARIATION OF BOND ANGLE WITH HYBRIDIZATION sp^n IN C_{3v} AND C_{2v} MOLECULES

n	θ (C_{2v})	θ (C_{3v})
1	109° 28′	101° 32′
2	120°	106° 37′
3	126° 52′	109° 28′
4	131° 44′	111° 21′
5	135° 34′	112° 39′
6	138° 34′	113° 35′
7	141° 04′	114° 20′
8	143° 08′	114° 54′
9	144° 54′	115° 23′
10	146° 26′	115° 46′

with σ bonding with the metal. Coulson (*150*) has showed that for C_{2v} ligands the internal angle

$$\theta = 2\cos^{-1}(n+2)^{-1/2} \tag{43}$$

and for a C_{3v} ligand,

$$\theta = \cos^{-1}\left[\frac{1.5}{2n+3} - \tfrac{1}{2}\right] \tag{44}$$

Table XII summarizes the bond angles for various hybridizations.

IV. Spin–Orbit Coupling and the Significance of the *g* Tensor

A. SPIN–ORBIT COUPLING

The angular momentum of an electron in an atom is made up of two components, the spin and the orbital angular momentum. Since angular momentum is a vector quantity, then the two such angular momenta parameters of an electron are able to couple together to form a resultant angular momentum. If in an atom there are two electrons, 1 and 2, with spin angular momenta s_1 and s_2 and orbital angular momenta l_1 and l_2, then there is the possibility of the two spin components combining (s_1 and s_2) and the two orbital components combining (l_1 and l_2) separately, as well as the spin of one electron combining with the orbital component of the same electron ($s_1 l_1$) or with the other ($s_1 l_2$). For most atoms of the periodic table, excluding the lanthanide and actinides groups of elements, the Russell–Saunders coupling* scheme dominates, which means that the order of the interaction is

$$s_1 s_2 > l_1 l_2 \gg \underset{\substack{\text{spin–orbit}\\ \text{coupling}}}{s_1 l_1 = s_2 l_2} \gg s_1 l_2 = s_2 l_1 \tag{45}$$

The energy due to spin–orbit coupling is considered as a comparatively small perturbation compared with the energy of electron interactions. In second and third row transition elements, spin–orbit coupling is more important, but does not become greater in magnitude than spin–spin or orbital–orbital interactions.

Two parameters are in common use to describe the action of spin–orbit coupling. The first of these is the single-electron spin–orbit coupling parameter ξ which measures the energy of the interaction between the

---

* An everyday example of classical spin–orbit coupling is the precession of the earth in its orbit around the sun. This is caused by mechanical coupling of the rotational and orbital angular momenta of the earth in the gravitational field of the sun.

spin and the orbital angular momenta of a *single* electron of the *configuration* and is a property of the electron configuration. ξ may be calculated from the expression

$$\xi = \frac{Z_{\text{eff}}\, e^2}{2m^2 c^2 \cdot \langle r^3 \rangle} \tag{46}$$

ξ is thus a positive quantity and is dependent upon the effective nuclear charge and the average distance of the electron from the nucleus $\langle r \rangle$. Whenever atoms in molecules are considered, the parameter ξ has to be reduced in magnitude because Eq. (46) is applicable only for atoms.

Since we are mainly concerned with the influence of spin–orbit coupling on *terms*, it is convenient to use a new parameter λ, which is a property of any given term but may vary from one term to another in a particular configuration. The two constants are related by

$$\lambda = \pm \frac{\xi}{2S} \tag{47}$$

where S is the spin multiplicity ($\sum s_i$). A proof of this equation has been given by Griffiths (*298*). λ is positive when the term arises from a subshell less than half full, and is negative for subshells more than half full. This latter is equivalent to a set of positive electrons in an empty subshell.

Some other general rules are applicable to spin–orbit coupling.

(*i*) Spin–orbit levels have quantum numbers J given by the vector sum of **S** and **L**

$$J = \mathbf{S} + \mathbf{L} \tag{48}$$

(*ii*) The level with lowest J quantum number lies lowest in energy for terms arising from levels less than half full ($\lambda + ve$). The reverse is true for levels more than half full, i.e., the highest J quantum number lies lowest in energy ($\lambda - ve$).

(*iii*) The separation between adjacent J levels is λJ_i where J_i is the larger J quantum number. This is called the Landé interval rule.

(*iv*) A magnetic field splits any J level into $2J + 1$ components.

(*v*) The energies of the J levels relative to the energy of the unperturbed term obeys the "center of gravity" rule.

Spin–orbit coupling is the mechanism by which a contribution from the orbital angular momentum is added to (or mixes with) the spin angular momentum, thus changing any magnetic parameter arising from pure spin angular momentum (spin-only case). It is also the mechanism whereby energy levels of different symmetries may mix.

The use of the words configuration, terms, states, etc. are summarized in Fig. 15 which refers to a d^2 ion in an octahedral crystal field. The energies given are approximate and are relevant to the V^{3+} ion.

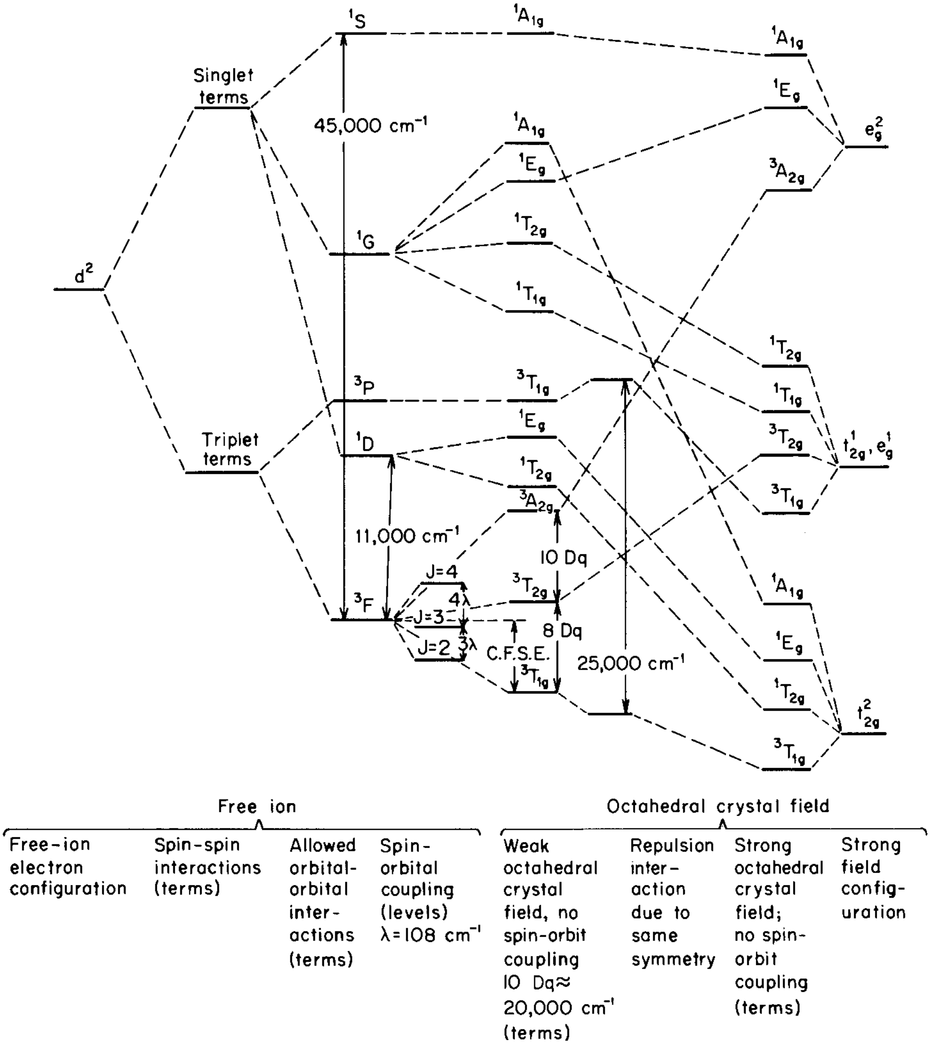

FIG. 15. The energy levels of a free d^2 ion, and in the presence of an octahedral crystal field.

B. THE MAGNETIC PROPERTIES OF ATOMS IN A CRYSTAL FIELD

In a crystal field, the degeneracy of orbitals is reduced or lost completely. The orbital angular momentum is then said to be partially or fully quenched. Orbital angular momentum about an axis is associated with the ability to rotate an orbital containing an unpaired electron about an axis to give an identical and degenerate orbital. Thus in a free atom, the d_{xy} orbital can be rotated about the z axis into the $d_{x^2-y^2}$ orbital and the two orbitals are said to commute about the z axis. Similarly, d_{xz} and d_{yz} will commute about the z axis, but about no other axis. In an octahedral crystal field the energy of the orbitals is split such that the d_{xy}, d_{xz}, d_{yz}, (t_{2g}) orbitals are degenerate, and the $d_{x^2-y^2}$, d_{z^2}, (e_g) orbitals are degenerate at a different energy. Commutation is possible in the t_{2g} set, thus allowing an orbital contribution, but not possible in the e_g set since the $d_{x^2-y^2}$ and d_{z^2} orbitals cannot be rotated into each other about any of the axes and so no angular momentum contribution is associated with it.

TABLE XIII

GROUND TERMS FOR WHICH ORBITAL ANGULAR MOMENTUM IS OR IS NOT QUENCHED BY A CUBIC LIGAND FIELD

		Stereochemistry					
		Octahedral			Tetrahedral		
No. of d electrons	Free-ion ground term	Nearest $t_{2g}^n \cdot e_g{}^m$ config.	Ground term in complex	Orbital contrib. expected	Nearest $t_2^n \cdot e^m$ config.	Ground term in complex	Orbital contrib. expected
1	^{2}D	t_{2g}^1	$^2T_{2g}$	Yes	e^1	^2E	No
2	^{3}F	t_{2g}^2	$^3T_{1g}$	Yes	e^2	$^3A_2$	No
3	^{4}F	t_{2g}^3	$^4A_{2g}$	No	$e^2 \cdot t_2{}^1$	$^4T_1$	Yes
4	^{5}D	$t_{2g}^3 \cdot e_g{}^1$	^5E_g	No	$e^2 \cdot t_2{}^2$	$^5T_2$	Yes
		t_{2g}^4	$^3T_{1g}$	Yes	—	—	—
5	^{6}S	$t_{2g}^3 \cdot e_g{}^2$	$^6A_{1g}$	No	$e^2 \cdot t_2{}^3$	$^6A_1$	No
		t_{2g}^5	$^2T_{2g}$	Yes	—	—	—
6	^{5}D	$t_{2g}^4 \cdot e_g{}^2$	$^5T_{2g}$	Yes	$e^3 \cdot t_2{}^3$	^5E	No
		t_{2g}^6	$^1A_{1g}$	No	—	—	—
7	^{4}F	$t_{2g}^5 \cdot e_g{}^2$	$^4T_{1g}$	Yes	$e^4 \cdot t_2{}^3$	$^4A_2$	No
		$t_{2g}^6 \cdot e_g{}^1$	^2E_g	No	—	—	—
8	^{3}F	$t_{2g}^6 \cdot e_g{}^2$	$^3A_{2g}$	No	$e^4 \cdot t_2{}^4$	$^3T_1$	Yes
9	^{2}D	$t_{2g}^6 \cdot e_g{}^3$	^2E_g	No	$e^4 \cdot t_2{}^5$	$^2T_2$	Yes

A further requirement for the existence of orbital angular momentum due to orbital rotation is that there must not be an electron in the second orbital with the same spin as that in the original orbital. With these rules, it is possible to deduce which electron configuration of transition metal ions will have its orbital angular momentum fully or partially quenched. This information is summarized in Table XIII.

It is seen that orbital angular momentum is fully quenched in ions whose ground state terms are A or E, i.e., singly or doubly degenerate. Conversely, there remains orbital angular momentum in triply degenerate ground states, e.g., T_1 and T_2. The exact amount of orbital contribution may be calculated for T terms and each configuration has to be considered individually.

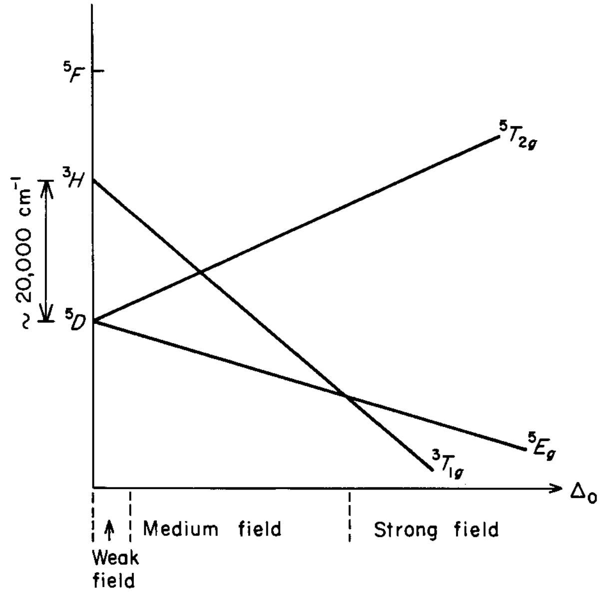

FIG. 16. Part of an Orgel energy level diagram for a d^4 ion in O_h symmetry, showing how the $^3T_{1g}$ level becomes lowest in energy in strong fields.

1. *The Strength of Crystal Fields*

The expressions weak, medium, and strong fields are often used in the discussion of the strength of a ligand or crystal field. A strong field is defined as one with sufficient strength to pair electrons so that they occupy t_{2g} orbitals (for an octahedral complex) in preference to e_g orbitals. Weak fields are rarely met with in transition metal complexes. Figure 16 summarizes these terms with respect to an Orgel energy level diagram for a d^4 ion in octahedral symmetry.

2. *The Magnetic Properties of Complexes with Ground State Term Configuration T*

Transition metal complexes have free ion ground state terms which (see Table XIII) may be S, D, or F. In the case of S or D ground state terms, there are no excited states of the same multiplicity, but with F ground state terms, there is always an excited state with the same multiplicity which arises from a P term. In cubic crystal fields, the free ion terms split into crystal field terms with symmetries A, E, T_1, or T_2 as follows:

$$\begin{aligned} &\mathrm{S} \rightarrow A_1 \\ &\mathrm{P} \rightarrow T_1 \\ &\mathrm{D} \rightarrow T_2 \text{ and } E \\ &\mathrm{F} \rightarrow A_2,\ T_1, \text{ and } T_2 \end{aligned}$$

Thus T_1 terms arise from free ion F ground state terms *and* associated P excited state terms, whereas T_2 terms may arise from *either* free ion F *or* D ground state terms. Thus in any complex with an F ground state term there will be two T terms, which are then capable of mixing since they have the same symmetry. When T_2 terms are present, however, there are never any others with the same symmetry; therefore they will be unperturbed by other terms. The mixing of the T_1 terms causes the energy levels to diverge and also to influence the magnetic properties so that, e.g., g and μ_{eff} are very dependent on the strength of the crystal field. A proof of this is given by Coulson (*151*) and is illustrated in Fig. 17. Table XIV gives the ground terms of first-row transition metal ions.

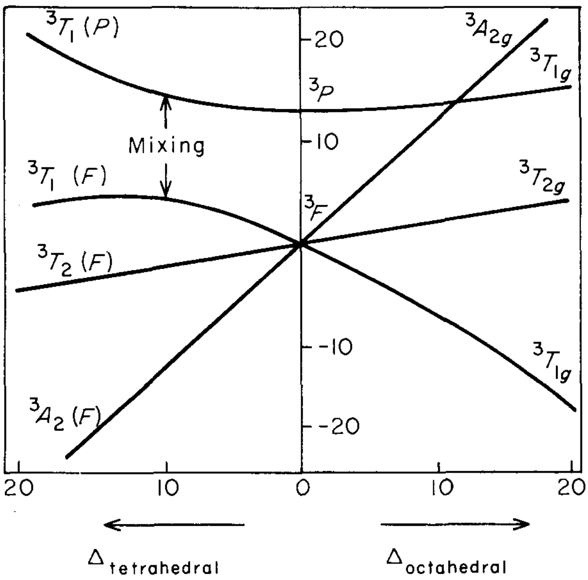

FIG. 17. Orgel energy level diagram for a d^3 ion in octahedral and tetrahedral crystal fields, showing the repulsion between the $^3T_1(F)$ and $^3T_1(P)$ energy levels. The units of energy are $10^3\,\mathrm{cm}^{-1}$.

The influence of spin–orbit coupling on T terms is simplified by the observation that they are triply degenerate like a free ion P term. It is thus possible to assign an effective total orbital angular momentum

TABLE XIV

FREE ION VALUES (cm^{-1}) OF SPIN–ORBIT COUPLING CONSTANTS FOR FIRST-ROW TRANSITION METAL IONS IN VARIOUS LIGAND FIELDS

			Weak octahedral		Strong octahedral		Weak tetrahedral	
Ion	ξ	No. of d electrons	Ground term	λ	Ground term	λ	Ground term	λ
Ti^{3+}	155	1	$^2T_{2g}$	155	$^2T_{2g}$	155	^2E	155
V^{3+}	210	2	$^3T_{1g}$	105	$^3T_{1g}$	105	$^3A_2$	105
V^{2+}	170	3	$^4A_{2g}$	57	$^4A_{2g}$	57	$^4T_1$	57
Cr^{2+}	230	4	^5E_g	58	$^3T_{1g}$	–115	$^5T_2$	58
Mn^{2+}	300	5	$^6A_{1g}$	—	$^2T_{2g}$	–300	$^6A_1$	—
Fe^{2+}	400	6	$^5T_{2g}$	–100	$^1A_{1g}$	—	^5E	–100
Co^{2+}	515	7	$^4T_{1g}$	–172	^2E_g	–515	$^4A_2$	–172
Ni^{2+}	630	8	$^3A_{2g}$	–315	$^3A_{2g}$	–315	$^3T_1$	–315
Cu^{2+}	830	9	^2E_g	–830	^2E_g	–830	$^2T_2$	–830

$L' = 1$ and a value for S depending upon the number of unpaired electrons. Values for J are $L' + S$, $L' + S - 1$, …, $L' - S$ as before. For example,

$^2T_1$ $S = \frac{1}{2}$ $L' = 1$ $J = \frac{3}{2}$ or $\frac{1}{2}$
$^3T_1$ $S = 1$ $L' = 1$ $J = 2, 1,$ or 0
$^4T_1$ $S = 1\frac{1}{2}$ $L' = 1$ $J = 2\frac{1}{2}, 1\frac{1}{2}, \frac{1}{2}$
$^5T_2$ $S = 2$ $L' = 1$ $J = 3, 2, 1$

The g value for T_2 terms is computed using the general equation

$$g = \frac{1 + S(S+1) - L(L+1) + J(J+1)}{2J(J+1)} \tag{49}$$

substituting L' for L, whereas that for T_1 terms will be dependent upon the strength of the crystal field. The appropriate equation is

$$g = -A + (2 + A)\frac{[S(S+1) - L(L+1) + J(J+1)]}{2J(J+1)} \tag{50}$$

For strong fields, $A = 1$, but for weak fields, the maximum value of A is $\frac{3}{2}$. Intermediate fields thus have values of A intermediate between $\frac{3}{2}$

and 1. Ground states with T terms are said to be orbitally degenerate because they are split by spin–orbit coupling.

3. *The Magnetic Properties of Complexes with Ground State Term Configuration A or E*

The effective total orbital angular momentum L' for an A or E term is zero and so there is no splitting of the term by spin–orbit coupling (since $J = L' + S = S$), i.e., the ground state term is not orbitally degenerate. It would thus be expected that the orbital angular momentum would be fully quenched and the magnetic parameters equal to the spin-only value. In fact, small but significant deviations of g and μ_{eff} from the spin-only value are found. The small orbital contribution arises from a mixing of the ground state term with a suitable excited state term by the mechanism of spin–orbit coupling. There are several approaches to this and these will be described in turn.

C. MIXING OF ORBITALS VIA SPIN–ORBIT COUPLING

1. *Rigorous Determination of Which Orbitals May Mix*

Spin–orbit coupling can be studied on a quantitative basis with the aid of quantum mechanical operators. The operator for spin–orbit coupling is

$$\lambda \hat{L} \cdot \hat{S} \tag{51}$$

Since the electron spin of the ground state and the excited state must be the same, the two states will mix via spin–orbit coupling if the integral

$$I = \int \psi_{ground}\, \hat{L} \cdot \psi_{excited}\, dT \tag{52}$$

is not zero. This may be written, using a different notation, as

$$I = \langle \psi_i | \hat{L} | \psi_j \rangle \neq 0 \tag{53}$$

This problem may be readily solved using group theory. The operator $\hat{L}$ $(= \hat{L}_x + \hat{L}_y + \hat{L}_z)$ possesses the symmetry properties of rotations about the three Cartesian axes. If its irreducible representation is $\Gamma_{R_{x,y,z}}$, then Eq. (53) may be rewritten

$$I = \Gamma_{\psi_i} \cdot \Gamma_{R_{x,y,z}} \cdot \Gamma_{\psi_j} \tag{54}$$

This integral (I) is nonzero *only* if the direct product $\Gamma_{\psi_i} \cdot \Gamma_{R_{x,y,z}} \cdot \Gamma_{\psi_j}$ includes Γ_{A_1}. A proof of this is given by Cotton (*147*). This is so, because whenever we have an integral of the product of several functions, the value of this integral will be equal to zero unless the integral is invarient under all operations of the symmetry group to which the molecule belongs. It must then form a basis for the totally symmetric representation of the group.

Let us apply this to the example of the d^1 (D_{4h}) ion (Table XV).

TABLE XV

CHARACTER TABLE FOR POINT GROUP D_{4h}

D_{4h}	E	$2C_4$	C_2	$2C_2'$	$2C_2''$	i	$2S_4$	σ_h	$2\sigma_v$	$2\sigma_d$		
A_{1g}	1	1	1	1	1	1	1	1	1	1	—	x^2+y^2, z^2
A_{2g}	1	1	1	−1	−1	1	1	1	−1	−1	R_z	—
B_{1g}	1	−1	1	1	−1	1	−1	1	1	−1	—	x^2-y^2
B_{2g}	1	−1	1	−1	1	1	−1	1	−1	1	—	xy
E_g	2	0	−2	0	0	2	0	−2	0	0	(R_x, R_y)	(yz, zx)
A_{1u}	1	1	1	1	1	−1	−1	−1	−1	−1	—	—
A_{2u}	1	1	1	−1	−1	−1	−1	−1	1	1	z	—
B_{1u}	1	−1	1	1	−1	−1	1	−1	−1	1	—	—
B_{2u}	1	−1	1	−1	1	−1	1	−1	1	−1	—	—
E_u	2	0	−2	0	0	−2	0	2	0	0	(x, y)	—

Rotations about z belong to the irreducible representation A_{2g}. Rotations about x and y belong to the irreducible representation E_g.

Consider the mixing of the ground state B_{2g} with (*i*) E_g (*ii*) B_{1g}, and (*iii*) A_{1g} when the applied field is parallel to z.

(*i*) $\Gamma_{B_{2g}} \cdot \Gamma_{A_{2g}} \cdot \Gamma_{E_g} = \Gamma_{E_g}$ i.e., does not include $\Gamma_{A_{1g}}$

(*ii*) $\Gamma_{B_{2g}} \cdot \Gamma_{A_{2g}} \cdot \Gamma_{B_{1g}} = \Gamma_{A_{1g}}$

(*iii*) $\Gamma_{B_{2g}} \cdot \Gamma_{A_{2g}} \cdot \Gamma_{A_{1g}} = \Gamma_{B_{1g}}$ i.e., does not include $\Gamma_{A_{1g}}$

When the applied field is along x or y

(*i*) $\Gamma_{B_{2g}} \cdot \Gamma_{E_g} \cdot \Gamma_{E_g} = \Gamma_{A_{1g}} + \Gamma_{A_{2g}} + \Gamma_{B_{1g}} + \Gamma_{B_{2g}}$ includes $\Gamma_{A_{1g}}$

(*ii*) $\Gamma_{B_{2g}} \cdot \Gamma_{E_g} \cdot \Gamma_{B_{1g}} = \Gamma_{E_g}$ i.e., does not include $\Gamma_{A_{1g}}$

(*iii*) $\Gamma_{B_{2g}} \cdot \Gamma_{E_g} \cdot \Gamma_{A_{1g}} = \Gamma_{E_g}$ i.e., does not include $\Gamma_{A_{1g}}$

Therefore $g_{\parallel}$ and $g_{\perp}$ will both deviate from 2 and in both cases will be <2 since the orbital containing the unpaired electron will commute with an empty orbital.

2. *Qualitative "Orbital Rotation" Method*

This method is suitable for the case where there is one unpaired electron in a singly degenerate orbital. This case will not occur in truly

O_h or T_d symmetry, but almost invariably there are distortions which will separate degenerate orbitals. Spin–orbit coupling is possible if this ground state orbital can commute with an excited state orbital about any of the axes x, y, or z. Consider the particular case of a d^1 ion in a tetragonally distorted octahedral environment (D_{4h}) such that the unpaired electron is in the d_{xy} orbital (see Fig. 18).

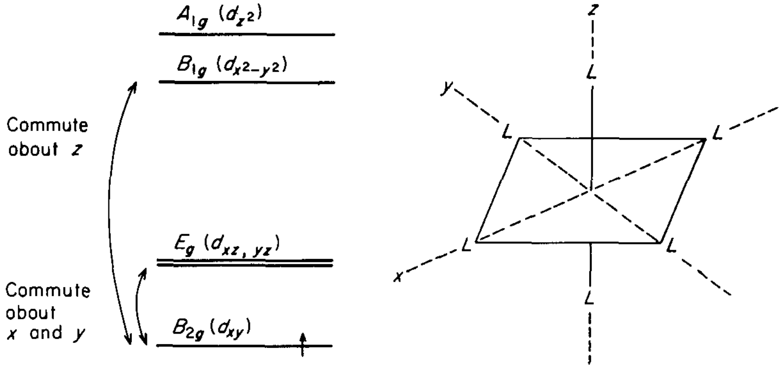

FIG. 18. Molecule of D_{4h} symmetry with compression of axial ligands and the corresponding energy level diagram.

When the applied magnetic field is along z (the "parallel" direction), the electron can weakly commute from d_{xy} to the $d_{x^2-y^2}$ orbital. The effect of the applied field $H_\parallel$ is to make the electron "rotate" about the z axis, giving rise to a small current flowing in a circle. Such an electric current will generate a small opposing magnetic field ΔH, and so to achieve the original field at the electron for the resonance condition, the original field must be increased by ΔH. The original resonance condition

$$h\nu = g_\parallel \beta H \tag{55}$$

now becomes

$$h\nu = g'_\parallel \beta(H + \Delta H) \tag{56}$$

Since the frequency ν is constant, $g'_\parallel$ (along the z axis) must now be less than 2.0023 to maintain the right-hand side of the equation equal to $h\nu$. For applied fields perpendicular to z, ($H_\perp$), i.e., along x or y, the d_{xy} orbital may commute with the d_{xz} and d_{xz} orbitals and so there is an orbital contribution and $g_\perp < 2.0023$.

In the case where the ground state orbital commutes with a filled level, the electron may be treated as a positron and the induced magnetic field is now in the same direction as the original field. The new resonance condition will be

$$h\nu = g' \beta(H - \Delta H) \tag{57}$$

giving rise to g' larger than 2.0023.

D. Molecules with Symmetry Lower than O_h or T_d

Very few molecules have perfect octahedral or tetrahedral symmetry. Jahn–Teller or crystal distortions are frequent, as well as the inherent low symmetry of molecules with mixed ligands. In low symmetry molecules, the energy levels are usually singly degenerate (symmetry A or B) or occasionally doubly degenerate (E). Almost never will they be triply degenerate (T_1 or T_2). It follows that the ground state will not be split by spin–orbit coupling, and that g values will be close to 2. It is found (to a first approximation) that the ground state is allowed (by the operator $\lambda \hat{L} \cdot \hat{S}$) to mix with other states. The deviation of the g value from 2 (Δg) will then be inversely proportional to the energy separation between those states. It is possible to calculate such g values by first-order perturbation theory (*117*) and the results of these calculations are given below.

For the case of a single electron in a nondegenerate d orbital, the g value along any direction x, y, or z is given by the expression

$$g = g_0 \pm \frac{n\lambda}{\Delta} \tag{58}$$

where $g_0 = 2.0023$, λ is the spin–orbit coupling constant, and Δ is the energy separation between the orbital containing the unpaired electron and the orbital with which it may mix by spin–orbit coupling. The $+$ or $-$ sign applies to the case of mixing with a filled or empty orbital, respectively. The coefficient n may be deduced from the magic pentagon below, n being the number on the line linking the orbitals under consideration.

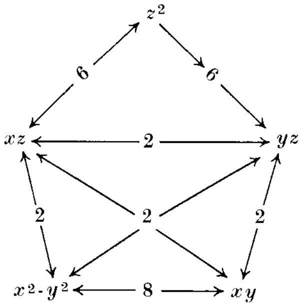

If the orbital containing the unpaired electron is allowed to mix with other orbitals, then further terms of the same format are needed.

Consider the case of a d^9 ion of near-octahedral symmetry, but with a tetragonal distortion such as to elongate the charges along the z axis.

The symmetry is D_{4h} and the unpaired electron is in the $d_{x^2-y^2}$ orbital. It follows that

$$g_{\parallel} = g_0 + \frac{8\lambda}{\Delta E(d_{x^2-y^2} - d_{xy})} \tag{59}$$

$$g_{\perp} = g_0 + \frac{2\lambda}{\Delta E(d_{x^2-y^2} - d_{xz,\, yz})} \tag{60}$$

If, however, there was a compression of charges, then the unpaired electron would be in d_{z^2} and

$$g_{\parallel} = g_0 \tag{61}$$

$$g_{\perp} = g_0 + \frac{6\lambda}{\Delta E(d_{z^2} - d_{xz,\, yz})} \tag{62}$$

These equations are only useful providing λ/Δ is small. A reasonable maximum value is 0.1. Further quadratic correction terms need to be used when λ/Δ is larger. Some of these expressions for g are given in

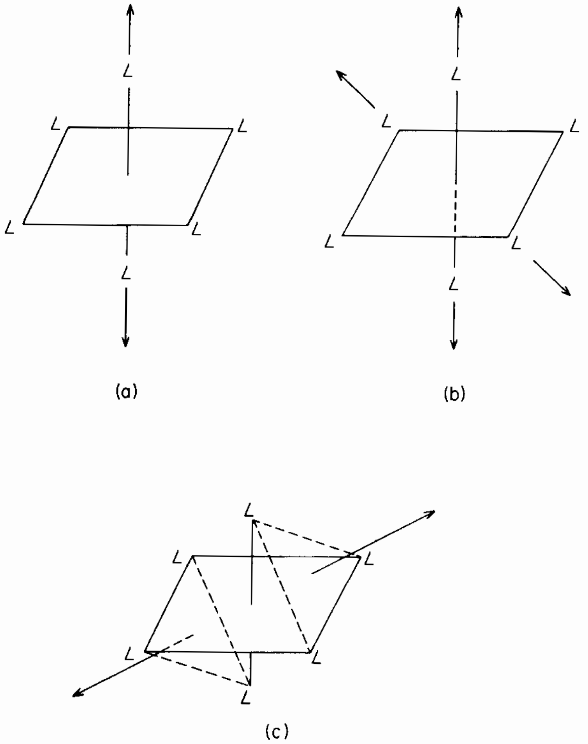

(a)

(b)

(c)

FIG. 19. (a) Tetragonal, (b) rhombic, and (c) trigonal distortions to an octahedron. The arrows indicate the directions of the distortions.

Section V,C which also includes some for the case of two or more unpaired electrons.

In cubic symmetry distortions are usually tetragonal, trigonal, or rhombic. Tetragonal distortions arise from alteration of the charge distribution along the z axis, maintaining a fourfold axis. Trigonal distortions maintain the threefold axis, but rhombic distortions may be envisaged as destroying the fourfold axis of tetragonal symmetry by altering the charge distribution along the x or the y axis. This is illustrated in Fig. 19.

E. ELECTRON DELOCALIZATION

So far, it has been assumed in deriving the g values, etc., that the unpaired electron is localized entirely on the metal atom, i.e., the crystal field approximation. This is not usually the case since the formation of molecular orbitals results in the transfer of some of the unpaired electron density onto the ligands. The effect is to reduce the orbital angular momentum, i.e., further quench the orbital contribution and so make the magnetic parameters have values closer to spin-only, i.e., $g = 2$.

The orbital angular momentum is reduced by a factor k to kL. Similarly the free ion spin–orbit coupling constant λ now becomes λ_L ($=k\lambda$); k is unity for no delocalization and zero for complete delocalization. The spin–orbit coupling operator $\lambda\hat{L}\cdot\hat{S}$ now becomes $k\lambda\cdot k\hat{L}\cdot\hat{S}$ and the equations for g and μ_{eff} are modified by a factor k^2; thus g for a d^3 ion in O_h ligand field

$$2 - \frac{8\lambda}{10Dq} \quad \text{becomes} \quad 2 - \frac{8k^2\lambda}{10Dq} \tag{63}$$

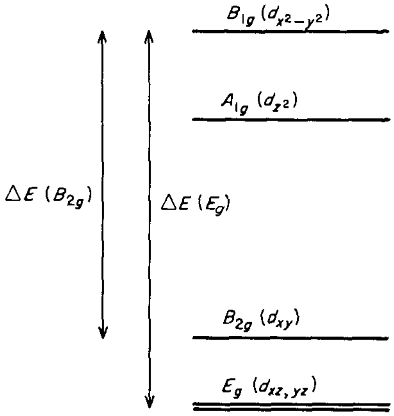

FIG. 20. Order of energy levels for a $d^9(D_{4h})$ complex. The axis notation is the same as in Fig. 18.

For T terms, the effect of delocalization may be found by writing kA instead of A.

It is usually more convenient to use the molecular orbital coefficients rather than k. This is illustrated for a d^9 complex in D_{4h} symmetry. The relevant molecular orbitals (see Fig. 20) are

$$\Psi B_{1g}^{*} = \beta_1 \psi d_{x^2-y^2} - \frac{\sqrt{1-\beta_1{}^2}}{2} (\phi_1 - \phi_2 + \phi_3 - \phi_4) \tag{64}$$

$$\Psi B_{2g}^{*} = \beta_2 \psi d_{xy} - \frac{\sqrt{1-\beta_2{}^2}}{2} (\pi_{1h} - \pi_{2h} + \pi_{3h} - \pi_{4h}) \tag{65}$$

$$\Psi E_g{}^{*} = \epsilon \psi d_{xz,\, yz} - \frac{\sqrt{1-\epsilon^2}}{\sqrt{12}} (\pi_{1v} + \pi_{2v} - \pi_{3v} - \pi_{4v} + \pi_{5hx,\, y} + \pi_{6hx,\, y}) \tag{66}$$

The g values are now

$$g_{\parallel} = 2 + \frac{8\xi\beta_1{}^2\beta_2{}^2}{\Delta E(B_{2g})} \tag{67}$$

$$g_{\perp} = 2 + \frac{2\xi\beta_1{}^2\epsilon^2}{\Delta E(E_g)} \tag{68}$$

F. VARIATIONS IN THE VALUE OF THE FREE-ION SPIN–ORBIT COUPLING CONSTANT λ

Since λ is related to ξ by

$$\lambda = \pm \frac{\xi}{2S} \tag{69}$$

and ξ itself is proportional to the effective nuclear charge and inversely proportional to the cube of the distance of the electron from the nucleus, then λ will increase (*i*) as the valency of the ion increases, (*ii*) as the atomic number increases across each transition metal series, and (*iii*) very greatly down a group.

It has already been said that λ decreases with delocalization of the electrons, but there are some less-well understood effects which influence λ and consequently g values. Marshall and Stuart (*487*) have proposed that λ could be reduced from the free ion value as a result of shielding of the nucleus by the ligand bonding electrons. In order to explain the presence of some g values greater than 2.0023 for some d^5 high-spin complexes, Fidone and Stevens (*213*) have found it necessary to promote electrons from inner filled ligand levels to the half-filled levels containing the unpaired electrons. In other words, there is a mixing in of excited states, which produces a positive contribution to g, but of course is not specific to the d^5 case [see, e.g., Watanabe (*694*)]. Thus we might expect g shifts to arise from the mixing via spin–orbit coupling of ligand orbitals involved in molecular orbitals containing unpaired electrons, with filled or empty ligand orbitals to produce positive and negative g shifts ($g \pm \Delta g$), respectively. This will be dependent on the degree of covalency

TABLE XVI

FREE ION VALUES (cm^{-1}) OF SPIN–ORBIT COUPLING CONSTANTS ξ[a]

	Valency						
Ion	0	1	2	3	4	5	6
Sc	67	53	80	—	—	—	—
Ti	111	88	121	155	—	—	—
V	158	136	170	210	248	—	—
Cr	223	222	230	273	327	380	—
Mn	239	254	300	352	402	475	540
Fe	391	356	400	460	514	590	665
Co	517	456	515	580	650	715	790
Ni	603[b]	603	630	715	790	865	950
Cu	817[c]	828[b]	830	890	960	1030	1130
Y[d]	212	212	290	—	—	—	—
Zr	335	339	403	500	—	—	—
Nb	475	490	554	670	748	—	—
Mo	552	672	670	817	887	900	—
Tc	647	656	950	1200	1300	1500	1700
Ru	878	887	990	1250	1400	1500	1700
Rh	968	1212	1235	1360	1700	1850	2100
Pd	1412[b]	1420	1460	1640	1830	2000	2230
Ag	1790[c]	1830[b]	1844	1930	2100	2300	2500
La[d]	798	—	—	—	—	—	—
Hf	1307	1336	—	—	—	—	—
Ta	1657	1776	—	1400	—	—	—
W	2089	2561	1500	1800	2300	2700	—
Re	2285	—	2100	2500	3300	3700	4200
Os	—	—	—	3000	4000	4500	5000
Ir	—	—	—	2000	5000	5500	6000
Pt	4052[b]	4910	—	—	—	—	—
Au	3368[c]	5091[b]	5000	2000	—	—	—

[a] From ref. (*191*).

[b] d^9s^1.

[c] d^9s^2.

[d] Values for the second and third transition series must be treated as approximate.

of the complex (i.e., the amount of unpaired electron density on the ligands), Δg decreasing with increasing covalency.

Table XVI gives the free ion spin–orbit coupling constant for various transition metal ions.

V. The Case of Two or More Unpaired Electrons: Fine Structure

A. The Two Electrons on Different Ions

In magnetically dilute compounds it is usually assumed that there is negligible interaction between the paramagnetic ions. Occasionally, however, radicals are trapped in pairs due to one of the following reasons: (*i*) too high a concentration of radicals are present, (*ii*) there is a chemical preference for the radicals to be associated, i.e., paramagnetic dimers, as in hydrated cupric acetate; (*iii*) radicals are formed in pairs within a lattice, e.g., by radiation damage, and consequently migration is hindered.

The first problem (*i*) can usually be avoided by using a lower concentration of radical ions, but mechanisms (*ii*) and (*iii*) are sometimes unavoidable. Also, since useful information may often be obtained by a study of radicals trapped in pairs in crystals or in powders, the nature of the interaction between them will be briefly considered here.

Since nearest neighbor metal ions in a crystal lattice are usually separated by at least a few Ångstroms (very seldom less than 5 Å), the interaction between an electron on each metal ion is represented quite well to a first-order approximation by a simple classical dipolar interaction between electrons located at a point on each metal atom. The splitting ΔH produced by this spin–spin interaction is given by

$$\Delta H = \frac{3\beta_e}{r^3}(3\cos^2\theta - 1) \tag{70}$$

where r is the mean separation of the two electrons (taken as the atom–atom bond distance) and θ is the angle between the dipole–dipole axis and the external magnetic field.

This approach breaks down completely if there is appreciable delocalization of the unpaired electron onto the ligands, since r would take a wide range of values, producing a splitting spread over a wide range, and yielding very broad lines.

When there is an interaction between an unpaired electron and a magnetic nucleus, hyperfine structure may be detected. Different spectra are obtained when an isolated pair of ions, each with $S = \frac{1}{2}$ and $I = 1$ is allowed to interact under different conditions. A single ion would give

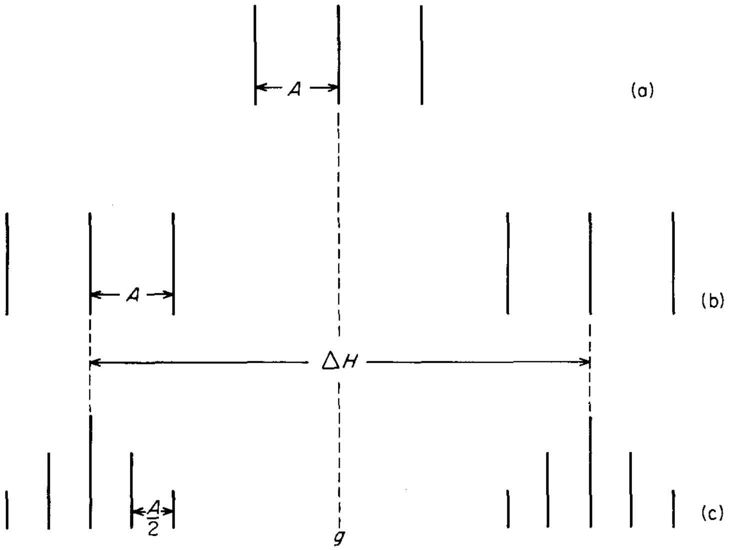

FIG. 21. (a) Spectrum of isolated ions with $S = \frac{1}{2}$ and $I = 1$. (b) Slow exchange between a pair of such ions, while (c) shows the spectrum where there is fast exchange.

a 3-line spectrum (Fig. 21a) with hyperfine splitting A. If another identical molecule is allowed to approach it so that there is appreciable dipolar interaction between the electron spins, then either of the following cases may arise.

(*i*) If the rate of exchange between the electrons is slow compared with the electron resonance frequency (10^{-10} sec), then during resonance each electron experiences interaction with the other electron and its own magnetic nucleus to give the spectrum in Fig. 21b.

(*ii*) If the rate of exchange is fast compared to the resonance frequency, then during resonance each electron spends half of its time on each magnetic nucleus and hence interacts with two equivalent nuclei as well as with the other electron. Slichter (*628*) has shown that since each electron spends only half as long on each nucleus as in the previous example a hyperfine splitting of $A/2$ is obtained (Fig. 21c). The observation of pairwise trapping may be useful in experiments on rates of spin–spin exchange and may give information on the separation of ions in a lattice.

B. IONS WITH MORE THAN ONE UNPAIRED ELECTRON

In ions with more than one unpaired electron there are interactions between the individual electron magnetic moments and the magnetic fields generated by the other electron(s). In this case, however, the ground state levels may not be degenerate in the absence of a magnetic field, i.e., spin–orbit coupling between various terms in the ground state may produce a zero-field splitting. When such a splitting is present the levels will no longer be equally spaced in the external magnetic field and the various magnetic resonance transitions will no longer coincide. A series of lines is thus obtained, which is commonly called the fine structure (Fig. 22).

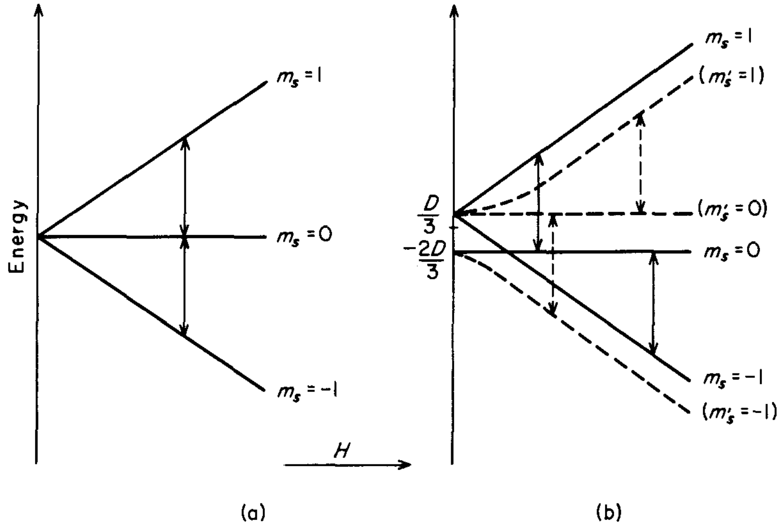

FIG. 22. $S = 1$ ion (a) with no zero-field splitting and (b) with zero-field splitting. The solid lines are the energy levels and transitions when the applied field lies parallel to the z axis. The dotted lines pertain to a field perpendicular to the z axis.

The variation of the energy levels with the magnetic field does not follow a simple relationship except when the magnetic field is parallel or perpendicular to the principal axis of the splitting, which is conventionally the z axis. In the following cases the field has been taken as parallel to the z axis, and $g = g_{\parallel}$. In many cases, if there is a metal ion with $I > 0$, then hyperfine structure may be detected.

There are two important theorems which determine whether a spectrum is likely to be seen for various numbers of electrons in an ion.

(*i*) *Jahn–Teller theorem* (*364*, *365*). This theorem states that in any orbitally degenerate ground state, there will be a distortion to remove the degeneracy *except* in linear molecules and in systems having Kramer's doublets.

(*ii*) *Kramer's theorem* (*414*). Any system containing an odd number of electrons will show at least twofold degeneracy in the absence of a magnetic field.

It follows from (*ii*) that in ions having an even number of electrons, the splitting of energy levels will be complete and all ground state levels will be nondegenerate. Since in most cases the separation between levels is very large ($>1\ \mathrm{cm}^{-1}$), the observation of paramagnetic resonance will not be expected. In paramagnetic ions having an odd number of electrons, levels showing Kramer's degeneracy will be present. Paramagnetic resonance is then expected, since in an external magnetic field, the Kramer's doublets are split and transitions between their components are induced (*409*).

In this description, the Russell–Saunders coupling scheme is assumed, whereby spin–orbit coupling acts as a perturbation to crystal field effects. It is necessary to use a new notation to describe the splitting of crystal field levels by spin–orbit coupling. This involves double group notation. Some points to note in connection with this are as follows (*659*).

In a cubic crystal field, the various J levels are split as follows:

$$\begin{aligned}
J &= \tfrac{1}{2} \rightarrow \Gamma_6 \\
J &= \tfrac{3}{2} \rightarrow \Gamma_8 \\
J &= \tfrac{5}{2} \rightarrow \Gamma_7 + \Gamma_8 \\
J &= \tfrac{7}{2} \rightarrow \Gamma_6 + \Gamma_7 + \Gamma_8 \\
J &= \tfrac{9}{2} \rightarrow \Gamma_6 + 2\Gamma_8
\end{aligned}$$

The splitting of these is proportional to the magnitude of the spin–orbit coupling. The degeneracy of these states is given below:

Γ_1 and Γ_2 are singly degenerate states
Γ_3 is a twofold degenerate state
Γ_4 and Γ_5 are threefold degenerate states
Γ_6 and Γ_7 are twofold degenerate states
Γ_8 is a fourfold degenerate state.

The literature on spin–orbit coupling is in a very confused state. The effect is often incorrectly ignored for first-row transition metal ions. For most complexes an inorganic chemist meets, however, the symmetry is low, and this, in general, greatly helps the observation of ESR spectra since the complications mostly occur in cubic crystal fields.

C. THE ESR SPECTRA OF METAL IONS IN OCTAHEDRAL AND TETRAGONAL CRYSTAL FIELDS

1. $d^1, S = \frac{1}{2}$

In octahedral crystal fields, the ground state is ${}^2T_2$ with the ${}^2E$ excited state much higher in energy. Spin–orbit coupling splits the ground state into a lower quartet Γ_8 and an upper doublet Γ_7. The Γ_8 state is not split by a magnetic field to first-order and no ESR spectrum is seen. A tetragonal distortion (D_{4h}) will split the ${}^2T_2$ ground state into ${}^2B_2$ and ${}^2E$, whereas a trigonal distortion will split it into ${}^2A_1$ and ${}^2E$. Spin–orbit coupling will split these states into Kramer's doublets. ESR spectra will only be seen if the distortion is large or if the temperature is considerably reduced (to liquid helium). The spin–lattice relaxation time will be short if the distortion is small because there are excited states (${}^2E$ in D_{4h}) close by (perhaps 100 cm^{-1}). When spectra are observed, the transition is between the Kramer's doublet levels $m_s \pm \frac{1}{2}$ which are split by the magnetic field (see Fig. 23a). There is no Jahn–Teller

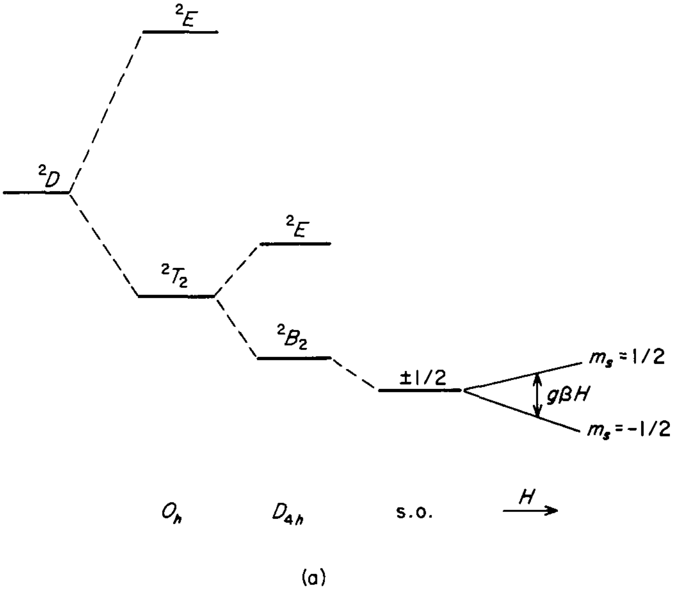

FIG. 23. Lowest energy levels for d^n ions in O_h and D_{4h} symmetry. The effect of spin–orbit coupling (s.o.) and an applied magnetic field H is indicated, along with the ESR transition $\leftrightarrow$. (a) d^1; (b) d^2, the m_s ● 1 level is a Kramer's doublet; (c) d^3, the $m_s \pm \frac{3}{2}$ and $\pm\frac{1}{2}$ levels are Kramer's doublets; (d) d^4, the $m_s \pm 2$ and ± 1 levels are Kramer's doublets; and (e) d^5, the m_s $\pm\frac{5}{2}$, $\pm\frac{3}{2}$ and $\pm\frac{1}{2}$ levels are Kramer's doublets.

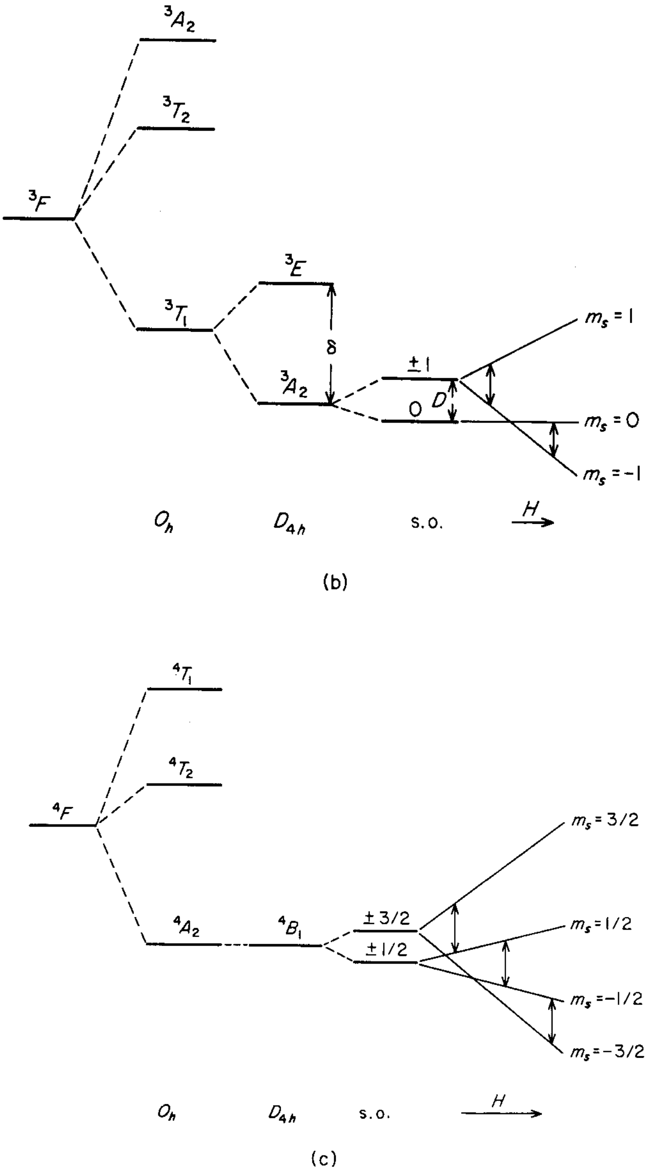

FIG. 23 (b) and (c): Complete caption on page 197.

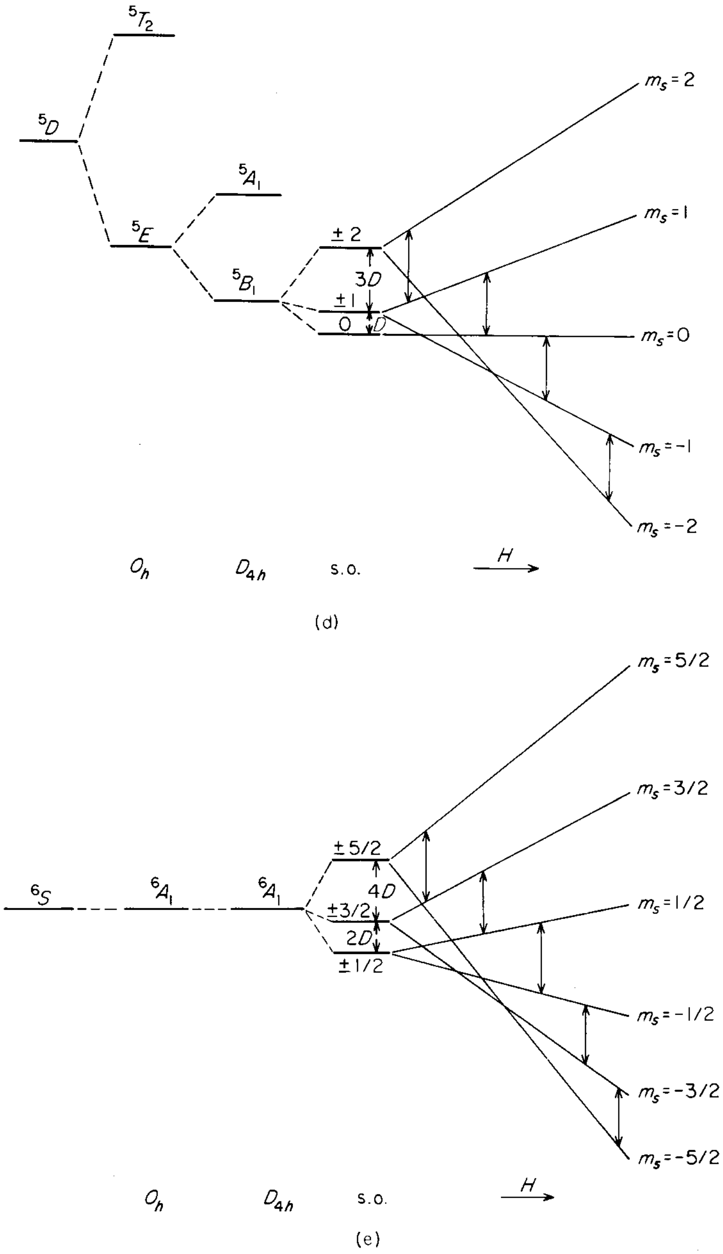

FIG. 23 (d) and (e): Complete caption on page 197.

distortion since there is Kramer's degeneracy. The g values are given as follows (*504*) for D_{4h} symmetry and $^2B_{2g}$ ground state.

$$g_{\parallel} = \frac{3(2\delta + \lambda)}{[(2\delta + \lambda)^2 + 8\lambda^2]^{1/2}} - 1 \tag{71}$$

$$g_{\perp} = \frac{(2\delta - 3\lambda)}{[(2\delta + \lambda)^2 + 8\lambda^2]^{1/2}} + 1 \tag{72}$$

where $\delta = \Delta E(e_g - b_{2g})$.

Spin–orbit mixing of e_g orbitals into the ground state produces the following corrections which must be added to Eqs. (71) and (72).

$$\Delta g_{\parallel} = -\frac{4\lambda}{\Delta}\left\{1 + \frac{2\delta + 3\lambda}{[(2\delta + \lambda)^2 + 8\lambda^2]^{1/2}}\right\} \tag{73}$$

$$\Delta g_{\perp} = \frac{2\sqrt{2}\lambda}{\Delta}\left\{1 + \frac{3\lambda + 2\delta}{[(2\delta + \lambda)^2 + 8\lambda^2]^{1/2}}\right\} \tag{74}$$

where $\Delta = \Delta E(e_g - t_{2g})$.

In D_{3d} symmetry and $^2A_{2g}$ ground state, $g_{\parallel}$ and $g_{\perp}$ are identical to Eqs. (71) and (72), but where $\delta = \Delta E(e_g - a_{1g})$. The corrections for spin–orbit mixing of the e_g orbitals into the ground state are as follows:

$$\Delta g_{\parallel} = \frac{2\lambda}{\Delta}\left\{1 - \frac{2\delta - 3\lambda}{[(2\delta + \lambda)^2 + 8\lambda^2]^{1/2}}\right\} \tag{75}$$

$$\Delta g_{\perp} = \frac{-2\lambda}{\Delta}\left\{1 + \frac{2\delta + 3\lambda}{[(2\delta + \lambda)^2 + 8\lambda^2]^{1/2}}\right\} \tag{76}$$

2. $d^2, S = 1$

A Jahn–Teller distortion will split the ground state ($^3T_1, O_h$) into $^3A_2$ (lowest) and ^3E if the distortion is trigonal. Spin–orbit coupling on $^3A_2$ produces a nondegenerate lower level $m_s = 0$ and a higher (~10 cm^{-1}) doubly degenerate level $m_s = \pm 1$, all the remaining levels (^2E) being several hundred reciprocal centimeters higher. The large zero-field splitting D prevents an ESR signal from being readily obtainable. This is shown in Fig. 23b where the energies of the levels are given

$$E_{\pm 1} = \tfrac{1}{2}D \pm g_{\parallel}\beta_e H \tag{77}$$

$$E_0 = -\tfrac{2}{3}D \tag{78}$$

If the symmetry is lower than D_{3h} or D_{4h}, the energy levels are further split at zero field such that their energeis are

$$E_{\pm 1} = \tfrac{1}{3}D \pm (g_{\parallel}{}^2\beta_e{}^2H^2 + E^2)^{1/2} \tag{79}$$

$$E_0 = -\tfrac{2}{3}D \tag{80}$$

For a ${}^3A_{2g}$ ground state (*12*)

$$g_{\parallel} \sim 2 - \frac{63\lambda^2}{8\Delta^2} \tag{81}$$

$$g_{\perp} \sim 2 - \frac{9\lambda}{2\Delta} \tag{82}$$

3. $d^3, S = \frac{3}{2}$

In an octahedral crystal field, the ground state is ${}^4A_2$ and the fourfold degeneracy is not removed by spin–orbit coupling since the state so formed is Γ_8. The Jahn–Teller theorem will not be applicable. With m_s values $\pm\frac{3}{2}$, $\pm\frac{1}{2}$, however, Kramer's theorem is applicable and so an ESR spectrum is readily obtainable. When the symmetry is reduced from O_h, by axial distortion, the energy levels and transitions are represented in Fig. 23c. Each level has energies:

$$E_{+3/2} = \tfrac{3}{2}g\beta_e H + D \tag{83}$$

$$E_{+1/2} = \tfrac{1}{2}g\beta_e H - D \tag{84}$$

$$E_{-1/2} = -\tfrac{1}{2}g\beta_e H - D \tag{85}$$

$$E_{-3/2} = -\tfrac{3}{2}g\beta_e H + D \tag{86}$$

If the distortion is large, the $+\frac{1}{2} \leftrightarrow +\frac{3}{2}$ or $-\frac{1}{2} \leftrightarrow -\frac{3}{2}$ transitions may not be visible, but the $+\frac{1}{2} \leftrightarrow -\frac{1}{2}$ transition is always observable. Also, since the ground state in O_h symmetry is spherically symmetrical, the spectrum will be isotropic and $g = 2 - 72\lambda/5\Delta$, where $\Delta = \Delta E(t_{2g} - e_g)$.

4. $d^4, S = 2$

In an octahedral crystal field, the ground state is ${}^5E$ and spin–orbit coupling splits this state into Γ_1, Γ_2, Γ_3, Γ_4, and Γ_5. These are very close in energy, and some doubly degenerate states will be populated; this will allow the Jahn–Teller theorem to be applicable. Axial fields split this state into ${}^5A_1$ and ${}^5B_1$. In zero magnetic field, the $m_s = 0$ level lies lowest, and since it is not a Kramer's doublet and higher spin–orbit levels lie too high, ESR is not easily seen. The energy levels are given in Fig. 23d, each level having energies as follows:

$$E_{+2} = 2g\beta_e H + 2D \tag{87}$$

$$E_{+1} = g\beta_e H - D \tag{88}$$

$$E_0 = -2D \tag{89}$$

$$E_{-1} = -g\beta_e H - D \tag{90}$$

$$E_{-2} = -2g\beta_e H + 2D \tag{91}$$

For a $^5B_{1g}$ ground state (D_{4h})

$$g_{\parallel} = 2 - \frac{8\lambda}{\Delta E(d_{x^2-y^2} - d_{xy})} \tag{92}$$

$$g_{\perp} = 2 - \frac{2\lambda}{\Delta E(d_{x^2-y^2} - d_{xz,\,yz})} \tag{93}$$

For a $^5A_{1g}$ ground state

$$g_{\parallel} = 2 \tag{94}$$

$$g_{\perp} = 2 - \frac{6\lambda}{\Delta E(d_{z^2} - d_{xz,\,yz})} \tag{95}$$

In D_{3d} symmetry,

$$g = 2 - \frac{4\lambda}{\Delta} \text{ (isotropic)} \tag{96}$$

In spin-paired d^4 ions, the ground state is $^3T_1$ and this behaves as a $S = 1$ ion which means that resonance is also not readily seen. Spin–orbit coupling splits this state into Γ_1, Γ_4, Γ_5, Γ_3, with Γ_1 lowest. Since this is singly degenerate, the Jahn–Teller theorem is inapplicable.

5. $d^5, S = \frac{5}{2}$

The ground state of both octahedral and tetrahedral d^5 ions (spin free) is $^6A_1$. Six degenerate levels (Γ_6 and Γ_8)are present, and since the Γ_8 is 4-degenerate then it may be split by a Jahn–Teller distortion. Since there is no other sextuplet term of the d^5 configuration, the ground state cannot mix with any other by spin–orbit coupling and so there is no zero-field splitting. The energy levels are at $\pm\frac{5}{2}$, $\pm\frac{3}{2}$, $\pm\frac{1}{2}(g\beta H)$ and a single isotropic resonance at $g = 2$ is easily seen. If there is an axial distortion, there is a zero-field splitting and three Kramer's doublets appear. The energy levels are shown in Fig. 23e and five transitions are observed. The energies of the levels are as follows:

$$E_{\pm 5/2} = \pm\tfrac{5}{2}g\beta_e H + \frac{10D}{3} \tag{97}$$

$$E_{\pm 3/2} = \pm\tfrac{3}{2}g\beta_e H - \frac{2D}{3} \tag{98}$$

$$E_{\pm 1/2} = \pm\tfrac{1}{2}g\beta_e H - \frac{8D}{3} \tag{99}$$

If there is interaction with a nucleus with spin $I > 0$, then there will be hyperfine structure on each fine structure line. This is seen, e.g., in certain Mn^{2+} salts (*92*). In the absence of a zero-field distortion the fine structure lines would coalesce and all that would be seen would be the six hyperfine lines from ^{55}Mn. For spin-paired d^5 ions, $S = \frac{1}{2}$ and ESR spectra are readily observed if distortions are present, so that mixing with excited states is minimal. The g values are the same as for the d^1 case, except that δ is negative.

6. $d^6, S = 2$

In an octahedral crystal field, the ground state is $^5T_2$. Spin–orbit coupling splits this state, with Γ_5 lowest, hence allowing the Jahn–Teller theorem to be applicable. This splits the state into $^5B_2$ and ^5E. Spin–orbit coupling splits these levels and the $m_s = 0$ level lies lowest in zero field. Since the lowest level is not a Kramer's doublet, no ESR spectrum is expected. The levels split as for the d^4 ion. $g_{\parallel}$ varies from 4 to 10.

7. $d^7, S = \frac{3}{2}$

In an octahedral crystal field, the ground state is $^4T_1$ and spin–orbit coupling splits this into Γ_6, Γ_7, and $2\Gamma_8$, with Γ_6 lowest. Since a Kramer's doublet is lowest, no Jahn–Teller distortions are possible. Axial fields split the ground state into A_2 and E. Since there are Kramer's doublets in either level, an ESR spectrum is obtainable, but spin–orbit coupling may mix these states and cause short spin–lattice relaxation times. In practice, the ground state is $^4A_2$ and the system behaves in a similar fashion to the $d^3(O_h)$ case. Distortions are unlikely and spectra readily seen. The g values vary in a complex manner (*14*).

In spin-paired d^7 ions, $S = \frac{1}{2}$, and provided that the symmetry is low, spectra are readily seen.

8. $d^8, S = 1$

In an octahedral crystal field, the ground state is $^3A_2$ and since spin–orbit coupling on this state produces Γ_5, which is threefold degenerate, then the Jahn–Teller effect is possible. The symmetrical ground state is reminiscent of the d^3 ion and spectra are usually readily observed. Spin–orbit coupling does not split the $m_s = 0$ and ±1 levels and the energies of the levels is similar to that shown in Fig. 22a. Like d^3 ions, the symmetrical ground state yields isotropic g and A values. When the symmetry is reduced, the zero-field splitting becomes large and since the lowest level is not a Kramer's doublet, an ESR spectrum is not easily observed. $g = 2 + 4\lambda/\Delta$ and is isotropic.

9. $d^9, S = \frac{1}{2}$

In octahedral crystal fields the ground state is ${}^2E$ which produces Γ_8 by spin–orbit coupling. Since this is 4-degenerate, then a Jahn–Teller distortion is possible and is often very large. In lower symmetries, the ground state is a Kramer's doublet and spectra are readily observed at room temperature. In octahedral complexes, the g values are the same as for the d^4 ion, but with the signs changed. For tetrahedral complexes, the g values are the same as the d^1 octahedral case, but with δ and Δ both negative.

D. OBSERVING THE SPECTRUM

In the high-field limit, i.e., when $g\beta H$ is large compared to any zero-field splitting, the transitions are of the type $m_s \leftrightarrow (m_s + 1)$. Thus a spectrum is obtained which arises from transitions between $2S + 1$ levels whose values of m_s differ by unit; the energies of the levels being given approximately by the relationship

$$E = g\beta H m_s + \tfrac{1}{2}D(3\cos^2\theta - 1)\,[m_s{}^2 - \tfrac{1}{3}S(S + 1)] \tag{100}$$

where θ is the angle between H and the z axis. The intensity of the various lines varies according to the rule that for the transition $m_s \leftrightarrow (m_s + 1)$ the intensity is proportional to $(S + m_s + 1)(S - m_s)$. Thus, for example, in the $S = \frac{3}{2}$ case, three lines are observed with relative intensities 3:4:3.

Measurement of an ESR spectrum from an ion which has more than one electron is often fraught with difficulties. The spectrum may exhibit only a part of the expected fine structure and hyperfine structure may not be resolved. From the spectra obtained, however, the parameters D and E, and in the case of $S = \frac{5}{2}$, a further parameter a may be calculated. D is a measure of the zero-field splitting and is proportional to the square of the spin–orbit coupling constant ξ. It is inversely proportional to δ, the separation between the ground state and the next higher state with which it can mix by spin–orbit coupling. Thus for any one ion, the greater the distortion (tetragonal) the larger will δ become and the smaller D. Hence D is a measure of the distortion of a complex ion. This is illustrated for a d^2 ion in Fig. 23b. The parameter E is zero if the ion is axially symmetric and hence the magnitude of E is a measure of further asymmetric distortion. Carrington (*122*), Figgis (*214*), König (*409*), and McGarvey (*504*) have reviewed this subject in more detail.

VI. Linewidths and Relaxation Mechanisms

This section deals with some of the main factors which contribute to the width of ESR spectral lines, an understanding of which is important in achieving maximum resolution of spectra and hence the maximum amount of information.

In general, Heisenberg's uncertainty principle relates line width with the lifetime of the excited state by the equation

$$\Delta t \cdot \Delta E \approx \frac{h}{2\pi} \tag{101}$$

where t is the lifetime of the excited state and ΔE is the effective width of the energy band involved.

A. SPIN–LATTICE RELAXATION

This is a mechanism whereby magnetic energy absorbed by the paramagnetic ion is transferred to vibrational degrees of freedom of the lattice. It is to the fluctuating magnetic field due to lattice motions that the spin magnetic moment of the electron must couple, since this gives rise to magnetic energy, and hence allows magnetic energy to be emitted. Because of this easy loss of energy, the length of time which a particular spin spends in the upper state Δt is reduced and hence the state becomes less well defined and the resonance line broadened. Alternatively, this conclusion may be deduced from Heisenberg's uncertainty principle, since Δt is small, it follows that ΔE will be large, and the absorption will be observed over a range of energies, i.e., over a range of magnetic field.

Spin–lattice relaxation predicts a line width of $\sim(2\pi T_1)^{-1}$, where T_1 is the relaxation time for the transfer of energy from the spin system to the lattice. T_1 has been found to be sensitive in particular to:

(*a*) Temperature. A decrease in temperature decreases the violence of the interatomic motion and leads to a longer relaxation time and correspondingly narrower lines.

(*b*) The presence of nearby electronic excited states. Where these are close ($\sim$100 cm^{-1}), the relaxation time will be very short and it will be necessary to reduce the temperature considerably (even to 4.2°K) in order to reduce the width of the lines.

Theoretical analyses of spin–lattice relaxation have been performed by Kubo and Tomita (*420*), Redfield (*579*), and Kivelson (*390*). This mechanism is applicable to solids and liquids. The line shape for this type of relaxation is Lorentzian.

B. SPIN–SPIN RELAXATION

1. Dipolar Interactions: Concentration Broadening

Because the local magnetic field produced by an electron at a distance r(cm) is given to a first approximation by

$$H = \frac{3\beta_e}{r^3} \text{ (gauss)} \tag{102}$$

then even at a distance of 4 Å, the local field is about 600 gauss. This large local field will affect neighboring electron spins, alter the field there, and cause a precessing of magnetic dipoles. This interaction causes the lifetime of the excited state to be reduced and hence broadens the line. Reduction of this line width is easily achieved by diluting the compound in a diamagnetic host lattice. The dilution factor should be in excess of 100. The line shape is gaussian.

2. Exchange Coupling

This is important only in undiluted crystals where the paramagnetic sites are so close together that the orbitals of the unpaired electrons overlap. If the exchange frequency (or magnitude of the exchange interaction or energy) is very small (i.e., $\ll$ hyperfine splitting measured in frequency units), then the hyperfine splitting may be well resolved, but as the exchange frequency is increased the hyperfine lines are broadened (a process known as *exchange broadening*) and start to shift toward the center of the spectrum. When the exchange frequency is of the same order of magnitude as the hyperfine splitting, a single broad line is obtained, which narrows as the exchange interaction is further increased. This is called *exchange narrowing*. This exchange narrowing is common in solid free radicals, e.g., diphenylpicrylhydrazyl, which often exhibits single narrow lines.

C. OTHER EFFECTS

1. Anisotropic Interactions

In viscous liquids or if the paramagnetic molecules are very large, there is not free motion of the molecules and an isotropic spectrum is not seen. Instead, there is residual anisotropy and the effect is seen as broadening or an asymmetry in the spectrum. In the extreme, a pseudo-anisotropic spectrum is seen. Improved resolution may be obtained by increasing the temperature to reduce the viscosity, and such narrowing is called motional narrowing. The occurrence of both motional narrowing and exchange broadening has been used by Pake and Tuttle (*552*) to explain the appearance of an optimum viscosity (or temperature) for the observation of narrow hyperfine lines (*316*). An initial appearance of hyperfine structure with temperature increase can be understood in terms of the theory of motional narrowing since the correlation time for molecular reorientation

$$\tau_c = 4\pi\eta a^3/(3kT) \tag{103}$$

decreases with increase in temperature. The motional narrowing theory predicts that for decreasing τ_c, a monotonic decrease in the width of each hyperfine component should also occur. That this does not occur arises from the fact that exchange interaction does occur even in dilute solutions since the paramagnetic ions will occasionally come into contact with one another as a consequence of unrestricted motion. As the temperature is increased (and viscosity decreased) the frequency of collisions between paramagnetic ions and hence exchange interactions, will be increased. This leads to a broadening of the hyperfine lines as the exchange interaction becomes more important than the motional narrowing and may even lead to a complete smearing out of the hyperfine structure at higher temperatures.

2. Chemical Effects

Another source of line broadening in solutions arises from the fluctuation in spectra parameters due to chemical reactions, e.g., solvent–ligand exchange, ion-pair formation, or complex formation.

If the effect of solvent–ligand exchange is to produce a strong perturbation of the electron-spin system, effecting considerable mixing of the spin states (e.g., exchange involving intermediates of a different structure viz. 5- or 7-coordinated species for an octahedral arrangement), then the spin state lifetimes are limited to the chemical lifetime of the complex. Linewidths of various hyperfine transitions would be identical. Alternatively, chemical exchange in the absence of a large ligand field change would act as a weak perturbation of the electron-spin system and would be similar to solvent fluctuations, i.e., fluctuations in the solvent shell surrounding the complex which would cause transient distortions of the complex. These introduce a symmetry in the spin–orbit coupling which mixes spin states.

Hayes and Myers (*323*) have shown that the difference between the behavior of $MnSO_4$ and $MnCl_2$ in aqueous solution at room temperature may be explained by the difference in size of the equilibrium constants for complex formation of Cl^- and SO_4^{2-} with Mn^{2+}, i.e., Mn^{2+} is not appreciably complexed by Cl^- but some complex with SO_4^{2-} is found. The formation of both inner sphere and outer sphere solvation must be considered, e.g., in $NiCl_2$ in H_2O or NH_3 (*556*), the linewidth is determined by the rate of formation of the second coordination sphere complex, whereas in $MnCl_2/H_2O$ (*323*) it is the rate of formation of the inner sphere complex which affects the line width. In $MnSO_4/H_2O$ the linewidth depends on both rates.

The formation of ion pairs may also be important in determining line widths. The theory concerning this mechanism has been conveniently presented by Fraenkel (*218*) and will not be enlarged on here.

3. Unresolved Structure

This includes any broad lines obtained by the presence of unresolved fine or hyperfine structure due to the separation between the lines being less than the component line widths. This is a very common source of broad lines in transition metal complexes where component linewidths of the order of a few gauss are common.

4. Spin-Rotational Effects

Another effect is the modulation of the rotational angular momentum of the ion and the interaction of this momentum with the spin angular momentum by means of its spin-rotational coupling. This mechanism (*43*) may be used to explain the absence of ^{14}N hyperfine splitting from vanadyl prophyrin in solution, whereas it is observed in the glassy state where spin-rotational relaxation will not be present.

VII. Experimental Technique

A. Preparation of Samples

Paramagnetic compounds are usually studies by ESR either in solution or in the solid state. Gas phase ESR will not be considered here. In a solid state study the radicals may be aligned in specific directions relative to one another as is the case in a single crystal, or randomly oriented in a dilute powder or frozen solution (glass).

A concentration of the order of 0.001 *M* is usual in ESR experiments since this allows optimum resolution and signal strength by keeping to a minimum most line-broadening mechanisms while at the same time working well within the sensitivity range of the instrument. Such solutions are referred to as magnetically dilute, i.e., the paramagnetic ions separated from each other by a large number of diamagnetic molecules thus preventing any magnetic exchange between paramagnetic molecules.

1. Fluid Solution

A paramagnetic compound in fluid solution usually gives an isotropic ESR spectrum, i.e., average *g* and *A* values, the exception being some large molecules of biochemical origin in viscous media where anisotropic spectra are obtained due to the tumbling frequency being less than the frequency at which resonance occurs.

With stable paramagnetic compounds, there is usually no difficulty in sample preparation. It is sufficient to make up a solution of approximate concentration, although removal of oxygen from the solvent sometimes helps to produce narrower lines. Often, however, it is desirable to study radicals which are unstable and which can only be generated in solution with short lifetimes. In these cases it is usual to generate the radicals *in situ* in the ESR cavity by one of the following methods.

a. Flow Method. If the radical to be studied is an intermediate of short lifetime it is necessary to use a "rapid-flow" arrangement to obtain the ESR spectrum. Here, the reactants are passed along separate tubes and mixed in, or just prior to flow into, the resonance cavity. By adjusting the rates of flow and the time between mixing and the sample passing through the cavity the lifetimes of any paramagnetic species produced during the reaction may be obtained from the spectrum recorded. The method is particularly suitable for studying the mechanisms which proceed via paramagnetic intermediates.

b. Irradiation in situ. When a solution of a diamagnetic complex ion placed in the resonance cavity is irradiated with light (usually UV or higher energy) it often happens that either an electron is removed from the complex ion or an electron is removed from the solvent and trapped on the complex. The net effect is to produce the oxidized or reduced species which is likely to be paramagnetic.

c. Electrolytic Oxidation and Reduction. By the application of an external potential to an ESR sample tube equipped with two electrodes it is possible to cause oxidation or reduction of the diamagnetic species in solution to occur. The radicals formed in the vicinity of the anode and cathode may be observed separately; however, it is usual for only one relatively stable paramagnetic complex to be formed, the other undergoing further reaction to form a diamagnetic compound. A typical experimental arrangement is shown in Fig. 24.

The arrangement is such that only radicals formed in the vicinity of the platinum electrode are observed, but this may be either the anode or cathode of the cell depending on the direction of the applied potential

The usual sample tube used for the ESR experiments is basically very similar to that shown in Fig. 24 but without the electrodes. The same tube, without the ends stoppered, may be used for flow experiments. It is possible to use a cylindrical tube drawn out into a capillary where it enters the ESR cavity. It is necessary to use quartz glass for all these sample tubes since Pyrex and other glasses contain small traces of paramagnetic impurities. It is also essential that only a thin sample should be exposed to the microwave radiation since all solvents absorb the microwaves to varying degrees and if much absorption occurs a process known as damping is observed and it is not possible to obtain resonance. Good solvents are those which cause the minimum of damping, and, in general, these are characterized by having low permittivity (dielectric constant). The presence of solute ions in the solvent raises the permittivity of the solution considerably. Some solvents have

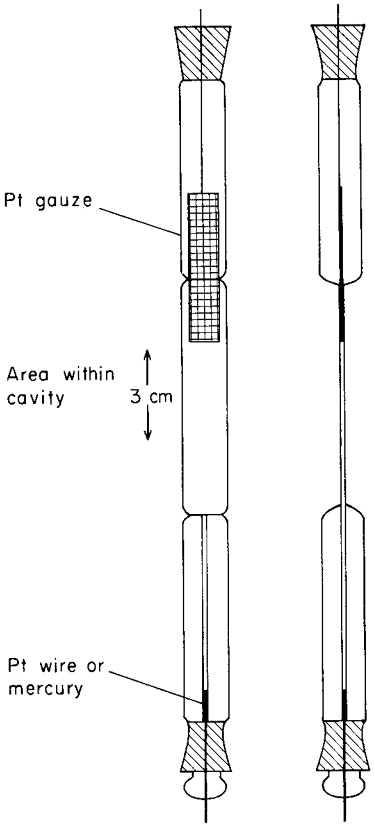

FIG. 24. Two views at right angles of solution cell showing the position of electrodes for reduction or oxidation.

anomalous damping behavior, e.g., ethylamine at temperatures below 263°K damps badly. Once frozen, most solvents cause much less damping.

2. *Single Crystals*

The most common method of production of a magnetically dilute single crystal of a paramagnetic compound is simply to grow a crystal of an isomorphous diamagnetic compound containing about 0.1 moles of the paramagnetic compound as an impurity. Any of the standard crystal growing methods may be used, e.g., slow evaporation or cooling of solution, pulling from melt, etc., the choice depending on the nature of the radical being studied.

Alternatively a single crystal containing a paramagnetic impurity may be produced by the use of high-energy radiation. This is done either by irradiating a pure crystal and studying the damage sites or by placing a diamagnetic transition metal complex in a host which easily produces or absorbs electrons or irradiation, e.g., KCl readily produces *F* centers, whereupon there is a good chance of this trapped electron adding to the complex. This is slightly less haphazard than the former method. Usually one cannot form a specific radical by irradiation and a number of paramagnetic species may be seen. The latter method is also limited to metal ions (or complexes) with a high negative charge, since a $(KCl_6)^{5-}$ unit in the KCl crystal lattice has to be replaced by an ion of similar size and charge.

3. *Dilute Powders or Glasses*

A "dilute glass" is a frozen dilute solution of a complex in any suitable solvent. A convenient method for the study of many compounds is to observe their ESR spectra in solution and then to rapidly freeze the solution and observe the solid state spectrum. The former spectra give the isotropic parameters for the various species, while the latter yield the anisotropic data.

A "dilute powder" consists of a large number of randomly oriented magnetically dilute crystals, the resulting spectrum being identical to that obtained from a glass, which contains a large number of randomly oriented molecules. Provided that the principal directions of the g and A tensors are colinear, the single crystal and powder methods should produce identical results, except that the latter is unable to give the directions of the principal tensors, but with powders resolution is often poorer and hyperfine structure are not always seen. There may also be some ambiguities in the interpretation of powder spectra. The powder method does have one big advantage over the single crystal method, namely, ease of preparation of samples. Here, all that is necessary is to freeze a dilute solution or to coprecipitate the radical with about 10^3 times as much of the host material. Almost all organic solvents form glasses at liquid nitrogen temperature; EPA (a mixture of ethanol, isopentane, and ether in 2:5:5 proportions) is perhaps the best. (*O*-Terphenyl is very suitable for use in glasses at room temperature.) Water is a very poor glass-forming solvent due to the presence of strong hydrogen bonds which makes it extremely unwilling to accommodate an impurity within the crystal structure, with the consequence that local concentrations of the paramagnetic ion are usually obtained, thus producing a spectrum broadened by dipolar and exchange interactions. Narrow lines may be obtained by the addition of some diamagnetic impurity, e.g., an alcohol or phosphoric acid.

B. MICROWAVE FREQUENCY

ESR measurements are usually recorded at *X*-band frequencies because of the convenience of the electronic components. *Q*-band frequency spectrometers are now becoming more widely used for special applications. Other frequencies, e.g., *K*- and *S*-band frequencies are also sometimes used. The frequencies, wavelength, and magnetic field of the more common spectrometers are given in Table XVII. The following are recommended volumes on instrumentation (*361*, *562*, *681*, *711*).

TABLE XVII

REPRESENTATIVE FREQUENCY AND MAGNETIC FIELDS FOR RESONANCE AT $g = 2$ FOR VARIOUS WAVE BANDS

Band	Nominal wavelength (cm)	Frequency (MHz)	Magnetic field (gauss)
Q band	0.8	34,222	12,225
K band	1.5	18,252	6,520
X band	3	9,126	3,260
S band	10	2,737	978

C. INTERPRETATION OF SPECTRA

1. *Solution Spectra*

A molecule in solution takes up all orientations with respect to the external magnetic field in a short time compared with the time that an electron exists in a particular energy state; consequently all the anisotropies of the spectrum are averaged to zero. The spectrum is analyzed by recording the microwave frequency and magnetic fields at which resonances occur. The values of A_{iso} and g_{av} may then be determined either directly from this data or if necessary by application of the Breit–Rabi equation (see Section VII,D). The isotropic spectrum of the species present when $[Fe(NO)(H_2O)_5]^{2+}$ is made alkaline at pH 11 is shown in Fig. 25a. The spectrum shows that there are two equivalent ^{14}N atoms in the molecule. Ambiguities of interpretation sometimes occur, particularly in multiline spectra; e.g., it may not be clear whether a line is a hyperfine component or whether it is due to another species. Such ambiguities may be resolved in the following ways.

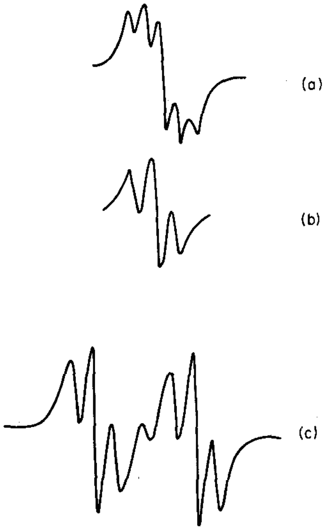

FIG. 25. Effect of isotopic substitution on the ESR spectra of an alkaline solution of $[Fe(NO)(H_2O)_5]^{2+}$ (a) ^{56}Fe and ^{14}N showing two equivalent ^{14}N; (b) ^{56}Fe and ^{15}N; and (c) ^{57}Fe and ^{15}N.

(*i*) *Isotopic substitution.* A new isotope having a different magnetic moment or spin will produce a spectrum in which the hyperfine interaction is changed in accord with these new parameters. The effect on the species shown in Fig. 25a of isotopic replacement is shown in Fig. 25b. In Fig. 25a $^{15}N(I = \frac{1}{2})$ replaces $^{14}N(I = 1)$.

Since, for two isotopes 1 and 2

$$\frac{A(1)\cdot I(1)}{\mu_N(1)} = \frac{A(2)\cdot I(2)}{\mu_N(2)} \tag{104}$$

then the ^{15}N hyperfine coupling is 1.403 times that for ^{14}N. Also, the number of lines is reduced from five with intensity ratio 1:2:3:2:1 to three with intensity ratio 1:2:1. In Fig. 25c ^{57}Fe replaces ^{56}Fe, and each line in the spectrum of Fig. 25b is split into two by $^{57}Fe(I = \frac{1}{2})$. If some lines do not change upon isotopic substitution, the spectrum is probably due to two species.

(*ii*) *Power saturation.* If the spectrum is due to two species, they will not usually have the same relaxation times. Thus, if the microwave power is increased progressively, one of the species will saturate before the other. This is shown as a broadening and gradual disappearance of the line.

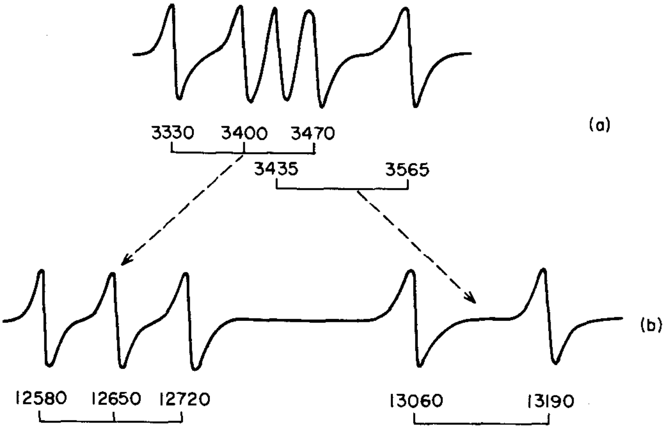

FIG. 26. ESR spectrum of two species, $I = 1$ and $I = \frac{1}{2}$, (a) at X band and (b) at Q band. The field position of each line is in gauss.

(*iii*) *Changing the microwave frequency.* Since to a good approximation the magnitude of the hyperfine interaction is independent of the external field, if the microwave frequency is increased (e.g., by going from X to Q band), hyperfine interactions associated with each g value (whether belonging to the same or different species) will be separated by a factor of 3.75. This is illustrated in Fig. 26 for the isotropic spectrum of two species 1($A = 80$ gauss, $I = 1$) and 2($A = 120$ gauss and $I = \frac{1}{2}$). The effect has been to separate the two spectra and thus make interpretation less ambiguous.

2. *Single Crystal Spectra*

The object is to rotate the crystal about three mutually perpendicular directions which are known relative to the crystal faces and hence relative to the unit cell or principal molecular directions. Some form of goniometer is used, whereby a crystal is either mounted on a rod or in a perspex cube which can be glued to a rod and rotated in the magnetic field as illustrated. It is generally time-consuming to attempt to discover the orientations of the crystal corresponding to the principal directions of the various tensors and the following procedure (*608*) is commonly used. The method is based on the expression for the g value at a general orientation of the crystal

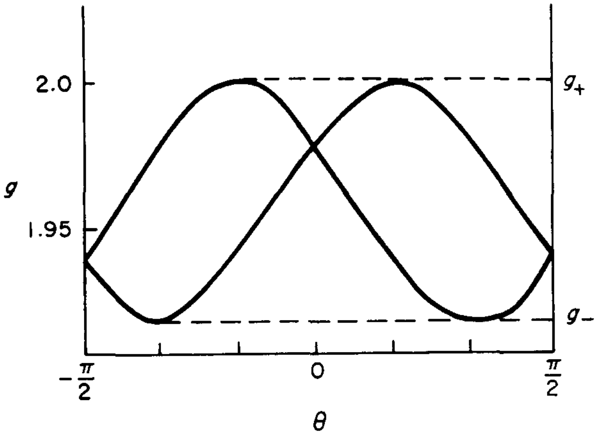

FIG. 27. Plot of g versus θ in one plane for Ti(acac)$_3$. There are two equivalent ions with a separation of 60°. In this case, $g_+ = g_{\parallel} = 2.000$ and $g_- = g_{\perp} = 1.921$.

$$g^2 = \sum_i l_i G_{ij} l_j \tag{105}$$

where l_i, l_j are direction cosines which relate that particular general orientation to some chosen system of axes set in the crystal and to which G refers. The problem is to determine the matrix G and then to diagonalize it, i.e., to determine the principal values of the g tensor and the orientation of the principal axes relative to the chosen axes.

(*i*) The diagonalization of G is straightforward. The roots of Eq. (105)

$$\det|G - \lambda I| = 0 \tag{106}$$

must be determined, then λ_i are the squares of the desired principal values of the g tensor.

(*ii*) Determination of G. The most general expression for g is

$$g^2 = \alpha + \beta \cos 2\theta + \gamma \sin 2\theta \tag{107}$$

where θ is a rotation angle and α, β, and γ are parameters which must be determined. If the maximum and minimum values of g during a rotation is denoted by $g_{\pm}$ and occurs at $\theta_{\pm}$ (see Fig. 27), then

$$2\alpha = g_{+}^{2} + g_{-}^{2} \tag{108}$$

$$2\beta = (g_{+}^{2} - g_{-}^{2}) \cos 2\theta_{+} \tag{109}$$

$$2\gamma = (g_{+}^{2} - g_{-}^{2}) \sin 2\theta_{+} \tag{110}$$

Therefore if the g-value variation is measured in three mutually perpendicular planes, nine pieces of information are obtained from which the six independent components of G may be determined and cross-checked.

For the experimental determination of G the most sensible set of axes of the crystal are chosen, e.g., if orthorhombic, the a, b, and c axes, are chosen or if monoclinic, a and b axes and an axis orthogonal to these are chosen. In any case measurements are taken in two mutually perpendicular planes (1, 2 and 3, 1) and a third plane containing the axis 2 and making an angle ϵ with axis 3.

The crystal is rotated so that θ is measured from axes 1, 2, and 3 in the positive right-handed sense. If the values of α, β, and γ are denoted by i for a rotation in the jk plane, the matrix G can be constructed as follows:

$$\begin{array}{c|c|c}
\begin{matrix}\alpha_3 + \beta_3 \\ \alpha_2 - \beta_2\end{matrix} & \gamma_3 & \gamma_2 \\
\hline
\gamma_3 & \begin{matrix}\alpha_3 - \beta_3 \\ \alpha_1 + \beta_1\end{matrix} & \dfrac{\gamma_1 - \gamma_3 \sin\epsilon}{\cos\epsilon} \\
\hline
\gamma_2 & \dfrac{\gamma_1 - \gamma_3 \sin\epsilon}{\cos\epsilon} & \alpha_2 + \beta_2
\end{array} \tag{111}$$

Also

$$G_{33} \cos^{2}\epsilon + G_{11} \sin^{2}\epsilon + 2G_{31} \sin\epsilon \cos\epsilon = \alpha_1 - \beta_1 \tag{112}$$

The case of three mutually perpendicular planes is particularly simple since $\epsilon = 0$ and $G_{11} = \alpha_2 + \alpha_3 - \alpha_1$

$$G_{12} = \pm[(\delta_3 + \alpha_1 - \alpha_2)(\delta_3 - \alpha_1 + \alpha_2)]^{1/2} \tag{113}$$

where

$$\delta = \tfrac{1}{2}({g_+}^2 - {g_-}^2)$$

The other components of G are generated by a cyclic permutation of 1, 2 throughout the expression for G_{12}. The sign of G_{12} is that for γ_3 and this is also cyclic.

It is now necessary to resolve the sign of γ. This may be done by performing a rotation in a plane other than those three already employed. The results for this rotation may be predicted from the expression

$$g_2{}^2 = g_{xx} l^2 + g_{yy} m^2 + g^2_{zz} n^2 \tag{114}$$

where g^2_{ii} are the principal values of G and l, m, and n are the direction cosines which specify the rotation with respect to the principal axes of G. One orientation is usually sufficient.

The whole process is repeated for each hyperfine coupling and their principal values and directions obtained. It frequently happens that the principal value of the g and A tensors are coincident, and this simplifies the interpretation of the g and A tensors considerably.

3. *Powder (or Polycrystalline) Spectra*

The powder spectrum is the envelope of the spectra from all possible orientations of the paramagnetic ion; all that is required is a method of determining the principal values directly from the spectrum in which they are present implicitly. The major loss of information is that the orientation of the radical in the crystal cannot be determined. The advantage is that doped single crystals need not be prepared and this saves considerable time.

In the following, the line shape results of Kneubühl (*393*) are used and for the sake of convenience, only one magnetic nucleus will be considered. Also it is necessary to assume the principal directions of g and A to be coincident.

When the axis of the molecule lies parallel to the applied magnetic field, there will be an absorption at the field value corresponding to $g_{\parallel}$. Only a small proportion of molecules will be near this position. There will be a larger number of molecules, however, lining up at right angles to this field direction. A larger absorption will occur at a field position corresponding to $g_{\perp}$. In a powder, there will be molecules lining up in all possible intermediate directions giving absorptions at all intermediate field positions between $g_{\parallel}$ and $g_{\perp}$. The resultant absorption curve is shown in Fig. 28. In the upper diagrams (Fig. 28a) the full line is the idealized absorption and the dotted line the real absorption. In the lower diagrams (Fig. 28b), the dotted lines are the first derivative traces

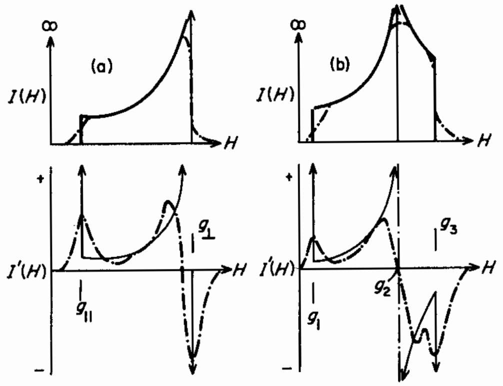

FIG. 28. Absorption and first derivative curves for radicals with a g tensor that is (a) axially symmetric and (b) anisotropic (*44*).

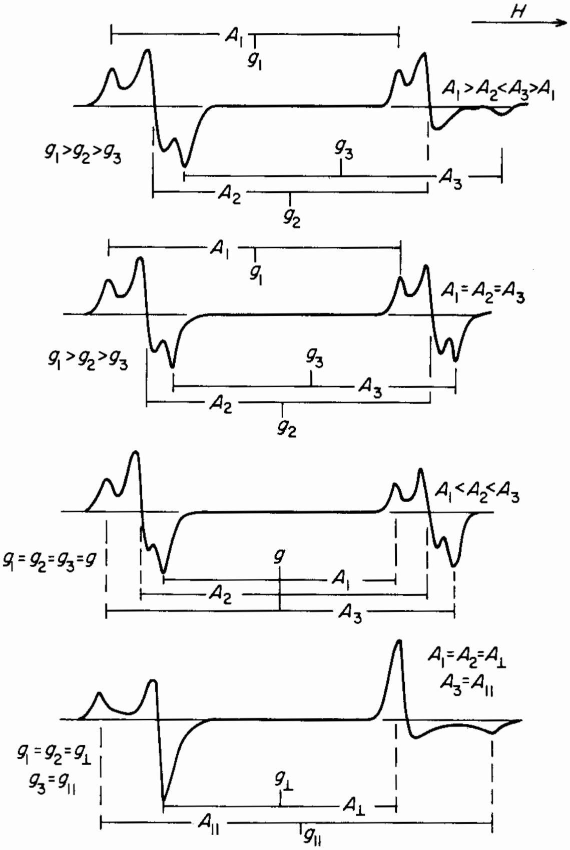

FIG. 29. Typical powder spectra for radicals with one $I = \frac{1}{2}$ nucleus (*44*).

normally observed. When there is a magnetic nucleus present, the spectra are more complicated (see Figs. 29 and 30).

Sometimes the species contains a nucleus with more than one magnetic isotope in appreciable natural abundance, e.g., Cr. (90.5% ^{50}Cr, ^{52}Cr, and ^{54}Cr, $I = 0$; 9.5% ^{53}Cr, $I = \frac{3}{2}$). The spectrum then consists of the superposition of spectra due to these isotopes. The relative intensity of the lines from each isotope is proportional to their abundance and inversely proportional to $2I + 1$, the number of lines for each isotope. Thus with chromium, there is one central line, with four other lines of relative intensity

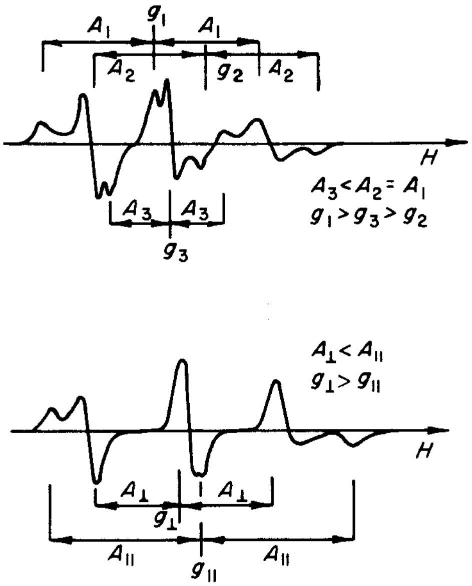

FIG. 30. Typical powder spectra for radicals with one $I = 1$ nucleus (*44*).

$$\frac{9.5}{90.5} \times \frac{1}{4} = \frac{1}{38}$$

The powder method has many limitations and inaccuracies and on occasions the data may fit a number of consistent interpretations. Inaccuracies arise, for example, from the difficulty of precisely locating a shoulder on a line.. Also, if the g and A tensors are not coaxial the powder spectra will not give accurate values for the principal values of the A and g tensors, but will give values corresponding to the turning points in a single crystal study. Usually, however, the agreement between powder and crystal results is good and much useful information can be obtained from studies on polycrystalline or glassy samples.

4. Forbidden Transitions

In ESR spectra involving interactions with nuclei with quadrupole moments, i.e., $I \geqslant 1$, there is the possibility of the selection rules breaking down. In addition to the transitions due to $\Delta m_s = 0$, $\Delta m_s = \pm\frac{1}{2}$, transitions associated with $\Delta m_I = \pm 1$ may be observed (*13*, *92*). The effect is seen as weak lines midway between the principal hyperfine lines. An example is shown in Fig. 31 which concerns the molecule hexakis(penta-

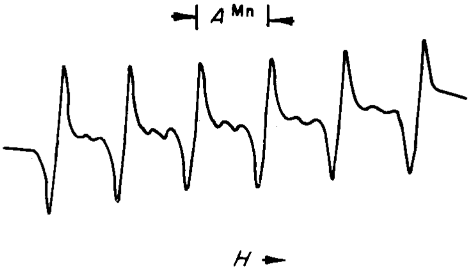

FIG. 31. ESR spectra of hexakis(pentamethylenetetrazole)manganese(II) ion, showing the pairs of $\Delta m_I = \pm 1$ forbidden transitions between the $\Delta m_I = 0$ transitions (*422*).

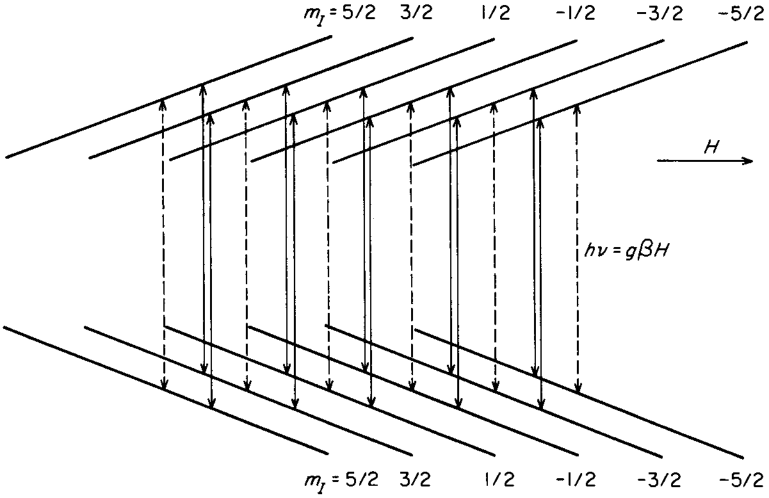

FIG. 32. The forbidden $\Delta m_I = \pm 1$ transitions —— and the allowed $\Delta m_I = 0$ transitions - - - for a ^{55}Mn complex (^6S, $I = \frac{5}{2}$). There is no zero-field splitting.

methylenetetrazole)manganese perchlorate (*422*). The forbidden lines are themselves split into doublets by spin–spin interaction (*125*) of the sextuplet state. This causes a variation in the hyperfine spacings with consequent separation of the two $\Delta m = \pm 1$ transitions which are otherwise degenerate. The transitions are indicated in Fig. 32.

D. THE BREIT–RABI EQUATION: SECOND-ORDER CORRECTIONS

It has been assumed, so far, that there is no coupling between the spin of the electron and the spin of the nucleus, i.e., as the electron spin is reversed, the nuclear spin remains unchanged. This is true at high fields, but becomes progressively less true at weaker fields, with the result that m_s and m_I are not good (pure) quantum numbers. In fact, there is a nonlinear divergence of energy levels as H increases. For an electron interacting with a nucleus with $I = 1$, the energy levels are as shown in Fig. 33. F is the quantum number such that

$$F = \mathbf{S} + \mathbf{I} \tag{115}$$

and m_F has values

$$m_F, m_F - 1, m_F - 2 \ldots - m_F$$

At the high applied fields which are usual for ESR any effect due to the nonparallel nature of the energy levels is small. At low fields (<100

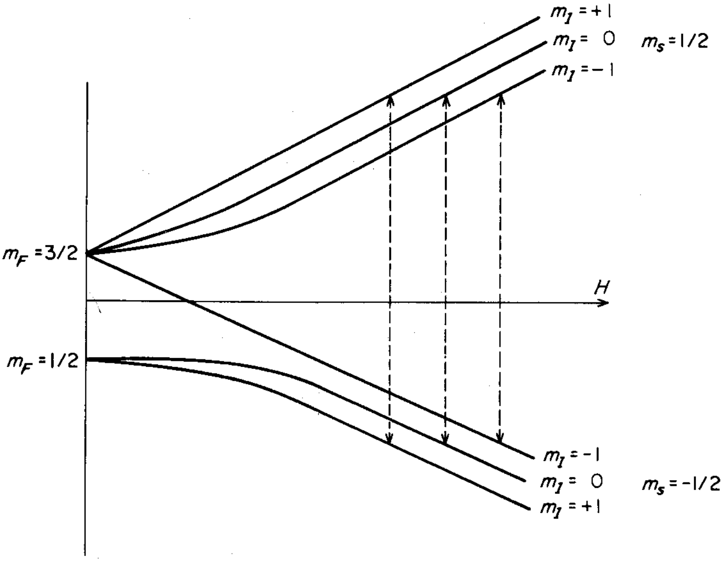

FIG. 33. Energy levels for a $S = \frac{1}{2}$, $I = 1$ system showing the transitions in the high field region.

gauss) the effect is significant. If the hyperfine coupling A is large, however, as occurs with some transition metals, the hyperfine spacings A will not be equal. The observed hyperfine spacings between lines may be corrected by use of the Breit–Rabi equation [Eq. (116)].

$$E_I = \frac{-\Delta W}{2(2I+1)} + g_N \beta_N m_F H \pm \frac{\Delta W}{2}\left\{\frac{1 + 4m_F x + x^2}{2I+1}\right\}^{1/2} \tag{116}$$

where $\Delta W = (2I + 1)A/2$ and

$$x = (g - g_N)\beta H/\Delta W \approx g\beta H/\Delta W \tag{117}$$

For the case of an ion with $S = \frac{1}{2}$, $I = \frac{1}{2}$, the energy levels may be represented as in Fig. 4. The highest level

$$\begin{aligned}
E_1 &= g\beta(H/2 + A/4) \\
E_2 &= g\beta\left(-A/4 + \sqrt{\frac{H^2 + A^2}{4}}\right) \\
E_3 &= g\beta(-H/2 + A/4) \\
E_4 &= g\beta\left(-A/4 - \sqrt{\frac{H_2 + A^2}{4}}\right)
\end{aligned} \tag{118}$$

and when $H = 0$,

$$E_1 = E_2 = E_3 = \frac{g\beta A}{4}, \; E_4 = \frac{-3g\beta A}{4} \tag{119}$$

at high field $H \gg A$

$$\sqrt{\frac{H^2 + A^2}{4}} \approx H/2 \tag{120}$$

which is the first-order approximation. But if A is not negligible compared with H, then

$$\sqrt{\frac{H^2 + A^2}{4}} = H/2 + \frac{A^2}{4H} \tag{121}$$

Since

$$(1 + x)^{1/2} \approx 1 + x/2 \qquad \text{if } x \ll 1$$

$$\begin{aligned}
\therefore \quad E_2 &= g\beta\left[-A/4 + \frac{H}{2}\left(1 + \frac{A^2}{H^2}\right)^{1/2}\right] \qquad (122) \\
&= g\beta(H/2 - A/4 + A^2/4H) \\
E_4 &= g\beta(-H/2 - A/4 - A^2/4H) \qquad (123)
\end{aligned}$$

Energy levels 2 and 4 have been moved to higher and lower energies, respectively. Thus there is a shift in the position of the lines of the spectrum as shown in Fig. 34.

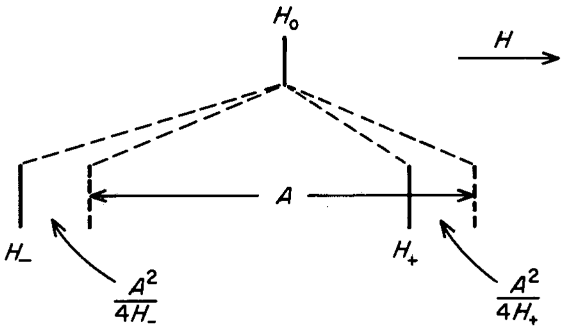

FIG. 34. Second-order corrections for nucleus $I = \frac{1}{2}$, ······, expected lines; ——, experimental lines.

The center of the spectrum H_0 is now

$$\begin{aligned} H_0 &= H_- + A/2 + A^2/4H_- \\ &= H_+ - A/2 + A^2/4H_+ \end{aligned} \tag{124}$$

where H_+, H_- are the field values at which resonance lines are observed.

$$\therefore \quad A = (H_+ - H_-)\left(1 - \frac{A^2}{4H_+H_-}\right) \tag{125}$$

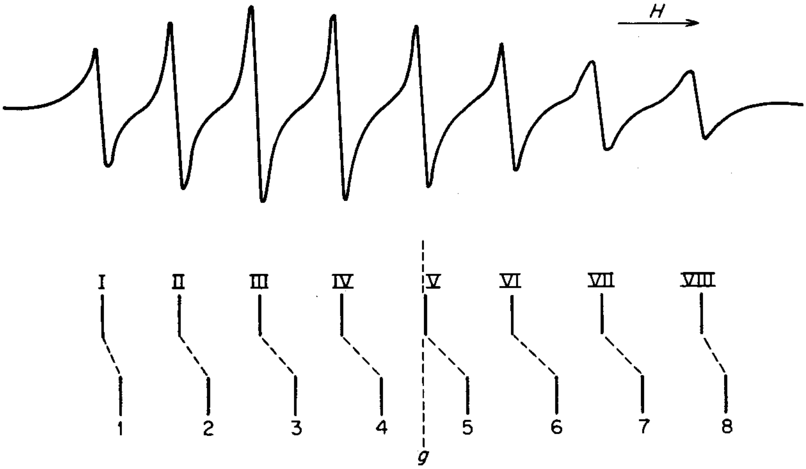

FIG. 35. Spectrum of the VO^{2+} ion in water showing the relationship between the experimental lines I–VIII and the corrected lines 1–8.

The magnitude of the second-order shifts to each line may be worked out as follows. If $x = A^2/4H$, the coefficient of x for various nuclear spins is given by

$$\begin{array}{ll}
I = 0 & 0 \\
I = \frac{1}{2} & 1 \quad 1 \\
I = 1 & 2 \quad 4 \quad 2 \\
I = \frac{3}{2} & 3 \quad 7 \quad 7 \quad 3 \\
I = 2 & 4 \quad 10 \quad 12 \quad 10 \quad 4 \\
I = \frac{5}{2} & 5 \quad 13 \quad 17 \quad 17 \quad 13 \quad 5 \\
I = 3 & 6 \quad 16 \quad 22 \quad 24 \quad 22 \quad 16 \quad 6 \\
I = \frac{7}{2} & 7 \quad 19 \quad 27 \quad 31 \quad 31 \quad 27 \quad 19 \quad 7
\end{array}$$

Figure 35 shows the spectrum and analysis of the lines of the VO^{2+} ion, $S = \frac{1}{2}$, $I = \frac{7}{2}$. The second-order corrected lines (H_1, H_2, etc.) are related to the experimental lines as follows

$$\begin{aligned}
H_{\mathrm{I}} &= H_1 - 7A^2/4H_1 \\
H_{\mathrm{II}} &= H_2 - 19A^2/4H_2 \\
H_{\mathrm{III}} &= H_3 - 27A^2/4H_3 \\
H_{\mathrm{IV}} &= H_4 - 31A^2/4H_4 \\
H_{\mathrm{V}} &= H_5 - 31A^2/4H_5 \\
H_{\mathrm{VI}} &= H_6 - 27A^2/4H_6 \\
H_{\mathrm{VII}} &= H_7 - 19A^2/4H_7 \\
H_{\mathrm{VIII}} &= H_8 - 7A^2/4H_8
\end{aligned}$$

where $H_{\mathrm{I,II}}$, etc. are the field positions of the lines measured from the spectrum. In this case the actual hyperfine coupling is thus approximately equal to H_{V}–H_{IV}.

The g values have to be corrected in a similar manner. It is seldom necessary to go to higher order approximations to explain observed spectra.

When the second-order correction is applied to a system with several equivalent magnetic nuclei, then there will be a splitting of the hyperfine lines in addition to the expected shifts. This may best be illustrated with the PF_4 radical. The system may be described by $S = \frac{1}{2}$, $4 \equiv I_F = \frac{1}{2}$. The total nuclear spin $I = 2$ and may, in general, have other values

$$I, I-1, I-2, \ldots, 0 \qquad (126)$$

here, the possible values are 2, 1, and 0. Four equivalent nuclei with spin $\frac{1}{2}$ may align themselves with respect to an applied magnetic field in 1, 4, 6, 4, and 1 ways for $m_I = 2, 1, 0, -1$, and -2, respectively. The relative intensities arise from I values of 2, 1, and 0 as follows, where the numbers represent relative intensities.

	$m_I = 2$	1	0	−1	−2
$I = 2$	1	1	1	1	1
$I = 1$		3	3	3	
$I = 0$			2		
Total intensity assuming no need for a second-order correction	1	4	6	4	1

Thus the five lines are made up of nine components, *each* of *which* is shifted to a different extent by the second-order correction. A reconstruction of the spectrum is shown in Fig. 36. The shifts are in multiples of x where $x = A^2/4H$.

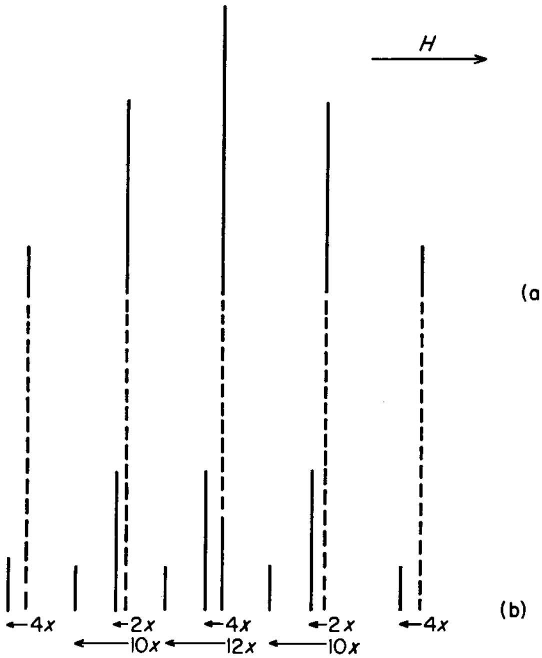

FIG. 36. The relationship between the experimental lines (b) and the lines corrected to second-order (a) for a system $S = \frac{1}{2}$, $4 \equiv I = \frac{1}{2}$. The coefficients of x represent the magnitude of the shifts from ideality.

E. Choice of Units and Conversion Factors

The resonance condition may be expressed in various ways depending on the units of A (*n.b.*, H_0 is measured in gauss)

(*i*) $h\nu = g\beta H_0 + Am_I$ where A is in ergs
(*ii*) $h\nu = g\beta H_0 + 10^6 hAm_I$ where A is in MHz
(*iii*) $h\nu = g\beta H_0 + hcAm_I$ where A is in cm^{-1}
(*iv*) $h\nu = g\beta(H_0 + Am_I)$ where A is in gauss

TABLE XVIII

Conversion Factors

	gauss (mT)	MHz	cm^{-1}	ergs (10^{-7} J)
gauss (mT)	1	$g\beta/10^6 h$	$g\beta/hc$	$g\beta$
MHz	$10^6 h/g\beta$	1	$10^6/c$	$10^6 h$
cm^{-1}	$hc/g\beta$	$c/10^6$	1	hc
ergs (10^{-7} J)	$1/g\beta$	$1/10^6 h$	$1/hc$	1

To convert from a unit in a row to the unit in a column in Table XVIII, multiply by the conversion factor in that row and column.

$$\text{NOTE:}\quad 10^6 h/\beta = 0.71449$$

$$hc/\beta = 2.1420 \times 10^4$$

$$\therefore\quad 1\ \text{gauss} = g/0.71449\ \text{MHz}$$

$$= g/2.1420 \times 10^4\ \mathrm{cm}^{-1}$$

The problem now arises as to which units one should use when reporting ESR spectra. The gauss has often been used purely as a matter of convenience since the parameters are always measured from the spectrum in terms of differences in magnetic field. The erg, being the energy unit, is the more fundamental but has not found favor and it is usually the reciprocal centimeter (or, less frequently, MHz) which are used as alternative units to the gauss. These are both independent of the g value, and are directly proportional to the energy. In principle, they are preferable to the gauss, but this latter unit still finds favor with quite a number of workers simply because of its convenience. SI units affect the above units in that the tesla is preferred to the oersted or gauss

(=1 mT) and the reciprocal meter is preferred to the reciprocal centimeter, i.e., 10^{-4} $cm^{-1} = 10^{-6}$ m^{-1}. Furthermore the unit of energy, erg, is to be replaced by the joule (1 erg = 10^{-7} J). Symbols for magnetic parameters are changed as follows: μ_B replaces β_e (Bohr magneton) and μ_N replaces β_N (nuclear magneton). A Royal Society publication (*649*) deals with units in detail.

VIII. Discussion of the Literature

A. d^1 IONS

1. *ESR of* Sc^{2+}, Y^{2+}, *and* La^{2+}

The divalent state of scandium, yttrium, and lanthanum is thermodynamically unstable and has only deen detected in certain host lattices. The available data are given in Table XIX. Höchli and Estle (*344, 345*) observed ^{45}Sc hyperfine structure (h.f.s.) together with nine lines attributable to eight equivalent F nuclei with a spacing of 2.2 gauss in calcium and strontium fluoride host lattices. The trapped species is a distorted $[ScF_8]^{6-}$ ion. The only other reported ESR (*378*) is for the oxides ScO, YO, and LaO trapped in a solid argon matrix by condensation of the oxide vapor at 4.2°K. The high metal h.f.s. is in accordance with expectation since the unpaired electron is in a σ-molecular orbital ($^2\Sigma$ ground state).

TABLE XIX

ESR DATA for d^1 IONS OF Sc^{2+}, Y^{2+}, AND La^{2+}

Ion	g	A (10^4 cm^{-1})	$A(^{19}F)$ (gauss)	References
ScO in argon, 4·2°K	2.00	2680	—	(*378*)
YO in argon, 4·2°K	2.003	270	—	(*378*)
LaO in argon, 4·2°K	2.01	5190	—	(*378*)
$[ScF_8]^{6-}$ in CaF_2 (1.5°K)				
Species 1	1.951	89.5	2.2	(*344, 345*)
Species 2	1.995	40.4	2.2	(*344, 345*)
Species 3	1.969	65.5	2.2	(*344, 345*)
$[ScF_8]^{6-}$ in SrF_2				
Species 1	1.936	91.2	2.2	(*344, 345*)
Species 2	1.991	43.0	2.2	(*344, 345*)
Species 3	1.963	67.0	2.2	(*344, 345*)

2. *ESR of Ti^{3+}*

Only two of the naturally occurring isotopes of titanium have nonzero nuclear spin; ^{47}Ti with $I = \frac{5}{2}$ (7.75%) and ^{49}Ti with $I = \frac{7}{2}$ (5.51%). Hyperfine spectra in solution will thus consist of a strong central line ($I = 0$) flanked by a sextet ($I = \frac{5}{2}$) and an octet ($I = \frac{7}{2}$) state superimposed on each other since μ_N/I is nearly the same for both nuclei. The spectrum will thus consist of a series of lines of approximate relative intensities 1:3:3:3:120:3:3:3:1. A typical spectrum is shown in Fig. 37.

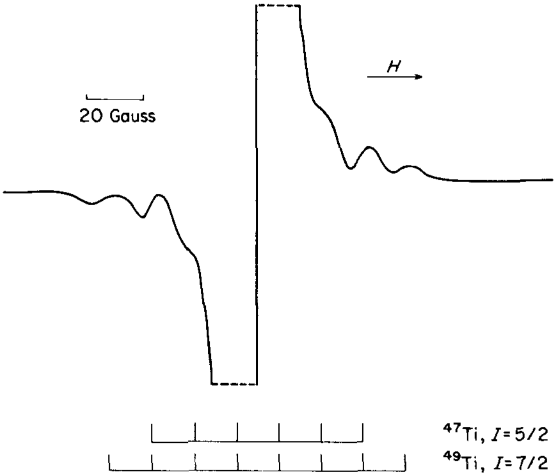

FIG. 37. ESR spectrum of transient species in reaction between Ti^{3+} and H_2O_2, showing ^{47}Ti and ^{49}Ti hyperfine coupling.

Small trigonal distortion occurs (*271*) in $CsTi(SO_4)_2 \cdot 12H_2O$ where the Ti^{3+} ion is surrounded by six H_2O molecules in D_{3h} symmetry. The $^2T_{2g}$ ground state in O_h symmetry splits into ^2E_g and $^2A_{1g}$ with a separation of about 140 cm^{-1}. The presence of a low-level excited state results in a short spin–lattice relaxation time and resonance is only seen at 4.2°K. The distortion is somewhat greater (*182*, *271*, *717*) for Ti^{3+} in $RbAl(SO_4) \cdot 12H_2O$. Similar distortions are found for the systems Ti^{3+} in Al_2O_3 (corundum, C_3), Ti^{3+} in $AlCl_3 \cdot 6H_2O$, $Ti_2(SO_4)_3 \cdot 4H_2O$, and $KTi(C_2O_4)_2 \cdot 2H_2O$. These systems have been critically reviewed by Gladney and Swalen (*271*). It is interesting that for Ti^{3+} in CaF_2 the spectrum is isotropic even at 2°K, showing the absence of a Jahn–Teller splitting. Fluorine super hyperfine splittings (s.h.f.s.) are detected (*461*, *728*). The ESR data are given in Table XX.

Titanium h.f.s. are resolved (*500*) at 77°K in Ti^{3+} doped $Al(acac)_3$. The symmetry here is D_3 and the large trigonal distortion ($\delta = 2000$–$4000\ cm^{-1}$) increases the spin–lattice relaxation time so that resonance is observed at 77°K. The electron is in the $a_1(d_{z^2})$ orbital in contrast with most other d^1 ions. Titanium h.f.s. are observed on the F-center line in H_2-reduced $BaTiO_3$ (*664*).

Waters and Maki (*695*) dissolved TiF_3 in CH_3OH and observed h.f.s. from Ti and two equivalent F atoms. The species in solution is likely to be TiF_2^{2+}(solv.). A(Ti) is almost identical to that in $(TiOCH_3)^{2+}$ prepared by the reaction of $TiCl_3$ in CH_3ONa/CH_3OH and is 13.7 gauss. Flow experiments (*651*) suggest that a transient species exists when $TiCl_3$ and alkaline H_2O_2 solutions in water mix in the ESR cavity. Titanium h.f.s. are observed and are attributed to 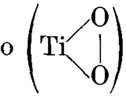 In neutral solution, another species is detected. The very small coupling to titanium observed by Fisher (*215*) (0.85 and 0.95 gauss) of two apparently different species indicates that the electron is located primarily on the peroxy group. This is supported by the g value slightly in excess of free spin, in contrast to complexes where the electron is mainly on the metal. Other studies of the reaction between Ti^{3+}, H_2O_2, and various organic compounds show the presence of organic free radicals (*133*, *653*). Fujiwara, Fisher, and others (*140*, *215*, *227*) have observed poorly resolved h.f.s. in complexes between Ti^{3+} and organic chelating groups of the ethylenediaminetetraacetic acid (EDTA) type. Semenova (*612*) has investigated the reaction of $TiCl_3$ in concentrated solutions of formic, acetic, and oxalic acids and suggested that the species formed are $Ti(HCOO)_3$, $Ti(OH)(CH_3COO)_2$, and $Ti_2(C_2O_4)_3 \cdot 10H_2O$. No hyperfine structure is observed in their ESR spectra.

There are numerous reports of ESR signals from organotitanium compounds and from Ziegler-type catalysts. Hyperfine structure from Ti is observed (*173*) from electrochemically reduced Cp_2TiCl_2 and $Cp_2Ti(TDT)$, where the paramagnetic species are thought to be

Cp_2TiCl and 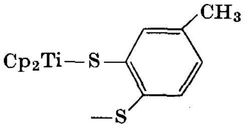

Solutions of $(Cp_2TiCl)_2$, $Cp_2TiC_2H_5$, $CpTiCl_2$, and Cp_2Ti^+ all give spectra with a single broad line with no h.f.s. (*59*, *134*, *257*, *534*). The product of the reaction between Cp_2TiCl_2 and aluminum alkyls usually

TABLE XX

ESR DATA FOR d^1 IONS OF Ti^{3+} AND Zr^{3+}

Ion	g_{av}	$g_{\parallel}$	$g_{\perp}$	A_{iso} ($10^4 cm^{-1}$)	$A_{\parallel}$ ($10^4 cm^{-1}$)	$A_{\perp}$ ($10^4 cm^{-1}$)	$A_{ligands}$ ($10^4 cm^{-1}$)	References
$BaTiO_3$ reduced by H_2	—	1.930	1.911	—	19 G	~8 G	—	*(664)*
Ti^{3+} in CaF_2	1.9452	—	—	20.0 G	—	—	$A(^{19}F) = 1.97$ G	*(461, 728)*
$Ti_2(SO_4)_3 \cdot 4H_2O$	—	—	—	12 G	30 G	2 G	—	*(252)*
Ti^{3+} in $CsTi(SO_4)_2 \cdot 12H_2O$	—	1.25	1.14	—	—	—	—	*(87)*
Ti^{3+} in Al_2O_3	—	1.067	<0.1	—	—	—	—	*(410)*
Ti^{3+} in $Al(acac)_3$	(1.947)	1.921	2.000	—	6.3	17.5	—	*(500)*
Ti^{3+} in CH_3OH, $[Ti(MeOH)_4Cl_2]^+$	1.951	—	—	20 G	—	—	—	*(253)*
Ti^{3+} in C_2H_5OH	—	2.00	1.90	(12 G)	30 G	2 G	—	*(252)*
Ti^{3+} in glycerine	—	1.99	1.93	(12 G)	30 G	2 G	—	*(252)*
$TiCl_3$ in $CH_3OH/NaOCH_3$, $(TiOCH_3)^{2+}$	1.9532	—	—	16.6	—	—	—	*(695)*
$(TiF_2)^+$ in CH_3OH	1.9465	—	—	16.7	—	—	$A(^{19}F) = 7.0$	*(695)*
$Ti(HCOO)_3$	—	1.95		—	—	—	—	*(612)*
$Ti(OH)(CH_3COO)_2$	1.93	—		—	—	—	—	*(612)*
$Ti^{3+} + H_2O_2$								
Species 1	2.01335	—		0.95 G	—	—	—	*(215)*
Species 2	2.01195	—		0.85 G	—	—	—	*(215)*
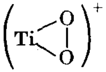	1.955	—		16.25 G	—	—	—	*(651)*
$Ti^{3+} + EDTA$	—	—		17.9 G	—	—	—	*(215)*
$[Ti(en)_3]Cl_3$	—	1.958		—	—	—	—	*(139)*
$[Ti(pn)_3]Cl_3$	—	1.966		—	—	—	—	*(139)*
$Ti_2(C_2O_4)_3 \cdot 10H_2O$	—	1.97, 1.94, 1.93		—	—	—	—	*(612)*

Cp_2TiCl	1.9789	—	13.14 G	—	—	—	*(173)*
$(Cp_2Ti)^+$	1.975	—	—	—	—	—	*(257)*
$CpTiCl_2$	1.975	—	—	—	—	—	*(59)*
$Cp_2TiC_2H_5$	1.94	—	—	—	—	—	*(134)*
$(Cp_2TiCl)_2$	1.980	—	—	—	—	—	*(534)*
$Cp_2Ti(TDT)$	1.9857	—	9.58 G	—	—	—	*(173)*
$Cp_2TiCl_2 + AlEt_3$	1.976	—	11 G	—	—	—	*(24)*
$Cp_2TiCl_2 + Al(i\text{-}Bu)_3$	1.976	—	12 G	—	—	—	*(24)*
$Cp_2TiCl_2 + Al(i\text{-}Bu)_3$, 1:100	1.988	—	—	—	—	$A(^{27}Al) = 4$ G; $A(^1H) = 4$ G; 2 ≡ H	*(617)*
$Cp_2TiCl_2 + Al(i\text{-}Bu)_3$, 1:12	1.987	—	—	—	—	$A(^{27}Al) = 3.7$ G; $A(^1H) = 3.7$ G	*(24)*
$Cp_2TiCl_2 + Al(CH_3)_2Cl$	1.9759	—	—	—	—	$A(^{27}Al) = 4$ G	*(57)*
$Cp_2TiCl_2 + Al(CH_3)Cl_2$	1.9747	—	—	—	—	$A(^{27}Al) = 4$ G	*(57)*
$Cp_2Ti(CH_3)Cl + AlCl_3$	1.9753	—	—	—	—	$A(^{27}Al) = 6.9$ G	*(57)*
$Cp_2Ti(CH_3)Cl + Al(CH_3)Cl_2$	1.9759	—	—	—	—	$A(^{27}Al) = 4$ G	*(57)*
$CpTi(OC_2H_5)_3 + Al(CH_3)_3$	1.973	—	—	—	—	$A = 3$ G, 11 components	*(192)*
$CpTi(OC_2H_5)_3 + Al(C_2H_5)_3$	1.976	—	—	—	—	$A = 3$ G, 11 components	*(192)*
$CpTi(OC_2H_5)_3 + Al(C_2H_5)_2Cl$	1.972	—	—	—	—	$A = 3$ G, 11 components	*(192)*
$CpTi(OC_2H_5)_3 + Al(C_2H_5)Cl_2$	1.973	—	—	—	—	$A = 3$ G, 11 components	*(192)*
$Ti(OC_4H_9)_4 + Al(C_2H_5)_3$	1.959	—	—	—	—	$A(^{27}Al) = 1.98$ G	*(28)*
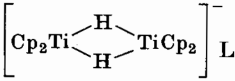 Li^+ or Na^+	1.993	—	6.8 G	—	—	$A(^1H) = 9.5$ G, $A(^1H, cp) = 0.23–0.27$ G $A(Li) = 2.4$ G; $A(Na) = 6.3$ G	(*107*, *109*, *339*)
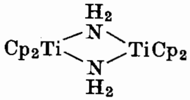	1.987	—	—	—	—	$A(^{14}N) = 2.3$ G	*(108)*
$[Cp_2TiMe_2]^-$ (?)	1.990	—	—	—	—	$A(^1H, CH_3) = 4.2$ G	*(109)*
$[Cp_2TiEt_2]^-$ (?)	1.990	—	—	—	—	$A(^1H, \alpha\text{-}H) = 2.3$ G	*(109)*
$[Cp_2Ti\text{-}i\text{-}Pr_2]^-$ (?)	1.991	—	—	—	—	$A(^1H, \alpha\text{-}H) = 1.8$ G	*(109)*

TABLE XX—*cont.*

ESR DATA FOR d^1 IONS OF Ti^{3+} AND Zr^{3+}

Ion	g_{av}	$g_\parallel$	$g_\perp$	A_{iso} ($10^4 cm^{-1}$)	$A_\parallel$ ($10^4 cm^{-1}$)	$A_\perp$ ($10^4 cm^{-1}$)	$A_{ligands}$ ($10^4 cm^{-1}$)	References
$Cp_2TiH(solv)$ (?)	1.992	—		—	—	—	$A(^1H) = 7.3$ G, $A(^1H, cp) = 1.7$ G	(*109*)
$Cp_2TiCH_3(solv)$	1.986	—		—	—	—	$A(^1H, \alpha\text{-}H) = 4.4$ G	(*109*)
CpTiX, X $=C_3H_5$, $C_3H_3Me_2$, or C_3H_4Et	1.991	—		—	—	—	28 lines $A = 0.4$ G	(*109*)
$Cp_2TiCl_2BCl_2$	1.975	—		10.8 G	—	—	$A(^{11}B) = 5.9$ G	(*340, 341*)
$Cp_2TiCl_2GaCl_2$	1.974	—		10.7	—	—	$A(^{69}Ga) = 30.3$	(*341*)
$Cp_2TiCl_2AlCl_2$	1.975	—		11.5 G	—	—	$A(^{27}Al) = 6.9$ G	(*340*)
Cp_2TiPMe_2	1.988	—		10.8 G	—	—	$A(^{31}P) = 20.5$ G	(*385*)
Cp_2TiPPh_2	1.980	—		9.5 G	—	—	$A(^{31}P) = 7.74$ G	(*385*)
$[Cp_2Ti(PMe_2)_2]^-Na^+$	1.992	—		9.0 G	—	—	$2 \equiv A(^{31}P) = 12.7$ G, $A(^{23}Na) = 1.3$ G	(*385*)
$[Cp_2Ti(PPh_2)_2]^-$	1.989	—		9.5 G	—	—	$2 \equiv A(^{31}P) = 9.4$ G	(*385*)
$[Cp_2Zr(PPh_2)_2]^-$	1.989	—		—	—	—	$2 \equiv A(^{31}P) = 11.7$ G	(*385*)

has weak ESR signals. The major products are diamagnetic and the signals in all cases are attributable to free radical intermediates. Titanium h.f.s. are observed (*24*) in the reaction of Cp_2TiCl_2 with $Al(C_2H_5)_3$ and $Al(i\text{-}Bu)_3$. In all other cases (*24, 57, 476, 617, 731*), or where large excesses of aluminum alkyl are used, the h.f.s. arise from ^{27}Al. In these cases bridged structures of the type

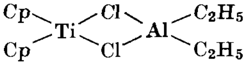

are postulated. The unpaired electron shows no interaction with the titanium nucleus and the very small $A(^{27}Al)$ value suggests it is mainly in a *p* or *d* orbital on the aluminum. In several cases (*24, 476, 617*) further splittings have been interpreted as interaction with two equivalent H atoms. The radical here is thought to involve bridging hydrogen atoms. Other papers concerning the Ziegler-type catalysts are given in references *17, 18, 58, 135, 534, 536, 663.*

Of particular importance is the spectrum obtained from the reaction of Cp_2TiCl_2 with EtMgCl in ether. Hyperfine structure from Ti and from two equivalent H atoms are observed (*107*), the latter being proved conclusively by replacement of the ethyl protons in EtMgCl by deuterium, whereby the 1:2:1 triplet was replaced by a 1:2:3:2:1 quintet. The paramagnetic species was originally thought to be

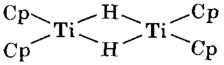

but later Brintzinger (*109*) suggested it was $[Cp_2TiH_2]^-$. He also prepared the corresponding alkyl complexes and some postulated as $[Cp_2TiR\cdot S]^0$ where R = H, CH_3, or C_4H_7 and S is solvent. In addition, π complexes of the type $[Cp_2TiX]^0$ where $X = \pi\text{-}C_3H_5$, $\pi\text{-}C_3H_3Me_2$, or $\pi\text{-}C_3H_4Et$. The Olivés (*339*), however, reduced Cp_2TiCl_2 by Na or Li naphthalide in tetrahydrofuran (THF) and found strong coupling to Na and Li, but no Ti h.f.s. Since there was no evidence of a triplet state, there could not be a Ti^{3+}–Ti^{3+} interaction. They conclude that the species is

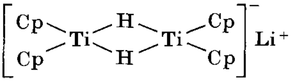

largely because when the reaction is carried out under nitrogen (*108, 339*), the solution shows a 1:2:3:2:1 quintet from two equivalent N atoms with a separation of 2.3 gauss. Complexes of the type Cp_2TiPR_2

and $[Cp_2Ti(PR_2)_2]^-$ yield h.f.s. to Ti and P. (*385*). Corresponding complexes of the type $Cp_2TiCl_2XCl_2$ with X = B, Al, and Ga have been prepared (*340*, *341*) and B, Al, Ga, and Ti h.f.s. observed in each case. The reaction between $Ti(OC_4H_9)_4$ and $Al(C_2H_5)_3$ produces a signal with hyperfine structure comprising 11 lines. This is thought (*28*) to arise from two equivalent Al atoms in an intermediate of the type

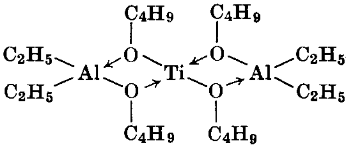

The absence of lines due to Ti makes this formulation improbable.

General trends. A plot of g against A(Ti) is almost linear for all titanium complexes which have strong axial symmetry where h.f.s. are observed (see Fig. 38); g values close to 2 and low A(Ti) values are

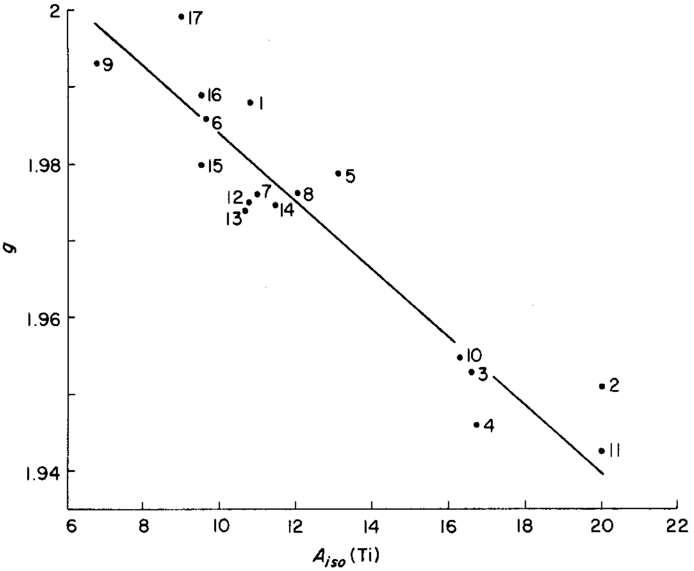

FIG. 38. Plot of g_{av} versus A_{iso} (Ti) for d^1, Ti^{3+} ions with a strong axial distortion. (1) Cp_2TiPMe_2, (2) $[Ti(OMe)_4Cl_2]^+$, (3) $(TiOMe)^{2+}$, (4) $(TiF_2)^+$, (5) Cp_2TiCl, (6) $Cp_2Ti(TDT)$, (7) $Cp_2TiCl_2 + AlEt_3$, (8) $Cp_2TiCl_2 + Al(i\text{-}Bu)_3$, (9) 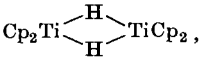 $Cp_2Ti(\mu\text{-}H)_2TiCp_2$, (10) 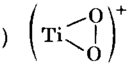 $(Ti\langle O_2 \rangle)^+$, (11) Ti^{3+} in CaF_2, (12) $Cp_2TiCl_2 \cdot BCl_2$, (13) $Cp_2TiCl_2 \cdot GaCl_2$, (14) $Cp_2TiCl_2 \cdot AlCl_2$, (15) Cp_2TiPPh_2, (16) $[Cp_2Ti(PPh_2)_2]^-$, and (17) $[Cp_2Ti(PMe_2)_2]^-Na^+$.

compatable with delocalization of the electron onto the ligands and a lowering of orbital contribution and spin–orbit coupling. The trend to delocalization is associated with chemical species having aromatic constituents and increased covalent bonding (see Section III,C,2).

3. *ESR of Zr^{3+} and Hf^{3+}*

Hyperfine coupling to Zr or Hf has not been detected. Zr^{3+} in silicate glasses (*254*) gives a broad line with $g = 1.906$. Reduction of Cp_2ZrCl_2 with $NaPPh_2$ yields a spectrum suggesting two equivalent phosphorus atoms and is attributable to $[Cp_2Zr(PPh_2)_2]^-$ with $g = 1.989$ and $A(^{31}P) = 11.7$ gauss (*385*).

4. *ESR of V^{4+} and VO^{2+}*

^{51}V is in 99.8% natural abundance and has a nuclear spin $I = \frac{7}{2}$. In fluid solution, eight hyperfine lines are observed exhibiting a variation in linewidth of which Fig. 35 is typical. Hyperfine couplings are large (~100 gauss), but a large nuclear moment and spin cause a large line width which tends to obscure s.h.f.s. A typical anisotropic spectrum of a molecule with axial symmetry is shown in Fig. 39, and the ESR data are summarized in Table XXI.

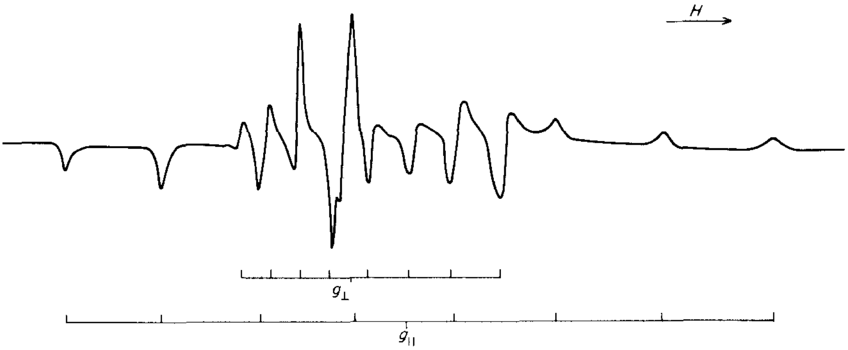

FIG. 39. Frozen solution spectrum of $VO(acac)_2$.

Almost all vanadium compounds have symmetry less than O_h and T_d, and so ESR signals are readily observed because of the longer relaxation time. Spectra of V^{4+} in the host lattices of TiO_2, GeO_2, Al_2O_3, and SnO_2 have been detected (*258, 580, 621*). In the case of SnO_2, s.h.f.s. to Sn were detected (*388*) which are largely isotropic. This system has been reviewed by McGarvey (*504*).

A system of theoretical interest (*572*) is that of VO^{2+} substituted in KNO_3 and $CsNO_3$. It seems probable from the g tensor that the vanadyl

TABLE XXI

ESR DATA FOR d^1 V^{4+} IONS

	g_{av}	$g_{\parallel}$	$g_{\perp}$	$A_{iso}(^{51}V)$ ($10^4 cm^{-1}$)	$A_{\parallel}(^{51}V)$ ($10^4 cm^{-1}$)	$A_{\perp}(^{51}V)$ ($10^4 cm^{-1}$)	$A_{ligands}$ ($10^4 cm^{-1}$)	References
VO^{2+}								
in KNO_3	1.966	1.9352	1.974	116 G	199 G	78 G	—	(*572*)
in $CsNO_3$	1.964	1.919	1.984	115 G	218 G	67 G	—	(*572*)
in GeO_2, amorphous	1.960	1.929	1.976	—	175.5	68.2	—	(*621*)
V^{4+}								
in TiO_2	—	1.915, 1.913, 1.956		—	31, 43, 142		—	(*258, 580*)
in Al_2O_3	—	1.97		—	132		—	(*258*)
in GeO_2, rhombic	—	1.921, 1.921, 1.963		—	36.69, 37.54, 134.36		—	(*621*)
in GeO_2, tetragonal	—	1.929	1.976	—	175.5	68.2	—	(*621*)
in SnO_2	—	1.943, 1.939, 1.903		—	140.3, 21.1, 41.9		(a) $A_x = 166$ G, $A_y = 172.6$ G, $A_z = 165.2$ G(Sn) (b) $A_x = A_y = A_z$ $= 28$ G(Sn)	(*388*)
VO_n, $1.5 < n < 2.5$	~1.96	—	—	—	—	—	—	(*19*)
$[VO(H_2O)_5]^{2+}$								
in Tutton salt	—	1.9331, 1.9813, 1.9801		—	182.28, 71.2, 72.44		$A(^1H) = 2.6$ G	(*100, 448*)
in $RbAl(SO_4)_2 \cdot 12H_2O$	—	1.923	1.975	—	182.2	66.6	—	(*481*)
$VOCl_2$								
in H_2O	—	—	—	117 G	—	—	—	(*250*)
in C_2H_5OH	—	—	—	110 G	~200 G	76 G	—	(*250*)
in acetone	1.962	1.92	1.960	110 G	200 G	76 G	—	(*413*)
in 3 *N* HCl	1.965	1.932	1.981	106.3	182.6	71.8	—	(*406*)
in 12 *N* HCl	1.968	1.933	1.978	101.9	182	70.4	—	(*406*)
	1.968	1.941	1.977	101.9	177.9	69.5	—	(*406*)
in HAc/HCl	1.969	1.944	1.979	101.4	172.9	66.2	—	(*406*)

$[VO(Ox)_2]^{2-}$ in $[TiO(Ox)_2]^{2-}$	1.9624	1.940	1.972	107 G	180 G	65 G	—	*(274, 718)*
$[VOF_5]^{3-}$	1.962	—	—	105.2	—	—	—	*(406)*
$[VO(H_2O)_5]Cl_2$	1.965	—	—	105.6	—	—	—	*(55, 391)*
$[VOF_5]^{3-}/HF/H_2O$	—	—	—	116.0 G	—	—	—	*(427)*
$[VOCl_5]^{3-}$ in $[InCl_5H_2O]^{2-}$	—	—	—	109.4	173	63.8	—	*(171)*
$[VO(CN)_5]^{3-}$	—	—	—	79.9 G	—	—	$A(^{13}C) = 11.3$ G	*(427)*
$[VO(NCS)_5]^{3-}$	—	—	—	104.75 G	—	—	—	*(427)*
$VOSO_4$								
in H_2O	1.961	—	—	115.5 G	—	—	—	*(718)*
in KNCS, $VO(NCS)_n$	1.964	—	—	108.0 G	—	—	—	*(718)*
$VO(acac)_2$								
in CH_3OH	1.9688	—	—	102.35 G	—	—	—	*(74, 303, 690)*
in C_6H_6	1.9695	—	—	108.19 G	—	—	—	*(74, 303, 427, 690)*
in C_5H_5N	1.971	—	—	103.6 G	—	—	—	*(74, 303)*
in CH_3COCH_3	1.968	—	—	106.0 G	—	—	—	*(74, 303)*
in CH_3CN	1.969	—	—	105.3 G	—	—	—	*(74, 303)*
in $C_6H_5NO_2$	1.972	—	—	104.6 G	—	—	—	*(74, 303)*
in CS_2	1.968	—	—	99.5	—	—	—	*(303, 391)*
in $CHCl_3$	1.968	1.948	(1.981)	97.8	106.5	63.5	—	*(303, 391)*
in THF	1.967	1.945	(1.981)	97.5	169.0	61.8	—	*(303, 391)*
in CH_3NH_2	1.967	1.944	(1.982)	95.5	167.4	59.5	—	*(303, 391)*
in NH_3	1.968	1.947	(1.983)	95.0	165.0	59.9	—	*(303, 391)*
$VO(tfac)_2$	1.9693	—	—	110.09 G	—	—	—	*(690)*
in C_5H_5N	1.9704	—	—	107.10 G	—	—	—	*(690)*
$VO(hfac)_2$	—	—	—	112.6 G	—	—	—	*(427)*
$[VO(TIR)]^{2-}$	1.966	—	—	101.5 G	—	—	—	*(719)*
$[VO(TIR)_6]^{6-}$	1.972	—	—	86.0 G	—	—	—	*(719)*
$[VO(SSS)]^{-}$	1.963	—	—	106.0 G	—	—	—	*(719)*
$[VO(SSS)_2]^{4-}$	1.966	—	—	96.5 G	—	—	—	*(719)*
$[VO(malonate)_2]^{2-}$	1.967	—	—	102.0 G	—	—	—	*(718)*

TABLE XXI—*cont.*

ESR DATA FOR d^1 V^{4+} IONS

	g_{av}	$g_{\parallel}$	$g_{\perp}$	$A_{iso}(^{51}V)$ ($10^4 cm^{-1}$)	$A_{\parallel}(^{51}V)$ ($10^4 cm^{-1}$)	$A_{\perp}(^{51}V)$ ($10^4 cm^{-1}$)	$A_{ligands}$ ($10^4 cm^{-1}$)	References
$[VO(phthalate)_2]^{2-}$	1.963	—	—	109.0 G	—	—	—	*(718)*
$[VO(dipy)_2]^{2+}$	1.974	—	—	95.0 G	—	—	—	*(718)*
VO(iminodiacetate)	1.966	—	—	104.0 G	—	—	—	*(718)*
$[VO(EDTA)]^{2-}$	1.967	—	—	102.5 G	—	—	—	*(718)*
$[VO(DTPA)]^{3-}$	1.967	—	—	102.0 G	—	—	—	*(718)*
$[VO(NTA)]^{-}$	1.963	—	—	109.0 G	—	—	—	*(718)*
$[VO(NTA)(OH)]^{2-}$	1.963	—	—	106.5 G	—	—	—	*(718)*
VO(PIDA)	1.966	—	—	105.0 G	—	—	—	*(718)*
$[VO(PIDA)(OH)]^{-}$	1.966	—	—	100.0 G	—	—	—	*(718)*
$VO(picolinate)_2$	1.970	—	—	99.0 G	—	—	—	*(718)*
$[VO(picolinate)_2(OH)]^{-}$	1.968	—	—	96.0 G	—	—	—	*(718)*
$VO(acac)_2 \cdot C_5H_5N$	1.9699	—	—	105.25 G	—	—	—	*(303, 690)*
$VO(acac)_2 \cdot$4-picoline	1.9695	—	—	105.24 G	—	—	—	*(303, 690)*
$VO(acac)_2 \cdot$2-picoline	1.9697	—	—	105.17 G	—	—	—	*(303, 690)*
$VO(acac)_2 \cdot$3,4-lutidine	1.9698	—	—	105.20 G	—	—	—	*(690)*
$VO(acac)_2$.piperidine	1.9699	—	—	105.38 G	—	—	—	(303, 690)
$VO(acac)_2$.3,5-lutidine	1.9698	—	—	105.08 G	—	—	—	(690)
$VO(acac)_2$.2-Me-piperidine	1.9697	—	—	105.95 G	—	—	—	(690)
$VO(acac)_2$.dibutylamine	1.9699	—	—	105.82 G	—	—	—	(303, 690)
$VO(acac)_2.OPPh_3$	1.9692	—	—	105.46 G	—	—	—	(690)
$VO(acac)_2.P(NMe_2)_3$	1.9692	—	—	103 G	—	—	—	(690)

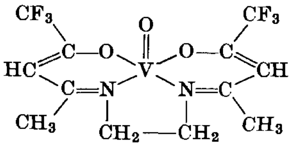

in CH_3CN	1.974	—	—	103.5 G	—	—	—	(*101*)
in THF	1.974	—	—	104.6 G	—	—	—	(*101*)
in C_5H_5N	1.974	—	—	101.0 G	—	—	—	(*101*)
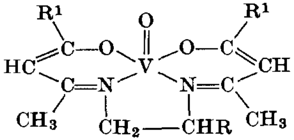								
$R=H, R^1=CH_3$	1.974	1.954	1.984	102.2 G	182 G	62 G	—	(*102*)
$R=CH_3, R^1=CH_3$	1.974	1.954	1.984	102.6 G	183 G	62 G	—	(*102*)
$R=H, R^1=C_6H_5$	1.974	1.952	1.986	102.6 G	183 G	62 G	—	(*102*)
$R=CH_3, R^1=C_6H_5$	1.975	1.957	1.984	103.4 G	182 G	64 G	—	(*102*)
VO(*d*-tartrate)$_2$	1.974	—	—	88.5 G	—	—	—	(*423, 654*)
[(VO-*dl*-tartrate)$_2$]$^{4-}$	1.98	—	—	40 G	—	—	—	(*654*)
VOTPP								
in $CHCl_3$	1.9797	1.966	1.985	89.4	161	55	$A_\parallel(^{14}N)=2.9$ G, $A_\perp(^{14}N)=2.8$ G	(*37, 391*)
in CS_2	1.981	1.965	1.990	91	159	57	$A_\parallel(^{14}N)=2.9$ G, $A_\perp(^{14}N)=2.8$ G	(*37, 391*)
in H_2TPP	(1.979)	1.966	1.985	—	161	55	—	(*37*)
VOPc								
in H_2SO_4	(1.980)	1.965	1.988	—	159	59	—	(*39*)
in H_2Pc	(1.981)	1.966	1.989	—	158	56	—	(*39*)
in ZnPc	—	1.966, 1.993, 1.981		—	158, 55, 52		—	(*39*)
VO etioporphrin I in pet. oil	1.974	1.948	1.987	89	159	52	—	(*541*)
VO etioporphrin II in C_6H_6	1.975	1.947	1.988	89	158	54	—	(*590*)
VO mesoporphrin IX diMe ester	1.975	1.947	1.988	89	158	54	—	(*590*)
VO deuteroporphrin IX diMe ester	1.975	1.947	1.988	89	158	54	—	(*590*)
$V(OC_5H_9)_4$	1.964	1.940	1.984	64	125.0	36	—	(*399*)
$VO(acac)_2+Al(C_2H_5)_3$	1.9915	—	—	46.8 G	—	—	—	(*28, 529*)

TABLE XXI—*cont.*

ESR DATA FOR d^1 V^{4+} IONS

	g_{av}	$g_\parallel$	$g_\perp$	$A_{iso}(^{51}V)$ ($10^4\,cm^{-1}$)	$A_\parallel(^{51}V)$ ($10^4\,cm^{-1}$)	$A_\perp(^{51}V)$ ($10^4\,cm^{-1}$)	$A_{ligands}$ ($10^4\,cm^{-1}$)	References
$V(NEt_2)_4$	1.976	1.946	1.991	−61	−124	−29	—	*(351)*
VCl_4								
in $TiCl_4$, 9° *K*	—	1.920	1.899	—	72 G	120 G	—	*(134, 373)*
4.2° *K*	1.931	1.941	1.915	—	97 G	113 G	—	*(134, 563)*
$+Al(C_2H_5)_3$	—	—	—	60 G	—	—	—	*(530)*
$+Al(C_2H_5)_3$	1.992	—	—	73 G	—	—	—	*(619)*
$+Al(i\text{-}Bu)_3$	1.992	—	—	73 G	—	—	—	*(619)*
$[VCp_2]^{2+}$	1.937	—	—	—	—	—	—	*(257)*
$VOCp_2$	1.99	—	—	75 G	—	—	—	*(495)*
Cp_2VCl_2	1.987	—	—	75 G	—	—	—	*(173, 534)*
in C_6H_6	1.994	—	—	71.2 G	—	—	—	*(5, 134)*
in $CHCl_3$	1.995	—	—	74.1 G	—	—	—	*(5, 134)*
$[Cp_2V(tropolone)]ClO_4$	1.983	—	—	65.9 G	—	—	—	*(188)*
$[Cp_2V(dibenzoylmethane)]^+$	1.985	—	—	74.6 G	—	—	—	*(188)*
Cp_2VCl_2	1.988	—	—	74.3 G	—	—	—	*(188)*
$Cp_2V(N_3)_2$	1.985	—	—	72.0 G	—	—	—	*(188)*
$Cp_2V(CN)_2$	1.999	—	—	60.3 G	—	—	—	*(188)*
$Cp_2V(NCO)_2$	1.985	—	—	76.1 G	—	—	—	*(188)*
$Cp_2V(NCS)_2$	1.991	—	—	73.0 G	—	—	—	*(188)*
$Cp_2V(NCSe)_2$	1.990	—	—	73.6 G	—	—	—	*(188)*
Cp_2VCl_2								
$+Al(CH_3)Cl_2$	1.990	—	—	72 G	—	—	—	*(5)*
$+Al(OCH_3)Cl_2$	1.998	—	—	72 G	—	—	—	*(5)*
$+Al(C_2H_5)Cl_2$	1.990	—	—	72 G	—	—	—	*(5)*
$+Al(OC_2H_5)Cl_2$	1.989	—	—	72 G	—	—	—	*(5)*

$+AlCl_3$	1.988	—	—	72 G	—	—	—	*(5)*
$+AlBr_3$	1.988	—	—	72 G	—	—	—	*(5)*
$+AlI_3$	1.988	—	—	72 G	—	—	—	*(5)*
$+Al(C_2H_5)_2Cl$	1.999	—	—	39.5 G	—	—	—	*(5)*
$+Al(CH_3)_3$	2.001	—	—	44 G	—	—	—	*(5)*
$+Al(C_2H_5)_3$	1.988	—	—	40 G	—	—	—	*(5)*
$+Al(CH_3)_3+O_2$	1.994	—	—	61.5 G	—	—	—	*(5)*
	1.990	—	—	72 G	—	—	—	*(5)*
$+Al(C_2H_5)_3+O_2$	1.992	—	—	62 G	—	—	—	*(5)*
	1.989	—	—	72 G	—	—	—	*(5)*
$+Al(Ph)_3+O_2$	1.988	—	—	72 G	—	—	—	*(5)*
$VO[S_2P(OC_2H_5)_2]_2$	1.980	1.98	1.998	96 G	169 G	60 G	$A_{iso}=A_{\parallel}=A_{\perp}(^{31}P)$ $=50$ G	*(242, 247)*
$VO[S_2CN(C_2H_5)_2]_2$	1.978	1.968	1.989	92 G	168 G	55 G	—	*(242)*
$VOCl_2+NaDTC+HCl$ $+$nonpolar solvent	1.974	1.960	1.948	72 G	139 G	39 G	—	*(242)*
$V(S_2CHOC_4H_9)_2$	1.974	1.960	1.948	72 G	139 G	39 G	—	*(242)*
$[VO(MNT)_2]^{2-}$	1.992	1.975	2.000	70 G	132 G	43 G	—	*(42)*
$[V(S_2C_2Ph_2)_3]^{2-}$	1.9811	—	—	63.9 G	—	—	—	*(168)*
$[V(TDT)_3]^{2-}$	1.9782	—	—	65.8 G	—	—	—	*(168)*
$[V(BDT)_3]^{2-}$	1.9779	—	—	65.2 G	—	—	—	*(168)*
$\{V[S_2C_2(CF_3)_2]_3\}^{2-}$	1.9829	—	—	62.4 G	—	—	—	*(168)*
$[V(MNT)_3]^{2-}$	1.980	1.974	—	63.3 G	100 G	45 G	—	*(167, 168)*
$V(S_2C_2Ph_2)_3$	1.9900	—	—	61.5 G	—	—	—	*(168, 697)*

group is in a four-coordinate site since the g tensor is similar to that for $V(NEt_2)_4$. At room temperature, there is free rotation of the vanadyl group, as manifest by the isotropic spectrum. At lower temperatures, the spectrum becomes anisotropic.

The particular stability and large number of vanadyl complexes is reflected in the number of ESR studies on these systems. Most VO^{2+} complexes have the square pyramid structure and may frequently add on Lewis bases to the sixth coordination position. The VO^{2+} ion has been substituted in various alums (*481*) and the spectrum attributed to $[VO(H_2O)_4]^{2+}$. Substitution in $(NH_4)_2Zn(SO_4)_2 \cdot 6H_2O$ yielded (*100*, *448*) s.h.f.s. attributable to protons from four equatorial water ligands. After subtraction of the dipolar contribution, $A_{iso}(^1H)$ was 2.6 gauss. Bernal (*74*), Kivelson and Lee (*391*), Walker (*690*), Kuska and Rogers (*427*), and Guzy, Raynor, and Symons (*303*) have measured g and $A_{iso}(^{51}V)$ for vanadyl acetylacetonate in numerous solvents and bases. There is a trend to lower A_{iso} values with increase in basicity (because of greater delocalization of the unpaired electron), and the systems are very sensitive to solvation and coordination. There is a close relationship between the energy of the first electronic absorption ($b_2 \rightarrow e_\pi{}^*$) and g_{av} with the solvent parameter E_T. Furthermore, the third transition is now assigned to $e_\pi \rightarrow b_2$ and a shoulder at about 23,600 cm^{-1} appears in solvents which are known to complex in the sixth position and may be used to characterize other such complexes. The large influence that water and alcohols have on the energy of the first electronic transition is attributed to hydrogen bonding with the vanadyl oxygen. The unpaired electron is in the $b_{2g}^*(d_{xy})$ orbital and is localized on the metal, and since this does not interact directly with incoming ligands, it is not surprising that no s.h.f.s. are observed (*391*). It is instructive to compare the decrease in A_{iso} with that of the V═O-stretching frequency (*611*) which also decreases as the basicity of the sixth ligand increases. The same trend (*611*) is observed as the basicity of the chelating ligands is increased, i.e., ν (V═O) decreases in the order hfac > tfac > acac.

Walker *et al.* (*690*) and Kuska and Rogers (*427*) compared the spectra of $VO(acac)_2$ with that of vanadyl trifluoroacetoacetonate and hexafluoroacetoacetonate and observed h.f.s. of 108.19, 110.09, and 112.6 gauss, respectively. The higher $A_{iso}(^{51}V)$ value is associated with greater localization of the electron on the metal because of the increased electrophilic nature of the ligands and consequent reduced covalency of the V—O(chelate) bonds. Solutions of $VOCl_2$ in water, acetone, dilute HCl, and concentrated HCl have A_{iso} values of 117, 110, 115.9, and 110.9 gauss, respectively, showing how the basicity of the primary solvation sphere affects the hyperfine coupling to the vanadium.

A study (*654*) of the VO^{2+}–tartrate system at varying pH has shown that at *p*H 7, the complex is a dimer with the two VO groups bridged by two tetranegative tartrate groups

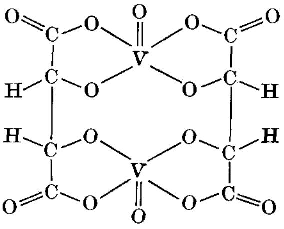

It is noteworthy that the spectrum shows two equivalent ^{51}V nuclei with splitting half that of the ^{51}V in $VO(tartrate)_2$ at higher *p*H. This means that there is rapid electron exchange between the two vanadium nuclei and establishes the type of structure depicted above. This has since been proved by X-ray analysis and the V—V distance shown to be 4.06 Å. Similar dimer formation has been postulated for the vanadyl–citrate system (*190*). Several mixed chelates which have two oxygen and two nitrogen-bonding atoms have been studied (*101*, *102*, *464*). Their ESR parameters are, in general, like those of $VO(acac)_2$.

Vanadyl phthalocyanine (*39*) and substituted vanadyl porphrins (*37*, *391*, *541*, *590*) have been extensively studied. In the case of the tetraphenylporphrin, Kivelson and Lee (*391*) found that the ^{14}N s.h.f. tensor is almost isotropic which indicates that the unpaired electron in the b_{2g}^* orbital is localized mainly on the metal and that in-plane π bonding is slight.

Splitting of the vanadium perpendicular features into A_x and A_y has only been seen in a few cases and arises from the asymmetry of the chelating ligand (*305*). In all these cases $g_{\parallel} < g_{\perp} < 2$ which is in agreement with prediction [see Eq. (58)].

In vanadyl diethyldithiophosphate (*242*, *247*) $VO[S_2P(OC_2H_5)_2]_2$, ^{31}P s.h.f.s. are observed and the tensor is completely isotropic. The coupling to the P atoms must be entirely via a σ interaction. The ^{51}V tensor for this molecule and for $VO[S_2CN(C_2H_5)_2]_2$ are very similar to that of $VO(acac)_2$. In vanadyl maleonitriledithiolate, $VO(MNT)_2$, however, the ^{51}V tensor is much smaller indicating significant delocalization of the electron into the π orbitals on the chelate ring. The vanadium trisditholene complexes are discussed in Section VIII,M,2. The reaction of $VOCl_2$ with sodium diethyldithiocarbamate or potassium butylxanthate in the presence of strong acid followed by extraction into nonpolar solvents produces a species (*242*) whose spectrum has a much lower ^{51}V h.f.s. indicating significant delocalization of the electron over the ligand. The species has axial symmetry (from frozen solution spectrum) and the proposed structures are

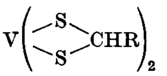

or

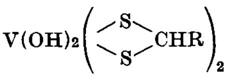

where $R = N(C_2H_5)_2$ or OC_4H_9. The former is considered more probable. No V=O-stretching frequency is seen in the infrared.

In $V(NEt_2)_4$, the symmetry is D_{2d} and the unpaired electron is in a $d_{x^2-y^2}$ orbital (*351*). The g tensor is given by

$$g_{\parallel} = 2 - \frac{8\lambda}{\Delta E(d_{x^2-y^2} - d_{xy})} \tag{127}$$

$$g_{\perp} = 2 - \frac{2\lambda}{\Delta E(d_{x^2-y^2} - d_{xy,yz})} \tag{128}$$

The values of the g and A tensors are very similar to those (*399*) for $V(OBu)_4$. In VCl_4, signals have been detected by two groups of workers (*373*, *563*), one in a $TiCl_4$ host lattice, and the other in fluid solution. In both cases, $g_{\parallel} > g_{\perp}$ which contrasts with the cases above. The difference may be reasonably attributed to changes in ΔE which could have a large effect on $g_{\parallel}$ and $g_{\perp}$. In all these cases, the distortion seems to be due to a Jahn–Teller effect. The theory of the d^1 ion in this symmetry has been given by Griffiths (*298*, pp. 280, 284, and 437).

The g value (*5*, *134*, *173*, *188*, *534*) in Cp_2VCl_2 is close to free spin indicating considerable delocalization of the electron onto the ligands. The absence of h.f.s. in the spectrum (*257*) of $[VCp_2]^{2+}$ prevents useful comparison with the above molecule. The ESR spectrum of catalysts formed by the interaction of VCl_4 or Cp_2VCl_2 with aluminum alkyls shows (*5*, *530*, *619*) extensive delocalization of the electron (g close to 2), although no ^{27}Al h.f.s. are observed, unlike the corresponding titanium complexes. A remarkably small ^{51}V h.f.s. was observed by Angelescu *et al.* (*28*) (46.8 gauss) in the system $VO(acac)_2/Al(C_2H_5)_3$. These workers feel that the complex has a sandwich structure involving the toluene solvent. Nasirov (*529*) believes the species is V^{2+} with the $Al(C_2H_5)_3$ bonded to the O atom in each acetylacetonate ring. Neither formulation is convincing.

Kraus and Deffner (*416*) have investigated the charge transfer complexes between $VOCl_3$ and various aromatic compounds and find that with *p*-xylene, benzophenone, and toluene ESR spectra are obtained which show some ^{51}V h.f.s.

General trends. As with titanium, a plot of g against $A(^{51}V)$ is roughly linear for vanadyl complexes. Complexes of vanadium of approximately cubic symmetry (i.e., O_h or T_d) lie on another straight line with lower g values. The different trend for $VO(acac)_2$ in various solvents has been discussed by Guzy *et al.* (*303*). A plot of g_{av} versus A_{iso} (^{51}V) is given in Fig. 40 and may be accounted for by variations in the spin polarization of inner s electrons (see Section III,C,2).

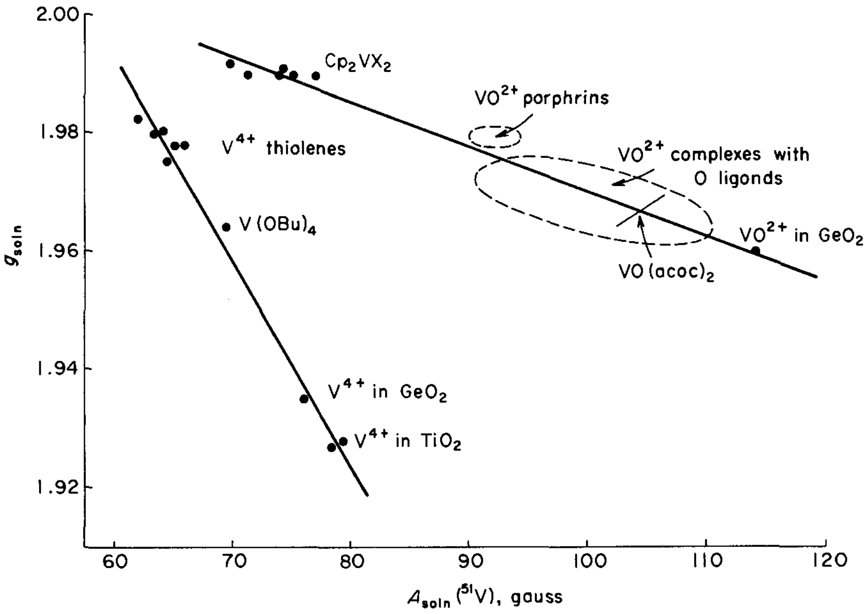

FIG. 40. Plot of g_{av} versus A_{iso} (^{51}V) for a series of vanadium complexes.

5. *ESR of* Nb^{4+} *and* Ta^{4+}

Little information (Table XXII) is known about the ESR of Nb^{4+} and Ta^{4+} because of the comparatively few complexes known. Data are available for the chemical systems $[Nb(OCH_3)Cl_5]^{2-}$, electrically reduced $NbCl_5$ in alcohols saturated with HCl, and $NbCl_4$. It is thought (*437*) that the species in reduced $NbCl_5$ is $[NbCl_6]^{2-}$, but since the ESR parameters are so similar to $[Nb(OCH_3)Cl_5]^{2-}$, it may be $[Nb(H_2O)Cl_5]^{2-}$. The symmetry of $[NbCl_6]^{2-}$ is too high for spectra to be seen even at 77°K. In these two cases, $g_{\parallel}$ is surprisingly large and greater than $g_{\perp}$ (unlike V^{4+}). This could be accounted for if the separation between the b_{1g} and b_{2g} levels is less than the b_{2g} and b_{1g}^* levels (c.f. Cr^{5+}). The increased deviation of g from free spin compared with vanadium arises from increased spin–orbit coupling. Species attributable (*231*) to $NbO(acac)_2$,

TABLE XXII

ESR DATA FOR d^1 Nb^{4+} IONS

Ion	g_{av}	$g_{\parallel}$	$g_{\perp}$	$A_{iso}(^{93}Nb)$ (gauss)	$A_{\parallel}(^{93}Nb)$ (gauss)	$A_{\perp}(^{93}Nb)$ (gauss)	$A_{\text{other atoms}}$ (gauss)	References
Nb^{4+}								
in ZrO_2	—	1.862	1.908	—	309	138	—	(*615*)
in Silicates	—	1.89	1.92	—	310	145	—	(*723*)
$NbCl_4$ in C_2H_5OH	—	1.82	1.80	—	270	146	—	(*210*)
$[NbCl_6]^{2-}$ in CH_3OH	1.892	1.925	1.892	177.4	275	131	—	(*437*)
$[Nb(OCH_3)Cl_5]^{2-}$	1.869	1.923	1.842	178	248	144	—	(*573*)
$[Et_4N]_3[Nb_6Cl_{12}]Cl_6$ in CH_3NO_2	1.948	—	—	20.6	—	—	—	(*468*)
$NbO(acac)_2$	1.906	1.903	1.964	159	249	108	—	(*231*)
$[NbOCl_4]^{2-}$	—	1.943	1.932	—	260	122	—	(*231*)
$[NbOF_4]^{2-}$	—	1.897		—	215		—	(*231*)
$[NbO_4]^{2-}$ in $CaMoO_4$ (γ-irradiated)	—	2.0061, 2.0146, 2.0480		—	−25.5, −28.5, −30.5		$A_{iso}(Mo) = 2.2$ (not d^1)	(*200*)

$[NbOCl_4]^{2-}$, and $[NbOF_4]^{2-}$ have been prepared by Zn/acid reduction of $NbCl_5$ plus acetylacetone, $NbCl_5$, and NbF_5, respectively. The acetylacetonate was extracted with chloroform and the ESR parameters are as expected for an axially symmetric niobyl complex.

Well-resolved ^{93}Nb h.f.s. are observed (*468*) in solutions of $[Et_4N]_3[Nb_6Cl_{12}]Cl_6$. The cluster complex cation has one unpaired electron ($\mu = 1.615$ B.M.) and the splitting is only 20.6 gauss, less than one-sixth that of the splitting in other niobium complexes containing only one metal nucleus. Forty-nine of a possible 55 lines arising from interaction with six equivalent Nb atoms ($I = \frac{9}{2}$) are observed. This suggests that the electron is delocalized over the whole cation interacting equally with each niobium. The 15 metal electrons are likely to be in the following molecular orbitals in O_h local symmetry: A_{1g}^2, T_{1u}^6, T_{2g}^6 and A_{2u}^1 using the scheme devised by Kettle (*386*) and improved by Schneider and MacKay (*606*). The unpaired electron is in a delocalized orbital of a_{2u} symmetry which may be described as made up of metal d_{xy} orbitals and is involved only with metal–metal bonding. A thorough analysis of the electronic spectra of the cluster compounds of formulas $[Nb_6Cl_{12}]^{2+}$, $[Nb_6Cl_{12}]^{3+}$, and $[Nb_6Cl_{12}]^{4+}$, is given by Schneider and MacKay (*606*).

Niobium hyperfine splittings are observed (*200*) in γ-irradiated $CaMoO_4$ containing Sm and Nb. The low value of the niobium h.f.s. and the observation of s.h.f.s. to Mo suggest that the unpaired electron is largely located on the oxygen atoms in a t_1 molecular orbital. γ-Irradiation causes loss of an electron from the diamagnetic parent molecule, and so the species cannot be described as d^1. It is included here for convenience.

6. *ESR of* Cr^{5+}

Since ^{53}Cr, the only isotope with nuclear spin ($I = \frac{3}{2}$) is present in only 9.54% natural abundance, the spectrum in fluid solution consists of a strong line flanked by weak satellite lines. Often the width of the main line hides the inner pair of satellite lines. The spectrum of the $[CrO_8]^{3-}$ ion is shown in Fig. 41.

Almost all Cr(V) complexes contain oxygen and ESR data are known for many of these (see Table XXIII). Many of the compounds have unusually large $g_\parallel$ values which are greater than $g_\perp$ as against expectation (see Section IV,D). Kon and Sharpless (*404*) and Gray, Bernal, and Hare (*288*, *313*) have explained the unusually large value of $g_\parallel$ in terms of the energies of electron transitions in $[CrOCl_5]^{2-}$. The unpaired electron is in the $b_2(d_{xy})$ molecular orbital (see Fig. 42) and the expected transitions

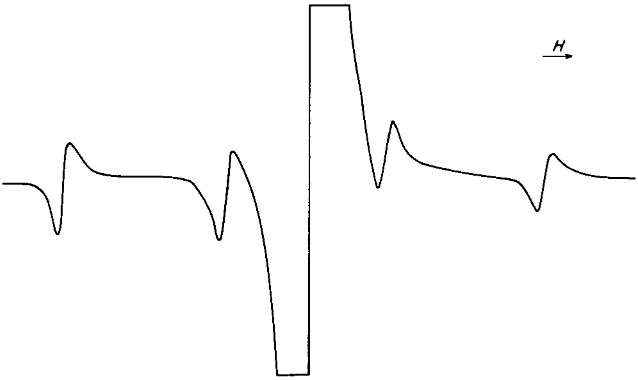

FIG. 41. ESR spectrum of $[CrO_8]^{3-}$ in water showing weak absorptions due to interaction with ^{53}Cr and a strong central line due to interaction with ^{50}Cr, ^{52}Cr, and ^{54}Cr.

are 1 and 2 (12,900 and 23,500 cm^{-1}). An additional transition 3 is also seen at 18,300 cm^{-1}. $_{\perp}$ and $g_{\parallel}$ are given by the following equations

$$g_{\perp} = 2.0023 - \frac{2\lambda}{\Delta E(e^* - b_2)} \tag{129}$$

$$g_{\parallel} = 2.0023 - \frac{8\lambda}{\Delta E(b_1{}^* - b_2)} + \frac{8\lambda}{\Delta E(b_2 - b_1)} \tag{130}$$

Since the b_1 level is closer to b_2 than $b_1{}^*$, there is theoretically a positive Δg shift for $g_{\parallel}$ and this is shown to be so in $[CrOCl_5]^{2-}$ where $g_{\parallel} = 2.008$, and almost so in $[CrOCl_4]^{2-}$ where $g_{\parallel} \sim 1.99$ ($>g_{\perp}$). This situation is also found in the corresponding Mo^{5+}, W^{5+} and Nb^{4+} ions.

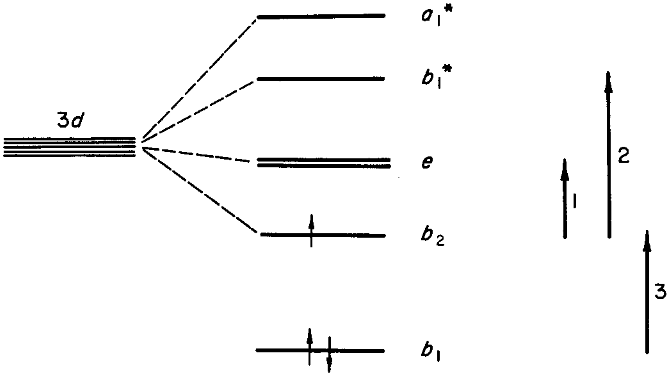

FIG. 42. Energy levels in $[CrOCl_5]^{2-}$, showing the three electronic transitions. The b_1 molecular orbital is bonding and the unpaired electron is in b_2.

TABLE XXIII

ESR DATA FOR d^1 Cr^{5+} IONS

Ion	g_{av}	$g_{\parallel}$	$g_{\perp}$	$A_{iso}(^{53}Cr)$ (10^4 cm^{-1})	$A_{\parallel}(^{53}Cr)$ (10^4 cm^{-1})	$A_{\perp}(^{53}Cr)$ (10^4 cm^{-1})	$A_{ligands}$ (10^4 cm^{-1})	References
$[CrOCl_5]^{2-}$	1.9877	2.008	1.974	18.3	36.1	(9.7)	$A_{\perp}(Cl) = 7.8$, $A_{\parallel}(Cl) = 0$	(*404, 405*)
in 20% HCl	1.986	1.995	1.937	19 G	—	—	—	(*235*)
$H[CrOCl_4]$	—	1.9883	1.9792	19.9	—	—	—	(*404*)
$[C_5H_6N][CrOCl_5]$	1.9877	2.008	1.974	19.9	—	—	—	(*403*)
CrO_3 in 20% HF	1.960	—	—	—	—	—	$A_{iso}(^{19}F) = 6$ G; $A_{\perp}(^{19}F) = 40$ and 22 G	(*6, 235*)
$[Cr_2O_7]^{2-}$ in glycerol	(1.976)	1.99	1.97	(20) G	37 G	12 G	—	(*233*)
CrO_3 in 70% H_2SO_4	1.966	1.969	1.976	28 G	—	—	—	(*235*)
$[Cr_2O_7]^{2-}$								
in 65% oleum	1.964	1.951	1.970	—	—	—	—	(*517*)
	1.964	1.936	1.986	—	—	—	—	(*517*)
in 30 and 100% oleum	1.970	—	—	23 G	—	—	—	(*517*)
	1.965	—	—	23 G	—	—	—	(*517*)
$[CrO_4]^{3-}$ in alkali	—	1.98	1.97	—	—	—	—	(*120*)
$K_3CrO_8 + H_2O_2$	1.973	1.951	1.985	19 G	—	—	—	(*235*)
$[CrO_8]^{3-}$	—	1.936	1.983	—	—	—	—	(*648*)
in $[NbO_8]^{3-}$	—	1.9434	1.9848	—	11 G	—	—	(*499*)
$[Cr(S_2C_2Ph_2)_3]^-$	1.996	—	—	19 G	—	—	—	(*697*)
$Cr[S_2C_2(CF_3)_2]_3^-$	1.9941	1.995	1.995	16.3 G	—	—	—	(*167*)
Cr(V) in ethylene glycol	1.981	—	—	17.6 G	35 G	8.9 G	$A(^1H) = 0.64$ G	(*246*)
$CrO[TDT]_2$	1.994	—	—	14.9	—	—	—	(*640*)

Chlorine s.h.f.s. are observed (*405*) in the $[CrOCl_5]^{2-}$ ion and are very anisotropic. Since the electron is largely in a metal d_{xy} orbital, most of the effect may be explained as a dipolar interaction between the d_{xy} electron and a $3p$ orbital on chlorine giving strong in-plane π bonding (unlike vanadyl porphrins where such π bonding is minimal). Fluorine s.h.f.s. are seen (*235*) in $[CrOF_5]^{2-}$ solutions (CrO_3 in HF) and are the same order of magnitude as the Cl s.h.f.s., although there appear to be two different pairs of fluorine atoms (*6*).

Chromates in oleums of various strengths produce paramagnetic species (*235, 517*) where there is much less electron delocalization. Several species appear to be formed, but their structure is not known.

In dodecahedral symmetry, the ground state is singly degenerate, $B_2(d_{xy})$ and spectra are readily seen. The $[CrO_8]^{3-}$ ion approximates to this symmetry (D_{2d}). The ground state configuration is readily proved (*499*) to be B_2 by inspection of the g tensor, since the only reasonable alternative is the A_1 ground state. Here

$$g_{\parallel} = 2.0023 \qquad \text{and} \qquad g_{\perp} = 2.0023 - \frac{6\lambda}{\Delta E(e - a_1)} \tag{131}$$

but for the B_2 ground state

$$g_{\parallel} = 2.0023 - \frac{8\lambda}{\Delta E(b_2 - b_1)} \tag{132}$$

$$g_{\perp} = 2.0023 - \frac{2\lambda}{\Delta E(e - b_2)} \tag{133}$$

Since $g_{\parallel} < g_{\perp} < 2$, the B_2 state is preferred. Taking $\Delta E(e - b_2) = 20{,}000$ cm^{-1}, λ is 175 cm^{-1} which is much smaller than the free ion value for Cr^{5+} (350 cm^{-1}). This reduction in the spin–orbit coupling constant indicates considerable covalent character in the complex. Further calculations (*648*) confirm that one O atom is nearer the Cr than the other O atom of the O—O group.

Cr(V) solutions in ethylene glycol (*246*) yield proton hyperfine coupling from eight equivalent protons, suggesting a structure

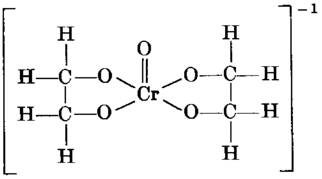

The dithiolene complexes are discussed in Section VIII,M,2.

7. *ESR of Mo^{5+} and W^{5+}*

The low symmetry of most Mo(V) and W(V) complexes splits the ground state and ESR spectra are readily observed. Both ^{95}Mo and ^{97}Mo have nuclear spin $I = \frac{5}{2}$ and their natural abundance is 15.8 and 9.6%, respectively. The nuclear magnetic moments are similar and the sextet of lines observed for each isotope in solution (in addition to the strong central line) overlap to give a broadening. ESR data are given in Tables XXIV and XXV. Most work has been carried out on halide complexes where s.h.f.s. are observed (*6*, *239*, *406*) in, e.g., $[MoOF_5]^{2-}$, $[MoOBr_5]^{2-}$, $[WOF_5]^{2-}$, and $[WOBr_5]^{2-}$ and in an uncharacterized ion found (*251*) when $Mo_2O_3(SO_4)_2$ is dissolved in H_2SO_4 in the presence of KCl. The spin density on each of the four equatorial Br atoms in $[MoBr_5]^{2-}$ and $[WOBr_5]^{2-}$ are 4.3–5.8% and 3.2–5.9%, respectively (*406*). Less delocalization is found in the tungsten complex, which is compatible with the increase in effective nuclear charge of the metal compared with molybdenum. This is supported by the lower g value which is indicative of larger spin–orbit coupling.

Dowsing and Gibson (*185*) have made a thorough study of the species present in HBr solutions of Mo(V). The solutions are not analogous to HCl solutions. At 9.4 M HBr, the species present is mainly $[MoOBr_5]^{2-}$. In 6 M acid, the species is different, but not characterized. A third unidentified species is thought to be present also. $[Et_4N][MoCl_6]$ is interesting in that it shows a spectrum (*185*) at room temperature. There must be a very large distortion (more than a few thousand cm^{-1}) to reduce the triple degeneracy of the ground state to leave an orbital singlet. There is spectroscopic evidence for such a distortion (*111*). Verbeek *et al.* have studied these systems from a more theoretical viewpoint (*673*, *684*, *685*) Mo h.f.s. are observed (*459*) for Mo(V) in K_2SnCl_6, but no chlorine s.h.f.s., although the line width is <14 gauss. Covalency is presumably small because of the small Cl coupling. Ryabchikov and Marov *et al.* (*483*, *596*, *598*) have studied mixed halide species of the type $MoOX_mY_n$. Each species is characterized by a different g value and usually Mo and ligand h.f.s. are observed particularly where fluorine is a ligand. Stepwise addition of ligands seems to occur, but the exact nature of the products is not known. The structure and interrelationship between species formulated in solution such as $MoOCl_3$, $[MoOCl_4]^-$, and $[MoOCl_5]^{2-}$ are not clear although one or other of the latter two is favored. Solutions of $[MoOCl_5]^{2-}$ in HCl varying from 12 → 2 M show a large variation in strength of ESR signal, which almost disappears at <4 *M*. Hare *et al.* (*313*) propose that the ion is a monomer in strong acid solutions (12 *M*). At about 6 *M*, a paramagnetic oxygen-bridged dimer exists and at lower *p*H, a diamagnetic dimer exists. This

TABLE XXIV: ESR OF d^1 Mo^{5+} IONS

Ion	g_{av}	$g_{\parallel}$	$g_{\perp}$	A_{iso}(Mo) (10^4 cm^{-1})	$A_{\parallel}$(Mo) (10^4 cm^{-1})	$A_{\perp}$(Mo) (10^4 cm^{-1})	$A_{ligands}$ (10^4 cm^{-1})	References
$[MoOF_5]^{2-}$ in 30% HF	1.906	1.874	1.918	70 G	114 G	54 G	$A_{iso}(^{19}F) = 11$ G, $A_{\perp}(^{19}F) = 55$ and 30 G	*(6, 239)*
$[MoOCl_5]^{2-}$	1.947	1.96	1.938	58 G	89 G	49 G	—	*(185, 237, 596)*
in $(NH_4)_2[InCl_5(H_2O)]$	(1.948)	1.9632	1.9400	(47)	74.7	32.6	—	*(15, 171, 406)*
in $K_3InCl_6 \cdot 2H_2O$	(1.943)	1.951	1.939	—	79	38.5	—	*(549)*
	(1.945)	1.959	1.939	—	77	38.5	—	*(549)*
$[MoOCl_4Br]^{2-}$	1.960	—	—	48 G	—	—	—	*(596)*
$[MoOCl_3Br_2]^{2-}$	1.970	—	—	47 G	—	—	—	*(596)*
$[MoOCl_2Br_3]^{2-}$	1.983	—	—	45 G	—	—	—	*(596)*
$[MoOBr_5]^{2-}$	1.993	2.090	1.945	41.7	66.0	30	$A_{\parallel}(Br) \leqslant 6.5$, $A_{\perp}(Br) = 35.9$	*(185, 406, 596)*
$[MoOCl_4]^-$	1.950	—	—	—	—	—	—	*(483)*
$[MoOBr_4]^-$	1.994	—	—	—	—	—	—	*(483)*
$[MoOI_4]^-$	2.058	2.258	1.97	—	—	—	—	*(483)*
$[MoOI_3Cl]^-$	2.033	—	—	—	—	—	—	*(483)*
$[MoOI_2Cl_2]^-$	2.000	—	—	—	—	—	—	*(483)*
$[MoOICl_3]^-$	1.978	—	—	—	—	—	—	*(483)*
$[MoOI_3Br]^-$	2.045	—	—	—	—	—	—	*(483)*
$[MoOI_2Br_2]^-$	2.030	—	—	—	—	—	—	*(483)*
$[MoOIBr_3]^-$	2.009	—	—	—	—	—	—	*(483)*
$[MoO(NCS)_5]^{2-}$	1.935	1.928	1.944	50 G	76 G	38 G	—	*(5, 244)*
$MoOCl_3$								
in EtOH	1.945	1.965	1.940	56 G	83 G	52 G	—	*(238, 733)*
in 20% HCl	1.949	—	—	52 G	—	—	—	*(251)*
$Mo_2O_3(SO_4)_2$								
in H_2SO_4	1.925	—	—	62 G	—	—	—	*(251)*
in H_2SO_4 + KCl	1.935	—	—	54 G	—	—	$A_{iso}(Cl) = 10$ G	*(251)*

$(Et_4N)[MoCl_6]$	—	1.977	1.935	—	—	—	—	*(185)*
Mo(V) in K_2SnCl_6	(1.950)	1.9739	1.9386	(48.9 G)	76.6 G	35.0 G	—	*(459)*
trans-$(C_5H_6N)[Mo(OCH_3)_2Cl_4]$	1.9453	1.9673	1.934	46.93	75.1	33.0	—	*(493)*
$MoOX_5 + S(SH)P(OC_2H_5)_2$								
X = F^-, Br^-, $(SO_4)^{2-}$	1.970	2.001	1.955	44 G	64 G	29 G	(^{31}P) $A_{iso} = 44$ G, $A_{\parallel} = 38$ G, $A_{\perp} = 40$ G	*(245)*
X = Cl^-	—	1.992	1.949	—	—	—	$A(Cl) = 9$ G, $A(^{31}P) = 39$ G	*(245)*
$\{(NH_4)_2[(OH)_2OCl_2Mo]_2\}^-$	—	1.969, 1.943, —		—	—	—	—	*(372)*
γ-irrad. $Mo_7O_{24}(NH_4)_6 \cdot 4H_2O$	(1.921)	1.915	1.924	(54 G)	78 G	42 G	—	*(554)*
$[Mo(CN)_8]^{3-}$ in glycerine	1.9920	1.9981	1.9889	30.7	14.0	39.1	$A(^{13}C) = 10.9$	*(320, 503, 702)*
$[Mo(CN)_8]^{3-}$ in $K_4Mo(CN)_8$	1.9848	1.9779	1.9882	—	—	—	—	*(503)*
Mo^{5+}								
in TiO_2	(1.842)	1.8155, 1.7923, 1.9167		(45.9)	24.32,[a] 30.48,[a] 65.08[a]		(Ti) $A_x = 2.8$, $A_y = 3.4$, $A_z = 3.1$	*(432, 670)*
in $CaWO_4$	(1.920)	1.987	1.887	(34.1)	8.39[a]	41.18[a]	—	*(47)*
$[Mo(S_2C_2Ph_2)_3]^-$	2.011	—	—	11.2 G	—	—	—	*(697)*
$Mo[S_2C_2(CF_3)_2]_3^-$	2.0097	2.011	2.009	12.2 G	17.4 G	9.6 G	—	*(167)*
$Mo_2(TDT)_5$	1.999	—	—	32 G	—	—	—	*(116)*
$[Mo(SCN)_6]^-$	1.940	—	—	49 G	—	—	$A(^{14}N) = 2.1$ G	*(597)*
$[MoO(H_2AsO_4)_4]^-$	1.916	1.898	1.925	61	—	—	$A(^{75}As) = 13$	*(484)*
$[SiMO_{12}O_{40}]^{n-}$ reduced	—	1.94		—	—	—	—	*(569)*
Mo^{5+}								
in H_3PO_4								
monomer	1.914	1.891	1.925	58 G	90 G	42 G	—	*(485)*
dimer	1.922	1.902	1.930	55 G	87 G	39 G	$A(^{31}P) = 5.1$ G	*(485)*
in H_2SO_4								
monomer	1.919	1.881	1.938	57.5 G	92 G	40 G	—	*(485)*
dimer	1.926	1.894	1.942	56 G	85.5 G	41 G	—	*(485)*
$[Cp_2MoCl_2]^+$	1.998	—	—	36 G	—	—	$A(Cl) = 3.3$ G	*(145)*
$[Cp_2MoBr_2]^+$	2.053	—	—	36 G	—	—	$A(Br) = 15.8$ G	*(145)*

[a] ^{95}Mo.

TABLE XXV

ESR OF d^1 W^{5+} IONS

Ion	g_{av}	$g_{\parallel}$	$g_{\perp}$	$A_{iso}(^{183}W)$ (10^4 cm^{-1})	$A_{\parallel}(^{183}W)$ (10^4 cm^{-1})	$A_{\perp}(^{183}W)$ (10^4 cm^{-1})	$A_{ligands}$ (10^4 cm^{-1})	References
$[WOF_5]^{2-}$	—	1.589	1.767	—	—	—	$A_{\perp}(^{19}F) = 64$ and 42 G	*(6)*
$[WOCl_5]^{2-}$	1.773	1.804	1.758	—	127	—	—	*(406)*
$[WOBr_5]^{2-}$	1.830	1.940	1.775	—	91	—	$A_{\perp}(Br) = 33.5$	*(406)*
$K_2[WO(NCS)_5]$	1.803	1.775	1.819	—	156 G	—	—	*(244)*
WCl_5								
in glycerol	1.754	1.79	1.757	(172)	216 G	>150 G	—	*(236)*
in HCl	1.745	1.78	1.756	(173)	220 G	>150 G	—	*(236)*
in C_2H_5OH	1.743	1.79	1.718	—	148 G	—	—	*(236)*
$[W(CN)_8]^{3-}$								
in glycerine	1.9724	1.9819	1.9677	51.9	18.7	68.5	—	*(320, 503, 703)*
in $K_4W(CN)_8$	1.963	1.942	1.973	—	—	—	—	*(503)*
W^{5+} in phosphates	1.716	1.604	1.763	220 G	—	—	—	*(724)*
γ-irrad. $CaWO_4$	(2.014)	2.0010, 2.0065, 2.0354		(9) G	9 G, 9 G, 9 G		—	*(732)*
	(1.684)	1.5716, 1.6334, 1.8482		—	Varies 35 → 65 G		—	*(732)*
$[W(S_2C_2Ph_2)_3]^-$	1.992	—	—	—	—	—	—	*(697)*
$W[S_2C_2(CF_3)_2]_3^-$	1.9910	1.987	1.993	—	—	—	—	*(167)*
W^{5+} in TiO_2	—	1.4725, 1.4431, 1.5944		—	40.8, 63.7, 92.5		$A(^{49}Ti) = 1.8, 1.8, 2.1$	*(129)*
$[Cp_2WCl_2]^+$	1.951	—	—	—	—	—		*(145)*
$[Cp_2WBr_2]^+$	2.013	—	—	—	—	—	$A(Br) = 23.35$ G	*(145)*

hypothesis explains the susceptibility data of Sacconi and Cini (*599*) and the electronic spectra of Haight (*306*). A Mo(V) species formulated as $[O(OH)_2Cl_2Mo{-}MoCl_2(OH)_2O]^{2-}$ with a Mo—Mo bond yields a poorly resolved spectrum (*372*) with no hyperfine structure. Marov *et al.* (*485*, *486*) suggest that Mo^{5+} in H_2SO_4 and H_3PO_4 can exist as a monomer and a $(SO_4)^{2-}$- or $(PO_4)^{3-}$-bridged dimer.

The reaction of $MoOX_5$ in halogen acids with dithiodiethylphosphate in ether produces (*245*) a spectrum attributed to $[X_5Mo{-}S{-}P(SH)(OC_2H_5)_2]$. ^{31}P s.h.f.s. are observed which are almost isotropic and approximate to ~10% electron density on the P atom. Where X = Cl, the spectrum is more confusing and both Cl and P s.h.f.s. are seen. The infrared spectrum shows no Mo—O bond. Although in $[Mo(NCS)_6]^{3-}$, infrared spectra (*447*) suggest that the NCS^- group bonds via N, Ryabchikov *et al.* (*597*) believe that in the corresponding Mo(V) complex, the low $A(^{14}N)$ value of 2.1 gauss suggests that there is a Mo—S bond with electron delocalization covering the whole ligand. This seems worthy of further investigation, as also (*15*, *244*) does the complex $[MoO(SCN)_5]^{2-}$.

Several species are observed (*484*) of the type $[MoOL_xM_{4-x}]^-$ in a solution of Mo(V) with mixtures of H_3AsO_4 and HCl. Arsenic as well as molybdenum h.f.s. are observed in the complex thought to be $[MoO(H_2AsO_4)_4]^-$.

The 8-coordinate ions $[Mo(CN)_8]^{3-}$ and $[W(CN)_8]^{3-}$ have been studied (*320*, *503*, *702*, *703*) in detail. The spectrum of $[Mo(CN)_8]^{3-}$ is

FIG. 43. ESR spectrum of $K_3[Mo(CN)_8]$ in H_2O. The large central line in the spectrum is from the nonmagnetic isotopes; the six smaller lines are the spectra from isotopes 95 and 97. The two small peaks on either side of the main peak are due to hyperfine interaction with ^{13}C in the cyanide ion which has $I = \frac{1}{2}$. Although the abundance of ^{13}C is only 1.1%, the ratio of $[Mo(CN)_8]^{3-}$ with one ^{13}C to that with none is 0.089, resulting in two ^{13}C hyperfine lines whose intensity is 4.5% that of the central line.

shown in Fig. 43. The crystal structure (*343*) of the diamagnetic analog $K_4Mo(CN)_8 \cdot 2H_2O$ shows that the ion has a dodecahedral structure belonging to D_{2d} symmetry. The structure of the d^1 ions is not known, but the power of ESR is apparent in the ability of the technique to determine the point group of this ion unambiguously. Considering (*320*, *503*) the two most likely structures, square antiprism D_{4d} and dodecahedral D_{2d}, crystal field theory predicts the ordering of the energy of the d orbitals as given in Fig. 44, where the axes are defined as in Fig. 45. The predicted g values are

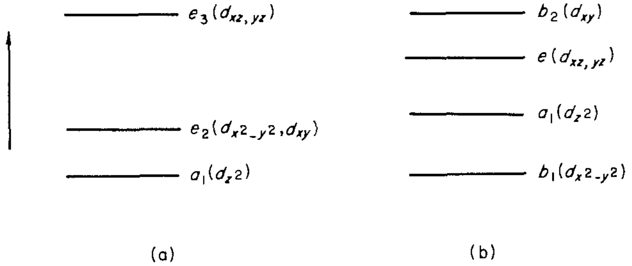

FIG. 44. Energy levels for eight-coordination. (a) D_{4d}, Archimedian square antiprism; (b) D_{2d}, dodecahedral.

D_{4d} symmetry.

$$g_{\parallel} = 2 \tag{134}$$

$$g_{\perp} = 2 - \frac{6\lambda}{\Delta E(e_2 - a_1)} \tag{135}$$

$$\therefore \quad g_{\parallel} > g_{\perp}$$

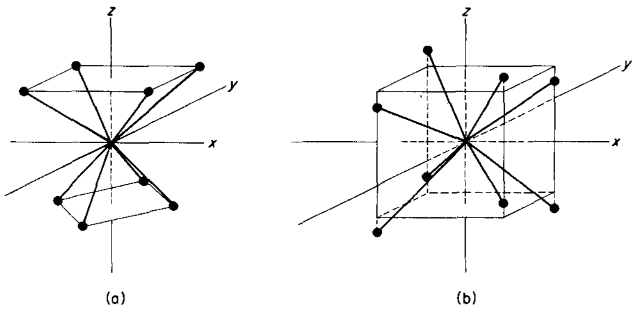

FIG. 45. Eight-coordination. (a) Archimedian square antiprism; (b) dodecahedral.

For D_{2d} symmetry

$$g_{\parallel} = 2 - \frac{8\lambda}{\Delta E(b_2 - b_1)} \tag{136}$$

$$g_{\perp} = 2 - \frac{2\lambda}{\Delta E(e - b_1)} \tag{137}$$

$$\therefore \quad g_{\parallel} < g_{\perp}$$

The observed g values for the ion in a random solvent matrix and in a $K_4Mo(CN)_8 \cdot 2H_2O$ host lattice show that the ion in the former has D_{4d} and, in the latter, D_{2d} symmetry. Thus dodecahedral symmetry has been forced upon the ion in the host lattice, but the crystal field is relaxed in solution and the square antiprism structure becomes more stable. Support for the assignments of solid $[Mo(CN)_8]^{4-}$ being D_{2d} and its aqueous solution being D_{4d} have since come from the Raman spectra of these compounds (*553*). The same authors conclude that solid $[Mo(CN)_8]^{3-}$, however, has D_{4d} symmetry. The corresponding tungsten compounds have the same symmetry. Adams (*16*) has reviewed the infrared and Raman evidence for $[M(CN)_8]$ systems. Weissman and Cohn (*702*) found that in solution the isotropic coupling constant to ^{13}C was nearly identical for all eight CN ligands, thus supporting D_{4d} symmetry where all the CN groups are equivalent. Confirmation of the $A_1(d_{z^2})$ ground state for the square antiprism structure comes from the metal hyperfine tensor for the Mo complex which is $|-16, +8, +8|$, of the form $|-2B, +B, +B|$, which is required for an electron in a d_{z^2} orbital. Exactly the same phenomena (*503*) occur with the corresponding W complex, where the tensor is $|-36.4, +18.2, +18.2|$. A similar tensor is found for Mo^{5+} in $CaWO_4$ (*47*) where $A_{\perp} > A_{\parallel}$ in contrast to Mo^{5+} in TiO_2 (*432, 670*) where $A_z > A_x \sim A_y$. The effect of the crystal field upon the Mo in these two host lattices must be totally different. In $CaWO_4$, the Mo^{5+} replaces Ca^{2+} ions with coordination number 8, whereas in TiO_2, the Mo^{5+} replaces Ti^{4+} ions with a coordination number 6. ESR signals have been detected (*623*) in hydrogen tungsten bronze $H_{0.1}WO_3$, a single line at $g = 1.97$ being obtained. The dithiolene complexes of Mo and W are discussed in Section VIII,M,2.

Some cyclopentadienyl complexes of molybdenum and tungsten yield h.f.s. and s.h.f.s. to halogens (*145*). These are $[Cp_2MX_2]^+$ where X = Cl and Br.

General trends. In the family of complexes $MoOX_5$, there is a clear trend in the value of the $2B$ term of the hyperfine tensor as the covalency of the ligand X varies. This is seen in Table XXVI. Increased covalency is associated with increased delocalization of the electron and consequent loss of spin density on the metal.

TABLE XXVI

ANISOTROPIC HYPERFINE TENSOR IN COMPLEXES OF TYPE $[MoOX_5]^{2-}$

Complex	$2B$ (gauss)
$[MoOF_5]^{2-}$	40
$[MoOCl_5]^{2-}$	27
$[MoO(NCS)_5]^{2-}$	26
$[MoOBr_5]^{2-}$	24

A plot of g_{av} versus A_{iso}(Mo) (Fig. 46) results in a useful correlation. Where the symmetry is strictly C_{4v}, the points lie on a straight line. As the symmetry is reduced slightly, the g and A values decrease slightly. The species formed on γ-irradiating (*554*) the polymolybdate $Mo_7O_{24}(NH_4)_6 \cdot 4H_2O$ and the complexes formed (*90*) between $MoOX_5$ with $S(SH)P(OC_2H_5)_2$ would appear to have a structure related to $MoOX_5$ since they lie close to this line. The structure of the complex

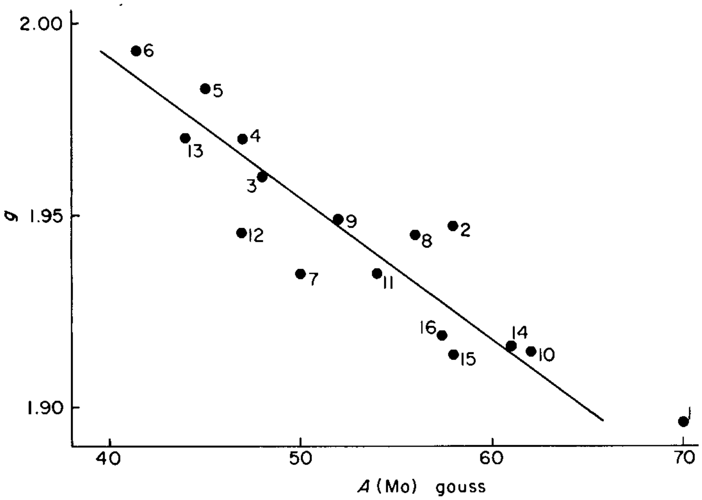

FIG. 46. Plot of g_{av} versus A_{iso} (Mo) for strongly axially symmetric complexes of molybdenum. (1) $(MoOF_5)^{2-}$, (2) $(MoOCl_5)^{2-}$, (3) $(MoOCl_4Br)^{2-}$, (4) $(MoOCl_3Br_2)^{2-}$, (5) $(MoOCl_2Br_3)^{2-}$, (6) $(MoOBr_5)^{2-}$, (7) $[MoO(SCN)_5]^{2-}$, (8) $MoOCl_3$ in EtOH, (9) $MoOCl_3$ in 20% HCl, (10) $Mo_2O_3(SO_4)_2$ in H_2SO_4, (11) $Mo_2O_3(SO_4)_2$ in $H_2SO_4 + KCl$, (12) *trans*-$[C_5H_5N][Mo(OCH_3)_2Cl_4]$, (13) $MoOX_5 + S(SH)P(OC_2H_5)_2$, (14) $[MoO(H_2AsO_4)_4]^-$, (15) Mo^{5+} in H_3PO_4, and (16) Mo^{5+} in H_2SO_4.

$Mo_2(TDT)_5$ is obviously very different from that of the other tris-dithiolenes which are D_{3h}. These, together with Mo^{5+} in $CaWO_4$, TiO_2, and $[Mo(CN)_8]^{3-}$ have totally different structures and would not be expected to fall near the C_{4v} line (see Section III,C,2).

8. ESR of Mn^{6+}, Re^{6+}, and Os^{7+}

The only recorded spectrum attributed (*119*) to Mn^{6+} giving h.f.s. seems to be the manganate ion in a chromate host lattice. For a regular tetrahedral ion, the ground state would be doubly degenerate, but the *g* values show that considerable distortion is present. The CrO_4^- ion in the host lattice itself is highly distorted, which will cause the Mn^{6+} substituent to be similarly distorted.

The ESR of $ReOCl_4$ in concentrated sulfuric acid or dioxane is observed (*234*) at 77°K, but not at room temperature. Since isotropic coupling to Re (admittedly Re^{4+} (*460*)) seems to be about 109 gauss, it seems likely that the measured values of $A_\parallel = 480$ and $A_\perp = 400$ gauss have opposite signs. The dithiolene complexes of Re are discussed in Section VIII,M,2. ESR data are recorded in Table XXVII. OsF_7 is reported to give an ESR signal, but no details are reported (*273*).

B. d^2 IONS

Detection of ESR signals from d^2 ions in octahedral fields is difficult because of the very short spin–lattice relaxation time (see Section V,C,2). Spectra from V^{3+} and Cr^{4+} ions (*357*, *435*, *734*) in Al_2O_3 (O_h with slight trigonal distortion) are only seen at 4.2°K, but in a tetrahedral field ESR signals are observed more readily because the ground state is a singlet, e.g., V^{3+} in CdS (*311*) and Ti^{2+} in ZnS (*604*). For this latter case, a small (2.2 gauss) isotropic coupling to ^{67}Zn is observed (see Table XXVIII). The only discrete chemical complexes where signals have been observed is the reduced form of Cp_2VCl_2 which is thought (*173*) to be Cp_2VCl, and $Cp_2VC_6H_5$, and $Cp_2VC_6H_4CH_3$ (*134*).

The hypomanganate anion MnO_4^{3-} in sodium vanadate shows (*123*) well resolved ^{55}Mn h.f.s. together with an isotropic *g* value close to 2. This means that the ground state of the ion must be well separated from the first excited state so that spin–orbit coupling is relatively ineffective.

C. d^3 IONS

1. ESR of V^{2+}

ESR signals are readily observed in d^3 systems because of the relatively long relaxation time. S.h.f.s. are rarely seen in d^3 ions because

TABLE XXVII

ESR DATA OF d^1 Mn^{6+} AND Re^{6+} IONS

Ion	g_{av}	$g_{\parallel}$	$g_{\perp}$	A_{iso} (10^4 cm^{-1})	$A_{\parallel}$ (10^4 cm^{-1})	$A_{\perp}$ (10^4 cm^{-1})	References
$[MnO_4]^{2-}$ in $[CrO_4]^{2-}$	—	1.970, 1.966, 1.938		—	25, 33, 135		(*119*)
$ReOCl_4$ in H_2SO_4 or dioxane	—	1.90	1.77	—	480 G	440 G	(*234*)
$Re(S_2C_2Ph_2)_3$	2.015	2.015		—	—	—	(*641*)
$Re(TDT)_3$	2.010	—		—	—	—	(*641*)

molecular orbitals involving the unpaired electrons in the t_{2g} metal orbitals and the ligand contain only the ligand π orbitals, σ bonded ligand orbitals cannot interact with the t_{2g} metal orbitals in octahedral symmetry.

The spectra of V^{2+} in MgO and MgS (*45*, *172*, *456*) are isotropic because of the cubic field (see Table XXIX). The ^{51}V h.f.s. are 80.3 and 76.1 gauss, respectively, and the decrease is related to the increase in π bonding between the $(t_{2g})^3$ electrons and O^{2-} or S^{2-} ions causing more delocalization of the electrons. The very small h.f.s. of ^{51}V in Cp_2V and the g value of 2.00 shows the large degree of delocalization of the electrons and consequent quenching of the orbital contribution which results in a g value close to free spin. The electron configuration is a_{1g}^1, e_{2g}^2. Cp_2V reacts with substituted acetylenes (*354*, *671*) to yield π complexes with a 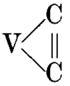 arrangement of atoms.

A similar π complex is formed with CS_2 which is formulated (48) as

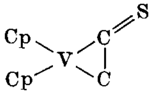

The $A_{iso}(^{51}V)$ value for V^{2+} in $K_4Fe(CN)_6$ is intermediate between that of V^{2+} in MgS and V^{2+} in Cp_2V showing that π bonding is significant in the hexacyanide. Dessy *et al.* (*173*, *174*) have electrolytically reduced the dithiolene bridged complex $[CpVS_2C_2(CF_3)_2]_2$ and found a complex ESR signal which was analyzed to consist of a principal set of ^{51}V h.f.s., each line of which was split into many lines separated by 10 gauss which could arise from either protons or fluorine atoms. Solid state systems are reviewed by McGarvey (*504*).

2. *ESR of Cr^{3+} and Mo^{3+}*

The relationship between increases in covalency associated with decreases in metal h.f.s. found in V^{2+} complexes is also observed with chromium. Almost all of the large number of ESR studies on Cr^{3+} have been carried out on Cr^{3+} ions replacing metal ions in a suitable host lattice. Nevertheless, when the host lattice is a recognized coordination complex, the ESR data obtained can justifiably be attributed to the equivalent Cr^{3+} complex (see Table XXX).

Sugano and Shulman (*646*) and Hall *et al.* (*308*, *309*) have shown that the traditional concept of ionic bonding in fluorides must be discarded. From the ^{19}F s.h.f.s. in $[CrF_6]^{3-}$ and the ^{13}C s.h.f.s. in $[Cr(CN)_6]^{3-}$, Kuska and Rogers (*425*) show that $[Cr(CN)_6]^{3-}$ has more covalent σ-bond

TABLE XXVIII

ESR Data for d^2 Ions

Ion	g_{av}	$g_{\parallel}$	$g_{\perp}$	A_{iso} (10^4 cm^{-1})	$A_{\parallel}$ (10^4 cm^{-1})	$A_{\perp}$ (10^4 cm^{-1})		References
V^{3+} in Al_2O_3	—	1.92	—	—	110 G	—	$D = 7.85$ cm^{-1}	(*435*, *734*)
Cr^{4+} in Al_2O_3	—	1.90	—	—	—	—	$D = 7$ cm^{-1}	(*357*)
V^{3+} in CdS	—	1.934	1.932	—	63	66	$D = 1.13$ cm^{-1}	(*311*)
Ti^{2+} in ZnS	—	1.9280		—	12.7		$A(^{67}Zn) = 2.0$	(*604*)
$(MnO_4)^{3-}$ in $(VO_4)^{3-}$	—	2		—	62.5		—	(*119*, *123*)
$(Fe_3O_4)^{2-}$ in $(CrO_4)^{2-}$	—	2		—	—		—	(*119*)
Cp_2VCl	1.98	—		89 G	—		—	(*173*)
Cr^{4+} in Si	—	1.9962		—	12.54		—	(*311*)
Mn^{5+} in Si	—	2.0259		—	63.09		—	(*311*)
V^{3+} in ZnS	—	1.9433		—	63		—	(*353*)
$Cp_2V(C_6H_5)$	2.13	—		—	—		—	(*134*)
$Cp_2V(C_6H_4CH_3)$	2.13	—		—	—		—	(*134*)

TABLE XXIX

ESR DATA FOR d^3 V^{2+} IONS

Ion	g_{av}	$g_{\parallel}$	$g_{\perp}$	$A_{iso}(^{51}V)$ $(10^4\,cm^{-1})$	$A_{\parallel}(^{51}V)$ $(10^4\,cm^{-1})$	$A_{\perp}(^{51}V)$ $(10^4\,cm^{-1})$		References
VCl_2 in H_2O	1.965	—	—	96 G	—	—	—	*(232)*
$K_4V(CN)_6$ in $K_4Fe(CN)_6$	—	1.9919	1.9920	—	55.5		$D = -0.0264$, $E = -0.0072\,cm^{-1}$	*(49)*
V^{2+}								
in NaCl								
orthorhombic site	—	1.969, 1.970, 1.976		—	81		$D = -0.0655$, $E = -0.0197\,cm^{-1}$	*(430)*
tetragonal field	—	1.9704	1.9754	—	80.5	88.8	$D = -0.05724$, $E = +0.00005\,cm^{-1}$	*(430)*
in MgO	—	1.9800		—	−80.3 G		—	*(172, 456)*
in MgS	—	1.9896		—	70.7		—	*(45)*
in CaF_2	—	1.935	1.943	—	79	92	—	*(729)*
$[CpVS_2C_2(CF_3)_2]_2 + e$	1.990	—	—	75 G	—	—	Other lines separated by 10 G	*(173, 175)*
Cp_2V in 2-Me-THF	—	2.002	1.99	27.4 G	37	21.5	$D = 2.3\,cm^{-1}$	*(495, 538, 566, 592)*
Cp_2VCS_2	2.0009	—	—	43.6 G	—	—	—	*(48)*
$Cp_2V(CH_3CO_2C{=}CCO_2CH_3)$	1.9976	—	—	44.0 G	—	—	—	*(671)*
$Cp_2V(CF_3C{=}CCF_3)$	1.9971	—	—	46.0 G	—	—	—	*(671)*
$Cp_2V(Ph_2C{=}C{=}O)$	1.9976	—	—	45.5 G	—	—	—	*(354)*

TABLE XXX

ESR Data for Some d^3 Ions of Cr^{3+} and Mo^{3+}

Ion	g_{av}	$g_\parallel$	$g_\perp$	$A_\parallel$ (10^4 cm^{-1})	$A_\perp$ (10^4 cm^{-1})		References
$Cr(acac)_3$ in $Co(acac)_3$	—	1.9802		16.2	16.9	$D = 0.06$, $E = 0.0085$ cm^{-1}	*(501)*
$Cr(hfac)_3$ in $Al(hfac)_3$	—	1.98		—	—	$D = 0.7$ cm^{-1}	*(366)*
$Cr(acac)_3 + Al(C_2H_5)_3$	1.987	—		—	—	2.7–3.8 G s.h.f.s.	*(28)*
Cr^{3+} in ScF_3	—	1.967		13 G		$A(^{19}F) = 11$ G	*(411)*
$[CrF_6]^{3-}$ in $KMgF_3$	—	—		—	—	$A_\parallel(^{19}F) = -10$ G, $A_\perp(^{19}F) = +2.6$ G	*(308, 309)*
Cr^{3+}							
in K_2NaGeF_6	—	—		—		$A_{iso}(^{19}F) = -1.1$ G, $A_\parallel = -10.1$ G, $A_\perp = 3.4$ G	*(334)*
in $AlCl_3 \cdot 6H_2O$							
violet	—	1.9761	1.9764	—		—	*(29)*
green	—	1.9769	1.9764	—		—	*(29)*
in $K_3Co(CN)_6$	—	1.993	1.991	14.7		$A_\parallel = -8.55$ G, $A_\perp = -10.5$ G(^{13}C)	*(49, 425)*

$[CrCl_5(H_2O)]^{2-}$ in $(NH_4)_2[InCl_5(H_2O)]$	—	1.9871	1.9828	15.4	14.7	$D = 0.05946$, $E = 0.00507$ cm^{-1}	(*255*)
$[Cr(triglycine)_2]SO_4$	—	1.985		<13		—	(*692*)
$[Cr(en)_3]Cl_2$	—	1.9871		—	—	$D = 0.0413$, $E = 0$ cm^{-1}	(*502*)
$[Cr(en)_3]Cl_3 \cdot 3H_2O$	—	1.9900		—	—	$D = 0.036$, $E = 0$ cm^{-1}	(*502*)
trans-$[CrCl_2(en)_2]Cl \cdot HCl \cdot H_2O$	—	1.9765		—	—	$D = 0.504$, $E = 0.036$ cm^{-1}	(*502*)
Cr^{3+} in $NH_4[CoEDTA] \cdot 4H_2O$	—	1.987	1.982	—	17	$D = 1.069$, $E = 0.203$ cm^{-1}	(*2*)
$[(NH_3)_5Cr–OH–Cr(NH_3)_5]Cl_5$	—	1.986		—	—	—	(*371*)
$[(NH_3)_5Cr–OH–Cr(NH_3)_4(H_2O)]Cl_5$	—	2.009		—	—	—	(*371*)
$[(NH_3)_5Cr–OH–Cr(NH_3)_4(OH)]Cl_4$	—	1.993		—	—	—	(*371*)
Cr^{3+}							
in $Co[S_2P(OC_2H_5)_2]$	—	1.9903, 1.9914 1.9901		—	—	$D = \pm 0.0138$, $E = \pm 0.0814$ cm^{-1}	(*291*)
in CaF_2	—	1.961	1.97	—	—	—	(*729*)
Mo^{3+}							
in $K_3InCl_6 \cdot 2H_2O$	—	1.93		—	39	—	(*548, 549*)
in $Al(acac)_3$	—	1.94		—	—	—	(*366*)
$[CpMo(SCH_3)_2]_2 - e$	2.027	—		—	—	—	(*174*)

TABLE XXXI

ESR DATA FOR d^3 Mn^{4+}, Tc^{4+}, AND Re^{4+} IONS

Ion	g	$A_{\parallel}$ (10^4 cm^{-1})	$A_{\perp}$ (10^4 cm^{-1})		References
Mn^{4+}					
in TiO_2	1.99	77		—	*(26)*
in $SrTiO_3$	1.994	75 G		—	*(524)*
$[MnF_6]^{2-}$ in Cs_2GeF_6	—	77 G		$A_{iso} = 5.5$ G, $A_{\parallel} = 13.5$ G, $A_{\perp} = 15.0$ G(^{19}F)	*(334)*
Re^{4+}					
in K_2PtCl_6	1.815	393		$U = -0.0037$, $u = -0.013$ cm^{-1}	*(184)*
in K_2PtCl_6	2.055	109 G		—	*(460)*
Tc^{4+}					
in K_2PtCl_6	1.9876 → 1.9896	133.7 → 136.1		—	*(460, 586)*
in K_2PtF_6	3.884	334	176	—	*(586)*

character than $[CrF_6]^{3-}$, but that the π-bond character is about the same in both. They calculate the unpaired electron-spin density in the σ bonds to be –0.03 and –2.64%, respectively, and that γ_π, a measure of the covalency of the π bond is 0.38 and 0.23, respectively.

The ^{53}Cr h.f.s. and g values found in Cr^{3+} compounds are all in the region expected and no unusual features are seen. The absence of s.h.f.s. reduces the value of the data in elucidating the structure or bonding in Cr^{3+} complexes. ^{19}F s.h.f.s. are detected (*729*) in the case of Cr^{3+} in CaF_2.

The D and E zero-field parameters give a measure of the symmetry of the crystal field. E gives a measure of the axial distortion; for a regular O_h complex, it should equal 0. In general, low values are observed for both D and E.

The s.h.f.s. observed (*28*) in the reaction between $Cr(acac)_3$ and excess $Al(C_2H_5)_3$ varies from 2.7 to 3.8 gauss depending on the solvent. Splittings are only observed in alkylbenzene solvents and the parameters are close to those for $[Cr(C_6H_6)_2]^+$ suggesting that a sandwich complex is formed and that the lines arise from interaction with protons.

Single crystal studies of the cluster complex $[Cr_3(CH_3COO)_6(OH)_2]Cl\cdot 8H_2O$ have been studied (*138*) at 4°K. Each Cr atom lies at the corners of an equilateral triangle and has three unpaired electrons. Broad line spectra are observed with principle g values between 1.78 and 1.90, but it is not clear how the axes are defined. Dessy (*174*) has found that $[CpMo(SCH_3)_2]_2$ may be electrolytically oxidized to yield a radical with one less electron.

3. *ESR of* Mn^{4+}, Tc^{4+}, *and* Re^{4+}

Helmholz *et al.* (*334*) have observed ^{55}Mn and ^{19}F splittings for $[MnF_6]^{2-}$ and find a large anisotropic term in the ^{19}F tensor indicating considerable π bonding, as observed in $[CrF_6]^{3-}$ and $[FeF_6]^{3-}$ ions. The small contribution due to σ bonding is consistant with the electrons being in the t_{2g} level as expected (see Table XXXI).

Re and ^{99}Tc h.f.s. have been detected (*184, 460*) in K_2PtCl_6 (*184, 460, 586*) and K_2PtF_6 (*586*) host lattices. No Cl h.f.s. are observed as for the classic case of Ir^{3+} in K_2PtCl_6 and is attributed to the greater line width of the Re and Tc lines. There is a major discrepancy between the work of Low (*460*) and Dorain (*184*) for Re^{4+} in K_2PtCl_6. The results of the latter are considered more reasonable.

D. d^4 IONS

Very few reports of ESR of d^4 ions have appeared. The difficulty in detecting ESR is probably due to short spin–lattice relaxation times together with large zero-field splittings. The complexes $Mo(CO)_2(C_5H_5N)_2X_2$ (X = Cl or Br) show a strong signal in the bulk solid (*143*). The available data are given in Table XXXII.

E. d^5 IONS: SPIN-FREE

The ground state is $^6S(^6A_1)$ for O_h symmetry and there are no other sextet terms of higher energy. Thus there can be no mixing of higher states and so ESR is readily observed in any crystal field symmetry. The absence of spin–orbit coupling means g values are isotropic and close to the free spin value of 2.0023. The hyperfine coupling constant is also isotropic, as expected for an S-state ion.

1. *ESR of* Cr^+

When chromium vapor is diffused into salts or when Cr^{2+} impurities are irradiated, Cr^+ species are trapped and are readily detected by ESR. S.h.f.s. are observed (*208*, *662*) in F^-, S^{2-}, Se^{2-}, and Te^{2-} crystals and in all cases are attributable to interaction with first and, in some cases, second sphere coordination of the anion (see Table XXXIII). In ZnS, ^{33}S splittings are observed, a rare event since the isotope is only in 0.74% natural abundance. The decrease in Δg ($g - 2.0023$) and in ^{53}Cr h.f.s. in the series of host lattices ZnS, ZnSe, and ZnTe follows the order of increase in covalency as expected. There are no paramagnetic chemical compounds of Cr^+ with $S = \frac{5}{2}$.

2. *ESR of* Mn^{2+}

Of the many papers reporting spectra of Mn^{2+} in various host lattices, only a few where important trends or where superhyperfine splittings are observed and which are of relevance to an inorganic chemist will be mentioned and listed in Table XXXIV.

No s.h.f.s. are observed for Mn^{2+} in H_2O where the species $[Mn(H_2O)_6]^{2+}$ exists (see Fig. 47). In a crystal of $AlCl_3 \cdot 6H_2O$, however,

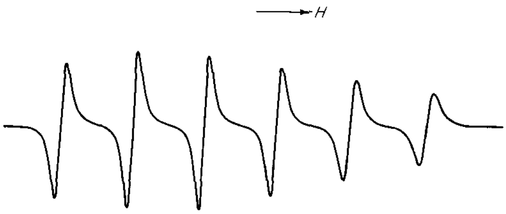

FIG. 47. ESR spectrum of Mn^{2+} in water.

TABLE XXXII

ESR DATA FOR d^4 IONS

Ion	$g_\parallel$	$g_\perp$	A_z (10^4 cm^{-1})	A_x (10^4 cm^{-1})	A_y (10^4 cm^{-1})		References
$CrSO_4 \cdot 5H_2O$	1.95	1.99	—	—	—	$D = 2.24$, $E = 0.10$ cm^{-1}	(*539, 540*)
Mn^{3+} in TiO_2	1.99	2.00	84.5	52.8	80.6	$D = -3.4$, $E = 0.116$, $a = 0.13$ cm^{-1}	(*260*)
Cr^{2+}							
in CdS	7.75	—	12.5	—	—	$A_\parallel(Cd) = 5.8$ G, $a = 0.30$ cm^{-1}	(*520*)
in ZnSe	7.837	—	12.6 G	—	—	$A(^{77}Se) = 4.31$ G	(*208*)
$Mo(CO)_2(C_5H_5N)_2X_2$; $X = Cl$ or Br	1.94		—	—	—	—	(*143*)

TABLE XXXIII

ESR DATA FOR SOME d^5 Cr^+ IONS

Cr^+	g	$A(^{53}Cr)$ (10^4 cm^{-1})		References
In NaF	2.000	14.0	—	(*324*, *326*)
In NaCl	1.998	18.3	$a = 7.2 \times 10^{-4}$ cm^{-1}	(*704*)
In ZnS	1.9995	13.4	$A(^{33}S) = 2.2$, $A(^{67}Zn) = 1.3$, $a = 3.9 \times 10^{-4}$ cm^{-1}	(*208*, *662*)
In ZnSe	2.0018	13.27	$A_{\parallel}(^{77}Se) = 6.83$; $A_{\perp}(^{77}Se) = 4.41$; $A^* = 1.65$; $a = 5.35 \times 10^{-4}$ cm^{-1}	(*208*, *662*)
In ZnTe	2.0026	12.43	$A_{\parallel}(^{125}Te) = 11.8$, $A_{\perp}(^{125}Te) = 21.83$, $A^* = 3.54$, $a = 6.59 \times 10^{-4}$ cm^{-1}	(*208*, *662*)
In CdTe	1.9997	12.78	$A(^{125}Te) = 10.6$, $a = 3.1 \times 10^{-4}$ cm^{-1}	(*662*)

TABLE XXXIV

ESR Data for Some d^5 Mn^{2+} Ions

Ion	g_{av}	$g_{\parallel}$	$g_{\perp}$	$A_{iso}(^{55}Mn)$ (10^4 cm^{-1})	$A_{\parallel}(^{55}Mn)$ (10^4 cm^{-1})	$A_{\perp}(^{55}Mn)$ (10^4 cm^{-1})		References
Mn^{2+}								
in NaF	—	2.002		—	95 G		$A_{iso}(^{19}F) = 11$ G	*(127)*
in LiF	—	2.000		—	90 G		$A_{\parallel} = 15$ G, $A_{\parallel}' = 25$ G, $A_{\perp} = 10$ G	*(127)*
in $CaCO_3$ (calcite)	—	—		−94.9 G	—		$A_{iso}(^{13}C) = 0.22$, $6 \equiv CO_3^{2-}$	*(347)*
[Mn(pentamethyl-tetrazole)$_6$](ClO_4)$_2$	—	2.0001		—	84.4		$D = 41 \times 10^{-4}$ cm^{-1}	*(422)*
$MnCl_2$ in molten KCl/LiCl	—	—		78 G	—		—	*(726)*
Mn^{2+}								
in Na[Co(EDTA)]·$4H_2O$	—	—		—	91		—	*(463)*
in $AlCl_3 \cdot 6H_2O$	—	2.0011	2.0015	—	95.2 G	96.4 G	$A(^1H) = 9.35$ G, $D = 146.8$, $F = 10.0$ G	*(412)*
in CaF_2	—	1.998		—	97.8		$A_s = 9.5$, $A_p = 2.7(^{19}F)$, $a = 0.6 \times 10^{-4}$ cm^{-1}	*(50)*
in CdF_2	—	2.0026		—	93		$A_s = 9.3$, $A_p = 2.4$, $a = 4 \times 10^{-4}$ cm^{-1}	*(310)*
in Cs_3ZnCl_5	—	2.0110	1.9926	—	73		$D = -89.6$, $a = +10.7 \times 10^{-4}$ cm^{-1}	*(336)*
in CdS	—	2.0016		—	76		$A(Cd) = 0.82$, $D = -216.9$, $a = 2.0 \times 10^{-4}$ cm^{-1}	*(183, 436)*
in CdTe	—	2.010		—	76		$A(Cd) = 2.6$	*(436)*
in ZnS	—	2.0024		—	64		$A(^{67}Zn) = 0.75$	*(605)*
$[Mn(CH_3CN)_6]^{2+}$ in CH_3CN	2.003	—		92	—		—	*(201)*
$[MnF_4]^{2-}$ in $CaWO_4$	—	1.9955	1.9885	—	94.2		$A(^{19}F) = 27.9$	*(77)*
$[MnCl_4]^{2-}$ in CH_3CN	2.007	—		79	—		—	*(201)*
$[MnBr_4]^{2-}$ in CH_3CN	2.008	—		75	—		—	*(201)*

^{1}H s.h.f.s. (9.35 gauss) are observed (*412*). Similar conclusions (*676*) are drawn from the spectrum of Mn^{2+} in $La_2Mg_3(NO_3)_{12} \cdot 24H_2O$ where each ^{55}Mn line is flanked by a doublet. The rare occurrence of such proton splittings to coordinated water warrants further investigation. These splittings should be compared with those found in $[VO(H_2O)_5]^{2+}$ in $(NH_4)_2Zn(SO_4)_2 \cdot 6H_2O$ where the splitting was only 2.6 gauss (*481*). Levanon and Luz (*444*) have considered the line widths of the ESR signal of methanol solutions of Mn^{2+} containing numerous anions and conclude from the line broadening that the species present are of the type $Mn(CH_3OH)_5X$. The complex (*422*)

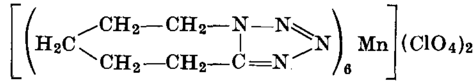

in the zinc analog shows no ^{14}N s.h.f.s. The line width is approximately 10 gauss and this puts an upper limit on the isotropic nitrogen splitting of about 4 gauss. This complex exhibits forbidden lines due to quadrupole interaction (Figs. 31 and 32). The complex is 91% ionic and intermediate between $[Mn(H_2O)_6]^{2+}$ and $[Mn(CN)_6]^{4-}$ (94 and 50%, respectively). There is a report of ^{55}Mn h.f.s. in the EDTA complex (*463*). ESR spectra (*186, 187*) of the family of complexes *trans*-MnL_4X_2, where L is a substituted pyridine and X = Cl, Br, or I have been shown to exhibit large zero-field splittings. The spectra show absorptions at $g = 2$ and $g = 6$ each with ^{55}Mn h.f.s.

Electron-spin resonance in fused salts has not received much attention and no s.h.f.s. have yet been observed. At low concentrations, the spectrum of Mn^{2+} in KCl/LiCl eutectic shows (*726*) six broad lines. As the concentration and the temperature are raised, the lines broaden, much more than at equivalent concentrations in water.

^{19}F s.h.f.s. are observed (*50, 130, 310*) in the spectra of Mn^{2+} in various fluoride host lattices such as CaF_2, LiF, and CdF_2, and for MnF_4^{2-} in $CaWO_4$ (*77*). S.h.f.s. are observed (*128*) by NMR in a $KMnF_3$ single crystal (16.8×10^{-4} cm^{-1}). The low coupling constant (*336*) for Mn^{2+} in Cs_3ZnCl_5, where the Mn^{2+} ion is in a distorted tetrahedral site, indicates considerable delocalization and the covalency is calculated to be 13%. S.h.f.s. attributed to ^{67}Zn and ^{111}Cd and ^{113}Cd are observed (*183, 436, 605*) for Mn^{2+} in CdS, CdTe, and ZnS. There must be some uncertainty concerning these assignments since in the case of Cr^{+} in these lattices (*208, 662*), it was shown that the splittings were due to interaction with the S or Te atom. ^{13}C s.h.f.s. are seen for Mn^{2+} in calcite where interaction with six equivalent CO_3^{2-} groups are seen. The total spin delocalization from the Mn^{2+} is only 0.86% and the spin density on ^{13}C is 0.072% (*347*).

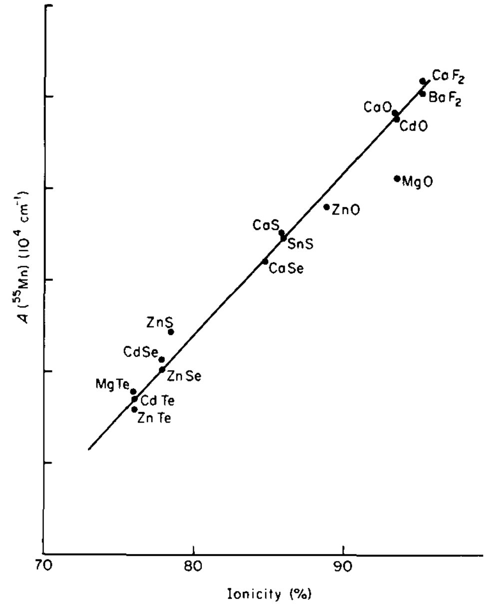

FIG. 48. $A(^{55}\text{Mn})$ versus ionicity of host lattice. From R. S. Title, *Phys. Rev.* **131**, 623 (1963).

There is a marked decrease in Mn h.f.s. as the covalency of the host lattice increases. The selected data in Table XXXV and Fig. 48 illustrate this point. The ionic character of the Mn^{2+}—X^- bond, I, is determined from Pauling's equation (*555*)

$$I = 1 - \exp\left[\frac{-(\chi_A - \chi_B)^2}{4}\right]$$

where χ_A and χ_B are the values of the electronegativity of the two atoms in the bond. The graph shows that these d^5 complexes are relatively ionic, but unfortunately the contributions to covalency from σ and π orbitals cannot be separated. In another correlation, Title (*660*) has related the zero-field and cubic field parameters a and D to the ionicity of the lattice.

Chan *et al.* (*128*) and others (*105*) have concluded that the reason why $A_{iso}(^{55}\text{Mn})$ in tetrahedral sites is 20–25% lower than in octahedral sites is not because there is a change in covalency in the ligand or that the ligands are closer, but because the different ligand field changes the $3d$-electron radial distribution. The same effect is observed by Mössbauer studies in Fe^{3+} substituted (*22, 61*) in both the octahedral and the tetrahedral sites in yttrium garnet. ESR of paramagnetic ions in a large number of host lattices have been reviewed by Larson and Jarrett (*442*).

TABLE XXXV

^{55}Mn h.f.s. (10^4 cm^{-1}) FOR Mn^{2+} IN VARIOUS LATTICES[a]

Anion	Li	Na	K	Ag	Mg	Ca	Sr	Ba	Zn	Cd	Pb
F	—	91.5	—	—	90.6	94.8	93	91.0	92.0	91.8	—
Cl	76.0	82.1	88.6	81.6	82.0	—	87.0	—	—	82.0	—
Br	—	—	88.6	77.0	—	—	—	—	—	78.0	—
I	—	—	—	—	—	—	—	—	—	80	—
O	—	—	—	—	81.6	84.5	—	—	77.0	87.3	—
S	—	—	—	—	71.9	75.7	75.2	—	63.9	63.6	71.8
Se	—	—	—	—	71.2	72.9	—	—	60.0	61.5	67.6
Te	—	—	—	—	58.1	67.2	—	—	56.0	57.0	61.2
Si	—	—	—	—	50.6	—	—	—	—	—	—

[a] The data is taken from references (*76*, *421*, *462*, *490*, *537*, *561*, *661*, *713*).

3. *ESR of Fe^{3+}*

Because of the low natural abundance of ^{57}Fe, it is difficult to detect h.f.s. unless the metal is enriched in the magnetic isotope. The data recorded in Table XXXVI contains, for dilute single crystal studies, only those where h.f.s. or s.h.f.s. are observed. The $[FeF_6]^{3-}$ ion has been trapped in K_2NaGaF_6 (*332, 333*), in CdTe containing trace amounts of Fe and annealed in contact with CaF_2 (*418*), in $KMgF_3$ and $KCdF_3$ (*308*), and in K_2NaAlF_6 (*332, 333*). In all cases, the ^{19}F s.h.f.s. are of similar magnitude and again show significant π bonding because of the relatively high anisotropic contribution. In an important paper by Levanon, Stein, and Luz (*445*), ^{19}F s.h.f.s. was observed in aqueous solutions of $Fe(ClO_4)_3$ containing a large excess of ammonium fluoride which indicated interaction with six equivalent fluorine atoms. The reason for the apparent narrow linewidth in solution (as is seen also in Mn^{2+} solutions) in contrast to Fe^{3+} in H_2O, is because of the symmetric structure of the complex ion. Line broadening is thought to occur because intermolecular collisions will reduce the symmetry of the complex. They went on further to suggest that the large linewidth of Fe^{3+} in H_2O was due to species of the type $[Fe(H_2O)_5OH]^{2+}$ being present. Coupling to ^{77}Se is also seen (*180*) in doped ZnSe. The site here is tetrahedral. When Fe^{3+} is introduced into AgCl and AgBr, the paramagnetic entity can be considered as $[FeX_4]^-$. Coupling to Br and Cl have been seen by Hennig (*335*) and Hayes *et al.* (*327*). Hennig concludes that the species in AgBr has $S = \frac{1}{2}$. He also assigns the s.h.f.s. to ^{109}Ag which is contrary to the conclusion of Hayes (*327*). This seems improbable if the trapped species is $[FeBr_4]^-$, which is known (*269*) in the complex $(NEt_4)[FeBr_4]$, to have $S = \frac{5}{2}$ from its magnetic moment.

The complex between Fe^{3+} and EDTA has been studied (*1*) as a single crystal in Rb[CoEDTA]. Single-crystal X-ray structure analysis shows that the Fe^{3+}EDTA complex is 7-coordinate with an H_2O molecule coordinating to the Fe, whereas the CoEDTA complex anion is 6-coordinate. Aasa *et al.* (*1*) consider that the Fe^{3+} remains 7-coordinate in the Rb[CoEDTA] host lattice from their ESR data. The $g \sim 4$ values and the second-order parameters D and E, which are sensitive to crystal field perturbations, are very close to those in the protein transferrin (*3*). The complex ferric phthalocyanine chloride in the solid state has been variously reported as having a g value of 3.8 (*362*) and 2.5 (*387*). It is thought to have a spin $S = \frac{3}{2}$ since its magnetic moment is 3.32 B.M.

4. *ESR of Fe^{3+} in Biological Systems*

Most ferric complexes where signals have been detected have been heme derivatives. Ehrenberg (*202*) has classified these as follows.

TABLE XXXVI

ESR DATA FOR SOME d^5 Fe^{3+} IONS

Ion	g_{av}	$g_\parallel$	$g_\perp$	$A(^{57}Fe)$ (10^4 cm^{-1})		References
Fe^{3+}						
in $RbCo(EDTA) \cdot 2H_2O$	—	4.092, 4.423, 4.259		5	$D/E = 0.06$, $E = 0.5$ cm^{-1}	(*1*)
in $Zn_3La_2(NO_3)_{12} \cdot 24H_2O$	—	2.0023		10.9	—	(*153*)
in MgO	—	—		10.8 G	—	(*595*)
in ZnS	—	2.0194		7.8	$a = 0.0128$ cm^{-1}	(*574*)
in $CaWO_4$	—	4.3		13.4	—	(*380*)
in $ZnWO_4$	—	2.0019		9.6	—	(*533*)
in $AlCl_3 \cdot 6H_2O$	—	2.0021		10.2	$D = +1494$, $a = +164$, $F = +13 \times 10^{-4}$ cm^{-1}	(*126*)
in AgCl	—	2.0156		—	$A_\parallel = 3.3$, $A_\perp = 2.0$(Cl), $a = 75 \times 10^{-4}$ cm^{-1}	(*327, 335*)
in AgBr	—	2.045		—	$A_\parallel = 16.2$, $A_\perp = 7.8$(Br)	(*327, 335*)
in ZnO	—	2.0060		9.02	—	(*691*)
in ZnSe	—	2.0464		6.75	$A_\parallel = 11.5$, $A_\perp = 6.7(^{77}Se)$, $a = 48.3 \times 10^{-4}$ cm^{-1}	(*180*)
$[FeF_6]^{3-}$						
in K_2NaGaF_6	—	—		—	$A_\parallel = 38$ G, $A_\perp = 17$ G(^{19}F), $a = 62$ G	(*332, 333*)
in CdTe	—	2.0029		10.7	$A_\parallel = 35.5$, $A_\perp = 14.66(^{19}F)$, $a = 499.28$	(*418*)
in K_2NaAlF_6	—	—		—	$A_s = 23.4$, $A_p = 6.5(^{19}F)$	(*332, 333*)
in $KMgF_3$	—	2.0031		—	$A_\parallel = 36.0$, $A_\perp = 18.0(^{19}F)$	(*308*)
in $KCdF_3$	—	2.0027		—	$A_\parallel = 34.0$, $A_\perp = 17.0(^{19}F)$	(*308*)
in H_2O	2.0036	—		—	$A_{iso}(^{19}F) = 23.0$ G	(*445*)

(*a*) *High spin* ($S = \frac{5}{2}$) with $g_\perp \sim 6$ and $g_\parallel \sim 2$ arising from very large zero-field splitting effects. Heme (Fig. 49) contains divalent Fe and no spectra have been detected from heme in this valence state. In the laboratory, hemoglobin (a tetranuclear species with four heme groups with the nitrogen atom from part of a protein donating in the fifth position of each Fe atom) may be oxidized to the ferric state and small molecules, e.g., O_2, CO, H_2O, N_3^-, F^-, CN^-, and NO, may add to the sixth position of the iron coordination sphere. Thiols may also be added (*62*). Myoglobin is a similar complex, but is mononuclear with only one heme group. With all groups except azide in the sixth position, the complexes are spin-free and give spectra with $g_\perp \sim 6$ and $g_\parallel \sim 2$. This is contrary to the behavior observed for typical d^5 (^6S) compounds where g is isotropic at 2 and is accounted for in terms of zero-field splitting by Griffiths (*297*). Similar behavior has only been observed in certain silicate glasses, e.g., by Castner *et al.* (*124*) and Sands (*600*). It is thought probable that in the O_2 adduct, the oxygen bonds with its axis parallel to the heme plane (*124*). Indirect chemical support for this lies in the observations (*360*) that $IrCl(CO)(PPh_3)_2$ is a reversible oxygen carrier and that in the adduct $IrCl(CO)(PPh_3)_2 \cdot O_2$,

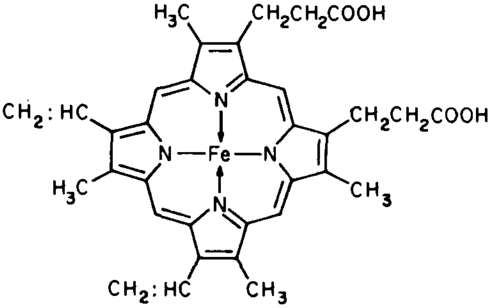

FIG. 49. Structure of heme.

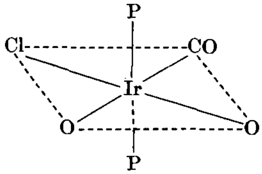

the two O atoms are equivalent and that the O—O distance is closer to that in O_2 than in H_2O_2.

(*b*) *Low spin* ($S = \frac{1}{2}$). The azide complex, metmyoglobin azide is spin-paired and has $g_\parallel = 2.8$ and $g_\perp = 1.70$. The iron atom in these adducts lies above the heme ring toward the sixth coordinating ligand (e.g., N_3^-). The N_3^- group is thought to bond with its axis parallel to the heme ring. Deviations from free spin arise from strong orbital contributions (*267*, *297*, *299*).

(*c*) *Low spin* ferrihemoproteins with minimal orbital contribution and consequently a g value close to 2, e.g., ferricytochrome C monomer (*521*).

(*d*) *Thermally balanced* mixtures of classes (*a*) and (*b*) or (*c*) in which the low-spin form is favored by lowering the temperature, e.g., Japanese radish and horseradish peroxidases (*511*).

Studies of the ESR of naturally occurring compounds of Fe(III) suffer from the inability to detect h.f.s. from the metal.

F. d^5 IONS: SPIN-PAIRED

In O_h symmetry, the ground state is $^2T_{2g}$. This is split by distortions and since the three orbital states will be close in energy and connected by spin–orbit coupling, ESR signals will only be obtained at low temperatures when the spin–lattice relaxation time will be longer. When the symmetry is much reduced (e.g., C_{4v}), spectra are readily observed and g values are nearer 2 because of the quenching of the orbital angular momentum. Theory predicts that $g_\parallel < 2$ and $g_\perp > 2$ for this system (see Section IV,C,5).

1. *ESR of Ti^- and V^0*

There are only a few spin-paired d^5 complexes of titanium and vanadium (Table XXXVII). Hausser (*317*) and the Olivés (*338*) have studied compounds of the type dibenzvanadium and detect proton s.h.f.s. The g values are of the same order as for $[Cr(C_6H_6)_2]^+$, suggesting

TABLE XXXVII

ESR DATA FOR SPIN-PAIRED d^5 Ti^{-1} AND V^0 IONS

Ion	g_{av}	$g_\parallel$	$g_\perp$	A_{iso}	$A_{ligands}$	References
Li[Ti(dipy)$_3$]	2.0074	—	—	—	—	(*206, 408*)
V(dipy)$_3$	1.9831	—	—	83.5 G	$A(^{14}N) = 2.3$ G	(*167, 206, 408*)
$V(C_6H_6)_2$	1.9624	—	—	63.5 G	$A(^1H) = 4.0$ G	(*317, 338*)
$V(C_6H_5\cdot CH_3)_2$	1.962	—	—	63 G	$A(^1H) = 3.9$ G	(*338*)
V(mesitylene)$_2$	1.962	—	—	63 G	$A(^1H) = 3.9$ G	(*338*)
$V(CO)_6$	2.062	1.981	2.103	—	—	(*563, 564*)

a similar electron configuration (*v.i*). A frozen pentane solution of vanadium hexacarbonyl (*563*, *564*) yields anisotropic g values which fit a $^2B_{2g}$ ground state for a tetragonally distorted octahedron. No ^{51}V h.f.s. is seen even at 4.2°K. The tris-dipyridyl complexes of titanium and vanadium (*206*, *408*) are readily reduced by lithium in tetrahydrofuran to d^5 species. The h.f.s. to ^{51}V, and hence the amount of electron delocalization, is intermediate between that for most vanadyl complexes and the cyclopentadienyl or dithiolene complexes.

2. *ESR of Cr⁺, Mo⁺, and W⁺*

There are very few compounds of Cr^+, all of which are spin-paired and most of these have been very intensively investigated (see Table XXXVIII). The family $Cr(NO)L_5$ where $L = CN^-$, H_2O, or NH_3 has been extensively studied (*72*, *75*, *114*, *162*, *207*, *216*, *279*, *280*, *319*, *342*, *424*, *511*, *634*) with the object of investigating the influence of the very electronegative NO^+ group upon the molecular orbital energy levels in the complex. The g tensor allows a determination of whether the unpaired electron is in the d_{xy} or d_{z^2} orbital (the only reasonable choice). In the case of $[Cr(CN)_5NO]^{3-}$, $g_{\parallel} = 1.9745$ and $g_{\perp} = 2.0051$ for the electron in the d_{xy} orbital, $g_{\parallel}$ is expected to be less than 2 (because it can commute with the empty $d_{x^2-y^2}$ orbital) and $g_{\perp} \sim 2$ (cannot commute with any orbital). For the electron in d_{z^2}, $g \sim 2$ and $g_{\perp} > 2$ (electron can commute with filled $d_{xz,yz}$). $^{14}N(NO)$ hyperfine coupling cannot arise from direct interaction between s or p orbitals on the N with d_{xy} orbital because they are of different symmetry with respect to the internuclear axis. The isotropic coupling must arise from spin polarization of the bonding orbitals and the anisotropic part from direct dipolar interaction of the electron in d_{xy} on the N nucleus. Even so, the coupling is too great, and it is postulated (*279*) that polarization occurs via the filled e (π) levels. There is some evidence (*506*) that the Cr—N—O bond angle is 7° from linear. This could possibly allow some mixing of levels to take place. S.h.f.s. to ^{13}C is detected for both equatorial and axial cyanide ligands. These are seen with ^{13}C in natural abundance, but characterization of the axial and equatorial ^{13}C coupling constants requires enriched ^{13}C. Of the several single crystal studies, that by Kuska and Rogers (*424*) is noteworthy in that they used alkali metal halides as the host lattice. The $[Cr(CN)_5NO]^{3-}$ ion replaces a $[MX_6]^{5-}$ group of the host lattice and the Cr—N—O direction is randomly distributed among the six possible positions. Spencer and Myers (*634*) determined the rate of exchange (by ESR) of the axial and equatorial CN^- groups using $^{13}CN^-$. They found that the axial cyanide was more labile in acid solution, but that all CN^- groups readily exchanged in neutral solution.

TABLE XXXVIII

ESR DATA FOR SPIN-PAIRED d^5 Cr^+ IONS

Ion	g_{av}	$g_\parallel$	$g_\perp$	$A_{iso}(^{53}Cr)$ ($10^4 cm^{-1}$)	$A_\parallel(^{53}Cr)$ ($10^4 cm^{-1}$)	$A_\perp(^{53}Cr)$ ($10^4 cm^{-1}$)	$A_{ligands}$ ($10^4 cm^{-1}$)	References
$[Cr(CN)_5NO]^{3-}$	1.9949	1.9745	2.0051	18.5 G	32.5 G	11.8 G	$(^{14}N)A_{iso} = 5.3$ G, $A_\parallel = 2.0$ G, $A_\perp = 7.0$ G $(^{13}C\ eq)A_{iso} = 12.4$ G, $A_\parallel = (10.5$ G), $A_\perp = 13.4$ G $(^{13}C\ ax)A_{iso} = 9.0$ G, $A_\parallel = 7.1$ G, $A_\perp = 10.0$ G	(*72, 162, 207, 216, 279, 319, 342, 424, 506, 634*)
$[Cr(NO)(NH_3)_5]^{2+}$	1.979	1.946	1.992	23.5 G	39.5 G	(20.0 G)	—	(*75, 280,* 480, 511)
$[Cr(NO)(H_2O)_5]^{2+}$	1.9671	1.9130	1.9952	26.9 G	42.8 G	(19.0 G)	$A_{iso} = 5.83$ G, $A_\parallel = (2.65$ G), $A_\perp = 7.42$ G(^{14}N)	(*75, 280, 511*)
$[Cr(CN)_4(CNH)(NO)]^{2-}$	1.9948	—	—	18.5 G	—	5.3 G	—	(*114*)
$[Cr(CN)_3(NO)(H_2O)_2]^-$	1.9880	—	—	20.0 G	—	5.8 G	—	(*114*)
$[Cr(CN)_2(NO)(H_2O)_3]$	1.9832	—	—	21.55 G	—	5.8 G	—	(*114*)
$[Cr(CN)(NO)(H_2O)_4]^+$	1.9748	—	—	23.2 G	—	5.8 G	—	(*114*)
$[Cr(C_6H_6)_2]^+I^-$ in DMF–$CHCl_3$	1.9865	2.0023	1.9785	18.1 G	—	26.9 G	$(A(^1H) = 3.46$ G	(*211, 212, 318, 368, 377, 576, 686*)

$[Cr(C_6H_6)(C_{12}H_{10})]^+$	1.98	—	—	17 G	—	—	$A(^1H) = 4$ G	*(205, 211, 686)*
$[Cr(C_{12}H_{10})_2]^+$	1.98	—	—	17 G	—	—	$A(^1H) = 3.30$ G	*(205, 211)*
$[Cr(cumene)_2]^+$	—	—	—	19 G	—	—	$A(^1H) = 1.0$ G(α), 3.6 G(ring)	*(686)*
$[Cr(dipy)_3]^+$	1.9972	—	—	21.8 G	—	—	$A(^{14}N) = 3.05$ G	*(206, 408)*
$[(CO)_4CrP(CH_3)_2]_2 + e$	1.9936	—	—	—	—	—	$A(^{31}P) = 12.87$ G, $A(^1H) = 1.19$ G, $2 \equiv P$	*(174, 177)*
$[Cr(C_6H_5 \cdot CH_3)_2]^+$	1.987	—	—	—	—	—	$A(^1H) = 3.5$ G	*(338)*
$[Cr(biphenyl)_2]^+BPh_4^-$	—	1.994	1.974	—	—	—	—	*(377)*
$[Cr(p\text{-terphenyl})_2]^+BPh_4^-$	—	1.994	1.974	—	—	—	—	*(377)*
$CpCr(CO)_3$	—	1.996, 2.030, 2.117		—	—	—	—	*(381)*
$[CrPc]^-$								
in THF								
species 1	1.975	—	—	—	—	—	$A(^{14}N) = 3.05$ G	*(301, 302)*
species 2	1.981	1.975		21.6 G	35 G	—	$A(^{14}N) = 3.15$ G	*(301, 302)*
in HMPA	2.0029	2.0035		—	—	—	$A(^{14}N) = 2.04$	*(301, 302)*
$[Mo(CN)_5NO]^{3-}$	—	1.9736	2.0168	—	54.4	25.5	$^{14}N(NO)\ A_\parallel = 1.27$, $A_\perp = 3.77$; $^{13}C(CN\ eq) A = 11$; $^{14}N(CN\ eq) A_\parallel = 2.21$, $A_\perp = -0.9$	*(321)*
$[Mo(C_6H_6)]^+$	1.9845	1.970	1.991	—	—	—	$A(^1H) = 4.45$ G	*(318)*
$\{[(Ph_4C_4)(CO)Mo]_2PhC{=\!=}CPh\} + e$	1.9953	—	—	—	—	—	—	*(175)*
$[W(C_6H_6)]^+$	1.9707	1.960	1.991	—	—	—	$A(^1H) = 5.7$ G	*(318)*
$[(CO)_4WP(CH_3)_2]_2 + e$	1.994	—	—	—	—	—	$A(^{31}P) = 15$ G, $2 \equiv P$	*(174)*

A full single crystal study (*321*) of the ion $[Mo(CN)_5NO]^{3-}$ in $K_3Co(CN)_6$ has yielded s.h.f.s. to the $^{14}N(NO)$, $^{13}C(CN)$ and, interestingly, $^{14}N(CN)$. This is the first time that coupling to the nitrogen of cyanide has been seen in a complex. Calculations show that unpaired electron delocalization onto this nitrogen is 0.053. This study has also given support to the formulation of the parent d^6 diamagnetic complex as $[Mo(CN)_5NO]^{4-}$ (*582*) rather than $[Mo(CN)_5NO(OH)_2]^{4-}$ (*293*). A recent crystal structure determination of $K_4[Mo(CN)_5NO]$ confirms the structure (*647*).

TABLE XXXIX

ESR PARAMETERS OF FAMILY $[Cr(NO)X_5]^a$

Ion	g_{av}	$A_{iso}(^{53}Cr)$ (gauss)	$A_{aniso}(^{53}Cr)$ (gauss)	ν(N—O) (cm^{-1})
$[Cr(NO)(H_2O)_5]^{2+}$	1.9671	26.9	15.9	1745
$[Cr(NO)(NH_3)_5]^{2+}$	1.979	23.5	15.8	1670
$[Cr(CN)_5NO]^{3-}$	1.9949	18.5	13.8	1645

[a] From ref. (*280*).

The ESR parameters for $[Cr(NO)(H_2O)_5]^{2+}$ and $[Cr(NO)(NH_3)_5]^{2+}$ are as expected and depend on the electronegativity of L in $Cr(NO)L_5$. Electron delocalization follows the order $CN^- > NH_3 > H_2O$. The more delocalization there is, the closer g_{av} is to 2.0023 and the smaller are the isotropic and anisotropic couplings to ^{53}Cr. This is also reflected in the NO-stretching frequency which decreases as back-bonding to NO increases (see Table XXXIX).

The acid hydrolysis of $[Cr(CN)_5NO]^{3-}$ has been followed by ESR and absorption spectroscopy (*114*, *280*). Each CN^- ligand is successively replaced by H_2O and the rate is sufficiently slow that spectra for each species can readily be obtained. Rate constants for the last two stages have been determined (*114*) by measuring the ESR peak heights as a function of time. A large number of controversial studies (*205*, *211*, *212*, *318*, *377*, *576*, *686*) have been made on the dibenzene chromium cation and similar sandwich complexes. Both ^{53}Cr and ^1H h.f.s. are observed, and whereas it was once thought that ^{13}C s.h.f.s. were observed, these have now been shown (*211*) to be too large to be attributed to ^{13}C and arise from coupling to ring protons. The symmetry is assumed to be D_{6h}, like $Cr(C_6H_6)_2$ (*532*). The electron configuration is probably e_{2g}^4, a_{1g}^1 rather than a_{1g}^2, e_{2g}^3. The next available orbitals, in increasing order of energy are calculated (*576*) to be e_{2u}, e_{1g}^*, and e_{2g}^*, and hence $g_\parallel$ will be expected to be close to 2, whereas $g_\perp$ will be less than 2 because a_{1g} can mix with the empty e_{1g}^* when H is perpendicular to z. Proton splittings are larger in $[(C_6H_6)_2Cr]^+$ than in $(C_6H_6)^-$ contrary to expectation. For aromatic radicals and ions the magnitude of the proton h.f.s. is proportional to the spin density ρ on the p_z orbital on the adjacent C atom, i.e., $A(^1H) = Q \cdot \rho$ where $Q = 22.5$ gauss. Taking $A(^1H) = 3.6$ gauss (*686*), the spin density on the p_z orbital of each carbon atom is 0.16. With 12 protons, the total spin density on both rings would be 1.92, which is clearly impossible. Calculations by Anderson and Drago (*27*) have shown that the spin density on the protons could arise from interaction of the d_{z^2} orbital with an extensively delocalized ring σ-molecular orbital with large proton coefficients rather than via a π-molecular orbital. Overlap is effectively between the d_{z^2} orbital and the inner small lobe of the sp^2 hybrids.

The g values for $[Mo(C_6H_6)_2]^+$ and $[W(C_6H_6)]^+$ show (*318*) less delocalization of the unpaired electron, but larger proton splittings, the reason for which is not clear.

The dipyridyl complex $[Cr(dipy)_3]^+$ yields (*206*, *408*) s.h.f. structure from interaction with the six equivalent nitrogen atoms. No proton splittings are seen, presumably these are lost in the linewidth.

Dessey (*174*, *177*) has shown that electrolytic reduction of

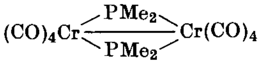

$$(CO)_4Cr\overset{PMe_2}{\underset{PMe_2}{\rightleftharpoons}}Cr(CO)_4$$

gives a very clear ESR signal consisting of a 1:2:1 triplet presumably due to two equivalent P atoms. Each line is split into 13 components arising from interaction with 12 equivalent protons. The signal is thought to arise from a singly charged anionic radical formed by equilibrium of the original neutral diamagnetic complex with the fully reduced doubly charged anion. The tungsten analog yields a similar spectrum upon electrolytic reduction (*174*). Electrolytic reduction of $\{[(Ph_4C_4)(CO)_2Mo]_2PhC{\equiv}CPh\}$ yielded a single line at $g = 1.9953$ (*175*).

When $[\pi\text{-}CpCr(CO)_3]_2$ is sublimed *in vacuo* at 80°K, the product yields an ESR spectrum showing three g values. The species is thought to be the monomer (*381*).

3. *ESR of* Mn^{2+}

The ion $[Mn(CN)_5NO]^{2-}$ has been studied in detail by several workers (*161*, *479*, *508*, *676*) (see Table XL) because of the interest in the ordering of the energy levels in the corresponding Cr^+ and Fe^+ complexes. The linewidths of the ^{55}Mn h.f.s. obscured any s.h.f. structure (see Fig. 50)

TABLE XL

ESR DATA FOR SPIN-PAIRED d^5 Mn^{2+} IONS

Ion	g_{av}	$g_{\parallel}$	$g_{\perp}$	$A_{iso}(^{55}Mn)$ (10^4 cm^{-1})	$A_{\parallel}(^{55}Mn)$ (10^4 cm^{-1})	$A_{\perp}(^{55}Mn)$ (10^4 cm^{-1})	$A_{ligands}$ (gauss)	References
$[Mn(CN)_5NO]^{2-}$	2.0146	1.9892	2.0265	79.0 G	161 G	38.7 G	$A_{\parallel}(^{14}N) \leqslant 1$, $A_{\perp}(^{14}N) \leqslant 4.5$	(*61, 216, 479, 508*)
$[Mn(CN)_6]^{4-}$ in $K_4Fe(CN)_6$	—	2.624, 2.182, 0.63		—	84.5, 46.5, 105		—	(*49*)
$[Mn(CO)_2(diphos)_2](ClO_4)_2$	—	2.080		—	—	—	—	(*631*)
Cp_2Mn	—	1.99–2.01		—	—	—	—	(*688*)
Mn phthalocyanine	2.07	1.90	2.16	—	170 G	24 G	—	(*560*)

and coupling to ^{14}N has only been detected in a dilute single crystal of sodium nitroprusside (*479*). Manoharan and Gray (*479*) attribute the spin density on the NO group to spin–orbit coupling which mixes the $e^4b_2{}^1(^2B_2)$ ground state with the $e^3b_2{}^2(^2E)$ excited state which has a large π^*(NO) character. Fortman and Hayes (*216*) reject this because this gives the wrong sign for the anisotropic coupling constant. They feel that the spin polarization mechanism is the most likely, but nevertheless only accounts for about one-third of the observed spin density. McNeil, Raynor, and Symons (*508*) found that γ-irradiation of the diamagnetic $K_3[Mn(CN)_5NO]$ produced the oxidized $[Mn(CN)_5NO]^{2-}$ species by simple electron addition. This should be contrasted with the analogous Fe compound which loses an electron on irradiation (*v.i.*). $K_4Mn(CN)_6 \cdot 3H_2O$ has been studied (*49*) in the corresponding iron host lattice.

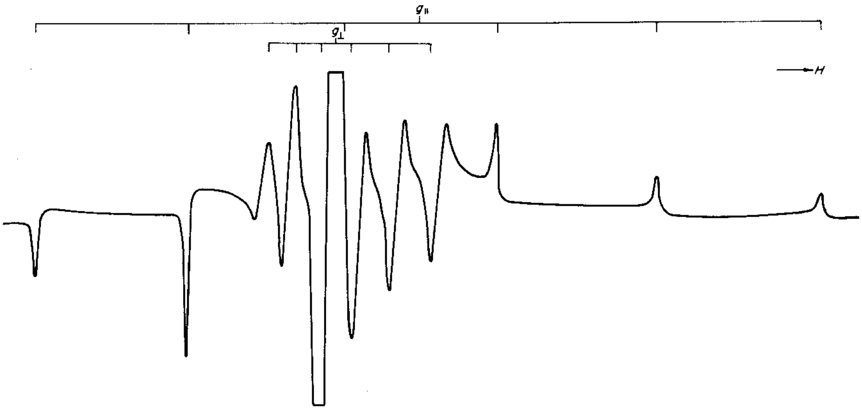

FIG. 50. ESR spectrum of a frozen solution of $[Mn(CN)_5NO]^{2-}$.

Manganese phthalocyanine has D_{4h} symmetry and the five electrons are partially paired such that the net spin is $\frac{3}{2}$ ($\mu = 4.55$ B.M.). The electron configuration is then d_{xy}^2, $d_{xz}^1 = d_{yz}^1$, $d_{z^2}^1$, $(b_{2g}^2, e_g{}^2, a_{1g}^1)$. This work (*362*) was carried out on a solid sample which gave a single broad line centered on $g = 2$. Recently (*560*), however, spectra from a solution has been obtained and the data suggest a single unpaired electron in a d_{xy} orbital. Presumably, solvation in the axial positions is sufficient to alter the energy levels to allow full spin-pairing.

Other molecules studied have been $[Mn(CO)_2(diphos)_2]ClO_4$ and $MnCp_2$ (*631, 688*), but no h.f.s. were detected because magnetically dilute samples were not used.

4. *ESR of Fe^{3+}, Ru^{3+}, and Os^{3+}*

$[Fe(CN)_6]^{3-}$ gives a single very broad line in solution (*49*) and as such will be expected to give an NMR signal. Shporer *et al.* (*451, 618*) have measured ^{13}C and ^{14}N chemical shifts of $K_4Fe(CN)_6$ and Knight shifts of $K_3Fe(CN)_6$ and have deduced the sign of the coupling constant from the direction of the shift. In the case of ^{13}C, the sign is negative, and for ^{14}N, it is positive. The coupling constants may be calculated from the contact shift by the method outlined by Eaton (*195*).

The lower symmetry $Fe(thioacac)_3$ yields (*415*) an ESR spectrum with three g values in a frozen solution at 77°K. Other complexes studied are some carborane "sandwich" compounds (*471*) of the type $[Fe(B_9H_9C_2R_2)_2]^-$ where a planar B_3C_2 five-membered ring π-bonds to the metal as in ferrocene. The g values are in accord with an electron configuration $(d_{z^2})^2$, $(d_{x^2-y^2}, d_{xy})^3$, i.e., (a_{1g}^2, e_{2g}^3), the order as in ferrocene (*156*). Spectra have been observed for the ferricinium cation at 4.2°K. Although Nöth *et al.* (*534*) observed a single line in the ESR of ferricinium salts in acetone at about $g = 2$, Golding and Orgel (*275*) attribute this to the decomposition product $[FeX_4]^-$ because, among other evidence, the $g = 2$ is suggestive of an $^6S(^6A_1)$ state. Table XLI summarizes the available data.

Dessy *et al.* (*174, 176*) have prepared electrolytically two organometallic species which yield ESR signals. These are thought to be $[\pi\text{-}C_5H_5Fe(CO)_2SCH_3]^+$ and $[\pi\text{-}C_5H_5Fe(CO)_2SCH_3]_2^+$ which presumably has bridging $>SCH_3$ groups. The compounds $[Cp(CO)FeSCH_3]_2$, $[Cp(CO)FePPh_2]_2$, and $[CpFe(CO)_2SCH_3]$ all can be electrolytically oxidized (*174*). The dithiocarbamate complex $Fe[S_2CN(iso\text{Pr})_2]_2Cl$ has the unusual $S = \frac{3}{2}$ configuration. Ferric maleonitriledithiolate yields a spectrum with three g values which are used to determine the separation of the molecular orbitals. The conclusion is that $d_{xz} < d_{xy} < d_{yz}$ with separations 282 and 338 cm^{-1}, respectively (*149*).

Chatt *et al.* (*131*) have observed a single broad line at 77°K in the first paramagnetic transition metal hydride to be prepared, namely, $OsHCl_2(PBu_2Ph)_3$. Its magnetic moment μ is 1.9 B.M.

The family of complexes MCl_3B_3, where M is Ru or Os, and B is a base such as tertiary phosphines and arsines, thio ethers, or pyridine has been studied in detail by Hudson and Kennedy (*358*). The complexes are mainly the meridianal isomer (C_{2v}), but in one case, $OsCl_3(PBu_2Ph)_3$, the g tensor indicates the other isomer, namely, facial (C_{3v}).

5. *ESR of Co^{4+} and Ir^{4+}*

Cobalt forms a complex (*52*) with

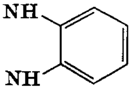

This, together with $[IrCl_6]^{2-}$ and $[IrBr_6]^{2-}$ in ammonium or sodium hexachloroplatinate host lattices, has been well studied (*136*, *294*, *295*, *546*). The $[IrCl_6]^{2-}$ spectrum (*296*, *546*) is an often-quoted classic since it was the first example of ligand s.h.f.s., proving for the first time that electron delocalization was possible and that the electron spent 30% of its time on the ligands. The g values of the tertiary arsine and phosphine complexes of $IrCl_4X_2$ have been measured (*358*) (see Table XLII).

In the case of $[Co(S_2C_2Ph_2)_2P(OPh)_3]$, ^{31}P s.h.f.s. has been detected (*256*) and the electron shown to be mainly in d_{xy} (bisecting the sulfur–cobalt bonds).

6. *ESR of* Ni^{5+}, Pt^{5+}, *and* Pd^{5+}

The complexes with

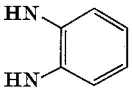

have been prepared (*52*, *54*) and behave rather like the dithiolenes, i.e., they undergo electrolytic oxidation and reduction. The available data is tabulated in Table XLII.

G. d^6 IONS

In O_h symmetry, the ground state is ^5D and thus is orbitally triply degenerate. The three t_{2g} orbitals are connected by spin–orbit coupling and the spin–lattice relaxation time is too short for ESR signals to be seen except at very low temperatures. The only ESR carried out has been on a few Fe^{2+} ions in host lattices. No biological systems yield ESR signals. Fe^{2+} in NaF at 4.2°K has the following parameters (*309*), $g = 3.420$, $A_{\parallel}(^{19}F) = 47.1$, and $A_{\perp}(^{19}F) = 19.2 \times 10^{-4}\ cm^{-1}$.

H. d^7 IONS: SPIN-FREE

1. *ESR of* Fe^{+}

Fe^{+} has been detected (*91*, *309*, *543*) in certain host lattices. ^{19}F s.h.f.s. are observed in NaF, LiF, and $KMgF_3$ lattices and the electron delocalization has been computed (*91*, *309*) (see Table XLIII).

2. *ESR of* Co^{2+}

Hyperfine coupling has been observed in numerous host lattices, but only in fluoride and selenide lattices are s.h.f.s. observed (*110*, *270*, *307*, *309*, *337*) (see Table XLIII).

TABLE XLI

ESR Data for Spin-Paired d^5 Ions of Fe^{3+}, Ru^{3+}, and Os^{3+}

Ion	g_{av}	$g_{\parallel}$	$g_{\perp}$	$A_{\parallel}$ ($10^4\,cm^{-1}$)	$A_{\perp}$ ($10^4\,cm^{-1}$)	$A_{ligands}$ (gauss)	References
$[Fe(PBu_3)(MNT)_2]^-$	2.046	—	—	—	—	$A(^{31}P) = 28.1$	(*144*)
$[Fe(CN)(MNT)_2]^{2-}$	2.054	—	—	—	—	—	(*144*)
$[Fe(dipy)(MNT)_2]^-$	2.085	—	—	—	—	—	(*144*)
$\{Fe(PEt_3)[S_2C_2(CF_3)_2]_2\}^-$	2.044	—	—	—	—	$A(^{31}P) = 27.9$	(*144*)
$\{Fe(o\text{-phen})[S_2C_2(CF_3)_2]_2\}^-$	2.084	—	—	—	—	—	(*144*)
$[Fe(CN)_6]^{3-}$	—	—	—	—	—	$A(^{14}N) = +0.78$, $A(^{13}C) = -11.8$	(*451, 618*)
$[Cp(CO)FeSCH_3]_2 - e$	1.998	—	—	—	—	—	(*174*)
$[CpFe(CO)_2SCH_3]_2 - e$	1.998	—	—	—	—	—	(*174*)
$[Cp(CO)FePPh_2]_2 - e$	1.977	—	—	—	—	—	(*174*)
Fe^{3+} in $K_3Co(CN)_6$	—	2.35, 2.10,	0.91	—	—	—	(*49*)
$(FeCp_2)^+$	—	4.68	0	—	—	—	(*376*)
$[Fe(B_9C_2H_{11})_2]^-$	—	3.994	1.532	—	—	—	(*471*)
$[Fe(B_9H_9C_2Me_2)_2]^-$	—	3.786	1.711	—	—	—	(*471*)
$CpFe(B_9C_2H_{11})$	—	3.579	1.778	—	—	—	(*471*)
$[Fe(B_9H_9C_2HPh)_2]^-$	—	3.572	1.799	—	—	—	(*471*)
$[CpFe(CO)_2SCH_3]^+$	1.9978	—	—	—	—	—	(*176*)
$[CpFe(CO)_2SCH_3]_2^+$	1.9982	—	—	—	—	—	(*176*)
$Fe(SacSac)_3$	—	2.14, 2.09,	2.01	—	—	—	(*415*)
$Fe(MNT)_3$	—	2.225, 2.140,	1.986	—	—	—	(*149*)
$Fe(NO)(S_2C_2Ph_2)_2$	2.009	—	—	—	—	—	(*492*)

Ru^{3+} in $K_3InCl_6 \cdot 2H_2O$	—	1.0,	1.22,	3.24	—	—	—	*(104)*
Na_3RuCl_6 in HCl	2.0	—		—	—	—	—	*(241)*
Ru^{3+} in Al(acac)$_3$	—	1.28,	1.74,	2.82	—	—	—	*(366)*
$[Ru(NH_3)_6]Cl_3 \cdot 3HgCl_2$	—	2.21,	2.05,	1.5	—	—	—	*(104)*
Ru^{3+} in YGa Garnet	—	3.113		1.148	63.8	38	—	*(512)*
Ru^{3+} in YAl Garnet	—	2.88		1.300	56.4	41	—	*(512)*
$RuCl_3(PMe_2Ph)_3$, C_{2v}	—	2.88,	2.03,	1.66	—	—	—	*(358)*
$RuCl_3(PEt_2Ph)_3$, C_{2v}	—	2.96,	2.01,	1.59	—	—	—	*(358)*
$RuCl_3(P\textit{n}\text{-}Bu_2Ph)_3$, C_{2v}	—	2.94,	2.02,	1.60	—	—	—	*(358)*
$RuCl_3(AsPr_3)_3$, C_{2v}	—	2.93,	2.06,	1.64	—	—	—	*(358)*
$RuCl_3(SMePh)_3$, C_{2v}	—	2.70,	2.29,	1.68	—	—	—	*(358)*
$RuBr_3(SMePh)_3$, C_{2v}	—	2.77,	2.37,	1.59	—	—	—	*(358)*
$RuCl_3(SEt_2)_3$, C_{2v}	—	2.76,	2.38,	1.60	—	—	—	*(358)*
$RuCl_3(S\textit{n}\text{-}PrPh)$, C_{2v}	—	2.69,	2.48,	1.56	—	—	—	*(358)*
$RuCl_3(C_5H_5N)_3$, C_{2v}	—	3.97,	—,	—	—	—	—	*(358)*
{*trans*-$RuCl_2[(PEt_2)_2C_2H_4]_2$}$ClO_4$	—	3.19,	1.87,	1.57	—	—	—	*(358)*
{*trans*-$RuCl_2[(PMe_2)_2C_2H_4]_2$}$ClO_4$	—	3.18,	1.88,	1.57	—	—	—	*(358)*
{*cis*-$RuCl_2[(PMe_2)_2C_2H_4]_2$}$ClO_4$	—	2.59,	2.13,	1.88	—	—	—	*(358)*
$(PEt_3H)[RuCl_4(PEt_3)_2]$, C_2	—	−2.51,	2.51,	−1.64	—	—	—	*(358)*
$OsCl_3(PMe_2Ph)_3$, C_{2v}	—	3.40,	1.46,	—	—	—	—	*(358)*
$OsCl_3(P\textit{n}\text{-}Bu_2Ph)_3$, C_{2v}	—	3.30,	1.65,	0.36	—	—	—	*(358)*
$OsBr_3(P\textit{n}\text{-}Bu_2Ph)_3$, C_{2v}	—	3.40,	1.44,	—	—	—	—	*(358)*
$OsCl_3(AsMe_2Ph)_3$, C_{2v}	—	3.35,	1.64,	—	—	—	—	*(358)*
$OsCl_3(C_5H_5N)_3$, C_{2v}	—	3.75,	1.37,	—	—	—	—	*(358)*
{*trans*-$OsCl_2[(PEt_2)_2C_2H_4]$}ClO_4	—	3.19,	1.73,	—	—	—	—	*(358)*
$OsCl_3(P\textit{n}\text{-}Bu_2Ph)_3$, C_{3v}	—	−1.83,	1.83,	1.28	—	—	—	*(358)*
Na_3OsCl_6 in HCl	1.8	—		—	—	—	—	*(241)*

TABLE XLII

ESR Data for Spin-Paired d^5 Co^{4+}, Ir^{4+}, Ni^{5+}, Pd^{5+}, and Pt^{5+} Ions

Ion	g_{av}	$g_{\parallel}$	$g_{\perp}$	A_{iso} (10^4 cm^{-1})	$A_{\parallel}$ (10^4 cm^{-1})	$A_{\perp}$ (10^4 cm^{-1})	$A_{ligands}$ (10^4 cm^{-1})	References
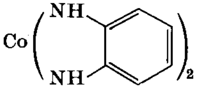	2.24	—	—	—	—	—	—	(*52*)
$Co(PPh_3)(S_2C_2Ph_2)_2$	2.013	—	—	26.4 G	—	—	—	(*144*)
$Co(PBu_3)(S_2C_2Ph_2)_2$	2.020	—	—	23.4 G	—	—	—	(*144*)
$[Co(S_2C_2Ph_2)_2(OPh)_3]$	2.010	2.019, 1.980, 2.006		23.7 G	56.4 G, 7.7 G, 0		$A(^{31}P)iso = 7.9$ G, $A_{\parallel} = 10.4$ G, $A_{\perp} = 6.6$ G	(*144, 256*)
$Co[P(OPh)_3][S_2C_2(CF_3)_2]_2$	2.0165	2.0160	—	26.4 G	62.95 G	—	$A(^{31}P) = 9.3$ G	(*51*)
$Co(PPh_3)[S_2C_2(CF_3)_2]_2$	2.0195	2.0193	—	28.8 G	74.99 G	—	—	(*51*)
$Co(AsPh_3)[S_2C_2(CF_3)_2]_2$	2.0197	2.0248	—	31.15 G	80.74 G	—	—	(*51*)
$Co(SbPh_3)[S_2C_2(CF_3)_2]_2$	2.0302	2.0497	—	—	81.28 G	—	—	(*51*)
Ir^{4+}								
in $(NH_4)_2PtCl_6$	—	1.786		—	25.3		$A(Cl) = 8.4$	(*136*)

in K_2PtCl_6	—	1.60	1.87	—	—	—	—	(*294*)
in Na_2PtCl_6	—	2.20, 2.07, 1.05		—	24.0	25.5	*A*(Cl) = 11.6, 10.7, <5	(*294, 296*)
in Na_2PtBr_6	—	2.25, 2.21, 0.75		—	—	25.5	$A_\perp$(Br) = 5.7	(*294*)
trans-$IrCl_4(AsPr_3)_2$	—	−2.43, 2.43, ±0.80		—	—	—	—	(*358*)
cis-$IrCl_4(PPr_3)_2$	—	2.65, 2.46, —		—	—	—	—	(*358*)
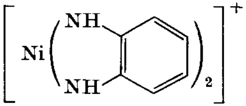	1.997	—	—	—	—	—	—	(*52, 54*)
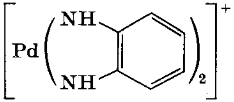	1.997	—	—	—	—	—	—	(*52*)
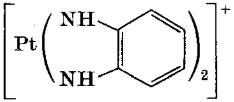	1.982	1.940	2.009	—	—	—	—	(*52*)

TABLE XLIII

ESR Data for Spin-Free d^7 Fe^+, Co^{2+}, and Ni^{3+} Ions

Ion	$g_\parallel$	$g_\perp$	$A_\parallel$ (10^4 cm^{-1})	$A_\perp$ (10^4 cm^{-1})	$A_{ligands}$ (10^4 cm^{-1})	References
Fe^+						
In MgO (octahedral field)	4.15		—	—	—	*(543)*
in NaF	4.344		—	—	$A_{iso}(^{19}F) = 14.0$ G	*(91)*
in NaF	4.351		—	—	$A_\parallel(^{19}F) = 44$, $A_\perp(^{19}F) = 16$	*(309)*
in LiF	4.251		—	—	$A_\parallel(^{19}F) = 66.5$, $A_\perp(^{19}F) = 28.3$	*(309)*
in $KMgF_3$	4.297		—	—	$A_\parallel(^{19}F) = 63$, $A_\perp(^{19}F) = 29$	*(309)*
Co^{2+}						
in $Mg(OAc)_2 \cdot 4H_2O$	6.018, 4.046, 2.518		192, 92, 31		—	*(152)*
in YGa garnet	7.037	2.675	306	17	—	*(643)*
in $Ce_2Mg_3(NO_3)_{12} \cdot 24H_2O$	4.43	4.05	103	80.7	—	*(154, 230)*
	7.23	2.31	278.8	<1	—	*(154, 230)*
in AgCl	5.38	3.87	233.3	89	—	*(630)*
in MgF_2	6.0327, 2.2970, 4.2391		75.5 G, 38.4 G, 35.4 G		$A(^{19}F)ax = 36.5$ G, 18.5 G, 12.8 G, $A(^{19}F)eq = 10.9$ G, 23.6 G, 27.3 G	*(270)*

in ZnF_2	6.05, 2.6, 4.1		77 G, 35 G, 36 G		$A(^{19}F) = 11.3$ G, 11.3 G, 11.0 G	(*110*)
in NaF	4.391		110		$A_{\parallel}(^{19}F) = 69.5$, $A_{\perp}(^{19}F) = 18.8$	(*309*)
in $KMgF_3$	4.371		104		$A_{\parallel}(^{19}F) = 77.5$, $A_{\perp}(^{19}F) = 26.1$	(*309, 714*)
in $CdBr_2$	—		—		$A_{\parallel}(Br) = 48$, $A_{\perp}(Br) = 20$	(*714*)
in CdI_2	—		—		$A_{\parallel}(^{127}I) = 57$, $A_{\perp}(^{127}I) = 15$	(*714*)
in TiO_2	2.19, 5.88, 3.75		40, 150, 26		—	(*725, 735*)
$Co[HCpz_3]_2\cdot(NO_3)_2$	8.534	0.807	369	<1	—	(*369*)
$Co[HBpz_3]_2$	8.46	0.97	362	<1	—	(*369*)
$Co[Bpz_4]_2$	8.48	0.94	365	—	—	(*369*)
Co^{2+} in $BaTiO_3$	4.347		109		—	(*730*)
$CoSeO_4\cdot 6H_2O$						
site a	5.60, 4.27, 2.26		110, 40, 40		—	(*644*)
site b	7.45, 2.36, 1.76		230, 40, 60		—	(*644*)
Co^{2+}						
in ZnSe (tetrahedral field)	2.2742		7.7		$A_{\parallel}(^{77}Se) = 16.4$, $A_{\perp}(^{77}Se) = 9.6$	(*337*)
in CdS	2.27		4.6	<12	—	(*434*)
in CdSe	2.295	2.303	13.6	20.1	—	(*356*)
in CdTe	2.30		23		—	(*307*)
in CaF_2	2.31		23		$A(^{19}F) = 6$ G	(*307*)
in Cs_3ZnCl_5	2.38	2.30	—	—	—	(*67, 677*)
Ni^{3+} in $KMgF_3$	4.163		—	—	$A_{\parallel}(^{19}F) = 147$, $A_{\perp}(^{19}F) = 24$	(*309*)

Jesson (*369*, *370*) has made a thorough study at 4.2°K of a series of pyrazolyl complexes of the type

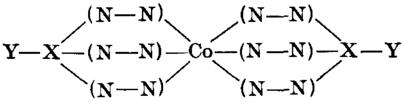

where (N—N) is

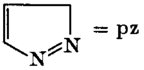

X is C or B, Y is H for $Co[HCpz_3]_2^{2+}$ or $Co[HBpz_3]_2^{2+}$, pz for $Co[BPz_4]_2$. The symmetry of the molecule is D_{3d} and the ligand field is effectively trigonally distorted octahedral. Proton NMR spectra may be seen from the ligand nuclei.

In general, coupling to ^{59}Co is about 2–3 times greater in magnitude for an octahedral crystal field than in a tetrahedral crystal field. This is supported by the predicted A values from the equations

$$O_h \qquad A = P[-\tfrac{5}{3}K + 1 + \tfrac{2}{63}] \tag{138}$$

$$T_d \qquad A = P[-K + g - 2] \tag{139}$$

where K is about 0.35.

The trend in metal h.f.s. in a series of lattices varying in anion electronegatively is opposite to earlier examples. In CdS, CdSe, and CdTe lattices, $A(^{59}Co)$ increases as the covalency increases. Covalent bonding in the series $[CoF_6]^{4-}$, $[CoBr_6]^{4-}$, and $[CoI_6]^{4-}$ has been studied by measuring the ligand s.h.f.s. in a series of host lattices (*714*). As expected, delocalization of the electrons increases as the covalency increases. The details are given in Table XLIV, where the figures refer to the probability of finding an electron in a ligand s, $p(\sigma)$, or $p(\pi)$ orbital.

TABLE XLIV

SPIN POPULATIONS IN s, p_σ, AND p_π LIGAND ORBITALS[a]

Orbital	$[CoF_6]^{4-}$	$[CoBr_6]^{4-}$	$[CoI_6]^{4-}$
f_s	0.43	0.57	0.54
$f_{p_\sigma} = f_{p_\pi}$	3.6	5.3	7.6

[a] Data given as percent.

3. *ESR of* Ni^{3+}

^{19}F s.h.f.s. have been observed (*309*) for Ni^{3+} in $KMgF_3$. The field here is essentially O_h, but is insufficiently great to cause spin-pairing, cf. Ni^{3+} in TiO_2 (*285*) where $S = \frac{1}{2}$.

I. d^7 IONS: SPIN-PAIRED

1. *ESR of* Cr^{-1}, Mo^{-1}, *and* Mn^0

S.h.f.s. is observed (*173*) in solution for the species thought to be [bipyridyl $Mo(CO)_4]^-$. Forth-five lines are observed with separation of 0.6 gauss. This splitting suggests well-defined spin density on the ligand and may usefully be compared with the largest proton splitting in the bipyridyl negative ion which is 4.71 gauss (*683*).

Similar electrolytic reduction (*174*) is achieved and ^{55}Mn h.f.s. observed in reduced $[(CO)_4MnS_2CN(C_2H_5)_2]$ and $[(CO)_3(SPh)Mn—]_2$. In the latter case, the spectrum shows two equivalent manganese atoms with the remarkably small h.f.s. of 14 gauss showing that the additional electron is delocalized very considerably. The available data is given in Table XLV. There is evidence for $[Cr(NO)(CN)_5]^{5-}$ and $[Mn(NO)(CN)_5]^{4-}$ ions in γ-irradiated KCl containing $[Cr(NO)(CN)_5]^{3-}$ and $[Mn(NO)(CN)_5]^{3-}$ (*93*).

TABLE XLV

ESR DATA FOR d^7 SPIN-PAIRED Mo^{-1} AND Mn^0 IONS

Ion	g_{av}	$A_{iso}(^{55}Mn)$ (gauss)		References
$[DipyMo(CO)_4]^-$	2.0031	—		(*173*)
$[(CO)_4MnS_2CN(C_2H_5)_2] + e$	—	40		(*174*)
$[(CO)_3(SPh)Mn-]_2 + e$	—	14	$2 \equiv {}^{55}Mn$	(*174*)

2. *ESR of* Fe^+

Most ESR of Fe^+ systems have been carried out on complexes of iron containing NO^+ as one or more ligand (see Table XLVI). Most of these complexes have been prepared by passing NO gas through an aqueous solution of ferrous ions containing various anionic ligands. The solution then contains the paramagnetic species of the form $Fe(NO)_{1\text{ or }2}L_n$. McDonald, Phillips, and Mower (*497*) obtained well-resolved isotropic spectra with a variety of ligands, L. ^{57}Fe-enriched material was used

TABLE XLVI

ESR DATA FOR d^7 SPIN-PAIRED Fe^+ IONS

Ion	g_{av}	$g_\parallel$	$g_\perp$	$A_{iso}(^{57}Fe)$ $(10^4 cm^{-1})$	$A_\parallel(^{57}Fe)$ $(10^4 cm^{-1})$	$A_\perp(^{57}Fe)$ $(10^4 cm^{-1})$	$A_{ligands}$	References
$[Fe(CN)_5NO]^{3-}$	2.026	2.006	2.031	−7.21 G	9 G	−14.3 G	$A_{iso}(^{14}N) = 14.8$ G, $A_\parallel = 17.1$ G, $A_\perp = 14.75$ G $A(^{13}C) = 9–10.1$ G	(*70, 158, 160, 322, 346, 508, 575, 679*)
$[Fe(CN)_5NO]^{2-} + S_2O_4^{-2}$ excess	2.0319	2.0215	2.041	—	—	—	$A_{iso}(^{14}N) = 2.18$ G	(*278*)
$[Fe(NO_2)(CN)_5]^{5-}$	—	1.9993, 1.9281, 2.0080		—	—	—	$A(^{14}N) = 32, 10, 15$ G	(*577, 679*)
$[Fe(CN)_5NO]^{2-} + Na_2S$	2.028	—		—	—	—	$A_{iso}(^{14}N) = 15$ G	(*278*)
	2.023	—		—	—	—	$A_{iso}(^{14}N) = 4.85$ G	(*278*)
γ-irrad. $Na_2Fe(CN)_5NO \cdot 2H_2O$	—	2.00, 1.98, 1.93		—	—	—	$A(^{14}N) = 25.9$ G, 18.3 G, 8.5 G	(*94, 679*)
$Fe(NO)[S_2CN(CH_3)_2]_2$	—	2.0461, 2.0397, 2.0277		—	—	—	$A_{iso}(^{14}N) = 12.7$ G	(*265, 281, 286, 492*)
$Fe(NO)(S_2CNEt_2)_2$	2.0368	2.025, 2.039, 2.035		8.6 G	2 G	14 G	$A_\parallel(^{14}N) = 16$ G, $A_\perp(^{14}N) = 13.2$ G	(*281*)
$Fe^{2+} + NO + Na_2S$	2.021	2.049	2.01	—	—	—	$A_{iso}(^{14}N) = 4.85$ G, $A_\parallel = 7.5$ G, $A_\perp = (3.6$ G$)$	(*278, 497*)
$Fe^{2+} + NO + H_2O$, pH 7	2.033	—	—	—	—	—	—	(*497*)
$Fe^{2+} + NO + OH^-$, pH 10	2.027	—	—	15.5 G	—	—	$A_{iso}(^{14}N) = 2.2$ G, $2 \equiv N$	(*497*)
$Fe^{2+} + NO + (PO_4)^{3-}$, pH 7	2.033	—	—	14.5 G	—	—	$A_{iso}(^{14}N) = 2.6$ G, $A_{iso}(^{31}P) = 2.6$ G, $2 \equiv N$ & P	(*497*)

$Fe^{2+} + NO + (AsO_3)^{3-}$	—	—	—	—	—	—	$A_{iso}(^{15}N) = 3$ G, $A_{iso}(^{75}As) = 3$ G, $2 \equiv N$ & As	*(497)*
$Fe^{2+} + NO + (P_2O_7)^{4-}$	2.040	—	—	12.9 G	—	—	$A_{iso}(^{31}P) = 5.5$ G, $2 \equiv N$ & P	*(497)*
Fe^{2+} + NO + AMP or ADP or ATP	2.038	—	—	—	—	—	—	*(497)*
Fe^{2+} + NO + cysteine or cysteine ethyl ester	2.032	—	—	—	—	—	$A_{iso}(^{15}N) = 3$ G, $2 \equiv N$ & S	*(497)*
Fe^{2+} + NO + β-mercaptoethanol	—	—	—	—	—	—	$A(^1H\text{-}CH_2) = 1.5$ G	*(497)*
$Fe^{2+} + NO + (MNT)^{2-}$	2.027	—	—	9.4 G	—	—	$A(^{14}N) = 15.5$ G	*(450, 492, 497)*
$Fe^{2+} + NO + (BDT)^{2-}$	2.028	—	—	9.3 G	—	—	$A(^{14}N) = 15.1$ G	*(497)*
Fe^{2+} + NO + 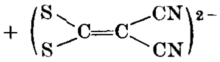	2.041	—	—	8.4 G	—	—	$A(^{14}N) = 12.8$ G	*(497)*
Black Roussins salt, pH 11	—	—	—	—	—	—	$A(^{14}N) = 4.7$ G	*(497)*
$[Fe(C_6Me_6)_2]^+$	—	1.865, 1.966, 2.086		—	—	—	—	*(110)*
$[(CO)_3FeAs(CH_3)_2]_2 + e$	2.064	—	—	—	—	—	—	*(174)*
$[(CO)_3FeP(CH_3)_2]_2 + e$	1.999	—	—	—	—	—	—	*(174)*
$[FePc]^-$ in THF	2.01	—	—	—	—	—	$A(^{14}N) = 2.4$ G	*(301, 302)*
$[Fe(CN)_5(NC)^{5-}$ in KCl	—	1.9998	2.0959	—	—	—	$A_\perp(^{14}N) = 1.95$ G	*(594)*
$\{Fe(NO)[S_2C_2(CF_3)_2]_2\}^{2-}$	2.027	—	—	—	—	—	$A(^{14}N) = 15.0$ G	*(492)*
$[Fe(NO)(S_2C_6Cl_4)_2]^{2-}$	2.027	—	—	—	—	—	$A(^{14}N) = 15.4$ G	*(492)*
$[Fe(NO)(S_2C_6H_3CH_3)_2]^{2-}$	2.028	—	—	—	—	—	$A(^{14}N) = 13.1$ G	*(492)*
$[Fe(NO)(S_2C_2Ph_2)_2]^{2-}$	2.026	—	—	—	—	—	$A(^{14}N) = 15.4$ G	*(492)*
$(CH_2CHCH_2)Fe(CO)_3$	2.0421	—	—	—	—	—	—	*(527)*
$(CH_3(CHCHCH_2)Fe(CO)_3$	2.0421	—	—	—	—	—	—	*(527)*
$(CH_3COOCH\cdot CHCH_2)Fe(CO)_3$	2.0447	—	—	—	—	—	—	*(527)*
$(CH_2CHCH_2)Fe(CO)_2(PPh_3)$	2.0462	—	—	—	—	—	$A(^{31}P) = 17.1$ G	*(527)*
$(CH_2CHCH_2)Fe(CO)_2(PBu_3)$	2.0423	—	—	—	—	—	$A(^{31}P) = 17.1$ G	*(527)*
$(CH_2CHCH_2)Fe(CO)(PBu_3)_2$	2.0408	—	—	—	—	—	$A(^{31}P) = 23.7$ G	*(527)*

to obtain metal h.f.s. No h.f.s. was obtained in the system Fe^{2+}–NO–H_2O at pH > (i.e., $[FeNO(H_2O)_5]^{2+}$), but at pH > 10, the spectrum indicates a species containing two equivalent NO groups is present (see Fig. 25). In the presence of phosphate, pyrophosphate, arsenate, molybdate, carbonate, maleate, benzoate, cystein, cysteine ethyl ester, β-mercaptoethanol, penicillamine, AMP, ADP, and ATP, the spectra indicated there were two equivalent NO groups and in many cases, two equivalent anion ligands. The structures proposed were of the type

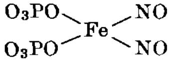

The complex with the bidentate pyrophosphate has a lower ^{57}Fe splitting and a higher ^{31}P splitting compared with the monophosphate, indicating greater delocalization of the unpaired electron. With maleonitrile dithiolate (MNT) and benzene *1:2* dithiol (BDT), complexes of the type $Fe(NO)(S_2)_2$ are formed and have since been isolated (*450*). It is noteworthy that when the chelate forms a five-membered ring, the ^{14}N s.h.f.s. is about 15 gauss, but when the chelate forms a four-membered ring with 1:1 dicyanoethylene 2:2 dithiol and with dimethyldithiocarbamate (*265*, *281*), the coupling to ^{14}N is about 12.7 gauss and the *g* value much higher, suggesting less delocalization of the unpaired electron.

Considerable attention has been paid to the species formed by reduction of sodium nitroprusside (*73*, *160*, *346*, *508*, *575*, *679*). Chemical reduction (*p*H 4), electrical reduction, or γ- or X-irradiation appear to produce the same species which has been assumed to be $[Fe(CN)_5NO]^{3-}$, although Van Voorst and Hemmerich (*679*) believe it to be protonated. Long irradiation of sodium nitroprusside with γ-rays produces sufficient number of damaged ions that many are adjacent and the resultant pairs of radicals have been analyzed. The species was originally thought (*525*) to be the $N_2O_2^+$, ion but has since been shown to be radical pairs (*277*, *509*). The directions of the pairs of ions in the crystal show (*277*) that the unpaired electron is mainly located on the Fe and confirms earlier proposals (*508*) that the unpaired electron was in an $a_1(d_{z^2})$ level, giving an electron configuration $e^4(d_{xz,yz})$, $b_2{}^2(d_{xy})$, $a_1{}^1(d_{z^2})$. This cannot be reconciled with the order of energy levels suggested by Manoharan and Gray (*289*, *478*) based on a study of the polarized visible and UV absorption spectrum of single crystals of d^5 and d^6 nitrosyl pentacyanides of V, Cr, Mn, and Fe. The proposed order of energy levels was $e(d_{xz,yz})$, $b_2(d_{xy})$, $e(\pi^*NO)$, $b_1(d_{x^2-y^2})$, $a_1(d_{z^2})$. The π^*(NO) level does not appear to be so deep as to become lower than the b_1 or a_1 levels in the d^7 Fe^+ case. An interesting further species in irradiated sodium nitroprusside is one where the electron seems to be located on the NO group which is no longer colinear with the Fe atom (*94, 667, 679*). Hayes (*322*) has suggested that the large coupling to ^{14}N in this species is due to a large contribution from orbital angular momentum. The interaction of sodium nitroprusside or $Fe^{2+} + NO$ solutions with sulfides has caused considerable interest (*65, 278, 497, 679*) largely because of its biochemical implications. Reduction of certain nonheme proteins produces similar spectra (*64*) and hence the $Fe^{+}/NO^{+}/S^{2-}$ system may act as a suitable model. Most of this work is in a very confused state largely because the species involved have not been characterized at all well.

The complex $Fe(NO)(S_2CNMe_2)_2$ has been studied in detail (*265, 281, 286*). The interest initially revolved around whether the Fe–N–O atoms were colinear. The d^8 diamagnetic $Co(NO)(S_2CNMe_2)_2$ has been shown to have a bent Co–N–O group (*21*). Since this was only a two-dimensional X-ray determination, too much reliance cannot be placed upon this observation, but the $Fe(NO)(S_2CNEt_2)_2$ complex has an Fe–N–O angle of 174° which may be taken as linear since there is a large thermal error in the position of the oxygen atom (*142*). The unpaired electron is in the $a_1^1(d_{z^2})$ molecular orbital (C_{2v} symmetry).

The detection of ESR signals from $[Fe(C_6Me_6)_2]^+$ illustrates some important principles (*110*). Since the electron is likely to be in the doubly degenerate E_{2u} ligand nonbonding orbital (*155*), this must be split by the Jahn–Teller effect. This is shown by the three g values which indicate that the hexamethylbenzene rings are oblique. Furthermore, signals were only detected between 25° and 80°K, the intensity decreasing rapidly with increase in temperature. This corresponds to increasing the population of a vibrational state where the Jahn–Teller distortion is dynamic.

There is an apparent correlation between the value of $A_{iso}(^{57}Fe)$ and the nature of the orbital containing the unpaired electron. When the electron is in orbitals other than of a_1 symmetry, the hyperfine coupling is about (—)14–15 gauss, a figure remarkably consistent with the theoretical hyperfine coupling χ, calculated by Freeman and Watson (*220*) (see Table V), but when the electron is known to be in a_1, the coupling is reduced to (—)8–9 gauss. This could arise from admixture of a small amount of 4*s* character to the orbital containing the unpaired electron which would make a positive contribution to A_{iso}.

Dessy *et al.* (*174*) have electrically reduced $[(CO)_3Fe(AsCH_3)_2]_2$ and $[(CO)_3FeP(CH_3)_2]_2$ and obtained simple absorptions with g values just greater than 2, suggesting that this and related systems have nominally a d^7 configuration. Murdoch and Lucken have shown (*527*) that reductive dehalogenation of $C_3H_5Fe(CO)_3Cl$ yields a diamagnetic dimer $[C_3H_5Fe(CO)_3]_2$ and a paramagnetic monomer. The paramagnetic species yields a single line at $g = 2.04$, and in the case of phosphine-substituted complexes, ^{31}P s.h.f.s.

3. *ESR of* Co^{2+}

Assour and Kahn (*38*, *41*) have shown from the absence of s.h.f.s. in cobalt phthalocyanine that the unpaired electron is in a d_{z^2} orbital. This is supported by the strong dependence of $g_\perp$ and $A_\parallel(^{59}Co)$ on solvent. Indeed, ^{14}N s.h.f.s. are observed from pyridine and other solvent molecules weakly coordinating to the 5- and 6-coordination positions. The two crystallographic forms of cobalt phthalocyanine, α and β, have markedly different g and $A(^{59}Co)$ parameters. In the β phase, the distance between nearest neighbor molecules must be less than in the α form. The low value of $g_\parallel$ (which should equal 2.0023) arises from admixture of $4s$ and $3d_{z^2}$ orbitals and interactions between cobalt and N atoms in molecules above and below the ring. Variations of $g_\perp$ with solvent arise as a result of the variation of $\Delta E(E_{d_{xz,yz}} - E_{d_{z^2}})$ in the equation

$$g_\perp = 2.0023 - \frac{6\lambda}{\Delta E} \tag{140}$$

ΔE must be twice as large for the α form than the β form. The values of $A_\parallel$ and $A_\perp$ change for similar reasons (see Table XLVII).

The ion $[Co(CN)_5]^{3-}$ has attracted a lot of interest because of its action as a hydrogenation catalyst (*431*). It readily adds a sixth ligand including cyanide, and as such is very reactive. ESR and optical measurements by Alexander and Gray (*23*) have shown it to be of C_{4v} symmetry with the unpaired electron in the $a_1(d_{z^2})$ orbital. In the solid state the molecule is a dimer, e.g., $K_6Co_2(CN)_{10}\cdot 4H_2O$. Danon *et al.* (*159*) have electron-irradiated $K_3Co(CN)_6$ and find unambiguous evidence for electron interaction with two equivalent nitrogen atoms attributed to reversal of two CN^- groups to form a complex of the type $[Co(CN)_4(NC)_2]^{4-}$. This is similar to that found by Root and Symons (*594*) in irradiated $[Fe(CN)_6]^{4-}$ in alkali halide host lattices where the species $[Fe(CN)_5NC]^{3-}$ is postulated. A typical frozen solution spectrum of a cobalt complex is shown in Fig. 51.

Various isonitrile (*565*) and phosphine (*355*, *489*) complexes have been studied and g values obtained, but without hyperfine structure. One phosphine complex is formulated as $[Co(Ph_2PC_2H_4PPh_2)_2X]^+X^-$ which is essentially a square based pyramid of C_{2v} symmetry. ESR and optical spectra fit such a symmetry where the unpaired electron is thought to be in a $d_{x^2-y^2}$ orbital. Had the complex been hexacoordinate, the electron would be in a d_{z^2} orbital and the spectral results cannot then be accom-

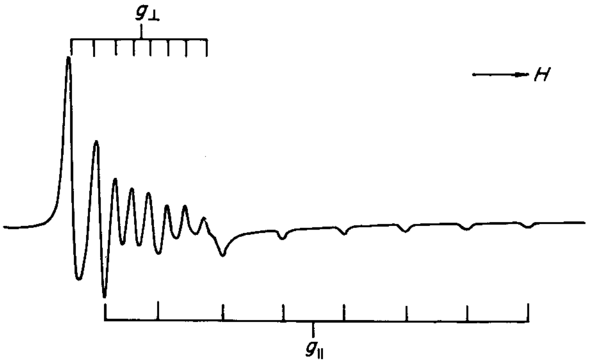

FIG. 51. ESR of a frozen solution of an axially symmetric cobalt complex.

modated on this model. The isonitrile complexes $[Co(PhNC)_5H_2O]^{2+}$ (blue) and $[Co(PhNC)_5]^{2+}$ (yellow) have been studied, but not properly characterized (*469*).

The series of complexes (*469*) $Co(CNR)_4X_2$ where $R = C_2H_5$, C_6H_{11}, *p*-tolyl, and X = I, Br, or Cl yield interesting spectra with h.f.s. attributed to two equivalent halogen atoms, and only in the case of the chloride is ^{59}Co coupling observed. If this interpretation is right, this shows that there is significant covalency in the Co–X bond in disagreement with conductivity measurements in solution which indicated an ionic structure. Detailed work by Maher (*469*) and Kimball *et al.* (*389*), however, have shown that there is a trend in g values for 4-, 5-, and 6-coordination of the complexes as shown in Table XLVIII, where the electron is in d_{z^2}. The absence of h.f.s. (^{59}Co) in the 5-coordinate complexes in solution is possibly due to rapid change from a trigonal bipyramid to a square-based pyramid structure. Theory shows that for C_{4v} symmetry, $g_\parallel = 2$, $g_\perp > 2$, whereas for D_{3h}, $g_\parallel > 2$. Signals are also detected for the square planar system *trans*-$R_2Co(PR_3)_2$, but no figures are given for Co h.f.s. which is said to be observed (*489*).

Hyperfine structure was observed (*601*) in a series of octahedral complexes with various organic bases. These h.f.s. were not measured, but bulk susceptibility measurements were correlated with the g values obtained from the undiluted solid.

Dessy *et al.* (*174*, *176*) have obtained well-resolved spectra from the species thought to be

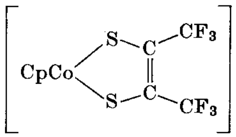

TABLE XLVII

ESR DATA FOR d^7 SPIN-PAIRED Co^{2+}, Rh^{2+}, AND Ir^{2+} IONS

Ion	g_{av}	$g_{\parallel}$	$g_{\perp}$	A_{iso} ($10^4\,cm^{-1}$)	$A_{\parallel}$ ($10^4\,cm^{-1}$)	$A_{\perp}$ ($10^4\,cm^{-1}$)	$A_{ligands}$ ($10^4\,cm^{-1}$)	References
α-Co-phthalocyanine	—	2.007	2.422	—	116	66	—	*(41)*
β-Co-phthalocyanine	—	1.89	2.94	—	150	280	—	*(41)*
Co-phthalocyanine								
in H_2SO_4	—	2.029	2.546	—	85	—	—	*(38)*
in pyridine	—	2.029	2.268	—	78	—	$A_{\parallel}(^{14}N) = 11.4$, $A_{\perp}(^{14}N) = 12.8$	*(38)*
in pyridazine	—	2.016	2.308	—	78	—	$A_{\parallel}(^{14}N) = 16.2$	*(38)*
in isoquinoline	—	2.018	2.336	—	84	—	$A_{\parallel}(^{14}N) = 13.3$	*(38)*
in quinoline	—	2.011	2.288	—	79	—	$A_{\parallel}(^{14}N) = 15.2$	*(38)*
in 3-Me-pyridine	—	2.013	2.326	—	88	—	$A_{\parallel}(^{14}N) = 15.1$	*(38)*
in 4-Me-pyridine	—	2.010	2.306	—	84	—	$A_{\parallel}(^{14}N) = 16.1$	*(38)*
in 2-Me-quinoline	—	2.007	2.317	—	91	—	$A_{\parallel}(^{14}N) = 16.1$	*(38)*
Co-tetraphenylporphrin in H_2TPP	—	1.798	3.322	—	315	197	—	*(37)*
$[CpCoPPh]_2 + e$	2.003	—	—	—	—	—	$A(^{31}P) = 9$ G($2 \equiv P$), $A(?) = 2$ G	*(174)*
$[CpCoSCH_3]_2 + e$	2.120	—	—	—	—	—	—	*(174)*
$[CpCoSCH_3]_2 - e$	2.107	—	—	—	—	—	—	*(174)*
$[CpCoS_2C_2(CF_3)_2] + e$	2.454	—	—	41 G	—	—	—	*(174, 176)*
$[Co(NO)(MNT)_2]^-$	2.063	—	—	31.9 G	—	—	—	*(492)*
$\{Co(NO)[S_2C_2(CF_3)_2]_2\}^-$	2.059	—	—	32.9 G	—	—	—	*(492)*
$[Co(NO)(S_2C_2Ph_2)_2]^-$	2.050	—	—	29.4 G	—	—	—	*(492)*
$[Co(CNR)_6]^{2+}$								
$R = CH_3$	2.055	2.025	2.092	24.6 G	65 G	75 G	—	*(389, 469)*
$R = C_2H_5$	2.067	—	2.089	23.95 G	—	72.1 G	—	*(469)*
$R = C_6H_{11}$	2.067	—	2.155	25.4 G	—	70.7 G	—	*(469)*
$R = C_6H_5$	2.059	—	2.083	28 G	—	74 G	—	*(469)*

$[Co(CNMe)_5(MeOH)]^{2+}$	2.0715	2.00	2.044	—	—	74 G	—	(*469*)
$[Co(CNEt)_5(MeOH)]^{2+}$	2.0765	2.00	2.058	—	—	75 G	—	(*469*)
$[Co(CNPh)_5(H_2O)]^{2+}$	2.0796	2.00	2.0865	—	73 G	70 G	—	(*469*)
$[Co(CNEt)_5C_5H_5N]^{2+}$	2.062	2.00	2.093	—	—	70.2 G	$A_{iso}(^{14}N) = 17{\cdot}5$ G	(*469*)
$[Co(CNR)_5]^{2+}$								
$R = CH_3$	2.0981	2.000	2.1227	—	77.2 G	59 G	—	(*389, 469*)
$R = C_2H_5$	2.093	2.0064	2.1275	—	80.2 G	50.3 G	—	(*469*)
$R = C_6H_{11}$	2.09	2.0061	2.1160	—	78 G	54 G	—	(*469*)
$R = C_6H_5$	2.081	2.004	2.118	—	86 G	50 G	—	(*469*)
$[Co(CN)_5]^{2-}$ in MeOH	2.115	2.006	2.156	—	87.4 G	28.6 G	—	(*23, 389, 469*)
$[Co(CNR)_4X_2]$								
$R = CH_3$, $X = Cl$	2.118	2·005	2·090	—	65·7 G	74·9 G	$A(Cl) = 13.2$ G	(*469*)
$X = Br$	2.097	—	—	—	—	—	$A(Br) = 73.7$ G	(*469*)
$X = I$	2.064	—	—	—	—	—	$A(I) = 95.6$ G	(*469*)
$R = C_2H_5$, $X = Cl$	2.104	—	—	—	—	—	—	(*469*)
$X = Br$	2.100	—	—	—	—	—	$A(Br) = 74.7$ G	(*469*)
$X = I$	2.068	—	—	—	—	—	$A(I) = 91.6$ G	(*469*)
$R = C_6H_{11}$, $X = Cl$	2.110	—	—	—	—	—	—	(*469*)
$X = Br$	2.100	—	—	—	—	—	$A(Br) = 69.7$ G	(*469*)
$X = I$	2.069	—	—	—	—	—	$A(I) = 89.6$ G	(*469*)
$R = p\text{-}MeC_6H_4$, $X = Cl$	2.094	—	—	—	—	—	—	(*469*)
$X = Br$	2.075	—	—	—	—	—	$A(Br) = 69.4$ G	(*469*)
$X = I$	2.044	—	—	—	—	—	$A(I) = 92.9$ G	(*469*)
$[Co(CN)_4(NC)_2]^{2-}$	—	2.006	2.095	—	54 G	70 G	$A(^{14}N) = 3.4–4.4$ G	(*159*)
$[Co(PhNC)_5{\cdot}H_2O](ClO_4)_2{\cdot}\frac{1}{2}H_2O$	—	2.12		—	—	—	—	(*565*)
$[Co(PhNC)_5](ClO_4)_2$	—	2.14		—	—	—	—	(*565*)
$[Co(Ph_2PC_2H_4PPh_2)_2]Cl_2$	—	2.257, 2.056, 2.041		—	—	—	—	(*355*)
$[Co(Ph_2PC_2H_4PPh_2)_2]Br_2$	—	2.258, 2.075, 2.037		—	—	—	—	(*355*)
$[Co(MNT)_2]^{2-}$	2.255	1.977, 2.798, 2.025		—	23, 50, 28		—	(*165, 166, 290, 473*)

TABLE XLVII—*cont.*

ESR DATA FOR d^7 SPIN-PAIRED Co^{2+}, Rh^{2+}, AND Ir^{2+} IONS

Ion	g_{av}	$g_{\parallel}$	$g_{\perp}$	A_{iso} (10^4 cm^{-1})	$A_{\parallel}$ (10^4 cm^{-1})	$A_{\perp}$ (10^4 cm^{-1})	$A_{ligands}$	References
$\{Co[S_2C_2(CF_3)_2]_2\}^{2-}$	—	2.04, 2.71, 2.04		—	—	—	—	(*166*)
$[Co(S_2C_2Ph_2)]^{2-}$	2.33	—	—	—	—	—	—	(*710*)
$\{Co_2[S_2C_2(CF_3)_2]_4\}^{-}$	2.042	—	—	—	—	—	—	(*53*)
Rh^{2+} in $ZnWO_4$	—	2.111, 2.130, 2.375		—	7 G, 8 G, 12 G		—	(*668, 669, 716*)
$[CpRh(\pi\text{-}C_2H_4)_2]^{+}$	1.9855	—	—	—	—	—	—	(*173*)
$[Rh(MNT)_2]^{2-}$	—	1.936, 2.447, 2.019		—	<4, <4, 7.5		—	(*81, 473*)
$RhCp_2$	—	2.033	2.003	—	—	—	—	(*384*)
$[CpRhS_2C_2(CF_3)_2] + e$	—	—	—	—	—	—	No figures quoted, 1 line	(*174*)
$IrCp_2$	—	2.033	2.001	—	1	5.1	—	(*384*)

and obtained a ^{59}Co splitting of 41 gauss. This seems anomalously high compared with other $S = \frac{1}{2}$ cobalt systems, although it is not known whether this compound really has $S = \frac{1}{2}$. Other complexes (*174*) which have been electrolytically reduced are $[CpCoPPh]_2$ and $[CpCoSCH_3]_2$, the latter may also be oxidized and yields an ESR signal. Vitamin B_{12} may be photolyzed or reduced to a species containing Co^{2+} (*350*). Numerous substituted cobalamin compounds are known, many of which yield similar ESR signals. Schrauzer (*610*) has shown that cobalt(II) dimethylglyoxime acts as a remarkably effective model for vitamin B_{12} derivatives, even to the extent of the methyl derivative being converted in the presence of hydrogen to methane by the bacterium *Methanobacillus omelanskii* with an efficiency nearly as great as the natural methylcobalamin.

TABLE XLVIII

g VALUES OF THE COMPLEXES $[Co(CNPh)_{4,\,5,\,or\,6}]^{2+}$

Ion	g_{av}	$g_{\perp}$	$\Delta(E_{d_{z^2}} - E_{d_{xz,yz}})$ (cm^{-1})
$[Co(CNPh)_4]^{2+}$	2.140	2.210	11,400
$[Co(CNPh)_5]^{2+}$	2.081	2.118	20,400
$[Co(CNPh)_6]^{2+}$	2.059	2.083	28,900

4. *ESR of Rh^{2+} and Ir^{2+}*

Hardly any ESR work has been carried out on rhodium complexes (*688*, *669*, *716*). In the host lattice $ZnWO_4$, ^{103}Rh splittings are seen, and Dessy *et al.* (*173*) have observed resonance from a species thought to be $[(\pi\text{-}C_5H_5)Rh(\pi\text{-}C_2H_2)_2]^+$ and also (*174*) from the one electron reduction product of $[CpRhS_2C_2(CF_3)_2]$ (see Table XLVII). The ^{103}Rh coupling (*81*, *473*) in $[Rh(MNT)_2]^{2-}$ is about half that in the $ZnWO_4$ host lattice case, showing the significant delocalization of the electron in the dithiolene complex. In $RhCp_2$, Keller and Wawersik (*384*) consider the electron to be in the $a_{2u}(d_{z^2})$ orbital as expected. The only ESR experiment on Ir(II) is that on Cp_2Ir, where a small metal hyperfine coupling is detected (*384*).

5. *ESR of Ni^{3+}, Pd^{3+}, and Pt^{3+}*

Resonance has been detected for Ni^{3+} in TiO_2 (*259*), where the crystal field is large enough to cause spin-pairing, and also in $KTaO_3$ (*312*) (see

Table XLIX). Pt^{3+} ions have been substituted in Al_2O_3 (*264*) and $BaTiO_3$ (*626*), ^{195}Pt coupling being observed in the latter case. In all cases, $g_{\parallel}$ is >2 and $g_{\perp} \sim 2$, indicating axial symmetry and suggesting the unpaired electron is in a d_{z^2} orbital. A single broad line ($\Delta H = 122$ gauss) is observed in powdered samples of $Ni[Ph_2P(CH_2)_3PPh_2]Br_3$ at 77°K. The stereochemistry of the complex is not known. Dessy *et al.* (*173*, *176*) have polarographically reduced some Ni–S complexes and obtained a single ESR line in solution. The products are thought to be $[CpNiSCH_3]^+$ and $CpNi[S_2C_2(CF_3)_2]$. $[CpNiSCH_3]_2$ may be both electrically oxidized and reduced, and [CpNi(PhC–CPh)NiCp] may be similarly reduced (*174*, *175*). Numerous dithiolene and related complexes of Ni, Pd, and Pt have been studied and are discussed in Section VIII,M,2.

The crystal structure (*419*) and ESR (*146*, *419*) of [*trans*-$Ni(diars)_2Cl_2]^+$ (where diars is *o*-phenylenebisdimethylarsine) have been determined. In methanolic solution, hyperfine coupling to four equivalent arsenic atoms are seen, but no interaction with Ni or Cl is observed. The complex $Ni(HBz)_2Br$ is thought to be square pyramidal, where H_2Bz represents α-benzoyloxime. ^{14}N s.h.f.s. are detected here (*240*). In the related complexes of Ni and Pd diphenylglyoxime with iodine and bromine, however, inclusion like molecular complexes stabilized by charge transfer interaction are thought to be formed rather than a square pyramidal halocomplex (*217*).

ESR signals are detected on some $Pd–SiO_2–Al_2O_3$ catalysts (*535*) and in the complex $Pt(NH_3)_2(SCN)_2I$ (*526*), prepared by oxidation of *cis*-$Pt(NH_3)_2(SCN)_2$ by I_2 in *t*-BuOH. This is one of the few paramagnetic Pt or Pd complexes.

J. d^8 IONS

In octahedral fields, g and A values are close to isotropic. As the field becomes distorted, the zero-field splitting becomes larger and ESR signals are more difficult to observe.

Most of the ESR of Ni^{2+} complexes have been carried out in host lattices. Since the spin of ^{58}Ni and ^{60}Ni is zero, and ^{61}Ni (spin $I = \frac{3}{2}$) is present in only 1.25% natural abundance, metal h.f.s. have only rarely been observed (*544*, *716*). McGarvey (*504*) lists many of the systems where g and zero-field parameters are known (see Table L for other data).

Resonance has been observed in various nickel–cyanide–ammonia clathrate compounds (*79*), but since these are not magnetically dilute, no hyperfine structure was observed. The pyridine clathrate is said to show fine structure, but no details are given.

Cu h.f.s. are observed for Cu^{3+} in a Al_2O_3 host lattice.

Owen and Thornley (*547*) have reviewed covalency in transition metal ions and, in particular, in nickel complexes. The NMR contact shift method has been used by Eaton *et al.* (*195*) to determine spin densities on organic ligands of paramagnetic molecules. In particular (*194*), a series of nickel aminotroponeiminates have been studied whereby conjugative and hyperconjugative effects within the molecule may be monitored. Similar studies of contact shifts have been carried out on Co^{II} and Ni^{II} pyrromethenes and porphyrins (*196*) and on many transition metal acetylacetonates (*193*) by Eaton *et al.*

K. d^9 IONS

1. ESR of Fe^{-1}

Dessy *et al.* (*173*, *176*) have electrically reduced numerous iron carbonyl derivatives. It is noticeable how close the g values are to free spin for the iron tricarbonyl cyclooctatetraene anion. This implies much delocalization of the electron onto the ring system compared with $[Fe(CO)_5]^-$ itself. No proton coupling was observed due to the large linewidth. Others which Dessy (*174*, *175*) has electrolytically reduced are listed in Table LI. A curious result is the reduction of the compound $[(NO)_2FePPh_2]_2$ where $g = 1.937$ (unusually low) and ^{31}P h.f.s. are detected but no ^{14}N. The solid compound Na[Fe(dipy)$_3$] gives a single narrow line (*470*), $\Delta H = 2.8$ gauss, at $g = 2.0031$. This is very similar to that in Na(dipy) where $g_\parallel = 2.0023$ and $g_\perp = 2.0046$ and suggests that the electron is almost entirely delocalized onto the dipyridyl ring systems. Under certain circumstances both spectra may be obtained simultaneously, showing that the spectrum due to the iron complex is not that due to sodium dipyridyl. These results should be compared with the phthalocyanine-type complexes described in Section VIII,L,1.

2. ESR of Co^0 *and* Rh^0

Trimeric $[\pi\text{-}C_5H_5Co(CO)]_3$ upon reduction (*173*) adds one electron and yields a complex ESR signal which has not been interpreted; this system is nominally $d^8d^8d^9$. The square planar species $Co(CO)_4$ is formed (*383*) by subliming $Co_2(CO)_8$ onto a cold finger (77°K). Cobalt h.f.s. is observed and the authors predict that the electron is in the a_{1u} antibonding molecular orbital.

$RhCl_3$ in AgCl produces Rh^0 in a lattice site with an environment of six Cl ions. The ESR spectrum (*708*) is interesting since three different spectra are observed as the temperature is raised. The vibrations of the surrounding Cl ions (ligands) causes mixing between the two possible

TABLE XLIX

ESR Data for d^7 Spin-Paired Ni^{3+}, Pd^{3+}, and Pt^{3+} Ions

Ion	g_{av}	$g_{\parallel}$	$g_{\perp}$	A_{iso} (10^4 cm^{-1})	$A_{\parallel}$ (10^4 cm^{-1})	$A_{\perp}$ (10^4 cm^{-1})	$A_{ligands}$ (10^4 cm^{-1})	References
$[Ni(diars)_2Cl_2]Cl$	2.09	2.05, 2.09, 2.14		—	—	—	$A_{iso}(As) = 70$ G	(*146, 419*)
$Ni(HBz)_2Br$	—	2.036	2.194	—	—	—	$A_{\perp}(^{14}N) = 19$ G	(*240*)
$Ni(Ph_2glyoxime)_2Br$	—	2.1118	2.0221	—	—	—	—	(*217*)
$Ni(Ph_2glyoxime)_2I$	—	2.0121	2.0222	—	—	—	—	(*217*)
$[CpNi\text{–}(PhC\text{–}CPh)\text{–}NiCp] + e$	2.0526	—	—	—	—	—	—	(*175*)
$[CpNiSCH_3]_2 - e$	2.007	—	—	—	—	—	—	(*174*)
Ni^{3+} in TiO_2	—	2.084, 2.085, 2.254		—	—	—	—	(*259*)
$Ni[Ph_2P(CH_2)_3PPh_2]Br_3$	—	2.218		—	—	—	—	(*672*)
$[CpNiSCH_3]_2^+$	2.0267	—	—	—	—	—	—	(*173*)
$[CpNiS_2C_2(CF_3)_2]$	2.0479	—	—	—	—	—	—	(*176*)
$[Ni(MNT)_2]^-$	2.063	1.198, 2.160, 2.042		—	—	—	$A_{\parallel}(^{33}S) = 14.27$ G, $A_{\perp}(^{33}S) = 4.55$ G	(*163, 164, 473, 602, 642*)
$[Ni(TDT)_2]^-$	2.082	2.016, 2.183, 2.048		—	—	—	$A_{\parallel}(^{33}S) = 13.3$ G	(*287, 602, 642, 710*)
$\{Ni[S_2C_2(CF_3)_2]_2\}^-$	2.0618	1.996, 2.137, 2.044		—	—	—	$A_{\parallel}(^{33}S) = 14.5$ G	(*163, 164, 166, 602*)
$[Ni(S_2C_2Ph_2)_2]^-$	2.0568	2.122, 2.041, 1.999		4.5 G	—	—	$A_{\parallel}(^{33}S) = 13.7$ G	(*163, 164, 602*)
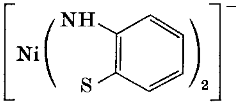	2.055	2.006, 2.123, 2.030		—	—	—	—	(*54, 352, 642*)
$[Ni(S_2C_2H_2)_2]^-$	—	2.126, 2.039, 1.996		—	—	—	$A_{\parallel}(^{33}S) = 13.9$ G	(*602*)
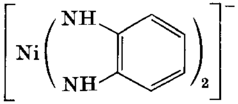	2.031	1.990, 2.102, 2.006		—	—	—	—	(*52*)

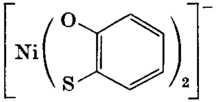	2.083	2.017, 2.191, 2.036	—	—	—	—	(*54*)
$\{Ni[Se_2C_2(CF_3)_2]_2\}^-$	—	2.008, 2.193, 2.116	—	—	—	$A(^{77}Se) = 69$ G	(*169*)
$[Ni(S_2C_2H_2)_2]^-$	2.056	1.996, 2.126, 2.039	—	—	—	$A_{\parallel}(^{33}S) = 13.9$ G	(*602, 609*)
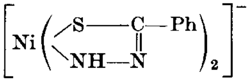	2.0435	2.006, 2.094, 2.025	—	—	—	—	(*352*)
$[NiH_2gma]^-$	2.051	2.009, 2.119, 2.027	—	—	—	—	(*352, 433, 472, 642*)
$[Pd(MNT)_2]^-$	2.0238	1.956, 2.065, 2.046	7.7 G	—	—	—	(*164*)
$[Pd(TDT)_2]^-$	2.022	—	—	—	—	—	(*710*)
$\{Pd[S_2C_2(CF_3)_2]_2\}^-$	2.023	1.955, 2.065, 2.049	7.7 G	—	—	—	(*166*)
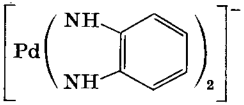	2.006	1.946, 2.062, 2.008	—	—	—	—	(*52*)
$Pd(HBz)_2Br$	—	2.008 2.019	—	—	—	—	(*240*)
$Pd(Ph_2glyoxime)_2Br$	—	2.0097 2.0177	—	—	—	—	(*217*)
$Pd(Ph_2glyoxime)_2]I$	—	2.0088 2.0166	—	—	—	—	(*217*)
Pt^{3+} in Al_2O_3	—	2.328 2.011	—	—	—	—	(*264*)
Pt^{3+} in $BaTiO_3$	—	2.459 1.950	—	0	135	—	(*626*)
$[Pt(MNT)_2]^-$	2.042	1.825, 2.221, 2.067	82 G	—	—	—	(*164*)
$[Pt(TDT)_2]^-$	2.031	1.810, 2.229, 2.059	—	—	—	—	(*710*)
$\{Pt[S_2C_2(CF_3)_2]_2\}^-$	2.039	1.823, 2.210, 2.074	82 G	118 G, 7 G, 129 G		—	(*166*)
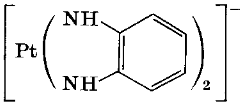	1.988	1.759, 2.217, 1.978	—	145 G, 68 G, 200 G		—	(*52*)
Pt in YAl Garnet	—	1.962, 2.361, 2.424	—	99 G, 88 G, 30 G		—	(*348*)

TABLE L

ESR DATA FOR SOME d^8 IONS

Ion	$g_{\parallel}$	$g_{\perp}$	$A_{\parallel}$ (10^4 cm^{-1})	$A_{\perp}$ (10^4 cm^{-1})		References
Ni in Ge–As	—		10.5 G		—	(*716*)
Ni^{2+} in MgO	2.225		8.3		—	(*544*)
$Ni(CN)_2 \cdot NH_3$	2.38		—		—	(*79*)
$Ni(CN)_2 \cdot NH_3 \cdot C_4H_5N$	2.14		—		—	(*79*)
$Ni(CN)_2 \cdot NH_3 \cdot C_6H_6$	2.11		—		—	(*79*)
$Ni(CN)_2 \cdot NH_3 \cdot C_5H_5N$	2.07		—		—	(*79*)
$Ni(CN)_2 \cdot NH_3 \cdot C_4H_4S$	2.05		—		—	(*79*)
Cu^{3+} in Al_2O_3	2.0784	2.0772	64.6	60.2	$D = -0.18838$ cm^{-1}	(*263*)

Jahn–Teller distorted ground states, d_{z^2} or $d_{x^2-y^2}$. At >160°K, the g values show that the wave function is a combination of $\frac{3}{4}\psi d_{x^2-y^2} + \frac{1}{4}\psi d_{z^2}$. The large admixture of d_{z^2} indicates considerable thermal vibration. At temperatures >200°K there is an equal amount of $\psi d_{x^2-y^2}$ and ψd_{z^2} in the wave function and consequently, the spectrum is isotropic. This is the dynamic Jahn–Teller effect. Below 160°K, the wave function is mostly $d_{x^2-y^2}$ and the low level of thermal vibration does not produce

TABLE LI

ESR DATA FOR d^9 Fe^{-1} IONS

Ion	g_{av}		References
$[Fe(CO)_5] + e$	2.038	—	(*176*)
$[(\pi\text{-}C_8H_8)Fe(CO)_3] + e$	2.0073	—	(*176*)
$[(\pi\text{-}C_6H_8)Fe(CO)_3] + e$	2.053	—	(*176*)
$[(\pi C_8H_8O)Fe(CO)_3] + e$	2.0403	—	(*173*)
$[(C_6H_{10}CO)Fe(CO)_3]$	2.0572	—	(*173*)
$\{Fe_2(CO)_6[(ClC_6H_4C)_4CO]\} + e$	2.0619	—	(*175*)
$[(Fe_2(CO)_6(PhC_2CH_3)_2CO] + e$	2.0322	2 lines sep. by 104 G	(*175*)
$[Fe_2(CO)_6(C_2H_5C_2C_2H_5)_3] + e$	2.0415	2 lines sep. by 27 G	(*175*)
$[Fe_3(CO)_8(PhC_2Ph)_2] + e$			
violet	2.0031	—	(*175*)
black	2.0106	—	(*175*)
$[(2,4\text{-Diphenyltropone})Fe(CO)_3] + e$	2.0247	—	(*175*)
$[(2,4,6\text{-Triphenyltropone})Fe(CO)_3] + e$	2.0251	—	(*175*)
$[(\text{Dithienyl})Fe_2(CO)_6] + e$	2.0291	2 lines sep. by 3.5 G	(*175*)
$[(\text{Thianaphthene})Fe_2(CO)_6] + e$	2.0261	2 lines sep. by 5.2 G	(*175*)
$[(NO)_2FePPh_2]_2 + e$	1.937	$A(^{31}P) = 20$ G, $2 \equiv P$	(*174*)
$NaFe(dipy)_3$	2.0031	Solid state g value	(*470*)
$FePc + 3e$	2.0030	—	(*301, 302*)

much mixing with d_{z^2}. S.h.f.s. is observed in the latter case which is due to two equivalent Cl ions. The available data are given in Table LII.

3. *ESR of Ni^+*

Stable paramagnetic organometallic compounds are exceedingly rare and so the few that are known have been studied in detail. ESR has shown (*455*) that in $(\pi\text{-}C_5H_5)_3Ni_3(CO)_2$, which has the structure shown in Fig. 52, this molecule has symmetry D_{3h} and the unpaired electron is in the A_2'' π-bonding molecular orbital linking the three nickel atoms

TABLE LII

ESR DATA FOR d^9, Co^0, Rh^0, Ni^+ IONS

Ion	g_{av}	$g_{\parallel}$	$g_{\perp}$	$A_{\parallel}$ (10^4 cm^{-1})	$A_{\perp}$ (10^4 cm^{-1})	$A_{ligands}$	References
$[CpCo(CO)]_3 + e$	—	—	—	—	—	No results given	*(173)*
$Co(CO)_4$	—	2.02	2.134	67 G	56.6 G	—	*(383)*
Rh^0 in AgCl							
<110°K	—	2.015	2.417	—	—	$A_{\parallel}(Cl) = 25.6$, $A_{\perp}(Cl) = 14.7$	*(708)*
160–350°K	—	2.436	2.207	—	—	—	*(708)*
200–430°K	—	2.287	2.287	—	—	—	*(708)*
Ni^+							
in TiO_2	—	2.272, 2.237, 2.050		—	—	—	*(259)*
in NaF	—	2.766	2.114	—	—	^{19}F s.h.f.s. seen	*(326)*
$Cp_3Ni_3(CO)_2$	—	2.110	2.027	—	—	—	*(173)*
	—	2.1050	2.0225	—	—	—	*(173)*
$[(CO)_2NiPPh_2]_2 + e$	1.979	—	—	—	—	—	*(174)*
$[CpNiPPh_2]_2 + e$	2.060	—	—	—	—	—	*(174)*
$[Ni(dbh)]^-$	2.0006	—	—	—	—	—	*(352)*
$[Nidtbh]^-$	1.9973	—	—	—	—	—	*(352)*
$[Nigma]^-$	2.0042	1.979, 2.028, 2.006		—	—	—	*(352, 433, 472)*
$NiPc + e$	2.0026	—	—	—	—	—	*(302)*

as shown in Fig. 53. Modifications to the theory for g values predict this and it is supported by the experimental values of $g_\perp$ and $g_\parallel$. The system is nominally $d^8d^8d^9$. A related complex (*545*) containing the $(CpNi)_3$ ring system but with a quarternary t-BuN$\lessdot$ group roughly centrally placed above the plane of the ring with the N atom acting as a multiple bridge to each nickel atom shows a $g = 2.035$ single line in the solid state.

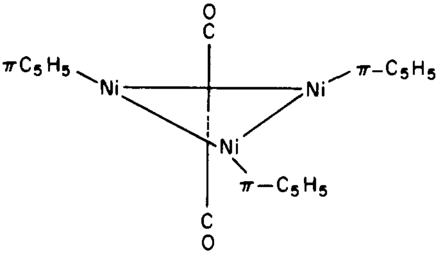

FIG. 52. $(\pi\text{-}C_5H_5)_3Ni_3(CO)_2$.

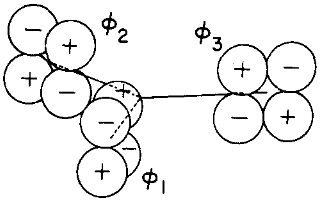

FIG. 53. The ground state molecular orbital of symmetry a_2'' consisting of a linear combination ($\psi = c_1\phi_1 + c_2\phi_2 + c_3\phi_3$) of $3d$ orbitals each centered on one of the metal atoms.

Irradiated Ni in TiO_2 (*259*), NaF (*326, 328*), and LiF (*328*) lattices yield spectra attributed to Ni^+. ^{19}F s.h.f.s. are observed in numerous species detected in the fluoride lattices.

Dessy *et al.* (*175*) have electrolytically reduced $[(CO)_2NiPPh_2]_2$ and $[CpNiPPh_2]_2$. In each case, one electron is added.

4. ESR of Cu^{2+}

a. The Jahn–Teller Effect. The Jahn–Teller effect causes distortions from O_h symmetry in all 6-coordinate cupric compounds. In almost all cases, the distortion is large and can be treated as an elongation of the charges along the z axis stabilizing the d_{z^2} orbital and leaving the unpaired electron in the $d_{x^2-y^2}$ orbital for which the g values are given by

$$g_{\parallel} = 2.0023 + \frac{8\lambda}{\Delta E(d_{x^2-y^2} - d_{xy})} \tag{141}$$

$$g_{\perp} = 2.0023 + \frac{2\lambda}{\Delta E(d_{x^2-y^2} - d_{xz,yz})} \tag{142}$$

thus making $g_{\parallel} > g_{\perp} > 2$.

When the Jahn–Teller effect stabilizes the $d_{x^2-y^2}$ orbital, the unpaired electron is in the d_{z^2} orbital for which the g values are given by

$$g_{\parallel} = 2.0023 \tag{143}$$

$$g_{\perp} = 2.0023 + \frac{6\lambda}{\Delta E(d_{z^2} - d_{xy,yz})} \tag{144}$$

thus making $g_{\perp} > g_{\parallel} = 2$.

Examples of this are rare, but the effect is observed in Cu^{2+} in $CdWO_4$ (and $ZnWO_4$ and $MgWO_4$) (*635*, *636*) and in NH_4Cl (*727*), although in this latter case the authors wrongly say the electron is in the $d_{x^2-y^2}$ orbital. In cupric citrate solutions at *p*H 7–11 (*189*), a dimeric form is postulated and the g values indicate that the electron is in the d_{z^2} orbital. In CuF_2 molecules trapped from the vapor state in an argon matrix, the ESR parameters show (*379*) that the molecules are linear with the electron in the d_{z^2} orbital. The high isotropic coupling to ^{63}Cu arises from mixing of the d_{z^2} orbital with the 4*s* orbital. The ^{19}F s.h.f.s. indicate about 8% electron delocalization and significant covalency.

The Jahn–Teller effect is usually static, i.e., the crystal environment is such as to force a distortion upon the degenerate e_g orbitals (in O_h symmetry) causing them to split.

In certain cases where the environment of the Cu^{2+} ion is almost truly octahedral, there is little difference in the stabilizing energy of the $d_{x^2-y^2}$ or d_{z^2} orbitals and the electron may jump from one to the other orbital. This is the dynamic Jahn–Teller effect and is recognized by isotropic A and g values, with values being the average of the anisotropic A and g values appropriate for a static distortion. Examples of this are Cu^{2+} in MgO (*178*), $Cu(en)_3SO_4 \cdot 3H_2O$ (*570*), Cu^{2+} in $MgCl_2$ and $CdCl_2$ (nearly isotropic) (*488*), and for $[Cu(H_2O)_6]^{2+}$ in $MgLa_2(NO_3)_{12} \cdot 24H_2O$, $Mg_3Bi_2(NO_3)_{12} \cdot 24H_2O$, and $ZnSiF_6 \cdot 6H_2O$ (*90*). In these latter cases, at 20°K, the distortion is static, but at 90°K, the distortion is dynamic.

A dynamic Jahn–Teller distortion occurs (*402*) in copper-doped zinc *tris-o*-phenanthralene nitrate. Since anisotropic nitrogen s.h.f.s. are observed, then the distortion must be tetragonal rather than trigonal, where the six nitrogen atoms would be equivalent and give an isotropic splitting. At 77°K the distortion is static, but at room temperature, the distortion is dynamic and the spectrum isotropic.

The Jahn–Teller effect has been reviewed by Mueller (*522*), and a detailed study of the dynamic aspects of it with particular reference to $[CuCl_6]^{4-}$ has been made by Lohr (*452*).

b. Square Planar Stereochemistry. Major distortions to Cu^{2+} in an approximately octahedral environment cause the g values to approach 2. Thus for a square planar molecule, $\Delta E(d_{x^2-y^2} - d_{xy})$ and $\Delta E(d_{x^2-y^2} - d_{xz,yz})$ become very large and so $g_{\parallel}$ and $g_{\perp}$ become smaller. This is readily seen in the phthalocyanine-type complexes and in other essentially square planar molecules, which are tabulated in Table LIII.

There have been numerous papers reporting results for the ESR of porphyrin-type complexes (see Table LIII). These complexes are of interest because of their rigid planar structure. The highly aromatic ring raises the question of the degree of in-plane and out-of-plane π bonding. This has been the subject of much controversy since measurement depends largely on the accuracy of the determination of the ^{14}N coupling constants. A recent redetermination of the spectrum of copper phthalocyanine (*304*) using enriched ^{63}Cu isotope has shown that most of the earlier workers had misinterpreted their spectra. This work has shown that, since the unpaired electron is in a $b_1{}^*(d_{x^2-y^2})$ molecular orbital and its interaction with the corresponding antibonding orbital on the pyrrole N atoms is sp^2, then there are no N orbitals available for in-plane π bonding between the metal d_{xy} orbital and the N. Out-of-plane π bonding is present, but the extent to which it is important depends on an accurate value for the $d_{x^2-y^2} - d_{xz,yz}$ energy gap. This is not known with any certainty. In the p-chloro derivative of copper tetraphenylporphrin, a large Cl s.h.f.s. splitting of about 100 gauss is observed (*69, 363*), showing that there is considerable unpaired spin density on the perifery of the ring system.

In the solid state, or indeed in solution, it is frequently difficult to consider truly square planar complexes because of the possibility of weak axial interactions.

Deviations from planarity affect to a major extent the g tensor, the metal, and the ligand h.f.s. Rist *et al.* (*583*) have studied single crystals of cupric 8-hydroxyquinolinate in a series of organic host lattices.

It is in the realm of cupric square planar complexes where the valence bond theory gives not only an inadequate, but an incorrect description of the bonding. Valence bond theory ignores the presence of antibonding orbitals and invokes the use of a linear combination of $d_{x^2-y^2}$, p_x, p_y, and s orbitals to form the σ bonds. For d^9 ions, the ninth electron can only

TABLE LIII

ESR DATA FOR SQUARE PLANAR d^9 Cu^{2+} IONS

Ion	g_{iso}	$g_{\parallel}$	$g_{\perp}$	A_{iso}Cu (10^4 cm^{-1})	$A_{\parallel}$Cu (10^4 cm^{-1})	$A_{\perp}$(Cu) (10^4 cm^{-1})	A_{iso}(^{14}N) (10^4 cm^{-1})	$A_{\parallel}$(^{14}N) (10^4 cm^{-1})	$A_{\perp}$(^{14}N) (10^4 cm^{-1})	References
^{63}CuPc in H_2Pc	—	2.160	2.045	—	217 G	31.5 G	—	19.5 G	15.4 G	(*304*)
CuPc										
in ZnPc	—	2.162	2.047	—	215	28	—	17.4	15.8	(*68, 170*)
in H_2SO_4	—	2.180	2.037	—	—	—	—	13.6 G	15.4 G	(*589*)
in H_2SO_4	—	2.1746	2.045	—	202	32	—	14.4 G		(*392, 531*)
in H_2Pc	—	2.179	2.050	—	202	19	—	14.5	17.8	(*40, 314*)
CuTPP										
in H_2Pc	—	2.170	2.042	—	180	53.6	—	17.0	12.4	(*36*)
in H_2TPP	—	2.193	2.071	—	202	29	—	14.5	16.1	(*37, 272, 363*)
in $CHCl_3$	2.1073	2.187	2.067	97.7	218	39	15.9	14.5	16.5	(*37*)
Cu etioporphrin	2.0975	2.169	2.061	91.2 G	—	—	14.6 G	—	—	(*588*)
Cu *p*-chloro TPP	—	2.17	2.05	—	250	30	—	($^{35/37}$Cl = 100 G)		(*69, 363*)
Cu Na chlorophyllin	2.1077	2.2033	2.0518	98	205.1	30.1	14.1	15.9	—	(*607*)
$[Cu(NH_4)_4][PtCl_4]$	—	2.217	2.051	—	211	28	—	17 G	10.2 G	(*225, 576*)
$(NH_4)_2CuCl_4$	—	2.234	2.046	—	—	—	—	—	—	(*709*)
$(EtNH_3)_2CuCl_4$	—	2.234	2.046	—	—	—	—	—	—	(*229, 709*)
$[Cu(CN)_4]^{2-}$ in MeOH	2.075	2.160	2.033	58	143	21	—	—	—	(*454*)
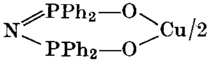	—	2.335	2.068	—	137.7 G	—	—	—	—	(382)

$Cu[S_2CN(i\text{-}Pr)_2]_2$	2.046	2.087	2.023	74	154	35	—	($A^{33}S = 11.2$ G)		(*4, 31, 261, 266, 292, 559, 624, 632, 674*)
$Cu[S_2P(OEt)_2]_2$	2.047	2.03	2.02	73	111	42	—	($A_{iso}{}^{31}P = 8$ G)		(*243, 682*)
$(Cu:Zn)(S_2CNEt_2)_2$	—	2.1085	2.023	—	142	22.4	—	—	—	(*578, 700*)
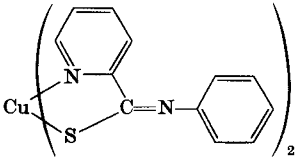	2.073	2.11	2.042	65 G	—	—	16 G	—	—	(*32–35, 513*)
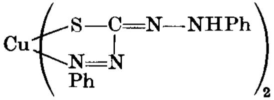	2.075	—	—	58.8 G	—	—	—	—	—	(*585*)
$[Cu(MNT)_2]^{2-}$	2.0458	2.086, 2.026, 2.023		75.99 G	158.9 G	43.4 G	—	—	—	(*82, 473, 637, 710*)
$[Cu(S_2C_2O_2)_2]^{2-}$	2.0427	2.083	2.024	81.26 G	176 G	51 G	—	—	—	(*82*)
$[Cu(i\text{-}MNT)_2]^{2-}$	2.046	—	—	75.9 G	—	—	—	—	—	(*706*)
$[Cu(TDT)_2]^{2-}$	2.046	—	—	77.6 G	—	—	—	—	—	(*710*)
$[Cu(cat)_2]^{2-}$	2.118	2.233	2.058	82	205	—	—	—	—	(*587*)
$[Cu(Clcat)_2]^{2-}$	2.124	2.254	2.056	79	200	—	—	—	—	(*587*)
[Cu(dbh)]	2.109	2.230	2.048	71.9	168	—	11.3	13.7	—	(*352*)
[Cu(dtbh)]	2.062	—	—	81.8	—	—	13.8	—	—	(*352*)

go into the $4p_z$ orbital. ESR results, however, show the unpaired electron to be in one of $d_{x^2-y^2}$ symmetry. Since the $d_{x^2-y^2}$ bonding orbital is filled, then the unpaired electron must be in the antibonding orbital with symmetry $d_{x^2-y^2}$ (*620*).

Electron diffraction measurements (*443*) of gaseous anhydrous cupric nitrate have suggested that the molecule is planar with the copper surrounded by four oxygen atoms in a square arrangement. This is confirmed by the ESR spectrum where the parameters are almost exactly that of cupric bisacetylacetonate (*474*). In ethyl acetate solutions, the ESR parameters indicate a tetragonally distorted octahedral structure with much less delocalization of the electron (i.e., more ionic bonding) in support of the structure

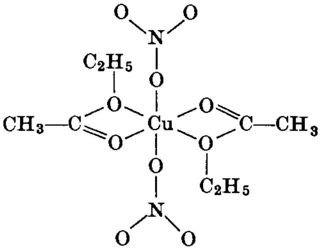

with weak bonding between the Cu^{2+} and NO_3^-.

Certain halide complexes, notably $(NR_4)_2CuCl_4$ (*709*), may be considered as square planar. One compound which is truly square planar is $[Cu(NH_3)_4](PtCl_4)$ (*225*), where planarity is forced upon the system by the host lattice, Magnus's salt $[Pt(NH_3)_4][PtCl_4]$. Analysis of the nitrogen tensor indirectly shows that the hybridization of the ammonia lone-pair electrons is $sp^{5.1}$. This is not unexpected, and shows how in certain cases, ESR data can be used to monitor the electrons in bonding orbitals (*576*).

c. Tetrahedral Stereochemistry. Cu^{2+} in a tetrahedral environment is rare, and distortions can be treated as perturbed square planar cases. Good approximations to t_d symmetry are found in Cs_2CuCl_4 (*613, 614*), Cu α,α′-dibromodipyrromethene (*60*), $[Cu(py)_4]\cdot S_2O_8$ (*329*), Cu^{2+} in ZnO (*178, 181, 375*), and Cu^{2+} in GeO_2 (*622*). In t_d symmetry, p orbitals have the same symmetry as the t_{2d} d orbitals of the metal, and thus there can be a mixing of $4p$ and $3d$ orbitals. Sharnhoff (*613*) has estimated that the unpaired electron in tetrahedral $[CuCl_4]^{2-}$ is in an orbital that is 70% $3d$ and 12% $4p$ on Cu and 17% $3p$ and 1.3% $3s$ on Cl. Using the ^{14}N coupling constants (*329*) in $[Cu(py)_4]^{2+}$, the $2p$ character of N is deduced from

$$\frac{A_{\parallel} - A_{iso}}{34.5} = \frac{7.8}{34.5} = 22.6\% \qquad (145)$$

and the 2*s* character of N is

$$\frac{A_{iso}}{550} = \frac{4.9}{550} = 0.9\% \qquad (146)$$

which are very close to the figures for Cl in $[CuCl_4]^{2-}$. In the case of Cu^{2+} in ZnO, the σ bonds are particularly strong and delocalization of the electron is as much as 40%. Certain salicylaldiminato complexes approximate closely to tetrahedral stereochemistry, particularly when the copper atom replaces a small proportion of zinc atoms in the diamagnetic host lattice. A detailed single crystal study has been made by Fritz *et al.* (*223*) on one of these complexes.

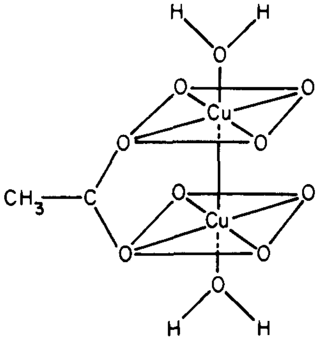

FIG. 54. Structure of cupric acetate, showing only one of the four bridging acetate groups.

The purple species in methanolic cupric solutions containing excess cyanide has been shown to be the square planar species $[Cu(CN)_4]^{2-}$ (*454*).

d. Dimers: copper–copper Interactions. The crystal structure (*675*) of cupric acetate is unique in that pairs of Cu^{2+} ions are only 2.64 Å apart. This is illustrated in Fig. 54. An exchange interaction between the two ions produces a singlet and a triplet state, with the singlet state lower in energy by 260 cm^{-1}. This manifests itself in the ESR spectrum (*396*) where the average Cu hyperfine coupling in $Cu_2(CH_3COO)_4 \cdot 2H_2O$ is about half that in $(Cu/Zn)_2(CH_3COO)_4 \cdot 2H_2O$ where the diamagnetic diluent prevents the exchange interaction and a "normal" copper spectrum is observed (see Table LIV). The same effect is seen (*689*) in copper-doped zinc formate, where for <0.5% Cu, $A_{iso}(^{63}Cu) = 100$ gauss, but for 3.4% Cu, $A_{iso}(^{63}Cu) = 49$ gauss, and in several other organic salts (*97, 99, 157, 189, 401, 446, 571, 721, 722*).

The importance of δ bonding has been discussed, and refined values of the spin–spin coupling constant have been given by Jotham and Kettle (*374*). Table LIV summarizes the available ESR data. An interesting molecule is cupric cyanoacetate, which forms a polymeric species

TABLE LIV

ESR DATA FOR DIMERIC AND RELATED SPECIES OF Cu^{2+}

Species	g_{av}	$g_{\parallel}$	$g_{\perp}$	A_{iso}(Cu) ($10^4 cm^{-1}$)	$A_{\parallel}$(Cu) ($10^4 cm^{-1}$)	$A_{\perp}$(Cu) ($10^4 cm^{-1}$)		References
(Cu:Zn)$(CH_3COO)_4 \cdot 2H_2O$	—	2.344	2.052	—	147, 18, 23		—	*(396, 571)*
$Cu_2(CH_3COO)_4 \cdot 2H_2O$	—	2.344, 2.052, 2.093		—	80	<10	—	*(9, 88, 396)*
$Cu_2(CH_2ClCOO)_4 \cdot 5H_2O$	—	2.40, 2.06, 2.09		—	—	—	—	*(157)*
(Cu:Zn)$(HCOO)_2 \cdot 2H_2O$	—	2.416	2.077	—	124	23	(^{63}Cu)	*(10, 417, 571, 689)*
$Cu_2(C_2H_5COO)_4$	—	2.368, 2.102, 2,100		—	120 G	35 G	—	*(7, 721)*
(Cu:Zn)$(C_3H_7COO)_4 \cdot H_2O$	—	2.348	2.060	—	74	<10	$D = 0.327$ cm^{-1}, $E < 0.001$ cm^{-1}	*(401)*
Cu *n*-valerate	—	2.29	2.03	—	115 G	39 G	—	*(721)*
Cu citrate, *p*H 2–7	—	2.37	2.07	—	140 G	—	—	*(189)*
$Cu_2(NC \cdot CH_2COO)_4$	—	2.40	2.08	—	—	—	—	*(693)*
Cu acetylsalicylate	—	2.36	2.07	—	80	—	$D = 0.36$ cm^{-1}. Similar values for 18 related acids	*(446)*
$Cu^+Cu^{2+}(CH_3COO)_2 \cdot$solv.	2.17	2.37	2.08	42 G	—	—	2 ≡ Cu in solution	*(625)*
Cu^{2+}								
in $[(C_5H_5NO)_2ZnCl_2]_2$	—	2.323, 2.056, 2.080		—	129	<10	$A_{\parallel}(^{35}Cl) = 25$, $A_{\perp}(^{35}Cl) = 7$	*(398)*
in $[(C_5H_5NO)ZnCl_2 \cdot H_2O]_2$	—	2.306, 2.056, 2.083		—	139	<10	—	*(398)*
in $[(C_5H_5NO)_2NiCl_2]_2$	—	2.14, 2.54, 2.49		—	35	<7	—	*(398)*
in $[(C_5H_5NO)NiCl_2 \cdot H_2O]_2$	—	2.15, 2.61, 2.50		—	40	<7	—	*(398)*

containing a Cu–Cu cage structure like the acetate (*174*). This paper gives a useful review of the theory and a general method for obtaining the magnetic parameters of dimeric copper compounds. Another related system investigated by Sigwart *et al.* (*625*) is a mixed valence Cu(I), Cu(II) acetate which exhibits seven lines with a spacing of 42 gauss and with appropriate relative intensities attributable to two equivalent copper atoms. The species so formed is considered to be a binuclear species with a pair of acetate bridges, the bridges being a single oxygen atom from the acetate.

The pyridine *N*-oxide complexes (*398*) of formula

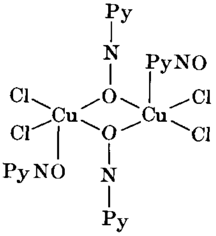

and the corresponding one with H_2O replacing PyN → O in the axial position have a Cu–Cu distance of 3.3 Å and show superexchange like cupric acetate. This is proven in the Cu/Zn case where the Zn diluent prevents exchange processes, but in the Cu/Ni case, there is still exchange between the Cu^{2+} and Ni^{2+}. This is because the Ni^{2+} is in a 5-coordinate position and has two unpaired electrons; this behaves like three coupled ions and the coupling to copper is about one-third that in $[(C_5H_5NO)_2Cu/ZnCl_2]_2$, i.e., 35×10^{-4} cm^{-1} compared with 129×10^{-4} cm^{-1}. This is the only known case where coupling between two different metals is found. It is interesting that superexchange does not seem to be dependent on Cu–Cu distance since in cupric acetate the Cu–Cu distance is 2.64 Å compared with 3.3 Å in the PyN → 0 complexes. In $CsCuCl_3$, however, the Cu–Cu distance is 3.06 Å, but no magnetic exchange properties are observed.

A detailed paper by Lohr (*453*) discusses and tabulates the theoretical g values for six-coordinated binuclear copper(II) complexes for all combinations of Jahn–Teller distortions along the axes x, y, and z. Interactions of this type have also been reviewed by Kokoszka and Gordon (*400*).

e. *Other Cupric Complexes.* ^{33}S s.h.f.s. have not been observed from ligands of the type dithiodialkylcarbamate except in the case of Cu^{2+} and Ag^{2+} complexes. Here, direct overlap between the $d_{x^2-y^2}$ orbital and the s orbitals places spin density on the sulfur atom. The reason why it is difficult to see ^{33}S s.h.f.s. is not only because of its low natural abundance (0.74%), but because there is usually little *s* character in the lone-pair hybrid orbital (unlike N where the lone-pair is usually *sp*, sp^2, or sp^3). This arises because of the availability of 3*d* orbitals means that 3*s* orbitals need not be used in hybridization. Pettersson and Vanngard (*559*) calculate that the *p*/*d*:*s* ratio in Ag and Cu dithiocarbamates is about 4.4:1. From the bonding parameters it is deduced (*559*) that the out-of-plane π bond is almost ionic.

A range of bisthiosemicarbazones and natural products with related groups have been studied by Blumberg and Peisach (*96*). The structurally related xanthates have also been investigated (*633*).

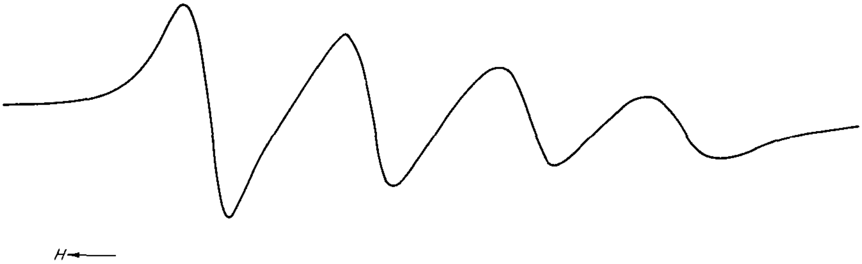

FIG. 55. Fluid solution spectrum of $Cu(acac)_2$ in $CHCl_3$.

The reaction (*585*, *707*) of cupric dithizonate and diphenylcarbazate with alkali is interesting in that the color change and ESR signal indicate that a ligand radical species is formed in solution. The reaction is reversible with acid.

Numerous copper complexes have been studied by Kivelson and Neiman (*392*) in great detail and this paper forms a good basis in understanding the significance of ESR to the problem of elucidating the nature of the bonding in copper complexes.

There has been a vast quantity of ESR work in the field of cupric complexes with organic bases. Much of this work is on poorly characterized species and the parameters obtained are usually incomplete and of little value. The series of complexes $[Cu(NH_3)_n(H_2O)_{6-n}]^{2+}$ yield (*657*) a trend in *g* and *A* values which could with interest be related to the optical work of Jorgensen *et al.* (*86*). Spin densities on the protons of the hexaamine have been determined from NMR Knight (Contact) shifts (*699*). Shupack has correlated the *g* tensors of $[Cu(NH_3)_6]^{2+}$ and $[Cu(NH_3)_4]^{2+}$ with the molecular orbital energy level diagram (*620*).

A series of papers by Hathaway *et al.* (*83–85*, *203*, *204*, *315*, *567*, *568*, *627*, *665*, *666*) have correlated the *g* tensors of a wide variety of cupric complexes with their optical spectra whose assignments are

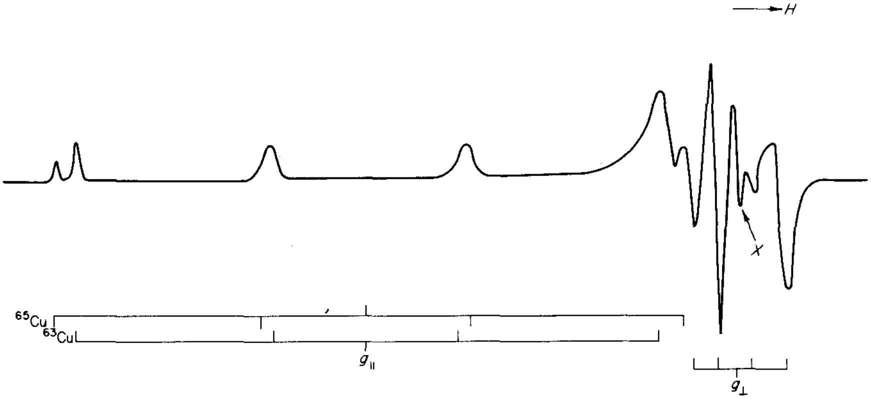

FIG. 56. Frozen solution spectrum of Cu(acac)$_2$ showing resolution of $g_{\parallel}$ into h.f.s. due to ^{63}Cu (69.1%) and ^{65}Cu (30.9%). The line X is a forbidden transition.

based on polarized light single-crystal studies. Considerable attention has been paid to cupric acetylacetonate and substituted derivatives in various solvents (see Figs. 55 and 56). It is concluded that the bonding is largely covalent (σ and in-plane π) and that there is virtually no out-of-plane π bonding (*474*). The parameters (*148*) of the homolog Cu[(CH$_3$)$_3$CCOCHCOC(CH$_3$)$_3$]$_2$ are similar. The influence of solvents like chloroform and toluene on the ESR spectra of cupric acetylacetonate suggests that there is axial coordination of toluene, but in the case of chloroform, a combination of axial coordination and hydrogen bonding as shown in Fig. 57 (*30*).

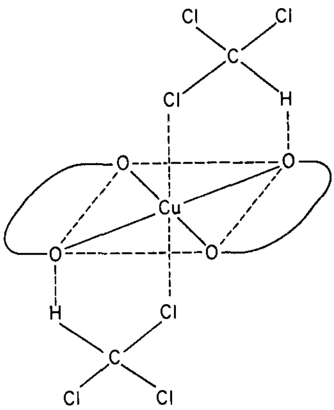

FIG. 57. Possible nature of solvent interaction between Cu(acac)$_2$ and chloroform.

Electron delocalization in a series of cupric salicylaldimines of the general formula

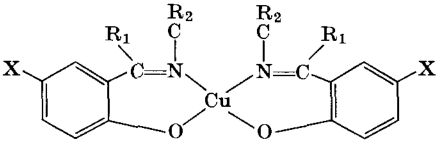

have been studied. Proton splittings of about 5–7 gauss (equivalent to a spin density of 1%) arising from R_1, which may be H or CH_3, are observed (*438, 440, 441, 475*). These have been discussed by Kuska, Rogers, and Drullinger who have compared these proton splittings with that observed in cupric diphenylacetylacetonate (*429*). It is not clear yet whether the spin density arises from σ or π delocalization of the unpaired electron.

The complex *trans*-CuI_2 (imidazole)$_4$ exhibits both Cu and N h.f.s. In this molecule, one pair of opposite imidazole groups are in the xy plane and the other pair are in the xz plane (*20*).

Electron nuclear double resonance has been used by Rist and Hyde (*584*) to determine the magnitude of the proton coupling in cupric 8-hydroxyquinolinate and also the signs of the ^{14}N s.h.f.s. The use of NMR for the determination of proton couplings in similar complexes of Ni(II) and Co(II) has been reviewed by Eaton and Phillips (*197*).

The Hofmann clathrate compounds of general formula $Cu(NH_3)_2M(CN)_4 \cdot 2G$ where $M = Ni^{2+}$, Pd^{2+}, or Pt^{2+} and G is an organic molecule have been studied (*523*). In the case of the magnetically dilute Cu/Cd complex, h.f.s. are detected and the g values indicate a tetragonal compression with the unpaired electron in the d_{z^2} orbital.

Copper is often found in biochemical systems, usually in peptides and proteins. Extensive reviews may be found (*66, 106, 557*). Semiquantitative discussion (*112*) of the significance of the results, which usually show that the copper environment has axial symmetry and with a distorted octahedral structure are numerous. The use of model compounds has been discussed by Malmstrom and Vanngard (*477*). In many cases there appears to be dimeric species present (*98*). A system of importance which has been extensively studied is the series of complexes with glycine and triglycine (*209, 638, 707, 712*). The ESR data are tabulated in Table LV.

5. *ESR of* Ag^{2+} *and* Au^{2+}

a. Ag^{2+} d^9. Hyperfine structure is resolved (*507*) in frozen acid solutions of Ag^+ oxidized with persulfate (see Fig. 58 and Table LVI). The species present is presumably $[Ag(H_2O)_6]^{2+}$. The complex with Ag^{2+} and α-picolinic acid also shows s.h.f.s. and the much larger $A_{\parallel}$ is indicative of some 5*s* orbital mixing of the ground state. The dithiocarbamate complex $Ag[S_2CN(i\text{-}Pr)_2]_2$ shows ^{33}S s.h.f.s. with sulfur in natural abundance (*559*). The bonding parameters (*559*) show that the Ag–S σ bond is almost completely covalent, but that the in-plane and out-of-plane π bonds have little covalent character. This lack of interaction between the metal and the π-ligand system is surprising since the stability of the complexes is usually attributed to the π bonding. γ-Irradiation of frozen solutions of $AgNO_3$ in alcohols and water yield Ag^{2+} ions which exhibit very large h.f.s. and are interpreted in terms of some 45% atomic character (*616*).

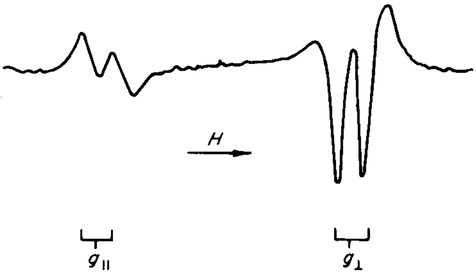

FIG. 58. ESR spectrum of a frozen solution of Ag^{2+} in nitric acid.

Comparison between $[Ag(C_5H_5N)_4]^{2+}$ and Ag porphrins is interesting because the anisotropic tensor for ^{109}Ag in the latter (*394*) is about three times larger than for the pyridine (*113*, *330*) complex. This is presumably due to the silver–nitrogen distance in silver porphrins being shorter than in the "free" pyridine complex. This is also reflected in the bonding parameters for Cu and Ag porphrins, where $\alpha^2 = 0.74$ and 0.58, respectively indicating that the b_{1g} orbital is much more covalent for the silver complex (*394*). A detailed study of solvent effects upon 14 different porphrins of Ag and Cu has been carried out by MacCragh *et al.* (*467*).

In irradiated Ag^+ in the alkali halides (*624*), the static (77°K) and dynamic (200°K) Jahn–Teller effects are observed. The g and A values for the dynamic distortion are found to be exactly the average of those for the static effect.

b. Au^{2+} d^9. The parameters obtained (*466*) from the ESR of gold phthalocyanine are not sufficiently accurately known to deduce details of the bonding as has been done for the copper and silver complexes. The instability of Ag and Au phthalocyanines is attributed mainly to the large size of the ions relative to the space available in the chelate ring. The available data are given in Table LVI.

TABLE LV

ESR DATA FOR d^9 Cu^{2+} IONS

Ion	g_{av}	$g_{\parallel}$	$g_{\perp}$	$A_{iso}(Cu)$ (10^4 cm^{-1})	$A_{\parallel}(Cu)$ (10^4 cm^{-1})	$A_{\perp}(Cu)$ (10^4 cm^{-1})	$A_{ligands}$ (10^4 cm^{-1})	References
$K_3Cu(NO_3)_5$, D_{3h}	—	2.30	2.04	—	183 G	38 G	—	*(70)*
$Cu(NO_3)_2$								
in argon matrix	—	2.2489	2.0522	—	190	17	—	*(379)*
in Et acetate	—	2.34	2.07	—	121	40	—	*(550)*
CuF_2 in argon matrix (linear)	—	1.913	2.601	—	722 G	574 G	$A_{\parallel}(^{19}F) = 115$ G, $A_{\perp}(^{19}F) = 56.7$ G	*(379)*
Cu^{2+}								
in BeO (C_{3v})	—	1.709	2.379	—	50	108	—	*(179)*
in KH_2PO_4	—	2.388	2.060	—	148.5	19.1	—	*(395)*
in MgO	—	2.19		—	19		—	*(141, 325)*
in ZnO(T_d)	—	0.7383	1.5237	—	198	224	—	*(178, 181, 375)*
in GeO_2, amorphous	2.143	2.318	2.056	68.9	164	21	—	*(622)*
in GeO_2, tetragonal (O_h)	2.166	2.380, 2.070, 2.049		62.8	128, 17, 43		—	*(622)*
in GeO_2, hexagonal (T_d)	2.175	2.382, 2.096, 2.047		53.8	83.22, 21.6, 56.4		—	*(622)*
in $CdWO_4$	—	2.018, 2.304, 2.494		—	84.5, <20, 0		—	*(635, 636)*
in K, Na, tartrate	2.13	2.324, 2.051, 2.060		66	153, 33, 19		—	*(528, 687)*
in $CdCl_2$	—	2.339	2.070	—	113	0	$A_{\parallel}(Cl) = 18.5$, $A_{\perp}(Cl) = 5.0$	*(655)*
in $CdCl_2$	—	2.162	2.144	—	101	80	—	*(488)*
in $MgCl_2$	—	2.178	2.154	—	92	75	—	*(488)*
in $Mg_3La_2(NO_3)_{12} \cdot 24H_2O$								
20°K	—	2.470	2.097	—	113, 19, 12.3		—	*(90)*
90°K	—	2.219		—	29		—	*(80, 90)*

in $ZnK_2(SO_4)_2 \cdot 6H_2O$	—	2.44	2.13	—	103	34	—	(89)
in $Mg_3Bi(NO_3)_{12} \cdot 24H_2O$								
20°K	—	2.454	2.096	—	110	17	—	(90)
90°K	—	2.219		—	27		—	(90)
in $ZnSiF_6$								
12°K	—	2.46	2.10	—	110	<30	—	(90)
90°K	—	2.221	2.230	—	21	28	—	(90)
in NH_4Cl	—	2.00	2.225	—	240	70	—	(727)
in NH_4Br	—	2.029	2.190	—	161	0	$A_\parallel(Br) = 8.5$, $A_\perp(Br) = 33.1$	(439)
$CuSO_4$ anhydrous	—	2.15, 2.2, 2.14		—	—	—	—	(705)
Cs_2CuCl_4 (T_d)	—	2.384, 2.083, 2.107		—	—	—	—	(613, 614)
Cu^{2+} in Cs_2ZnCl_4 (T_d)	—	2.446, 2.083, 2.101		—	25, 51, 46		—	(613, 614)
Cu $\alpha\alpha'$-bromodipyrromethene (T_d)	—	2.283, 2.084, 2.069		—	—	—	—	(60)
$CuCl_2$								
+tri-*n*-propylamine	2.112	2.213	2.062	104.8	−202.4	−56.0	—	(132)
+di-*n*-propylamine	2.121	2.204	2.061	77.1	−192.4	−19.4	—	(132)
+*n*-propylamine	2.128	2.236	2.074	57.8	−182.1	4.3	$A(^{14}N) = 11.7$	(132)
+dibenzylamine	2.107	2.225	2.049	75.5	−180.8	22.9	—	(132)
+benzylamine	2.136	2.235	2.086	60.5	−178.4	1.5	$A(^{14}N) = 12.2$	(132)
$Cu(NO_2)_2$ + *n*-propylamine	2.122	2.232	2.067	72.7	−181.3	18.4	—	(132)
CuF_2 + *n*-propylamine	2.125	2.232	2.072	66.0	−179.2	9.4	—	(132)
$CuBr_2$ + *n*-propylamine	2.130	2.233	2.078	61.7	−182.4	1.3	—	(132)
$(Cu,Cd)(NH_3)_2Ni(CN)_4(C_6H_6)_2$	—	2.027	2.257	—	90.1	−60.7	—	(523)
$Cu(dimethylglyoxime)_2$	2.086	2.155	2.035	87.5	144 G	14.6 G	$A_{iso}(^{14}N) = 15.0$ G	(367, 658, 707)
$Cu(N\text{–}biuret)_2$	2.09	2.20	2.04	—	158	135	—	(707)
Cu^{2+} in NH_4NO_3	2.187	—	—	33 G	—	—	—	(657)
$[Cu(NH_3)(H_2O)_5]^{2+}$	2.16	—	—	—	—	—	—	(657)
$[Cu(NH_3)_2(H_2O)_4]^{2+}$	2.14	—	—	—	—	—	—	(657)
$[Cu(NH_3)_3(H_2O)_3]^{2+}$	2.122	—	—	54 G	—	—	—	(657)
$[Cu(NH_3)_4(H_2O)_2]^{2+}$	2.108	—	—	79 G	—	—	—	(657)
$[Cu(NH_3)_5(H_2O)]^{2+}$	2.118	2.24	2.06	65 G	160 G	50 G	—	(657)

TABLE LV—*cont.*

ESR Data for d^9 Cu^{2+} Ions

Ion	g_{av}	$g_{\parallel}$	$g_{\perp}$	A_{iso}(Cu) ($10^4\,cm^{-1}$)	$A_{\parallel}$(Cu) ($10^4\,cm^{-1}$)	$A_{\perp}$(Cu) ($10^4\,cm^{-1}$)	$A_{ligands}$ ($10^4\,cm^{-1}$)	References
Cu^{2+}								
$+(\mathrm{en})_n, n>2$	2.103	—	—	90 G	—	—	—	*(656)*
$n<1$	2.139	—	—	74 G	—	—	—	*(656)*
$+[NH(CH_2CH_2OH)_2]_n, n>5$	2.116	—	—	83 G	—	—	—	*(656)*
$n<4$	2.126	—	—	61 G	—	—	—	*(656)*
$+(NH_2CH_2CH_2OH)_n, n>4$	2.109	—	—	87 G	—	—	—	*(656)*
$n<3$	2.112	—	—	56 G	—	—	—	*(656)*
$+N(CH_2CH_2OH)_3$	2.124	—	—	74 G	—	—	—	*(656)*
$+CH_3NHCH_2NHCH_3$	2.109	—	—	87 G	—	—	—	*(656)*
$+i\text{-}PrNH_2$	2.130	—	—	61 G	—	—	—	*(656)*
$+OH^-$	2.116	—	—	72 G	—	—	—	*(656)*
$[Cu(H_2O)_6]^{2+}$	2.200	2.400	2.099	−37	−127.8	12.6	—	*(449)*
$[Cu(\mathrm{en})(H_2O)_4]^{2+}$	2.137	2.281	2.058	−68.5	−181.2	−24.0	—	*(449)*
$[Cu(\mathrm{en})_2(H_2O)_2]^{2+}$	2.102	2.209	2.047	−83.9	−202.7	−28.0	$A_{iso}(^{14}N)=11.0$	*(449)*
$Cu(\mathrm{en})_3SO_4$	—	2.126	2.113	—	—	—	—	*(570, 645)*
$Cu(o\text{-phen})_3(NO_3)_2\cdot 2H_2O$	—	2.273	2.064	—	160	<7	$A_{\parallel}(^{14}N)=12.5$, $A_{\perp}(^{14}N)=10.5$	*(402)*
$[Cu(py)_6](NO_3)_2$	—	2.25	2.05	—	190 G	<15 G	—	*(8)*
Cu^{2+} in $[Cd(py)_4]S_2O_8$	—	2.264, 2.071, 2.034		—	169, 15.6, 13.9		$A(^{14}N)=12.7, 1, 1$	*(329)*
$Cu(py)_2Cl_2$	2.15	2.220	2.06	—	134 G	20 G	—	*(514)*
$Cu(2\text{-picoline})_2Cl_2$	2.14	2.246	2.06	—	127 G	20 G	—	*(514)*
$Cu(3\text{-picoline})_2Cl_2$	2.14	2.206	2.06	—	142 G	20 G	—	*(514)*
$Cu(2,6)\text{toluidine})_2Cl_2$	2.14	2.163	2.05	—	198 G	34 G	—	*(514)*
$Cu(\alpha\text{-Br-picoline})_2Cl_2$	2.14	2.296	2.05	—	115 G	20 G	—	*(514)*
$[Cu(py)_4]^{2+}$	—	2.22	—	—	174 G	—	$A_{\perp}(^{14}N)=14$ G	*(720)*
$[Cu(4\text{-picoline})_4]^{2+}$	—	2.21	—	—	174 G	—	$A_{\perp}(^{14}N)=14$ G	*(720)*
$[Cu(3\text{-picoline})_4]^{2+}$	—	2.21	—	—	177 G	—	$A_{\perp}(^{14}N)=15$ G	*(720)*

$[Cu(2\text{-picoline})_4]^{2+}$	—	2.25	—	—	146 G	—	$A_{\perp}(^{14}N) = 15$ G	*(720)*
$[Cu(2,3\text{-lutidine})_4]^{2+}$	—	2.25	—	—	142 G	—	$A_{\perp}(^{14}N) = 15$ G	*(720)*
$[Cu(2,4\text{-lutidine})_4]^{2+}$	—	2.23	—	—	153 G	—	$A_{\perp}(^{14}N) = 15$ G	*(720)*
$[Cu(2,5\text{-lutidine})_4]^{2+}$	—	2.25	—	—	153 G	—	$A_{\perp}(^{14}N) = 15$ G	*(720)*
$[Cu(2,6\text{-lutidine})_4]^{2+}$	—	2.21	—	—	174 G	—	$A_{\perp}(^{14}N) = 14$ G	*(720)*
$[Cu(2,4,6\text{-collidine})_4]^{2+}$	—	2.21	—	—	176 G	—	$A_{\perp}(^{14}N) = 14$ G	*(720)*
$Cu(8\text{-OH quinoline})_2 \cdot 2H_2O$	—	2.287	2.066	—	171	30	$A_{iso}(^{14}N) = 9$	*(397)*
$CuCl_2$–8-OH quinoline	—	2.172	2.042	—	168	25	$A_{iso}(^{14}N) = 10$	*(228, 261)*
$CuCl_2$–NH_3	2.13	2.228	2.056	66	160	15	$A_{iso}(^{14}N) = 13$	*(261)*
$CuCl_2$–morpholine	2.13	2.227	2.081	46	95	31	—	*(261)*
$CuCl_2$–pyridine	2.14	2.241	2.079	60	160	~1	$A_{iso}(^{14}N) = 14$	*(261)*
$CuCl_2$–*o*-phenanthroline	2.14	2.22	2.08	—	119	29	—	*(261)*
$CuCl_2$–CH_3NH_2	2.13	—	—	63	—	—	—	*(261)*
$CuCl_2$–$(C_2H_5)_2NH$	2.12	—	—	67	—	—	—	*(261)*
$CuCl_2$–$(C_2H_5)_3N$	2.13	—	—	70	—	—	—	*(261)*
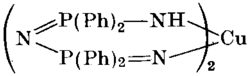	—	2.24	2.04	—	166 G	15 G	—	*(382)*
$Cu(CH_3COCHCOCH_3)_2$								
in Pd acac	—	2.266, 2.055, 2.052		—	160	19.5	—	*(474, 498)*
in $CHCl_3$	2.123	2.285	2.042	77.2	175	28.2	—	*(426, 429)*
in DMF	—	2.293	2.061	—	172	13.1	—	*(429)*
in Py	—	2.302	2.071	—	164	3.5	—	*(429)*
$Cu(CH_3COC(CH_3)COCH_3)_2$ in $CHCl_3$	2.121	2.269	2.047	78.5	186	25	—	*(261, 426, 429)*
$Cu(PhCOCHCOCH_3)_2$ in $CHCl_3$	2.124	2.281	2.046	76.4	176	26.6	—	*(426, 429)*
$Cu(PhCOCHCOPh)_2$ in $CHCl_3$	2.124	—	—	75.3	—	—	—	*(426)*
$Cu(CF_3COCHCOCH_3)_2$ in $CHCl_3$	2.129	2.308	2.040	72.5	167	25.2	—	*(426, 429)*
$Cu(CF_3COCHCOCF_3)_2$ in $CHCl_3$	2.136	2.306	2.051	84.0	173	24.5	—	*(426, 429)*
$Cu[(CH_3)_3CCOCHCOC(CH_3)_3]_2$	—	2.2438	2.0505	—	—	—	—	*(148)*
trans-$[Cu(DCO_2)_4(D_2O)_2]^{2-}$	—	2.391	2.079	—	130	20	$A(^{13}C) = 6.8$	*(56)*
$[Cu(DCO_2)_6]^{4-}$	—	2.407	2.081	—	129	21	—	*(56)*
trans-$[Cu(D_2O)_4(DCO_2)_2]$	—	2.420	2.066	—	134	26	—	*(56)*
$Cu(acac)_2en$	—	2.184	2.033	—	202 G	27 G	$A_{iso}(^{14}N) = 12.5$ G	*(221)*

TABLE LV—*cont.*

ESR Data for d^9 Cu^{2+} Ions

Ion	g_{av}	$g_{\parallel}$	$g_{\perp}$	A_{iso}(Cu) (10^4 cm^{-1})	$A_{\parallel}$(Cu) (10^4 cm^{-1})	$A_{\perp}$(Cu) (10^4 cm^{-1})	$A_{ligands}$ (10^4 cm^{-1})	References
Cu(bzac)$_2$en	—	2.215	2.027	—	196 G	28 G	$A_{iso}(^{14}N) = 13.5$ G	(*221*)
Cu(salicylamide)$_2$	—	2.14	2.08	—	156	10.8	—	(*707*)
Cu(salicylaldimine)$_2$	—	2.200, 2.040, 2.055		—	184	21	$A(^{14}N) = 11.1$ G, $A(^1H) = 5.5$ G	(*261, 475*)
Cu(N-*i*-Pr salicylaldimine)$_2$	2.124	2.287, 2.014, 2.095		65 G	117 G	15 G, 30 G	—	(*222, 224, 581*)
Cu(salicylaldoxime)$_2$	—	2.171	2.020	—	183	41	$A(^{14}N) = 14$	(*261, 707*)
cis-Cu(α-aminoacetate)$_2$	2.121	2.234	2.053	61 G	153 G	12.6 G	—	(*515*)
trans-Cu(α-aminoproprionate)$_2$	2.116	2.226	2.051	65 G	160 G	13 G	—	(*515*)
trans-Cu(β-aminoproprionate)$_2$	2.126	2.243	2.055	43 G	130 G	8 G	—	(*515*)
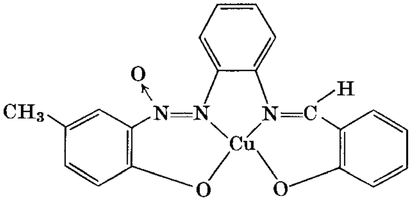	2.11	2.18	2.06	75 G	—	—	$A_{iso}(^{14}N) = 12.5$ G	(*438*)
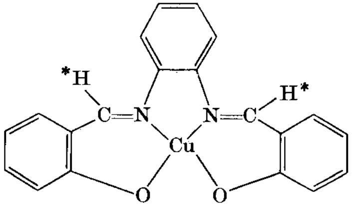	2.10	2.19	2.05	91 G	200 G	—	$A_{iso}(^{14}N) = 22$ G, $A_{iso}(^1H^*) = 7$ G	(*438*)

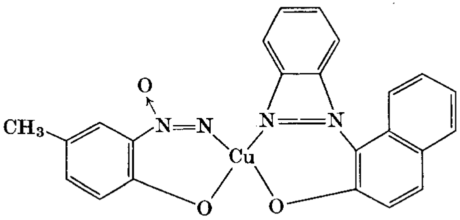	2.091	2.193	2.039	94.5 G	—	—	$A_{iso}(^{14}N) = 14.3$ G	(*438*)
trans-Cu(diphenylcarbazide)	2.12	2.24	2.20	—	140	11.0	—	(*585, 707*)
cis-Cu(glycylglycylglycine)	2.12	2.20	2.08	—	156	10.8	—	(*707*)
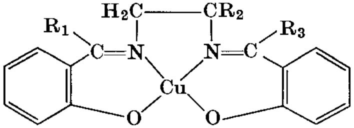 $R_1R_2R_3 = H$ or CH_3		—	—	—	—	—	$A(^{14}N) = 11$ G, $A(^1H) = 6$–7 G	(*440*)
5,5′-dibromo derivative of above	2.095	—	—	87.4 G	—	—	$A(^{14}N) = 12.6$ G, $A(^1H) = 6.3$ G	(*441*)

TABLE LVI

ESR DATA FOR d^9 Ag^{2+} AND Au^{2+} IONS

Ion	g_{av}	$g_{\parallel}$	$g_{\perp}$	A_{iso} (10^4 cm^{-1})	$A_{\parallel}$ (10^4 cm^{-1})	$A_{\perp}$ (10^4 cm^{-1})	$A_{ligands}$ (10^4 cm^{-1})	References
γ-irr $AgNO_3$/EtOH	—	2·001	1·974	848 MHz	876 MHz	834 MHz	—	*(616)*
$[Ag(H_2O)_6]^{2+}$ in acid	2.124	2.265	2.065	—	48 G	32.6 G	—	*(248, 507)*
$[Ag(\alpha\text{-picolinate})_2](S_2O_8)$	—	2.244, 2.044, 2.072		—	188 G	30 G	—	*(507)*
$[Ag(py)_4](S_2O_8)$	—	2.148, 2.048, 2.098		—	—	—	$A(^{14}N) = 24$ G	*(248, 268, 507)*
Ag^{2+} in $[Cd(Py)_4](S_2O_8)$	—	2.18	2.04	—	42.4	19.2	$A_{\parallel}(^{14}N) = 17$, $A_{\perp}(^{14}N) = 22$	*(113, 330)*
$[Ag(o\text{-phen})_2]S_2O_8$	—	2.168	2.046	—	—	—	—	*(103, 507)*
$[Ag(dipy)_2]S_2O_8$	—	2.164	2.032	—	—	—	—	*(507)*
$[Ag_2(dipy)_5](S_2O_8)_2$	—	2.176, 2.040, 2.056		—	—	—	—	*(507)*
$[Ag(dipy)_3](NO_3)_2$	—	2.168, 2.037, 2.047		—	—	—	—	*(507)*
$Ag[S_2CN(iso\text{-}Pr)_2]_2$	2.0194	2.035	2.011	−28	−37	−24	$A(^{33}S) = 11.9$ G	*(4, 559, 674)*
$Ag[S_2CNbz_2]_2$	2.020	—	—	20.76	—	—	—	*(249)*
$Ag[S_2CNEt_2]_2$	2.040	—	—	20.76	—	—	—	*(249)*
$[Ag(MNT)_2]^{2-}$	2.019	—	—	31.4 G	—	—	—	*(710)*
Ag-deuteroporphrin IX dimethyl ester	2.054	2.104	2.029	—	71	31	$A_{\parallel}(^{14}N) = 20$, $A_{\perp}(^{14}N) = 23$	*(394)*
Ag-phthalocyanine	2.042	2.093	2.014	—	—	—	$A_{\parallel}(^{14}N) = 21.4$, $A_{\perp}(^{14}N) = 23.2$	*(465)*
Ag^{2+} in LiCl	—	2.178	2.039	—	38	30	$A_{\parallel}(Cl) = 5$, $A_{\perp}(Cl) = 30$	*(624)*
Ag_2S and Ag_2Se in AgCl	—	2.163	2.040	—	35 G	30 G	—	*(349)*
AuPc	2.065	—	1.996	—	—	61	$A_{\perp}(^{14}N) = 15.8$	*(466)*
$Au[S_2CN(i\text{-}Pr)_2]_2$	2.040	—	—	28	—	—	—	*(674)*
$[Au(MNT)_2]^{2-}$	2.009	—	—	41.7 G	—	—	—	*(696, 710)*

L. ESR OF BIOLOGICAL SYSTEMS

Many of the important biochemical species found in natural biological systems contain transition metals, the most common being iron, copper, molybdenum, manganese, vanadium, and cobalt. These metals in complexes are also notable in being readily oxidized or reduced, and hence either naturally or under mild oxidative or reducing conditions are paramagnetic with the consequent possibility of detection by ESR.

In general, spectra from natural biochemical species are poorly resolved and better resolved spectra are usually only obtained if a much simpler complex is studied. In natural systems, the symmetry is usually completely lost and each ligand is different. The additional s.h.f.s. from several different nitrogen-bonded ligands causes further line broadening. In addition, impurities pose a very serious problem particularly if the signal under investigation is usually weak. It is for these reasons that simpler systems are studied, and hence most of the recent advances have been made with suitable model systems which bear a close chemical relationship to the natural system but with a higher symmetry and having simple ligands.

Model systems have the advantage that a reasonably accurate picture of electron delocalization, covalency, ordering of energy levels, structure, and bonding may be achieved. The more complicated natural system may then be compared if the general envelope of the spectrum is similar. The *g* value(s) and any hyperfine splittings can then be compared and some useful conclusions concerning the electronic structure of the natural system may then be deduced.

In this review, no attempt is made to survey in depth the enormous number of spectral measurements made on biological systems. The examples quoted are largely at random, and are notable only in that reasonably clear spectra are observed. A number of useful reviews have been published (*64*, *66*, *95*, *106*, *202*, *299*).

1. Metal Phthalocyanines and Porphrins

Metal phthalocyanines and porphrins are a group of complexes, many of which are found in biological systems. The structure of the molecules is also related to heme and vitamin B_{12}. The molecules are characterized by a rigid-square fully aromatic ring system (Fig. 59) whose low-lying π^*-molecular orbitals are close in energy to the metal iron bonding and antibonding *d* orbitals. For this reason, it is relatively easy to add electrons to the system and the orbital into which the electron goes depends on the relative energy of the metal and the ring orbitals. This differs from metal to metal and is also dependent on the porphrin and the solvent. Copper phthalocyanine has been well studied and the results

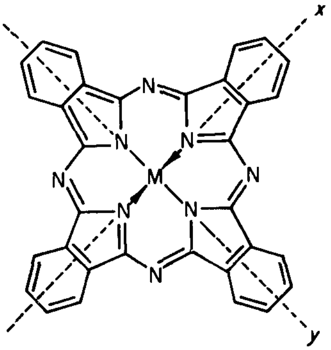

FIG. 59. Axis notation for phthalocyanine-type compounds.

are discussed in Section VIII,K,4. Other systems have been reviewed and the results collated and systematized using a qualitative energy-level scheme (Fig. 60) by Guzy *et al.* (*302*). Addition of one and three electrons to the d^{10} systems of both ZnPc and H_2Pc yield, respectively, a single line and a multiplet of lines attributable to N and H s.h.f.s. (*359*). This is explained by the electrons going into b_{1u} and e_g orbitals, respectively. In the latter case, spin density may reside on the inner nitrogen atoms and thus give rise to nitrogen coupling. Many ESR spectra have been recorded (*137*, *593*).

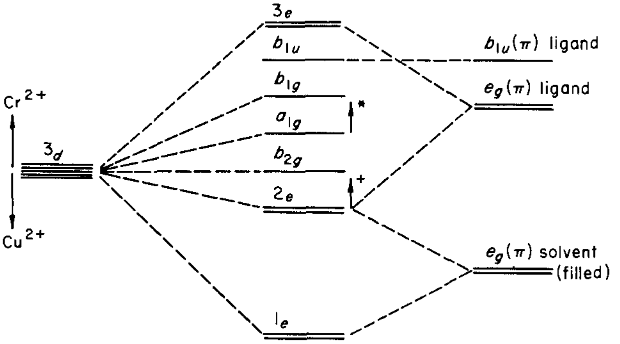

FIG. 60. Generalized energy-level diagram for metal phthalocyanines. *, the a_{1g} is raised by strong σ bonding from the solvent; †, the 2*e* level is raised by strong π bonding from the solvent.

M. UNPAIRED ELECTRONS LOCALIZED ON LIGANDS

1. *Binuclear Cobalt Complexes*

The family of binuclear paramagnetic complexes of cobalt of the type $[L_5Co^{III}O_2Co^{IV}L_5]$ and $[L_5Co^{III}O_2(NH_2)Co^{IV}L_5]$ have been studied in detail by several workers (*63*, *71*, *198*, *199*, *482*, *510*, *519*, *603*, *701*).

Spectra in sulfuric acid solution show that there are two equivalent cobalt nuclei indicating that the electron is delocalized over the CoO_2Co chromophore (see Fig. 61). This was confirmed by Weil and Kinnaird (*701*) who detected ^{17}O s.h.f.s. in $[(NH_3)_4Co(NH_2)(O_2)Co(NH_3)_4]^{4+}$ using 11.7% enriched ^{17}O in the –O–O– group. A coupling of 22.5 gauss was obtained. Since no ^{14}N s.h.f.s. are observed in the μ-amido complexes, from linewidths an upper limit of 0.5 gauss can be put on $A(^{14}N)$. Unfortunately, frozen solution spectra give only a single broad line thus making it impossible to estimate non-s-electron densities at the cobalt nuclei. It is interesting that the red and green isomers have different types of peroxo bridging groups, as shown in Fig. 62. The bond distance

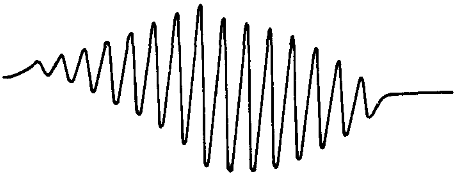

FIG. 61. The ESR spectrum of a dicobalt peroxo complex

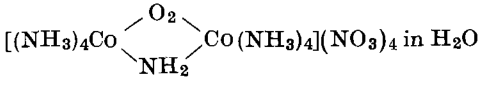

$$[(NH_3)_4Co\overset{O_2}{\underset{NH_2}{\diamond}}Co(NH_3)_4](NO_3)_4 \text{ in } H_2O$$

showing coupling to two equivalent ^{59}Co nuclei (*519*).

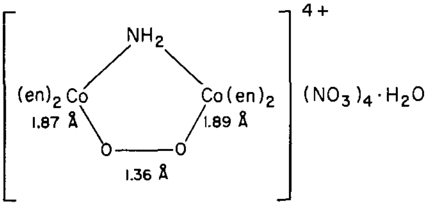

Green, paramagnetic

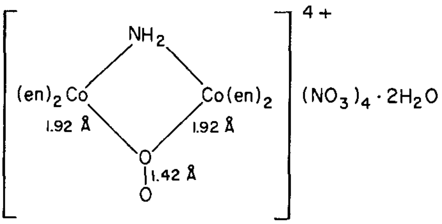

Red , diamagnetic

FIG. 62. Structure of the green and the red forms of the μ-amido dicobaltiperoxo complexes.

TABLE LVII

ESR DATA FOR COBALT PEROXY COMPLEXES

Complex	g_{av}	$g_{\parallel}$	$g_{\perp}$	$A_{iso}(^{59}Co)$ (gauss)	$A_{\parallel}(^{59}Co)$ (gauss)	$A_{\perp}(^{59}Co)$ (gauss)	$A_{iso}(^{17}O)$ (gauss)	References
$K_5[(CN)_5CoO_2Co(CN)_5]\cdot H_2O$	2.0200	—	—	8.50	—	—	—	*(63, 71, 199, 519, 603)*
$[(NH_3)_5CoO_2Co(NH_3)_5](NO_3)_5$	2.0249	2.076	2.003	11.4	18	18	—	*(63, 71, 199, 407, 519, 603)*
$K_4[(CN)_4CoO_2(NH_2)Co(CN)_4]\cdot 2H_2O$	2.0244	—	—	10.2	—	—	—	*(63, 71, 199, 519, 603)*
$K_3[(CN)_3(NH_3)CoO_2(NH_2)Co(CN)_4]\cdot 4H_2O$	2.0241	—	—	10.2	—	—	—	*(63, 71, 199, 519, 603)*
$K_2[(CN)_3(NH_3)CoO_2(NH_2)Co(NH_3)(CN)_3]\cdot H_2O$	2.0241	—	—	10.2	—	—	—	*(63, 71, 199, 519, 603)*
$K_2[(CN)_4CoO_2(NH_2)Co(CN)_2(NH_3)_2]\cdot H_2O$	2.0241	—	—	10.2	—	—	—	*(63, 71, 199, 519, 603)*
$[(NH_3)_4CoO_2(NH_2)Co(NH_3)_4](NO_3)_4$	2.0341	—	—	12.43	—	—	22.5	*(63, 71, 199, 519, 603, 701)*
Co^{2+}-bis(salicylal)-3,3′-diiminodipropylamine peroxide	2.033	2.108	1.995	13.4	18.5	16.9	—	*(407)*

(*482*) in the green complex is closer to that usually found in superoxides than in peroxides (1.28 and 1.48Å, respectively). The planarity of the

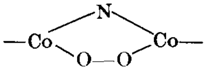

ring supports a superoxo configuration with the unpaired electron located mainly on the –O–O– group, with the cobalt atoms nominally 3+. The available data are given in Table LVII. The oxidation of the μ-amido–μ-peroxo complex by ceric ions has been followed by ESR (*518*).

2. Dithiolenes and Related Compounds

Complexes of the general type

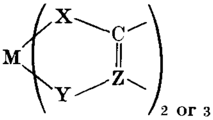

where X and Y are usually S, but may be Se, N–R, or O, and Z is usually C, but sometimes N–R, undergo reversible electron transfer reactions. Many of the complexes, in apparently unusual valency states have been isolated and characterized, and the paramagnetic ones have been extensively studied by ESR. The presence of a five-membered delocalized chelate ring appears to be a requirement for the reaction. The paramagnetic complexes are usually square planar for the Co, Ni, and Cu groups of elements and distorted octahedral or trigonal prismatic for the V, Cr, and Mn groups. Considerable controversy has occurred in the formulation of these complexes, since, for example, $Ni(MNT)_2^-$ could be formulated as $[Ni^{3+}(MNT^{2-})_2]^-$ or $[Ni^{2+}(MNT)_2^{3-}]^-$. That is, is the unpaired electron localized on the Ni or localized over the ligands? Agreement now seems to have been reached that the best formulation is somewhere between these extremes and the best description of the electron configuration of the molecule is in terms of molecular orbital theory. The lack of hyperfine structure in the ESR of most of these complexes has hindered calculations of electron delocalization. Where h.f.s. or s.h.f.s. are observed, the low values of metal h.f.s. and high values of ligand s.h.f.s. are consistent with much electron delocalization over the ligands. The g values are all close to 2, again suggesting delocalization and little metal spin–orbit coupling contribution to g. A satisfactory energy level scheme which is applicable for many of the square planar complexes is given in Figs. 63 and 64. This is applicable in particular to $[Ni(MNT)_2]^{2-}$. An extensive review by McCleverty has

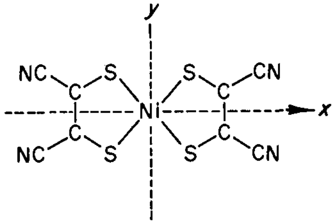

FIG. 63. The coordinate system for metal dithiolenes.

been published but the value of much of the extensive tabulated data is diminished by the absence of references (*491*).

In the survey of ESR results, the nomenclature for electron configuration used has been, for convenience, to take the unpaired electron to be *nominally* on the metal. In practice, this means that, e.g., $[\mathrm{Ni(MNT)_2}]^-$ has its unpaired electron in the $4a_g$-molecular orbital which

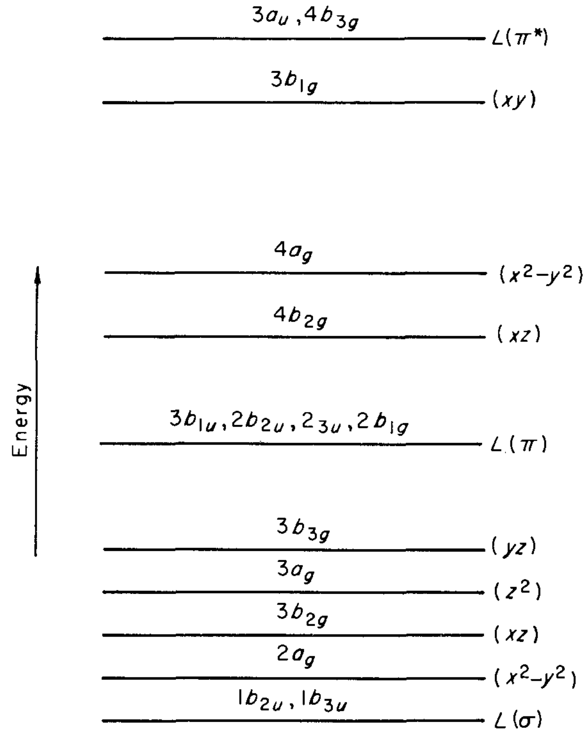

FIG. 64. Ordering of molecular orbitals for $\mathrm{Ni(MNT)}_2^{n-}$. For $n = 2$, the $4a_g$ level is filled.

is partly metal $d_{x^2-y^2}$, but, in practice, largely (~75%) delocalized over the ligand $4a_g$-antibonding molecular orbital. The $Ni[Se_2C_2(CF_3)_2]_2^-$ complex (*169*) has g values deviating from free spin to a greater extent than the S analog. This is because of larger spin–orbit coupling with the

TABLE LVIII

DITHIOLENE LIGAND FORMULAS

Abbreviation	Compound	Structure
MNT	Maleonitriledithiolate	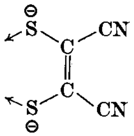
TDT	Toluene-3,4-dithiolate	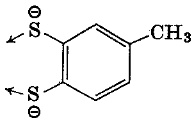
$S_2C_2R_2$	where R = CF_3, H, Ph	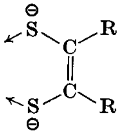
gma	Glyoxalbis(*o*-mercaptoanil)	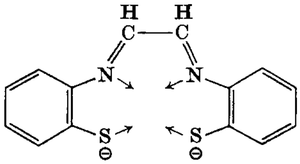
H_2(gma)	Dihydroglyoxalbis(*o*-mercaptoanil)	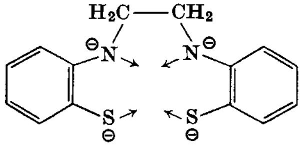
dbh	Bisacetylbis(benzoylhydrazone)	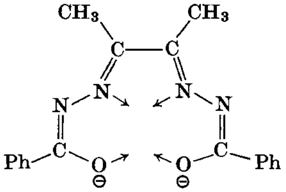
dtbh	Bisacetyl(thiobenzoylhydrazone)	as above but S instead of O

TABLE LVIII—*cont.*

DITHIOLENE LIGAND FORMULAS

Abbreviation	Compound	Structure
i-MNT	*Iso*maleonitriledithiolate (not a species which undergoes electron transfer reactions)	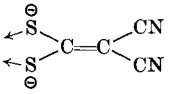
BDT	*o*-Benzene dithiolate	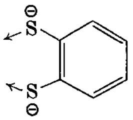
DTC	Dithiocarbamate	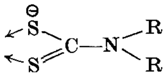

Se atoms of the ligand. The square planar complexes have also been reviewed by Gray (*283*, *284*). Table LVIII lists some of the ligands and their trivial formulas.

Some of the tris-chelate complexes have proved unique in that they have a trigonal prismatic coordination of ligands around the metal, with D_{3h} symmetry. The Mo, W, and Re tris-dithiolenes seem to have this structure, together with $V(S_2C_2Ph_2)_3$. The Ti, V, and Cr complexes are isomorphous and thought to have a distorted octahedral structure (*285*, *639*). The trigonal prismatic structure is maintained in solution since, for $Re(TDT)_3$ the magnetic moment, g value and electronic absorption spectrum is the same for the solid and its solution in benzene (*641*). Steifel, Dori, and Gray (*639*) have proposed that the tendency is for the highly reduced species to be octahedral and for the oxidized species to be trigonal prismatic.

The order of the M.O. energy levels (*285*) for trigonal prismatic $Re(S_2C_2Ph_2)_3$ is $(4e')^4$, $(2a_2')^2$ $(3a_1')^1$. The unpaired electron is in a molecular orbital formed by interaction of the metal d_{z^2} orbital and sp^2-hybrid orbitals in the plane of the chelate ring. The limiting formulations $[Re^{VI}(L_3)^{6-}]^0$, where the ligand is in a classical dianionic form and the metal is d^1, and $[Re^{II}(L_3)^{2-}]^0$, where the three dianionic ligands have four electrons removed, represent extreme configurations. The complex $V(S_2C_2Ph_2)_3{}^0$ is intriguing in that the unpaired electron is in the $2a_2'$ orbital which is ligand-based and non-bonding with the metal. This complex is known to have D_{3h} symmetry compared with $[V(S_2C_2Ph_2)_3]^{2-}$

which is distorted O_h (D_3). This latter complex would not be expected to have an electron in an A_1 orbital and so the sign of the metal anisotropic hyperfine coupling constant will be reversed (see Section III,B,1).

$[VO(MNT)_2]^{2-}$ and the binuclear (*116*) $[Mo_2(TDT)_5]$ have also been prepared. The former (*42*) is much more like a typical VO^{2+} complex, showing the dominance of the V=O system. A simpler method of preparing MNT complexes has been reported (*42*) which involves direct reaction of a metal salt with sodium dithiocyanoformate and eliminates the troublesome synthesis of Na_2MNT.

Certain reduced zinc and cadmium (gma) and (dtbh) complexes yield ESR signals with *g* close to free spin and no h.f.s. (*352*, *472*).

ACKNOWLEDGMENTS

We have been particularly indebted to Professor M. C. R. Symons, Drs. R. Catterall and D. J. A. Tinling, and Mr. N. V. Vugman for helpful discussions during the preparation of this Review.

REFERENCES

1. Aasa, R., Carlsson, K. E., Reyes, S. A., and Vänngard, T., *Arkiv. Kemi* **25**, 285 (1966).

2. Aasa, R., Falk, K. E., and Reyes, S. A., *Arkiv. Kemi* **25**, 309 (1966).

3. Aasa, R., Malmström, B. G., Saltman, P., and Vänngard, T., *Biochim. Biophys. Acta* **75**, 203 (1963).

4. Aasa, R., Petterson, R., and Vänngard, T., *Nature* **190**, 258 (1961).

5. Abakumov, G. A., Shilov, A. E., and Shulyndin, S. V., *Kinetika i Kataliz* **5**, 228 (1964); *Kinetics Catalysis* (*USSR*) (*Engl. Transl.*) **5**, 201 (1964).

6. Abdrakhmanov, R. S., Garif'yanov, N. S., and Semenova, E. I., *Zh. Strukt. Khim.* **9**, 530 (1968).

7. Abe, H., *J. Phys. Soc. Japan* **13**, 987 (1958).

8. Abe, H., and Ohtsuka, M., *J. Phys. Soc. Japan* **11**, 896 (1956).

9. Abe, H., and Shimada, J., *Phys. Rev.* **90**, 316 (1953); *J. Phys. Soc. Japan* **12**, 1255 (1957).

10. Ablov, A. V., Yablokov, Y. V., and Milkova, L. N., *Dokl. Akad. Nauk SSSR* **171**, 593 (1966).

11. Abragam, A., Horowitz, J., and Pryce, M. H. L., *Proc. Roy. Soc.* **A230**, 169 (1955).

12. Abragam, A., and Pryce, M. H. L., *Proc. Roy. Soc.* **A205**, 135 (1951).

13. Abragam, A., and Pryce, M. H. L., *Proc. Roy. Soc.* **A206**, 164 (1951).

14. Abragam, A., and Pryce, M. H. L., *Proc. Roy. Soc.* **A206**, 173 (1951).

15. Abraham, M. M., Abriata, J. P., Foglio, M. F., and Pasquini, E., *J. Chem. Phys.* **45**, 2069 (1966).

16. Adams, D. M., "Metal-Ligand and Related Vibrations." Arnold, London, 1967.

17. Adema, E. H., Bartelink, H. J. M., and Smidt, J., *Rec. Trav. Chim.* **80**, 173 (1961).

18. Adema, E. H., Bartelink, H. J. M., and Smidt, J., *Rec. Trav. Chim.* **81**, 73 (1962).

19. Airja, S. M., Akopgan, S. C., and Wintruff, W., *Z. Anorg. Chem.* **352**, 102 (1967).

20. Akhtar, F., Goodgame, D. M. L., Goodgame, M., Rayner-Canham, G. W., and Skapski, A. C., *Chem. Commun.* p. 1389 (1968).

21. Alderman, P. R. H., Owston, P. G., and Rowe, J. M., *J. Chem. Soc.* p. 668 (1962).

22. Alef, C., and Wertheim, G. K., *Phys. Rev.* **122**, 1414 (1961).

23. Alexander, J. J., and Gray, H. B., *J. Am. Chem. Soc.* **89**, 3356 (1967).

24. Allen, P. E. M., Brown, J. K., and Obaid, R. M. S., *Trans. Faraday Soc.* **59**, 1808 (1963).

25. Al'tshuler, S. A., and Kozyrev, B. M., "Electron Paramagnetic Resonance." Academic Press, New York, 1964.

26. Anderson, H. G., *Phys. Rev.* **120**, 1606 (1960).

27. Anderson, S. E., and Drago, R. S., *J. Am. Chem. Soc.* **91**, 3656 (1969).

28. Angelescu, E., Nicolau, C., and Simon, Z., *J. Am. Chem. Soc.* **88**, 3910 (1966).

29. Antipova-Karataeva, I. I., Grechushnikov, B. N., Koryagin, V. F., and Kutsenka, Y. I., *Fiz. Tverd. Tela* **7**, 2712 (1965); *Soviet. Phys.—Solid State* (*Engl. Transl.*) **7**, 2192 (1966).

30. Antosik, S., Brown, N. M. D., McConnell, A. A., and Porte, A. L., *J. Chem. Soc. A* p. 545 (1969).

31. Anufrienko, V. F., Kogan, T. M., Rukhadze, E. G., Dunnina, V. V., and Drobyshevskaya, E. V., *Teor. Eksp. Khim.* **3**, 370 (1967).

32. Anufrienko, V. F., Mamaeva, E. K., and Keier, N. P., *Dokl. Akad. Nauk SSSR* **168**, 116 (1966).

33. Anufrienko, V. F., Mamaeva, E. K., Keier, N. P., Kefeli, L. M., Terentev, A. P., and Rukhadze, E. G., *Dokl. Akad. Nauk SSSR* **159**, 1059 (1964)

34. Anufrienko, V. F., Mamaeva, E. K., Rukhadze, E. G., and Ilina, I. G., *Teor. Eksp. Khim.* **3**, 363 (1967).

35. Anufrienko, V. F., and Zeif, A. P., *Opt. i Spektroskopiya* **20**, 652 (1966).

36. Aoyagi, Y., Masuda, K., and Yamaguchi, J., *J. Phys. Soc. Japan* **23**, 1188 (1967).

37. Assour, J. M., *J. Chem. Phys.* **43**, 2477 (1965).

38. Assour, J. M., *J. Am. Chem. Soc.* **87**, 4701 (1965).

39. Assour, J. M., Goldmacher, J., and Harrison, S. E., *J. Chem. Phys.* **43**, 159 (1965).

40. Assour, J. M., and Harrison, S. E., *Phys. Rev.* **136**, A1368 (1964).

41. Assour, J. M., and Kahn, W. K., *J. Am. Chem. Soc.* **87**, 207 (1965).

42. Atherton, N. M., Locke, J., and McCleverty, J. A., *Chem. Ind.* (*London*) p. 1300 (1965).

43. Atkins, P. W., and Kivelson, D., *J. Chem. Phys.* **44**, 169 (1966).

44. Atkins, P. W., and Symons, M. C. R., "The Structure of Inorganic Radicals." Elsevier, Amsterdam, 1967.

45. Auzins, P., Orton, J. W., and Wertz, J. E., *in* "Paramagnetic Resonance" (W. Low, ed.), Vol. 1, p. 90. Academic Press, New York, 1963.

46. Ayscough, P. B., "Electron Spin Resonance in Chemistry." Methuen, London, 1967.

47. Azarbayejani, G. H., and Merlo, A. L., *Phys. Rev.* **137**, A489 (1965).

48. Baird, M. C., Hartwell, G., and Wilkinson, G., *J. Chem. Soc. A*, p. 2037 (1967).

49. Baker, J. M., Bleaney, B., and Bowers, K. D., *Proc. Phys. Soc.* (*London*) **B69**, 1205 (1956).

50. Baker, J. M., Bleaney, B., and Hayes, W., *Proc. Roy. Soc.* **A247**, 141 (1958).

51. Balch, A. L., *Inorg. Chem.* **6**, 2158 (1967).

52. Balch, A. L., and Holm, R. H., *J. Am. Chem. Soc.* **88**, 5201 (1966).

53. Balch, A. L., and Holm, R. H., *Chem. Commun.* p. 552 (1966).

54. Balch, A. L., Rohrscheid, F., and Holm, R. H., *J. Am. Chem. Soc.* **87**, 2301 (1965).

55. Ballhausen, C. J., and Gray, H. B., *Inorg. Chem.* **1**, 111 (1962).

56. Barbour, J. M., Morton-Blake, D. A., and Porte, A. L., *J. Chem. Soc. A* p. 878 (1968).

57. Bartelink, H. J. M., Bos, H., Smidt, J., Vrinssen, C. H., and Adema, E. H., *Rec. Trav. Chim.* **81**, 225 (1962).

58. Bartelink, H. J. M., Bos, H., van Raayen, W., and Smidt, J., *Arch. Sci.* (*Geneva*) **14**, 158, 197 (1961).

59. Bartlett, P. D., and Seidel, B., *J. Am. Chem. Soc.* **83**, 581 (1961).

59a. Basch, H., and Gray, H. B., *Theoret. Chim. Acta* **4**, 367 (1966).

60. Bates, C. A., Moore, W. S., Standley, K. J., and Stevens, K. W. H., *Proc. Phys. Soc.* (*London*) **79**, 73 (1962).

61. Bauminger, R., Cohen, S. G., Marinov, A., and Ofer, S., *Phys. Rev.* **122**, 743 (1961).

62. Bayer, E., Hill, H. A. O., Roder, A., and Williams, R. J. P., *Chem. Commun.* p. 109 (1969).

63. Bayston, J. H., Looney, F. D., and Winfield, M. E., *Australian J. Chem.* **16**, 557 (1963).

64. Beinert, H., *in* "Non-Heme Iron Proteins" (A. S. Pietro, ed.), p. 23. Antioch Press, Yellow Springs, Ohio, 1965.

65. Beinert, H., Devartanian, D. V., Hemmerich, P., Veeger, C., and Van Voorst, J. D. W., *Biochim. Biophys. Acta* **96**, 530 (1965).

66. Beinert, H., and Palmer, G., *Advan. Enzymol.* **27**, 105 (1965).

67. Beljers, H. G., Bongers, P. F., Van Stapele, R. P., and Zijlstra, H., *Phys. Letters* **12**, 81 (1964).

68. Bennett, J. E., and Ingram, D. J. E., *Nature* **175**, 130 (1955).

69. Bennett, J. E., and Ingram, D. J. E., *Phil. Mag.* [8] **1**, 970 (1956).

70. Bernal, I., *Inorg. Chem.* **3**, 1465 (1964).

71. Bernal, I., Ebsworth, E. A. V., and Weil, J. A., *Proc. Chem. Soc.* p. 57 (1959).

72. Bernal, I., and Harrison, S. E., *J. Chem. Phys.* **34**, 102 (1961); **38**, 2581 (1963).

73. Bernal, I., and Hockings, E. F., *Proc. Chem. Soc.* p. 361 (1962).

74. Bernal, I., and Rieger, P. H., *Inorg. Chem.* **2**, 256 (1963).

75. Bernal, I., Robinson, S. D., Meriwether, L. S., and Wilkinson, G., *Chem. Commun.* p. 571 (1965).

76. Bershov, L. V., and Marfunin, A. S., *Dokl. Akad. Nauk SSSR* **155**, 632 (1964).

77. Bershov, L. V., Marfunin, A. S., and Mineeva, R. M., *Zh. Eksp. i Teor. Fiz.* **49**, 743 (1965).

78. Bersohn, M., and Baird, J. C., "Electron Paramagnetic Resonance." Benjamin, New York, 1966.

79. Bhatnager, V. M., and Fujiwara, S., *Chem. Ind.* (*London*) p. 1471 (1962).

80. Biji, D., and Rose-Innes, A. C., *Proc. Phys. Soc.* (*London*) **A66**, 954 (1953).

81. Billig, E., Shupack, S. I., Waters, J. H., Williams, R., and Gray, H. B., *J. Am. Chem. Soc.* **86**, 926 (1964).

82. Billig, E., Williams, R., Bernal, I., Waters, J. H., and Gray, H. B., *Inorg. Chem.* **3**, 663 (1964).

83. Billing, D. E., Dudley, R., Hathaway, B. J., Nicholls, P., and Procter, I. M., *J. Chem. Soc. A* p. 312 (1969).

84. Billing, D. E., and Hathaway, B. J., *J. Chem. Phys.* **50**, 1476, 2258 (1969); *J. Chem. Soc. A* p. 1516 (1968).

85. Billing, D. E., Hathaway, B. J., and Nicholls, P., *J. Chem. Soc. A* p. 316 (1969).

86. Bjerrum, J., Ballhausen, C. J., and Jorgensen, C. K., *Acta Chem. Scand.* **8**, 1275 (1954).

87. Bleaney, B., Bogle, G. S., Cooke, A. H., Duffus, R. J., O'Brien, M. C. M., and Stevens, K. W. H., *Proc. Phys. Soc.* (*London*) **A68**, 57 (1955).

88. Bleaney, B., and Bowers, K. D., *Proc. Roy. Soc.* **A214**, 451 (1952); *Phil. Mag.* [7] **43**, 372 (1952).

89. Bleaney, B., Bowers, K. D., and Ingram, D. J. E., *Proc. Roy. Soc.* **A228**, 147 (1955); *Proc. Phys. Soc.* (*London*) **A64**, 758 (1951).

90. Bleaney, B., Bowers, K. D., and Trenam, R. S., *Proc. Roy. Soc.* **A228**, 157 (1955).

91. Bleaney, B., and Hayes, W., *Proc. Phys. Soc.* (*London*) **B70**, 626 (1957).

92. Bleaney, B., and Ingram, D. J. E., *Proc. Roy. Soc.* **A205**, 336 (1951).

93. Bloom, M. B. D., Raynor, J. B., Root, K. D. J., and Symons, M. C. R., unpublished results.

94. Bloom, M. B. D., Raynor, J. B., and Symons, M. C. R., unpublished results.

95. Blumberg, W. E., and Peisach, J., "Non-Heme Iron Proteins" (A. S. Pietro, ed.), p. 101. Antioch Press, Yellow Springs, Ohio, 1965.

96. Blumberg, W. E., and Peisach, J., *J. Chem. Phys.* **49**, 1793 (1968).

97. Boas, J. F., Dunhill, R. H., Pilbrow, J. R., Srivastava, R. S., and Smith, T. D., *J. Chem. Soc. A* p. 94 (1969).

98. Boas, J. F., Pilbrow, J. R., Hartzell, C. R., and Smith, T. D., *J. Chem. Soc. A* p. 572 (1969).

99. Boas, J. F., Pilbrow, J. R., and Smith, T. D., *J. Chem. Soc. A* pp. 721, 723 (1969).

100. Borcherts, R. H., and Kikuchi, C., *J. Chem. Phys.* **40**, 2270 (1964).

101. Boucher, L. J., and Teh Fu Yen, *Inorg. Chem.* **7**, 2665 (1968).

102. Boucher, L. J., Tynan, E. C., and Teh Fu Yen, *Inorg. Chem.* **7**, 731 (1968).

103. Bowers, K. D., *Proc. Phys. Soc.* (*London*) **A66**, 666 (1953).

104. Bowers, K. D., and Owen, J., *Rep. Progr. Phys.* **18**, 304 (1955).

105. Breivagel, F. W., and Sarkissian, V., *J. Chem. Phys.* **48**, 2442 (1968).

106. Brill, A. S., Martin, R. B., and Williams, R. J. P., "Electronic Aspects of Biochemistry" (B. Pullman, ed)., p. 519. Academic Press, New York, 1964.

107. Brintzinger, H., *J. Am. Chem. Soc.* **88**, 4305 (1966).

108. Brintzinger, H., *J. Am. Chem. Soc.* **88**, 4307 (1966).

109. Brintzinger, H., *J. Am. Chem. Soc.* **89**, 6871 (1967).

110. Brintzinger, H., Palmer, G., and Sands, R. H., *J. Am. Chem. Soc.* **88**, 623 (1966).

111. Brisdon, B. J., and Walton, R. A., *J. Inorg. Nucl. Chem.* **27**, 1101 (1965).

112. Bryce, G. F., *J. Phys. Chem.* **70**, 3549 (1966).

113. Buch, T., *J. Chem. Phys.* **43**, 761 (1965).

114. Burgess, J., Goodman, B. A., and Raynor, J. B., *J. Chem. Soc. A* p. 501 (1968).

115. Burns, G., *J. Chem. Phys.* **41**, 1521 (1964).

116. Butcher, A., and Mitchell, P. C. H., *Chem. Commun.* p. 176 (1967).

117. Carrington, A., *Quart. Rev.* (*London*) **14**, 427 (1960).

118. Carrington, A., *Chem. Britain* **4**, 301 (1968).

119. Carrington, A., Ingram, D. J. E., Lott, K. A. K., Schonland, D. S., and Symons, M. C. R., *Proc. Roy. Soc.* **A254**, 101 (1960).

120. Carrington, A., Ingram, D. J. E., Schonland, D., and Symons, M. C. R., *J. Chem. Soc.* p. 4710 (1956).

121. Carrington, A., and Longuet-Higgins, H. C., *Quart. Rev.* (*London*) **14**, 427 (1960).

122. Carrington, A., and McLachlan, A. D., "Introduction to Magnetic Resonance." Harper & Row, New York, 1967.

123. Carrington, A., and Symons, M. C. R., *Chem. Rev.* **63**, 443 (1963).

124. Castner, T., Newell, G. S., Holton, W. C., and Schlicter, C. P., *J. Chem. Phys.* **32**, 668 (1960).

125. Chakravarty, A. S., *J. Chem. Phys.* **39**, 1004 (1963).

126. Chamberlain, J. R., and Syms, C. H. A., *Proc. Phys. Soc.* (*London*) **84**,867 (1964).

127. Chan, K. K., and Shields, L., *J. Chem. Soc. A* p. 3114 (1968).

128. Chan, S. I., Fung, B. M., and Lutje, H., *J. Chem. Phys.* **47**, 2121 (1967).

129. Chang, T.-T., *Phys. Rev.* **147**, 264 (1966).

130. Chang, T.-T., and Tanttila, W. H., *J. Chem. Phys.* **38**, 571 (1963).

131. Chatt, J., Leigh, G. J., and Paske, R. J., *Chem. Commun.* p. 671 (1967).

132. Chiang, T-C., *J. Chem. Phys.* **48**, 1814 (1968).

133. Chiang, Y. S., Craddock, J., Mickewich, D., and Turkevich, J., *J. Phys. Chem.* **70**, 3509 (1966).

134. Chien, J. C. W., and Boss, C. R., *J. Am. Chem. Soc.* **83**, 3767 (1961).

135. Ch'iu, T-W., Chu, Y-F., T'ang, H-M., Hsiung, F-C., and Kung, H-Y., *Wu Li Hsueh Pao* **17**, 600 (1961).

136. Cipollini, E., Owen, J., Thornley, J. H. M., and Windsor, C., *Proc. Phys. Soc.* (*London*) **79**, 1083 (1962).

137. Clack, D. W., Hush, N. S., and Yandle, J. R., *Chem. Phys. Letters* **1**, 157 (1967).

138. Clad, R., and Wucher, J., *Compt. Rend.* **260**, 4318 (1965); **B262**, 113 (1966).

139. Clark, R. J. H., and Greenfield, M. L., *J. Chem. Soc. A* p. 409 (1967).

139a. Clementi, E., *Phys. Rev.* **135**, 980 (1964).

139b. Clementi, E., *J. Chem. Phys.* **41**, 295 (1964).

139c. Clementi, E., *J. Chem. Phys.* **41** (Part 2, Suppl.) (1964).

140. Codell, M., Fujiwara, S., Nagashima, K., and Seki, T., *Bull. Chem. Soc.* **38**, 21 (1965), and references therein.

141. Coffman, R. E., *Phys. Letters* **21**, 381 (1966).

142. Colapietro, M., Domenicano, A., Scaramuzza, L., Vaciago, A., and Zambonelli, L., *Chem. Commun.* p. 583 (1967).

143. Colton, R., and Rix, C. J., *Australian J. Chem.* **21**, 1155 (1968).

144. Connelly, N. G., McCleverty, J. A., and Winscom, C. J., *Nature* **216**, 999 (1967).

145. Cooper, R. L., and Green, M. L. H., *J. Chem. Soc. A* p. 1155 (1967).

146. Corraja, C., and Nordio, P. L., *Ric. Sci.* **38**, 44 (1968).

147. Cotton, F. A., "Chemical Application of Group Theory," p. 84. Interscience, New York, 1963.

148. Cotton, F. A., and Wise, J. J., *J. Am. Chem. Soc.* **88**, 3451 (1966); *Inorg. Chem.* **6**, 915 (1967).

149. Cotton, S. A., and Gibson, J. F., *Chem. Commun.* p. 883 (1968).

150. Coulson, C. A., "Contribution a l'Etude de la Structure Moléculaire," Volume Commémoratif Victor Henri, p. 15, 1948.

151. Coulson, C. A., "Valence," p. 69. Oxford Univ. Press, London and New York, 1961.

152. Cowen, J. A., and Johnson, G. T., *J. Chem. Phys.* **44**, 2217 (1966).

153. Culvahouse, J. W., and Olsen, L. C., *J. Chem. Phys.* **43**, 1145 (1965).

154. Culvahouse, J. W., Unruh, W., and Sapp, R. C., *Phys. Rev.* **121**, 1370 (1961).

155. Dahl, J. P., and Ballhausen, C. J., *Kgl. Danske Videnskab. Selskab. Mat.-Fys. Medd.* **33**, 22 (1961).

156. Dahl, J. P., and Ballhausen, C. J., *Kgl. Danske Videnskab. Selskab, Mat.-Fys. Medd.* **33**, 1 (1961).

157. Dall'olio, A., Dascola, G., and Varacca, V., *Nuovo Cimento* **B43**, 192 (1966).

158. Danon, J., Muniz, R. P. A., and Caride, A. O., *J. Chem. Phys.* **46**, 1210 (1967).

159. Danon, J., Muniz, R. P. A., Caride, A. O., and Wolfson, I., *J. Mol. Struct.* **1**, 127 (1967).

160. Danon, J., Muniz, R. P. A., and Panepucci, H., *J. Chem. Phys.* **41**, 2651 (1964).

161. Danon, J., Muniz, R. P. A., and Panepucci, H, *J. Chem. Phys.* **41**, 3651 (1964).

162. Danon, J., Panepucci, H., and Misetich, A. A., *J. Chem. Phys.* **44**, 4154 (1966).

163. Davison, A., Edelstein, N., Holm, R. H., and Maki, A. H., *Inorg. Chem.* **2** 1227 (1963).

164. Davison, A., Edelstein, N., Holm, R. H., and Maki, A. H., *J. Am. Chem. Soc.* **85**, 2029 (1963).

165. Davison, A., Edelstein, N., Holm, R. H., and Maki, A. H., *J. Am. Chem. Soc.* **85**, 3049 (1963).

166. Davison, A., Edelstein, N., Holm, R. H., and Maki, A. H., *Inorg. Chem.* **3**, 814 (1964).

167. Davison, A., Edelstein, N., Holm, R. H., and Maki, A. H., *J. Am. Chem. Soc.* **86**, 2799 (1964).

168. Davison, A., Edelstein, N., Holm, R. H., and Maki, A. H., *Inorg. Chem.* **4**, 55 (1965).

169. Davison, A., and Shawl, E. T., *Chem. Commun.* p. 670 (1967).

170. Deal, R. M., Ingram, D. J. E., and Srinivasan, R., *Proc. 12th Colloq. Ampère* p. 239 (1963).

171. DeArmond, K., Garrett, B. B., and Gutowsky, H. S., *J. Chem. Phys:* **42**, 1019 (1965).

172. Declerck, C., *Bull. Soc. Roy. Sci. Liege* **35**, 230 (1966).

173. Dessy, R. E., King, R. B., and Waldrop, M., *J. Am. Chem. Soc.* **88**, 5112 (1966).

174. Dessy, R. E., Kornmann, R., Smith, C., and Hayter, R., *J. Am. Chem. Soc.* **90**, 2001 (1968).

175. Dessy, R. E., and Pohl, R. L., *J. Am. Chem. Soc.* **90**, 1995 (1968).

176. Dessy, R. E., Stary, F. E., King, R. B., and Waldrop, M., *J. Am. Chem. Soc.* **88**, 471 (1966).

177. Dessy, R. E., Weissman, P. M., and Pohl, R. L., *J. Am. Chem. Soc.* **88**, 5117 (1966).

178. de Wit, M., and Estle, T. L., *Bull. Am. Phys. Soc.* [2] **8**, 24 (1963).

179. de Wit, M., and Reinberg, A. R., *Phys. Rev.* **163**, 261 (1967).

180. Dieleman, J., *Philips Res. Rep.* **20**, 206 (1965).

181. Dietz, R. E., Kamimura, H., Sturge, M. D., and Yariv, A., *Phys. Rev.* **132**, 1559 (1963).

182. Dionne, G. F., *Phys. Rev.* **137**, A743 (1965).

183. Dorain, P. B., *Phys. Rev.* **112**, 1058 (1958).

184. Dorain, P. B., and Rahn, R., *J. Chem. Phys.* **36**, 561 (1962); **42**, 3249 (1964).

185. Dowsing, R. D., and Gibson, J. F., *J. Chem. Soc. A* p. 655 (1967).

186. Dowsing, R. D., Gibson, J. F., Goodgame, D. M. L., Goodgame, M., and Hayward, P. J., *Nature* **219**, 1037 (1968).

187. Dowsing, R. D., Gibson, J. F., Goodgame, M., and Hayward, P. J., *J. Chem. Soc. A* p. 187 (1969).

188. Doyle, G., and Tobias, R. S., *Inorg. Chem.* **7**, 2479 (1968).

189. Dunhill, R. H., Pilbrow, J. R., and Smith, T. D., *J. Chem. Phys.* **45**, 1474 (1966).

190. Dunhill, R. H., and Smith, T. D., *J. Chem. Soc. A* p. 2189 (1968).

191. Dunn, T. M., *Trans. Faraday Soc.* **57**, 1441 (1961).

192. Dzahabiev, T. S., and Shilov, A. E., *Zh. Strukt. Khim.* **6**, 302 (1965); *J. Struct. Chem. (USSR) (Engl. Transl.)* **6**, 279 (1965).

193. Eaton, D. R., *J. Am. Chem. Soc.* **87**, 3097 (1965).

194. Eaton, D. R., Josey, A. D., and Benson, R. E., *J. Am. Chem. Soc.* **89**, 4040 (1967).

195. Eaton, D. R., Josey, A. D., Phillips, W. D., and Benson, R. E., *J. Chem. Phys.* **37**, 347 (1962); *J. Am. Chem. Soc.* **84**, 4100 (1962); *Discussions Faraday Soc.* **34**, 77 (1962).

196. Eaton, D. R., and LaLancette, E. A., *J. Chem. Phys.* **41**, 3534 (1964).

197. Eaton, D. R., and Phillips, W. D., *Advan. Magnetic Resonance* **1**, 103 (1966).

198. Ebsworth, E. A. V., and Hughes, R. G., *J. Inorg. Nucl. Chem.* **29**, 1799 (1967).

199. Ebsworth, E. A. V., and Weil, J. A., *J. Chem. Phys.* **63**, 1890 (1959).

200. Edwards, P. R., Subramanian, S., and Symons, M. C. R., *J. Chem. Soc. A* p. 2985 (1968).

201. Egashira, K., and Hirakawa, K., *J. Phys. Soc. Japan* **22**, 344 (1967).

202. Ehrenberg, A., *Arkiv. Kemi* **19**, 119 (1962).

203. Elliott, H., and Hathaway, B. J., *Inorg. Chem.* **5**, 885 (1966); *J. Chem. Soc. A* p. 1443 (1966).

204. Elliott, H., Hathaway, B. J., and Slade, R. C., *Inorg. Chem.* **5**, 669 (1966).

205. Elschner, B., and Herzog, S., *Z. Naturforsch.* **12a**, 860 (1957).

206. Elschner, B., and Herzog, S., *Arch. Sci. (Geneva)* **11**, 160 (1958).

207. Elschner, B., and Neubert, R., "Hochfrequenzspektroskopie," p. 185. Akademie Verlag, Berlin, 1961.

208. Estle, T. L., and Holton, W. C., *Phys. Rev.* **150**, 159 (1966).

209. Falk, K. E., Freeman, H. C., Jansson, T., Malmstrom, B. G., and Vanngard, T., *J. Am. Chem. Soc.* **89**, 6071 (1967); **90**, 2203 (1968).

210. Fedotov, V. N., Garif'yanov, N. S., and Kozyrev, B. M., *Dokl. Akad. Nauk SSSR* **145**, 1318 (1962); *Dokl. Phys. Chem. (Engl. Transl.)* **145**, 606 (1962).

211. Feltham, R. D., *J. Inorg. Nucl. Chem.* **16**, 197 (1961).

212. Feltham, R. D., Sogo, P., and Calvin, M., *J. Chem. Phys.* **26**, 1354 (1957).

213. Fidone, I., and Stevens, K. W. H., *Proc. Phys. Soc. (London)* **73**, 116 (1958).

214. Figgis, B. N., "Introduction to Ligand Fields." Wiley (Interscience), New York, 1966.

215. Fisher, H., *Ber. Bunsenges. Phys. Chem.* **71**, 685 (1967).

216. Fortman, J. J., and Hayes, R. G., *J. Chem. Phys.* **43**, 15 (1965).

217. Foust, A. S., and Soderberg, R. H., *J. Am. Chem. Soc.* **89**, 5507 (1967).

218. Fraenkel, G. K., *J. Phys. Chem.* **71**, 139 (1967).

219. Freeman, A. J., and Watson, R. E., *Phys. Rev.* **123**, 2027 (1961).

220. Freeman, A. J., and Watson, R. E., *in* "Magnetism" (G. T. Rado and H. Suhl, eds.), Vol. IIA, p. 167. Academic Press, New York, 1965.

221. Fritz, H. P., Golla, B. M., and Keller, H. J., *Z. Naturforsch.* **21b**, 97 (1966).

222. Fritz, H. P., Golla, B. M., and Keller, H. J., *Z. Naturforsch.* **21b**, 1015 (1966).

223. Fritz, H. P., Golla, B. M., and Keller, H. J., *Z. Naturforsch.* **23b**, 876 (1968).

224. Fritz, H. P., Golla, B. M., Keller, H. J., and Schwarzhans, K. E., *Z. Naturforsch.* **21b**, 725 (1966).

225. Fritz, H. P., and Keller, H. J., *Z. Naturforsch.* **20b**, 1145 (1965).

226. Fujiwara, S., "Spectroscopy and Structure of Metal Chelate compounds." Wiley, New York, 1968.

227. Fujiwara, S., and Codell, M., *Bull. Chem. Soc. Japan* **37**, 49 (1964).

228. Fujiwara, S., and Nagashima, K., *Anal. Chem.* **38**, 1464 (1966).

229. Furlani, C., Sgamellotti, A., Magrini, F., and Cordischi, D., *J. Mol. Spectry.* **24**, 270 (1967).

230. Gager, W. B., Jastram, P. S., and Daunt, J. G., *Phys. Rev.* **111**, 803 (1958).

231. Gainullin, I. F., Garif'yanov, N. S., and Kozyrev, B. M., *Dokl. Akad. Nauk SSSR* **180**, 858 (1968).

232. Garif'yanov, N. S., *Dokl. Akad. Nauk SSSR* **155**, 612 (1961).

233. Garif'yanov, N. S., *Fiz. Tverd. Tela* **4**, 2450 (1962); *Soviet Phys.—Solid State* (*Engl. Transl.*) **4**, 1795 (1963).

234. Garif'yanov, N. S., *Zh. Eksp. Teor. Fiz.* **45**, 1819 (1963); *Soviet Phys. JETP* (*Engl. Transl.*) **18**, 1246 (1964).

235. Garif'yanov, N. S., *Dokl. Akad. Nauk SSSR* **155**, 385 (1964); *Dokl. Phys. Chem.* (*Engl. Transl.*) **155**, 249 (1964).

236. Garif'yanov, N. S., and Fedotov, V. N., *Fiz. Tverd. Tela* **4**, 3537 (1962); *Soviet Phys.—Solid State* (*Engl. Transl.*) **4**, 2589 (1963).

237. Garif'yanov, N. S., and Fedotov, V. N., *Zh. Strukt. Khim.* **3**, 711 (1962); *J. Struct. Chem.* (*USSR*) (*Engl. Transl.*) **3**, 685 (1962).

238. Garif'yanov, N. S., and Fedotov, V. N., *Zh. Eksp. Teor. Fiz.* **43**, 376 (1962); *Soviet Phys. JETP* (*Engl. Transl.*) **16**, 269 (1963).

239. Garif'yanov, N. S., Fedotov, V. N., and Kucheryavenko, N. S., *Izvest. Akad. Nauk SSSR Ser. Khim.* **4**, 743 (1964); *Bull. Acad. Sci. USSR Div. Chem. Sci.* (*Engl. Transl.*) p. 689 (1964).

240. Garif'yanov, N. S., Kalinichenko, I. I., Ovchinnikov, I. V., and Mantyanova, Z. F., *Dokl. Akad. Nauk SSSR* **176**, 328 (1967); *Dokl. Chem.* (*Engl. Transl.*) **176**, 795 (1967).

241. Garif'yanov, N. S., and Karakhashyan, E. G., *Fiz. Tverd. Tela* **7**, 1274 (1965); *Soviet Phys.—Solid State* (*Engl. Transl.*) **7**, 1033 (1965).

242. Garif'yanov, N. S., and Kozyrev, B. M., *Teor. Eksp. Khim.* **1**, 525 (1965); *Theor. Exptl. Chem.* (*USSR*) (*Engl. Transl.*) **1**, 345 (1965).

243. Garif'yanov, N. S., and Kozyrev, B. M., *Zh. Strukt. Khim.* **6**, 773 (1965); *J. Struct. Chem.* (*USSR*) (*Engl. Transl.*) **6**, 734 (1965).

244. Garif'yanov, N. S., Kozyrev, B. M., and Fedotov, V. N., *Dokl. Akad. Nauk SSSR* **156**, 641 (1964); *Dokl. Phys. Chem.* (*Engl. Transl.*) **156**, 516 (1964).

245. Garif'yanov, N. S., Kozyrev, B. M., and Fedotov, V. N., *Teor. Eksp. Khim.* **1**, 118 (1965); *Theor. Exptl. Chem.* (*USSR*) (*Engl. Transl.*) **1**, 77 (1965).

246. Garif'yanov, N. S., Kozyrev, B. M., and Fedotov, V. N., *Dokl. Akad. Nauk SSSR* **178**, 808 (1968).

247. Garif'yanov, N. S., Kozyrev, B. M., and Gainullin, I. F., *Zh. Strukt. Khim.* **9**, 529 (1968).

248. Garif'yanov, N. S., Kozyrev, B. M., and Semenova, E. I., *Dokl. Akad. Nauk SSSR* **147**, 365 (1962); *Dokl. Chem.* (*Engl. Transl.*) **147**, 977 (1962).

249. Garif'yanov, N. S., Kozyrev, B. M., and Semenova, E. I., *Dokl. Akad. Nauk SSSR* **170**, 1324 (1966).

250. Garif'yanov, N. S., Kozyrev, B. M., Timerov, R. K., and Usachev, N. F., *Zh. Eksp. Theor. Fiz.* **41**, 1076 (1961); *Soviet Phys. JETP* (*Engl. Transl.*) **14**, 786 (1962).

251. Garif'yanov, N. S., Kucheryavenka, N. S., and Fedotov, V. N., *Dokl. Akad. Nauk SSSR* **150**, 802 (1963); *Dokl. Chem.* (*Engl. Transl.*) **150**, 452 (1963).

252. Garif'yanov, N. S., and Semenova, E. I., *Zh. Eksp. Teor. Fiz.* **41**, 337 (1962); *Soviet Phys. JETP* (*Engl. Transl.*) **14**, 243 (1962).

253. Garif'yanov, N. S., Semenova, E. I., and Usacheva, N. S., *Zh. Strukt. Khim.* **3**, 596 (1962); *J. Struct. Chem.* (*USSR*) (*Engl. Transl.*) **3**, 570 (1962).

254. Garif'yanov, N. S., and Yafaev, N. R., *Zh. Eksp. Teor. Fiz.* **43**, 1978 (1962); *Soviet Phys. JETP* (*Engl. Transl.*) **16**, 1392 (1963).

255. Garrett, B. B., DeArmond, K., and Gutowsky, H. S., *J. Chem. Phys.* **44**, 3393 (1966).

256. Genser, E. E., *Inorg. Chem.* **7**, 13 (1968).

257. German, E. D., and Dyatkina, M. E., *Zh. Strukt. Khim.* **6**, 898 (1965).

258. Gerritsen, H. J., and Lewis, H. R., *Phys. Rev.* **119**, 1010 (1960).

259. Gerritsen, H. J., and Sabisky, E. S., *Phys. Rev.* **125**, 1853 (1962).

260. Gerritsen, H. J., and Sabisky, E. S., *Phys. Rev.* **132**, 1507 (1963).

261. Gersmann, H. R., and Swalen, J. D., *J. Chem. Phys.* **36**, 3221 (1962).

262. Geschwind, S., *J. Appl. Phys.* **36**, 920 (1965).

263. Geschwind, S., and Remeika, J. P., *Bull. Am. Phys. Soc.* [2] **6**, 116 (1961).

264. Geschwind, S., and Remeika, J. P., *J. Appl. Phys.* **33**, 370 (1962).

265. Gibson, J. F., *Nature* **196**, 64 (1962).

266. Gibson, J. F., *Trans. Faraday Soc.* **60**, 2105 (1964).

267. Gibson, J. F., and Ingram, D. J. E., *Nature* **180**, 29 (1957).

268. Gijsman, H. M., Gerritsen, H. J., and van der Handel, J., *Physica* (*Utrecht*) **20**, 15 (1954).

269. Gill, N. S., and Nyholm, R. S., *J. Chem. Soc.* p. 3997 (1959).

270. Gladney, H. M., *Phys. Rev.* **143**, 198 (1966).

271. Gladney, H. M., and Swalen, J. D., *J. Chem. Phys.* **42**, 1999 (1965).

272. Glazkov, Y. V., and Solov'ev, K. N., *Zh. Prikl. Spektrosk.* **6**, 262 (1967).

273. Glemser, O., Roesky, H. W., Hellberg, K. H., and Werther, H. U., *Chem. Ber. 99*, 2652 (1966).

274. Golding, R. M., *Mol. Phys.* **5**, 369 (1962).

275. Golding, R. M., and Orgel, L. E., *J. Chem. Soc.* p. 363 (1962).

276. Goodings, D. A., and Heine, V., *Phys. Rev. Letters* **5**, 370 (1960).

277. Goodman, B. A., McNeil, D. A. C., Raynor, J. B., and Symons, M. C. R., *J. Chem. Soc. A* p. 1547 (1966).

278. Goodman, B. A., and Raynor, J. B., *J. Chem. Soc. A* (1970), in press.

279. Goodman, B. A., Raynor, J. B., and Symons, M. C. R., *J. Chem. Soc. A* p. 910 (1966).

280. Goodman, B. A., Raynor, J. B., and Symons, M. C. R., *J. Chem. Soc. A* p. 1973 (1968).

281. Goodman, B. A., Raynor, J. B., and Symons, M. C. R., *J. Chem. Soc. A* p. 2572 (1969).

282. Goodman, B. A., and Raynor, J. B., *J. Inorg. Nucl. Chem.* **32**, (1970), in press.

283. Gray, H. B., *Transition Metal Chem.* **1**, 240 (1965).

284. Gray, H. B., *Coord. Chem. Rev.* **1**, 156 (1966).

285. Gray, H. B., *Trans. N.Y. Acad. Sci.* [2] **28**, 898 (1966).

286. Gray, H. B., Bernal, I., and Billig, E., *J. Am. Chem. Soc.* **84**, 3404 (1962).

287. Gray, H. B., and Billig, E., *J. Am. Chem. Soc.* **85**, 2019 (1963).

288. Gray, H. B., and Hare, C. R., *Inorg. Chem.* **1**, 363 (1962).

289. Gray, H. B., Manoharan, P. T., Pearlman, J., and Riley, R. F., *Chem. Commun.* p. 62 (1965).

290. Gray, H. B., Williams, R., Bernal, I., and Billig, E., *J. Am. Chem. Soc.* **84**, 3596 (1962).

291. Gregorio, S., Weber, J., and Lacroix, R., *Helv. Phys. Acta* **38**, 172 (1965).

292. Gregson, A. K., and Mitra, S., *J. Chem. Phys.* **49**, 3696 (1968).

293. Griffith, W. P., Lewis, J., and Wilkinson, G., *J. Chem. Soc.* p. 872 (1959).

294. Griffiths, J. H. E., and Owen, J., *Proc. Roy. Soc.* **A226**, 96 (1954).

295. Griffiths, J. H. E., Owen, J., Park, J. G., and Partridge, M. F., *Phys. Rev.* **108**, 1345 (1957).

296. Griffiths, J. H. E., Owen, J., and Ward, I. M., *Proc. Roy. Soc.* **A219**, 526 (1953).

297. Griffiths, J. S., *Proc. Roy. Soc.* **A235**, 23 (1956).

298. Griffiths, J. S., "Theory of Transition Metal Ions." Cambridge Univ. Press, London and New York, 1961.

299. Griffiths, J. S., *Biopolymers Symp.* **1**, 35 (1964).

300. Griffiths, J. S., "Molecular Biophysics", p. 191. Academic Press, New York, 1965.

301. Guzy, C. M., Raynor, J. B., and Stodulski, L. P., *Nature* **221**, 551 (1969).

302. Guzy, C. M., Raynor, J. B., Stodulski, L. P., and Symons, M. C. R., *J. Chem. Soc. A* p. 997 (1969).

303. Guzy, C. M., Raynor, J. B., and Symons, M. C. R., *J. Chem. Soc. A* p. 2791 (1969).

304. Guzy, C. M., Raynor, J. B., and Symons, M. C. R., *J. Chem. Soc. A* p. 2299 (1969).

305. Guzy, C. M., Raynor, J. B., and Symons, M. C. R., unpublished results.

306. Haight, G. P., *J. Inorg. Nucl. Chem.* **24**, 663 (1962).

307. Hall, T. P. P., and Hayes, W., *J. Chem. Phys.* **32**, 1871 (1960).

308. Hall, T. P. P., Hayes, W., Stevenson, R. W. H., and Wilkins, J., *J. Chem. Phys.* **38**, 1977 (1963).

309. Hall, T. P. P., Hayes, W., Stevenson, R. W. H., and Wilkins, J., *J. Chem. Phys.* **39**, 35 (1963).

310. Hall, T. P. P., Hayes, W., and Williams, F. I. B., *Proc. Phys. Soc.* (*London*) **78**, 883 (1961).

311. Ham, F. S., and Ludwig, G. W., *in* "Paramagnetic Resonance" (W. Lowe, ed.), Vol. 1, p. 163. Academic Press, New York, 1963.

312. Hannon, D. M., *Phys. Rev.* **164**, 366 (1967).
313. Hare, C. R., Bernal, I., and Gray, H. B., *Inorg. Chem. 1*, 831 (1962).
314. Harrison, S. E., and Assour, J. M., *in* "Paramagnetic Resonance" (W. Low, ed.), Vol. 2, p. 855. Academic Press, New York, 1963; *J. Chem. Phys.* **40**, 365 (1964).
315. Hathaway, B. J., Billing, D. E., Nicholls, P., and Procter, I. M., *J. Chem. Soc. A* p. 319 (1969).
316. Hausser, K. H., *Z. Naturforsch.* **14a**, 425 (1959).
317. Hausser, K. H., *Z. Naturforsch.* **16a**, 1190 (1961).
318. Hausser, K. H., *Naturwissenschaften* **48**, 426, 666 (1961).
319. Hayes, R. G., *J. Chem. Phys.* **38**, 2580 (1963).
320. Hayes, R. G., *J. Chem. Phys.* **44**, 2210 (1966).
321. Hayes, R. G., *J. Chem. Phys.* **47**, 1692 (1967).
322. Hayes, R. G., *J. Chem. Phys.* **48**, 4806 (1968).
323. Hayes, R. G., and Myers, R. J., *J. Chem. Phys.* **40**, 877 (1964).
324. Hayes, W., *Discussions Faraday Soc.* **26**, 58 (1958).
325. Hayes, W., *Rep. Progr. Phys.* **22**, 204 (1959).
326. Hayes, W., and Jones, D. A., *Proc. Phys. Soc.* (*London*) **71**, 503 (1958).
327. Hayes, W., Philbrew, J. R., and Slifkin, L. M., *J. Phys. Chem. Solids* **25**, 1417 (1964).
328. Hayes, W., and Wilkens, J., *Proc. Roy. Soc.* **A281**, 340 (1964).
329. Hecht, H. G., and Frazier, J. P., *J. Chem. Phys.* **44**, 1718 (1966).
330. Hecht, H. G., and Frazier, J. P., *J. Inorg. Nucl. Chem.* **29**, 613 (1967).
331. Heine, V., *Phys. Rev.* **107**, 1002 (1957).
332. Helmholz, L., *J. Chem. Phys.* **31**, 172 (1959).
333. Helmholz, L., and Guzzo, A. V., *J. Chem. Phys.* **32**, 302 (1960).
334. Helmholz, L., Guzzo, A. V., and Sanders, R. N., *J. Chem. Phys.* **35**, 1349 (1961).
335. Hennig, K., *Phys. Status Solidi* **7**, 885 (1964).
336. Henning, J. C. M., and Bongers, P. F., *J. Phys. Chem. Solids* **27**, 745 (1966).
337. Henning, J. C. M., Van den Boom, H., and Dieleman, J., *Philips Res. Rept.* **21**, 16 (1966).
338. Henrici-Olivé, G., and Olivé, S., *Z. Phys. Chem.* (*Frankfurt*) **56**, 223 (1967).
339. Henrici-Olivé, G., and Olivé, S., *Angew. Chem. Intern. Ed.* **7**, 386 (1968).
340. Henrici-Olivé, G., and Olivé, S., *Angew. Chem.* **80**, 796 (1968).
341. Henrici-Olivé, G., and Olivé, S., *Chem. Commun.* p. 113 (1969).
342. Heuer, K., Neubert, R., and Sonneck, H. D., *Exptl. Tech. Phys.* **13**, 231 (1965).
343. Hoard, J. L., and Nordsieck, H. H., *J. Am. Chem. Soc.* **61**, 2853 (1939).
344. Höchli, U. T., *Phys. Rev.* **162**, 262 (1967).
345. Höchli, U. T., and Estle, T. L., *Phys. Rev. Letters* **18**, 128 (1967).
346. Hockings, E. F., and Bernal, I., *J. Chem. Soc.* p. 5029 (1964).
347. Hodges, J. A., Marshall, S. A., McMillan, J. A., and Serway, R. A., *J. Chem. Phys.* **49**, 2857 (1968).
348. Hodges, J. A., Serway, R. A., and Marshall, S. A., *Phys. Rev.* **151**, 196 (1966).
349. Hoehne, M., and Stasiw, M., *Phys. Status Solidi* **25**, K55 (1968).
350. Hogenkamp, H. P. C., Barker, H. A., and Mason, H. S., *Arch. Biochem. Biophys.* **100**, 353 (1963).
351. Holloway, C. E., Mabbs, F. E., and Smail, W. R., *J. Chem. Soc. A* p. 2980 (1968).

352. Holm, R. H., Balch, A. L., Davison, A., Maki, A. H., and Berry, T. E., *J. Am. Chem. Soc.* **89**, 2866 (1967).

353. Holton, W. C., Schneidu, J., and Estle, T. L., *Phys. Rev.* **133**, 1638 (1964).

354. Hong, P., Sonogashiva, K., and Hagihara, N., *Bull. Chem. Soc. Japan* **39**, 1821 (1966).

355. Horrocks, W. D., Van Hecke, G. R., and Hall, D. D., *Inorg. Chem.* **6**, 694 (1967).

356. Hoshina, T., *J. Phys. Soc. Japan* **21**, 1608 (1966).

357. Hoskins, R. H., and Soffer, B. H., *Phys. Rev.* **133**, A490 (1964).

358. Hudson, A., and Kennedy, M. J., *J. Chem. Soc. A* p. 1116 (1969).

359. Hush, N. S., and Rowlands, J. R., *J. Am. Chem. Soc.* **89**, 2976 (1967).

360. Ibers, J. A., and La Placa, S. L., *Science* **145**, 920 (1964).

361. Ingram, D. J. E., "Free Radicals as Studied by E.S.R.," Butterworths, Washington, D.C., 1958.

362. Ingram, D. J. E., and Bennett, J. E., *Discussions Faraday Soc.* **19**, 140 (1955).

363. Ingram, D. J. E., Bennett, J. E., George, P., and Goldstein, J. M., *J. Am. Chem. Soc.* **78**, 3545 (1956).

364. Jahn, H. A., *Proc. Roy. Soc.* **A164**, 117 (1938).

365. Jahn, H. A., and Teller, E., *Proc. Roy. Soc.* **A161**, 220 (1937).

366. Jarrett, H. S., *J. Chem. Phys.* **27**, 1298 (1957).

367. Jarrett, H. S., *J. Chem. Phys.* **28**, 1260 (1958).

368. Jellinek, F., *Nature* **187**, 871 (1960).

369. Jesson, J. P., *J. Chem. Phys.* **45**, 1049 (1966).

370. Jesson, J. P., *J. Phys. Chem.* **47**, 582 (1967).

371. Jezowska-Trzebiatowska, B., and Wojciechowski, W., *Theory Structure Complex Compounds, Symp. Wroclow, Poland, 1962* p. 375.

372. Jezowska-Trzebiatowska, B., and Wojciechowski, W., *Poznam. Towarz Przyjaciol Nauk Wydzial Mat.-Przyrod Prace Komisji Mat.-Przyrod* **11**, 679 (1966).

373. Johannesen, R. B., Candela, G. E., and Tung Tsang, *J. Chem. Phys.* **48**, 5544 (1968).

374. Jotham, R. W., and Kettle, S. F. A., *Chem. Commun.* p. 258 (1969).

375. Kamimura, H., and Yariv, A., *Bull. Am. Phys. Soc.* [2] **8**, 23 (1963).

376. Karimov, Y. S., and Rudashevskii, N., *Radiospektrosk. Kvantovokhim. Metody Strukt. Issled* p. 128 (1967); *Chem. Abstr.* **69**, 89755 (1968).

377. Karthe, W., and Kleinwalchter, W., *Ann. Phys. (Leipzig)* **21**, 137 (1968).

378. Kasai, P. H., and Weltner, W., *J. Chem. Phys.* **43**, 2553 (1965).

379. Kasai, P. H., Whipple, E. B., and Weltner, W., *J. Chem. Phys.* **44**, 2581 (1966).

380. Kedzie, R. W., Lyons, D. H., and Kostigan, M., *Phys. Rev.* **138**, A918 (1965).

381. Keller, H. J., *Z. Naturforsch.* **23b**, 133 (1968).

382. Keller, H. J., and Schmidpeter, A., *Z. Naturforsch.* **22b**, 231 (1967).

383. Keller, H. J., and Wawersik, H., *Z. Naturforsch.* **20b**, 938 (1965).

384. Keller, H. J., and Wawersik, H., *J. Organomet. Chem.* **8**, 185 (1967).

385. Kenworthy, J. G., Myatt, J., and Todd, P. F., *Chem. Commun.* p. 263 (1969).

386. Kettle, S. F. A., *Theor. Chim. Acta* **3**, 211 (1965).

387. Kholmogorov, V. E., and Glebovsky, D. N., *Opt. i Spektroskopiya* **12**, 728 (1962).

388. Kikuchi, C., Chen, I., From, W. H., and Dorain, P. B., *J. Chem. Phys.* **42**, 181 (1965).

389. Kimball, M. E., Pratt, D. W., and Kaska, W. C., *Inorg. Chem.* **7**, 2006 (1968).
390. Kivelson, D., *J. Chem. Phys.* **41**, 1904 (1964).
391. Kivelson, D., and Lee, S. K., *J. Chem. Phys.* **41**, 1896 (1964).
392. Kivelson, D., and Neiman, R., *J. Chem. Phys.* **35**, 149 (1961).
393. Kneubühl, F. K., *J. Chem. Phys.* **33**, 1074 (1960).
394. Kneubühl, F. K., Koski, W. S., and Caughey, W. S., *J. Am. Chem. Soc.* **83**, 1607, 5049 (1961).
395. Koga, H., and Hukuda, K., *J. Phys. Soc. Japan* **25**, 630 (1968).
396. Kokoszka, G. F., Allen, H. C., and Gordon, G., *J. Chem. Phys.* **42**, 3693 (1965).
397. Kokoszka, G. F., Allen, H. C., and Gordon, G., *J. Chem. Phys.* **42**, 3730 (1965).
398. Kokoszka, G. F., Allen, H. C., and Gordon, G., *J. Chem. Phys.* **46**, 3013, 3020 (1967).
399. Kokoszka, G. F., Allen, H. C., and Gordon, G., *Inorg. Chem.* **5**, 91 (1966).
400. Kokoszka, G. F., and Gordon, G., *Tech. Inorg. Chem.* **7**, 151 (1968).
401. Kokoszka, G. F., Linzer, M., and Gordon, G., *Inorg. Chem.* **7**, 1730 (1968).
402. Kokoszka, G. F., Reiman, C. W., Allen, H. C., and Gordon, G., *Inorg. Chem.* **6**, 1657 (1967).
403. Kon, H., *J. Inorg. Nucl. Chem.* **25**, 933 (1963).
404. Kon, H., and Sharpless, N. E., *J. Chem. Phys.* **42**, 906 (1965).
405. Kon, H., and Sharpless, N. E., *J. Chem. Phys.* **43**, 1081 (1965).
406. Kon, H., and Sharpless, N. E., *J. Phys. Chem.* **70**, 105 (1966).
407. Kon, H., and Sharpless, N. E., *Spectrosc. Letters* **1**, 49 (1968).
408. König, E., *Z. Naturforsch.* **19a**, 1139 (1964).
409. König, E., "Physical Methods of Advanced Inorganic Chemistry." Wiley (Interscience), New York, 1968.
410. Kornienko, L. S., and Prokhorov, A. M., *Zh. Eksp. Teor. Fiz.* **38**, 1651 (1960); *Soviet Phys. JETP* (*Engl. Transl.*) **11**, 1189 (1960).
411. Koryagin, V. F., and Grechushnikov, B. N., *Fiz. Tverd. Tela* **6**, 422 (1964); *Soviet Phys.—Solid State* (*Engl. Transl.*) **6**, 337 (1964).
412. Koryagin, V. F., and Grechushnikov, B. N., *Fiz. Tverd. Tela* **8**, 565 (1966); *Soviet Phys.—Solid State* (*Engl. Transl.*) **8**, 445 (1966).
413. Kozyrev, B. M., *Discussions Faraday Soc.* **19**, 135 (1955).
414. Kramers, H. A., *Proc. Acad. Sci. Amsterdam* **33**, 959 (1930).
415. Krauer, K., Hemmerich, P., and van Voorst, J. D. W., *Angew. Chem. Intern. Ed.* **6**, 262 (1967).
416. Kraus, H. L., and Deffner, U., *Z. Naturforsch.* **19b**, 1 (1964).
417. Kravchuk, L. S., Poznyak, A. L., and Erofeev, B. V., *Zh. Strukt. Khim.* **6**, 645 (1965); *J. Struct. Chem.* (*USSR*) (*Engl. Transl.*) **6**, 617 (1965).
418. Kravitz, L. C., and Piper, W. W., *Phys. Rev.* **146**, 322 (1966).
419. Krusman, P., Marsh, R., Preer, J. R., and Gray, H. B., *J. Am. Chem. Soc.* **90**, 1067 (1968).
420. Kubo, R., and Tomita, K., *J. Phys. Soc. Japan* **9**, 888 (1954).
421. Kunii, S., Tobita, S., and Hirahara, E., *J. Phys. Soc. Japan* **21**, 479 (1966).
422. Kuska, H. A., D'Itri, F. M., and Popov, A. I., *Inorg. Chem.* **5**, 1272 (1966).
423. Kuska, H. A., Krigas, T., and Rogers, M. T., *Abstr. 152nd Meeting Am. Chem. Soc., Pittsburgh, Pa., March 1966* (1966).
424. Kuska, H. A., and Rogers, M. T., *J. Chem. Phys.* **40**, 910 (1964); **42**, 3034 (1965).

425. Kuska, H. A., and Rogers, M. T., *J. Chem. Phys.* **41**, 3802 (1964).
426. Kuska, H. A., and Rogers, M. T., *J. Chem. Phys.* **43**, 1744 (1965).
427. Kuska, H. A., and Rogers, M. T., *Inorg. Chem.* **5**, 313 (1966).
428. Kuska, H. A., and Rogers, M. T., *in* "Radical Ions," p. 579. Wiley (Interscience), New York, 1968.
429. Kuska, H. A., Rogers, M. T., and Drullinger, R. E., *J. Chem. Phys.* **71**, 109 (1967).
430. Kuwabara, G., *Phys. Rev.* **138**, A99 (1965).
431. Kwiatek, J., Mader, I. L., and Seyler, J. K., *Advan. Chem. Ser.* **37**, 201 (1963).
432. Kyi, R., *Phys. Rev.* **128**, 151 (1962).
433. Lalor, F., Hawthorne, M. F., Maki, A. H., Darlington, K., Davison, A., Gray, H. B., Dori, Z., and Steifel, E. I., *J. Am. Chem. Soc.* **89**, 2278 (1967).
434. Lambe, J., Baker, J., and Kikuchi, C., *Phys. Rev. Letters* **3**, 270 (1959).
435. Lambe, J., and Kikuchi, C., *Phys. Rev.* **118**, 71 (1960).
436. Lambe, J., and Kikuchi, C., *Phys. Rev.* **119**, 1256 (1960).
437. Lardon, M., and Gunthard, H. H., *J. Chem. Phys.* **44**, 2010 (1966).
438. Larin, G. M., Dziomko, V. M., Dunaevskaya, K. A., and Syrkin, Y. K., *Zh. Strukt. Khim.* **6**, 391 (1965); *J. Struct. Chem.* (*USSR*) (*Engl. Transl.*) **6**, 370 (1965).
439. Larin, G. M., Miroshnichenko, I. V., and Chirkin, G. K., *Fiz. Tverd. Tela* **9**, 677 (1967).
440. Larin, G. M., Panova, G. V., and Rukhadze, E. G., *Zh. Strukt. Khim.* **6**, 699 (1965).
441. Larin, G. M., Panova, G. V., and Rukhadze, E. G., *Dokl. Akad. Nauk SSSR* **166**, 363 (1966).
442. Larson, G. H., and Jarrett, H. S., *Magn. Magn. Mater. Dig.* p. 98 (1966); *Chem. Abstr.* **67**, 68797 (1967).
443. LaVilla, R. E., and Bauer, S. H., *J. Am. Chem. Soc.* **85**, 3597 (1963).
444. Levanon, H., and Luz, Z., *J. Chem. Phys.* **49**, 2031 (1968).
445. Levanon, H., Stein, G., and Luz, Z., *J. Am. Chem. Soc.* **90**, 5292 (1968).
446. Lewis, J., Mabbs, F. E., Royston, L. K., and Smail, W. R., *J. Chem. Soc. A* p. 291 (1969).
447. Lewis, J., Nyholm, R. S., and Smith, P. W., *J. Chem. Soc.* p. 4590 (1961).
448. Lewis, W. B., *Inorg. Chem.* **6**, 1737 (1967).
449. Lewis, W. B., Alei, M., and Morgan, L. O., *J. Chem. Phys.* **45**, 4003 (1966).
450. Locke, J., McCleverty, J. A., Wharton, E. J., and Winscom, C. J., *Chem. Commun.* p. 677 (1966).
451. Loewenstein, A., Shporer, M., and Navon, G., *J. Am. Chem. Soc.* **85**, 2855 (1963).
452. Lohr, L. L., *Inorg. Chem.* **6**, 1890 (1967).
453. Lohr, L. L., *Proc. Natl. Acad. Sci. U.S.* **59**, 720 (1968).
454. Longo, A., and Buch, T., *Inorg. Chem.* **6**, 556 (1967).
455. Longuet-Higgins, H. C., and Stone, A. J., *Mol. Phys.* **5**, 417 (1962).
456. Low, W., *Phys. Rev.* **101**, 1827 (1956).
457. Low, W., *Solid State Phys. Suppl.* **2** (1962).
458. Low, W., ed., "Paramagnetic Resonance." Vols. 1 and 2. Academic Press, New York, 1963.
459. Low, W., *Phys. Letters* **24A**, 46 (1967).
460. Low, W., and Llewellyn, P. M., *Phys. Rev.* **110**, 842 (1958).
461. Low, W., and Rosenthal, A., *Phys. Letters* **26A**, 143 (1968).

462. Low, W., and Rubins, R. S., *in* "Paramagnetic Resonance" (W. Low, ed.), Vol. 1, p. 79. Academic Press, New York, 1963.

463. Lund, A., Aasa, R., and Vänngard, T. cited in Eaton *et al.* (*195*).

464. Lutskii, A. E., Kotelevskii, N. M., and Kogan, V. A., *Teor. Eksp. Khim.* **3**, 846 (1967).

465. MacCragh, A., and Koski, W. S., *J. Am. Chem. Soc.* **85**, 2375 (1963).

466. MacCragh, A., and Koski, W. S., *J. Am. Chem. Soc.* **87**, 2496 (1965).

467. MacCragh, A., Storm, C. B., and Koski, W. S., *J. Am. Chem. Soc.* **87**, 1470 (1965).

468. Mackay, R. A., and Schneider, R. F., *Inorg. Chem.* **6**, 549 (1967).

469. Maher, J. P., *Chem. Commun.* p. 632 (1967); *J. Chem. Soc. A* p. 2918 (1968).

470. Mahon, C., and Reynolds, W. L., *Inorg. Chem.* **6**, 1927 (1967).

471. Maki, A. H., and Berry, T. E., *J. Am. Chem. Soc.* **87**, 4437 (1965).

472. Maki, A. H., Berry, T. E., Davison, A., Holm, R. H., and Balch, A. L., *J. Am. Chem. Soc.* **88**, 1080 (1966).

473. Maki, A. H., Edelstein, N., Davison, A., and Holm, R. H., *J. Am. Chem. Soc.* **86**, 4580 (1964).

474. Maki, A. H., and McGarvey, B. R., *J. Chem. Phys.* **29**, 31 (1958).

475. Maki, A. H., and McGarvey, B. R., *J. Chem. Phys.* **29**, 35 (1958).

476. Maki, A. H., and Randall, E. W., *J. Am. Chem. Soc.* **82**, 4109 (1960).

477. Malmström, B. G., and Vänngard, T., *J. Mol. Biol.* **2**, 118 (1960).

478. Manoharan, P. T., and Gray, H. B., *J. Am. Chem. Soc.* **87**, 3340 (1965).

479. Manoharan, P. T., and Gray, H. B., *Chem. Commun.* p. 324 (1965).

480. Manoharan, P. T., Kuska, H. A., and Rogers, M. T., *J. Am. Chem. Soc.* **89**, 4564 (1967).

481. Manoogian, A., and MacKinnon, J. A., *Can. J. Phys.* **45**, 2769 (1967).

482. March, R. E., and Thewalt, U., *J. Am. Chem. Soc.* **89**, 6364 (1967).

483. Marov, I. N., Dubrov, Y. N., Belyaeva, V. K., and Ermakov, A. N., *Dokl. Akad. Nauk SSSR* **171**, 385 (1966).

484. Marov, I. N., Dubrov, Y. N., Belyaeva, V. K., and Ermakov, A. N., *Dokl. Akad. Nauk SSSR* **176**, 590 (1967).

485. Marov, I. N., Dubrov, Y. N., Belyaeva, V. K., and Ermakov, A. N., *Dokl. Akad. Nauk SSSR* **177**, 1106 (1967); *Dokl. Chem.* **177**, 1166 (1967).

486. Marov, I. N., Dubrov, Y. N., Belyaeva, V. K., and Ermakov, A. N., *Zh. Neorg. Khim.* **13**, 2140 (1968).

487. Marshall, W., and Stuart, R., *Phys. Rev.* **123**, 2048 (1961).

488. Matsumoto, H., *J. Phys. Soc. Japan* **20**, 1579 (1965).

489. Matsuzaki, K., and Yasukawa, T., *Chem. Commun.* p. 1460 (1968).

490. Matumura, O., *J. Phys. Soc. Japan* **14**, 108 (1959).

491. McCleverty, J. A., *Progr. Inorg. Chem.* **10**, 49 (1968).

492. McCleverty, J. A., Atherton, N. M., Locke, J., Wharton, E. J., and Winscom, C. J., *J. Am. Chem. Soc.* **89**, 6082 (1967).

493. McClung, D. A., Dalton, L. R., and Brubaker, C. H., *Inorg. Chem.* **5**, 1985 (1966).

494. McConnell, H. M., and Chesnut, D. B., *J. Chem. Phys.* **27**, 984 (1957).

495. McConnell, H. M., Porterfield, W. W., and Robertson, R. E., *J. Chem. Phys.* **30**, 442 (1959).

496. McConnell, H. M., and Strathdee, J., *Mol. Phys.* **2**, 129 (1959).

497. McDonald, C. C., Phillips, W. D., and Mower, H. F., *J. Am. Chem. Soc.* **87**, 3319 (1965).

498. McGarvey, B. R., *J. Phys. Chem.* **60**, 71 (1956).

499. McGarvey, B. R., *J. Chem. Phys.* **37**, 2001 (1962).

500. McGarvey, B. R., *J. Chem. Phys.* **38**, 388 (1963).

501. McGarvey, B. R., *J. Chem. Phys.* **40**, 809 (1964).

502. McGarvey, B. R., *J. Chem. Phys.* **41**, 3743 (1964).

503. McGarvey, B. R., *Inorg. Chem.* **5**, 476 (1966).

504. McGarvey, B. R., *Transition Metal Chem.* **3**, 89 (1966).

505. McGarvey, B. R., *J. Phys. Chem.* **71**, 51 (1967).

506. McGarvey, B. R., and Pearlman, J., *J. Chem. Phys.* **46**, 4992 (1967).

506a. McMillan, J. A., and Halpern, T., Based upon the wavefunctions of Charlotte Froese, "Hartree–Foch parameters for the atoms helium to radon," Department of Mathematics, University of British Columbia, Vancouver 8, B.C. (1966).

507. McMillan, J. A., and Smaller, B., *J. Chem. Phys.* **35**, 1698 (1961).

508. McNeil, D. A. C., Raynor, J. B., and Symons, M. C. R., *J. Chem. Soc.* p. 410 (1965).

509. McNeil, D. A. C., Raynor, J. B., and Symons, M. C. R., *Mol. Phys.* **10**, 297 (1966).

510. Mellor, D. P., and Stephenson, N. C., *Inorg. Nucl. Chem. Letters* **3**, 431 (1967).

511. Meriwether, L. S., Robinson, S. D., and Wikinson, G., *J. Chem. Soc. A* p. 1488 (1966).

512. Miller, I. A., and Offenbacher, E. L., *Phys. Rev.* **166**, 269 (1968).

513. Miroschnichenko, I. V., Larin, G. M., and Rukhadze, E. G., *Teor. Eksp. Khim. Akad. Nauk Ukr. SSR* **2**, 409 (1966); *Chem. Abstr.* **66**, 24301 (1967).

514. Miroshnichenko, I. V., Larin, G. M., Rukhadze, E. G., and Litvinyuk, M. A., *Zh. Neorg. Khim.* **11**, 331 (1966); *Russ. J. Inorg. Chem.* **11**, 180 (1966).

515. Miroshnichenko, I. V., Larin, G. M., and Syrkin, Y. K., *Zh. Strukt. Khim.* **7**, 361 (1966); *J. Struct. Chem.* (*USSR*) (*Engl. Transl.*) **7**, 345 (1966).

516. Miroshnichenko, I. V., Rukhadze, E. G., and Zapuskalova, S. F., *Izv. Akad. Nauk SSSR Ser. Khim.* p. 1658 (1966).

517. Mishra, H. C., and Symons, M. C. R., *J. Chem. Soc.* p. 4490 (1963).

518. Mori, M., and Weil, J. A., *J. Am. Chem. Soc.* **89**, 3732 (1967).

519. Mori, M., Weil, J. A., and Kinnaird, J. K., *J. Phys. Chem.* **71**, 103 (1967).

520. Morigaki, K., *J. Phys. Soc. Japan* **18**, 733 (1963) **19**, 187 (1964).

521. Morita, Y., and Mason, H. S., *Abstr. 6th. Intern. Congr. Biochem. New York* p. 323 (1964).

522. Mueller, K. A., *Proc. 14th Colloq. Ampere* p. 192 (1966).

523. Mujoshi, T., Iwamoto, T., and Sasaki, Y., *Inorg. Chim. Acta* **2**, 329 (1968).

524. Muller, K. A., *Phys. Rev. Letters* **2**, 341 (1959).

525. Muniz, R. P. A., and Danon, J., *Mol. Phys.* **9**, 599 (1965).

526. Muraveiskaya, G. S., Larin, G. M., and Sorokina, V. F., *Zh. Neorg. Khim.* **13**, 1466 (1966); *Russ. J. Inorg. Chem.* (*Engl. Transl.*) **13**, 771 (1968).

527. Murdock, H. D., and Lucken, E. A. C., *Helv. Chim. Acta* **47**, 1517 (1964).

528. Murphy, J. C., and Bohandy, J., *J. Chem. Phys.* **46**, 1215 (1967).

529. Nasirov, F. M., Karpacheva, G. P., Davydov, B. E., and Krentsel, B. A., *Izvest. Akad. Nauk SSSR* p. 1697 (1964); *Bull. Acad. Sci USSR* (*Engl. Transl.*) p. 1603 (1964).

530. Natta, G., Zambelli, A., Lanzi, G., Pasquon, I., Magnaschi, E. R., Segre, A. L., and Centola, P., *Makromol. Chem.* **81**, 161 (1965).

531. Neiman, R., and Kivelson, D., *J. Chem. Phys.* **35**, 156 (1961).

532. Ngai, L. H., Stafford, F. E., and Schafer, L., *J. Am. Chem. Soc.* **9**, 48 (1969).

533. Nilson, W. G., and Kurtz, S. K., *Phys. Rev.* **136**, A262 (1964).

534. Nöth, H., Voitländer, J., and Nussbaum, M., *Naturwissenschaften* **47**, 57 (1960).

535. Nozaki, F., *Shokubai* (*Tokyo*) **8**, 32 (1966); *Chem. Abstr.* **69**, 48131 (1968).

536. Nozawa, Y., and Takeda, M., *Kogyo Kagaku Zasshi* **71**, 189 (1968).

537. Nudelman, H. B., Johnson, S. H., and Barnes, R. G., *J. Phys. Chem. Solids* **26**, 1035 (1965).

538. Nussbaum, M., and Voitländer, J., *Z. Naturforsch.* **20a**, 1411, 1417 (1965).

539. Ono, K., *J. Phys. Soc. Japan* **12**, 1231 (1957).

540. Ono, K., Koide, S., Sekiyama, H., and Abe, H., *Phys. Rev.* **96**, 38 (1954).

541. O'Reilly, D. E., *J. Chem. Phys.* **29**, 1189 (1958); **30**, 591 (1959).

542. O'Reilly, D. E., and Anderson, J. H., *Phys. Chem. Org. Solid State* **1**, 121 (1965).

543. Orton, J. W., Auzins, P., Griffiths, J. H. E., and Wertz, J. E., *Proc. Phys. Soc.* (*London*) **78**, 554 (1961).

544. Orton, J. W., Auzins, P., and Wertz, J. E., *Phys. Rev.* **119**, 1691 (1960).

545. Otsuka, S., Nakamura, A., and Yoshida, T., *Inorg. Chem.* **7**, 261 (1968).

546. Owen, J., and Stevens, K. W. H., *Nature* **171**, 836 (1953).

547. Owen, J., and Thornley, J. H. M., *Rep. Progr. Phys.* **29** (2), 675 (1966).

548. Owen, J., and Ward, I. M., see Bowers and Owen (*104*).

549. Owen, J., and Ward, I. M., *Phys. Rev.* **102**, 591 (1956).

550. Owen, S. J. T., Standley, K. J., and Walker, A., *J. Chem. Phys.* **40**, 183 (1964).

551. Pake, G. E., "Paramagnetic Resonance." Benjamin, New York, 1962.

552. Pake, G. E., and Tuttle, T., *Phys. Rev. Letters* **3**, 423 (1959).

553. Parish, R. V., Simms, P. G., Wells, M. A., and Woodward, L. A., *J. Chem. Soc. A* p. 2882 (1968).

554. Pascaru, I., Constantinescu, O., Constantinescu, M., and Arizan, D., *J. Chim. Phys.* **62**, 1283 (1965).

555. Pauling, L., "The Nature of the Chemical Bond," 3rd ed., p. 98. Cornell Univ. Press, New York, 1960.

556. Pearson, R. G., and Buch, T., *J. Chem. Phys.* **36**, 1277 (1962).

557. Peisach, J., "Biochemistry of Copper." Academic Press, New York, 1966.

558. Petrakis, L., *J. Chem. Educ.* **44**, 432 (1967).

559. Petterson, R., and Vanngard, T., *Arkiv Kemi* **17**, 249 (1961).

560. Philips, L. K., *U.S. At. Energy Comm. Rep. U.C.R.L.-17853* (1967).

561. Pifer, J. H., *Phys. Rev.* **157**, 272 (1967).

562. Poole, C. P., "Electron Spin Resonance." Wiley (Interscience), New York, 1967.

563. Pratt, D. W., *U.S. At. Energy Comm. U.C.R.L.-17406* (1967). *Chem. Abstr.* **69**, 14737 (1968).

564. Pratt, D. W., and Myers, R. J., *J. Am. Chem. Soc.* **89**, 6470 (1967).

565. Pratt, J. M., and Silverman, P. R., *Chem. Commun.* p. 117 (1967); *J. Chem. Soc. A* p. 1286 (1967).

566. Prins, R., Bilsen, P., and van Voorst, J. D. W., *J. Chem. Phys.* **46**, 1216 (1967).

567. Procter, I. M., Hathaway, B. J., Billing, D. E., Dudley, R., and Nicholls, P., *J. Chem. Soc. A* p. 1192 (1969).

568. Procter, I. M., Hathaway, B. J., and Nicholls, P., *J. Chem. Soc. A* p. 1678 (1968).

569. Rabette, P., Ropars, C., and Grivet, J. P., *Compt. Rend.* **C265**, 153 (1967).

570. Rajan, R., and Reddy, T. R., *J. Chem. Phys.* **39**, 1140 (1963).

571. Ramasubba Reddy, T., and Srinivasan, R., *Proc. Indian Acad. Sci., Sect. A* **65**, 303 (1967).

572. Rao, K. V. S., Sastry, M. D., and Venkateswarlu, P., *J. Chem. Phys.* **49**, 1714 (1968).

573. Rasmussen, P. G., Kuska, H. A., and Brubaker, C. H., *Inorg. Chem.* **4**, 343 (1965).

574. Rauber, A., and Schneider, J., *Z. Naturforsch.* **17a**, 266 (1962).

575. Raynor, J. B., *Nature* **201**, 1216 (1965).

576. Raynor, J. B., *Z. Naturforsch.* **24b**, 775 (1969).

577. Raynor, J. B., and Symons, M. C. R., *J. Chem. Soc. A* p. 339 (1970).

578. Reddy, T. R., and Srinivasan, R., *J. Chem. Phys.* **43**, 1404 (1965).

579. Redfield, A. G., *IBM Res. Develop.* **1**, 19 (1957).

580. Rei, D. K., *Fiz. Tverd. Tela* **3**, 2539 (1961); *Soviet Phys.—Solid State* (*Engl. Transl.*) **3**, 1845 (1962).

581. Reiman, C. W., Kokoszka, G. F., and Allen, H. C., *J. Res. Natl. Bur. St.* **A70**, 1 (1966).

582. Riley, R. F., and Ho, L., *J. Inorg. Nucl. Chem.* **24**, 1121 (1962).

583. Rist, G. H., Ammeter, J., and Gunthard, H. H., *J. Chem. Phys.* **49**, 2210 (1968).

584. Rist, G. H., and Hyde, J. S., *J. Chem. Phys.* **49**, 2449 (1968).

585. Rivkind, A. I., and Yablokov, I. V., *Dokl. Akad. Nauk SSSR* **158**, 1401 (1964); *Zh. Strukt. Khim.* **7**, 30 (1966); *J. Struct. Chem.* **7**, 25 (1966).

586. Roemelt, G., and Schwochau, K., *Z. Naturforsch.* **22a**, 519 (1967).

587. Rohrscheid, F., Balch, A. L., and Holm, R. H., *Inorg. Chem.* **5**, 1542 (1966).

588. Roberts, E. M., and Koski, W. S., *J. Am. Chem. Soc.* **82**, 3006 (1960).

589. Roberts, E. M., and Koski, W. S., *J. Am. Chem. Soc.* **83**, 1865 (1961).

590. Roberts, E. M., Koski, W. S., and Caughey, W. S., *J. Chem. Phys.* **34**, 591 (1961).

591. Robertson, R. E., *Determination Org. Struct. Phys. Methods* **2**, 617 (1962).

592. Robertson, R. E., and McConnell, H. M., *J. Phys. Chem.* **64**, 70 (1960).

593. Rollman, L. D., and Iwamoto, R. T., *J. Am. Chem. Soc.* **90**, 1455 (1968).

594. Root, K. J., and Symons, M. C. R., *J. Chem. Soc. A* p. 2366 (1968).

595. Rosenvasser, E. S., and Feher, G., *Bull. Am. Phys. Soc.* [2] **6**, 117 (1961).

596. Ryabchikov, D. I., Marov, I. N., Dubrov, Y. N., Belyaeva, V. K., and Ermakov, A. N., *Dokl. Akad. Nauk SSSR* **165**, 842 (1965).

597. Ryabchikov, D. I., Marov, I. N., Dubrov, Y. N., Belyaeva, V. K., and Ermakov, A. N., *Dokl. Akad. Nauk SSSR* **167**, 629 (1966); *Dokl. Chem.* (*Engl. Transl.*) **167**, 183 (1966).

598. Ryabchikov, D. I., Marov, I. N., Dubrov, Y. N., Belyaeva, V. K., and Ermakov, A. N., *Dokl. Akad. Nauk SSSR* **169**, 1107 (1966); *Dokl. Chem.* (*Engl. Transl.*) **169**, 795 (1966).

599. Sacconi, L., and Cini, R., *J. Am. Chem. Soc.* **76**, 4239 (1954).

600. Sands, R. H., *Phys. Rev.* **99**, 1222 (1955).

601. Schmidt, J. G., Brey, W. S., and Stoufer, R. C., *Inorg. Chem.* **6**, 268 (1967).

602. Schmitt, R. D., and Maki, A. H., *J. Am. Chem. Soc.* **90**, 2288 (1968).

603. Schneider, E. E., and Weiss, J., *Proc. Chem. Soc.* p. 130 (1959).

604. Schneider, J., and Rauber, A., *Phys. Letters* **21**, 380 (1966).

605. Schneider, J., Sircar, S. R., and Rauber, A., *Z. Naturforsch.* **189**, 980 (1963).

606. Schneider, R. F., and Mackay, R. A., *J. Chem. Phys.* **48**, 843 (1968).

607. Schoffa, G., *Z. Naturforsch.* **23a**, 550 (1968).

608. Schonland, D. S., *Proc. Phys. Soc.* (*London*) **73**, 788 (1959).

609. Schrauzer, G. N., and Mayweg, V. P., *J. Am. Chem. Soc.* **87**, 3585 (1965).

610. Schrauzer, G. N., and Windgassen, R. J., *J. Am. Chem. Soc.* **89**, 143, 1999 (1967); **88**, 3738 (1966); *Chem. Ber.* **99**, 602 (1966); *Chem. Eng. News* p. 42 (21st Oct. 1968).

611. Selbin, V., Holmes, L. H., and McGlynn, S. P., *J. Inorg. Nucl. Chem.* **25**, 1359 (1963).

612. Semenova, E. I., *Zh. Neorgan. Khim.* **11**, 2158 (1966); *Russ. J. Inorg. Chem.* (*Engl. Transl.*) **11**, 1156 (1966).

613. Sharnoff, M., *J. Chem. Phys.* **41**, 2203 (1964); **42**, 3383 (1965).

614. Sharnoff, M., and Reimann, C. W., *J. Chem. Phys.* **43**, 2993 (1965).

615. Shekun, L. Ya., *Fiz. Tverd. Tela* **5**, 2034 (1963); *Soviet Phys.—Solid State* (*Engl. Transl.*) **5**, 1487 (1964).

616. Shields, L., and Symons, M. C. R., *Mol. Phys.* **11**, 57 (1966).

617. Shilov, A. E., Zefirova, A. K., and Tikhomirova, N. N., *Zh. Fiz. Khim.* **33**, 2113 (1959); *Russ. J. Phys. Chem.* (*Engl. Transl.*) **33**, 310 (1959).

618. Shporer, M., Ron, G., Loewenstein, A., and Navon, G., *Inorg. Chem.* **4**, 358 (1965).

619. Shulyndin, S. V., Tikhornirova, N. N., Shilov, A. E., and Shilova, A. K., *Zh. Strukt. Khim.* **2**, 740 (1961); *J. Struct. Chem.* (*USSR*) (*Engl. Transl.*) **2**, 682 (1961).

620. Shupack, S. I., *Inorg. Chim. Acta* **1**, 435 (1967).

621. Siegel, I., *Phys. Rev.* **134**, A193 (1964).

622. Siegel, I., and Lorenc, J. A., *J. Chem. Phys.* **45**, 2315 (1966).

623. Sienko, M. J., and Oesterricher, H., *J. Am. Chem. Soc.* **90**, 6568 (1968).

624. Sierro, J., *J. Phys. Chem. Solids* **28**, 417 (1967).

625. Sigwart, C., Hemmerich, P., and Spence, J. T., *Inorg. Chem.* **7**, 2545 (1968).

626. Simanek, E., Sroubek, Z., Zdansky, K., Kaczer, J., and Novak, L., *Phys. Status Solidi* **14**, 333 (1966).

627. Slade, R. C., Tomlinson, A. A. G., Hathaway, B. J., and Billing, D. E., *J. Chem. Soc. A* p. 61 (1968).

628. Slichter, C. P., *Phys. Rev.* **99**, 479 (1955).

629. Slichter, C. P., "Principles of Magnetic Resonance," Harper, New York, 1963.

630. Sliker, T. R., *Phys. Rev.* **130**, 1749 (1963).

631. Snow, M. R., and Stiddard, M. H. B., *J. Chem. Soc. A* p. 777 (1966).

632. Solozhenkin, P. M., and Kopitsya, N. I., *Dokl. Akad. Nauk Tadzh. SSSR* **10**, 21 (1967).

633. Solozhenkin, P. M., and Kopitsya, N. I., *Zh. Strukt. Khim.* **8**, 534 (1967).

634. Spencer, J. B., and Myers, R. J., *J. Am. Chem. Soc.* **86**, 522 (1964).

635. Sroubek, Z., and Zdansky, K., *J. Chem. Phys.* **44**, 3078 (1966).

636. Sroubek, Z., Zdansky, K., and Simanek, E., *Phys. Status Solidi* **6**, K149 (1964).

637. Standley, K. J., and Taylor, P. F., *J. Phys. C* **1**, 551 (1968).

638. Stankowski, J., *Phys. Status Solidi* **24**, 451 (1967).

639. Steifel, E. I., Dori, Z., and Gray, H. B., *J. Am. Chem. Soc.* **89**, 3353 (1967).

640. Steifel, E. I., Eisenberg, R., Rosenberg, R. C., and Gray, H. B., *J. Am. Chem. Soc.* **88**, 2956 (1966).

641. Steifel, E. I., and Gray, H. B., *J. Am. Chem. Soc.* **87**, 4012 (1965).

642. Steifel, E. I., Waters, J. H., Billig, E., and Gray, H. B., *J. Am. Chem. Soc.* **87**, 3016 (1965).
643. Sturge, M. D., Merritt, F. R., and Remeika, J. P., *Appl. Phys. Letters* **9**, 63 (1966).
644. Subramanian, S., Rahman, Z., and Witters, J., *J. Chem. Phys.* **49**, 473 (1968).
645. Subramanian, S., Witters, J., Van Itterbeek, A., Moreau, J., and Rahman, Z., *Physica* (*Utrecht*) **34**, 456 (1967).
646. Sugano, S., and Shulman, R. G., *Phys. Rev.* **130**, 517 (1963).
647. Svedung, D. H., and Vannerberg, N. G., *Acta Chem. Scand.* **22**, 1551 (1968).
648. Swalen, J. D., and Ibers, J. A., *J. Chem. Phys.* **37**, 17 (1962).
649. "Symbols, Signs and Abbreviations Recommended for British Scientific Publications." Roy. Soc., London, 1968.
650. Symons, M. C. R., *Advan. Phys. Org. Chem.* **1**, 284 (1963).
651. Symons, M. C. R., and Tinling, D. J. A., unpublished results.
652. Synek, M., and Stungis, G. E., *J. Chem. Phys.* **41**, 971 (1964).
653. Takakura, K., and Ranby, B., *J. Phys. Chem.* **72**, 164 (1968).
654. Tapscott, R. E., and Belford, R. L., *Inorg. Chem.* **6**, 735 (1967).
655. Thornley, J. H. M., Mangum, B. W., Griffiths, J. H. E., and Owen, *J. Proc. Phys. Soc.* (*London*) **78**, 1263 (1961).
656. Tikhomirova, N. N., and Zamaraev, K. I., *Zh. Strukt. Khim.* **4**, 224 (1963); *J. Struct. Chem.* (*USSR*) (*Engl. Transl.*) **4**, 200 (1963).
657. Tikhomirova, N. N., Zamaraev, K. I., and Berdnikov, V. M., *Zh. Strukt. Khim.* **4**, 449 (1963); *J. Struct. Chem.* (*USSR*) (*Engl. Transl.*) **4**, 407 (1963).
658. Timerov, R. K., Yablokov, Y. V., and Ablov, A. V., *Dokl. Akad. Nauk SSSR*, **152**, 160 (1963); *Dokl. Chem.* (*Engl. Transl.*) **152**, 786 (1963).
659. Tinkham, M., "Group Theory and Quantum Mechanics," p. 76. McGraw-Hill, New York, 1964.
660. Title, R. S., *Phys. Rev.* **130**, 17 (1963).
661. Title, R. S., *Phys. Rev.* **131**, 2503 (1963).
662. Title, R. S., *Phys. Rev.* **131**, 623 (1963); **133**, A1613 (1964).
663. Tkac, A., *Collection Czech. Chem. Commun.* **33**, 1629 (1968).
664. Tkaeda, T., and Watanabe, A., *J. Phys. Soc. Japan* **23**, 469 (1967).
665. Tomlinson, A. A. G., and Hathaway, B. J., *J. Chem. Soc. A* pp. 1685, 1905, 2578 (1968).
666. Tomlinson, A. A. G., Hathaway, B. J., Billing, D. E., and Nicholls, P., *J. Chem. Soc. A* p. 65 (1969).
667. Tosi, L., and Danon, J., *Compt. Rend.* **B263**, 970 (1966).
668. Townsend, M. G., *J. Chem. Phys.* **41**, 3149 (1964).
669. Townsend, M. G., and Orton, J. W., *J. Chem. Phys.* **45**, 4135 (1966).
670. Tse Chang, T., *Phys. Rev.* **136**, A1413 (1964).
671. Tsumura, R., and Hagihara, N., *Bull. Chem. Soc. Japan* **38**, 861 (1965).
672. Van Hecke, G. R., and Horrocks, W. DeW., *Inorg. Chem.* **5**, 1968 (1966).
673. van Kemenade, J. T. C., Verbeek, J. L., and Cornaz, P. F., *Rec. Trav. Chim.* **85**, 629 (1966).
674. Vänngard, T., and Akerstrom, S., *Nature* **184**, 183 (1959).
675. Van Niekert, J. N., and Schoening, F. R. L., *Acta Cryst.* **6**, 227 (1953).
676. Van Ormondt, D., and Thalhammer, T., *Phys. Letters* **14**, 169 (1965).
677. Van Stapele, R. P., Henning, J. C. M., Hardeman, G. E. G., and Bongers, P. F., *Phys. Rev.* **150**, 310 (1966).
678. Van Vleck, J. H., *J. Chem. Phys.* **7**, 72 (1939).

679. Van Voorst, J. D. W., and Hemmerich, P., *J. Chem. Phys.* **45**, 3914 (1966).

680. Van Wieringen, J. S., *Discussions Faraday Soc.* **19**, 118 (1955).

681. Varian Associates, "N.M.R.–E.P.R. Spectroscopy." Pergamon, Oxford, 1960.

682. Vashman, A. A., *Zh. Neorg. Khim.* **12**, 2857 (1967).

683. Veiga, J., Reynolds, W. L., and Bolton, J. R., *J. Chem. Phys.* **44**, 2214 (1966).

684. Verbeek, J. L., and Cornaz, P. F., *Rec. Trav. Chim.* **86**, 209 (1967).

685. Verbeek, J. L., and Vink, A. T., *Rec. Trav. Chim.* **86**, 913 (1967).

686. Vetchinkin, S. I., Solodovnikov, S. P., and Chibrikin, V. M., *Opt. i. Spektroskopiya* **8**, 137 (1960); *Opt. Spectrosy* (*USSR*) (*Engl. Transl.*) **8**, 71 (1960).

687. Voelkel, G., and Windsch, W., *Phys. Status Solidi* **17**, K75 (1966).

688. Voitländer, J., and Schmitschek, E., *Z. Elektrochem.* **61**, 941 (1957).

689. Wagner, G. R., Schumacher, R. T., and Friedberg, S. A., *Phys. Rev.* **150**, 226 (1966).

690. Walker, F. A., Carlin, R. L., and Rieger, P. H., *J. Chem. Phys.* **45**, 4181 (1966).

691. Walsh, W. M., and Rupp, L. M., *Phys. Rev.* **126**, 952 (1962).

692. Wartewig, S., and Windsch, W., *Phys. Status Solidi* **17**, K221 (1966).

693. Wasson, J. R., Shyr, C. I., and Trapp, C., *Inorg. Chem.* **7**, 469 (1968).

694. Watanabe, H., *Progr. Theoret. Phys.* (*Kyoto*) **18**, 405 (1957).

695. Waters, E. L., and Maki, A. H., *Phys. Rev.* **125**, 233 (1962).

696. Waters, J. H., and Gray, H. B., *J. Am. Chem. Soc.* **87**, 3534 (1965).

697. Waters, J. H., Williams, R., Gray, H. B., Schrauzer, G. N., and Finck, H. W., *J. Am. Chem. Soc.* **86**, 4198 (1964).

698. Watson, R. E., and Freeman, A. J., *in* "Hyperfine Interactions." Academic Press, New York, 1967.

699. Wayland, B. B., and Rice, W. L., *J. Chem. Phys.* **45**, 3150 (1966).

700. Weeks, M. J., and Fackler, J. P., *Inorg. Chem.* **7**, 2548 (1968).

701. Weil, J. A., and Kinnaird, J. K., *J. Phys. Chem.* **71**, 3341 (1967).

702. Weissman, S. I., and Cohn, M., *J. Chem. Phys.* **27**, 1440 (1957).

703. Weissman, S. I., and Garner, C. S., *J. Am. Chem. Soc.* **78**, 1072 (1956).

704. Welber, B., *Phys. Rev.* **138**, A1481 (1965).

705. Wells, J. S., Matarrese, L. M., and Sukle, D. J., *J. Chem. Phys.* **47**, 2259 (1967).

706. Werden, B. G., Billig, E., and Gray, H. B., *Inorg. Chem.* **5**, 78 (1966).

707. Wiersema, A. K., and Windle, J. J., *J. Phys. Chem.* **68**, 2316 (1964).

708. Wilkens, J., de Graag, D. P., and Helle, J. N., *Phys. Letters* **19**, 178 (1965).

709. Willett, R. D., Liles, O. L., and Michelson, C., *Inorg. Chem.* **6**, 1885 (1967).

710. Williams, R., Billig, E., Waters, J. H., and Gray, H. B., *J. Am. Chem. Soc.* **88**, 43 (1966).

711. Wilmshurst, J. H., "Electron Spin Resonance Spectrometers." Hilger, 1967.

712. Windsch, W., and Welter, M., *Z. Naturforsch.* **22a**, 1 (1967).

713. Windsor, C. G., Griffiths, J. H. E., and Owen, J., *Proc. Phys. Soc.* (*London*) **81**, 373 (1963).

714. Windsor, C. G., Thornley, J. H. M., Griffiths, J. H. E., and Owen, J., *Proc. Roy. Soc.* **80**, 803 (1962).

715. Wood, J. H., and Pratt, G. W., *Phys. Rev.* **107**, 995 (1957).

716. Woodbury, H. H., and Ludwig, G. W., *Phys. Rev. Letters* **1**, 16 (1958).

717. Woonton, G. A., and MacKinnon, J. A., *Can. J. Phys.* **46**, 59 (1968).

718. Wüthrich, K., *Helv. Chim. Acta* **48**, 779 (1965).

719. Wüthrich, K., *Helv. Chim. Acta* **48**, 1012 (1965).

720. Wüthrich, K., *Helv. Chim. Acta* **49**, 1400 (1966).

721. Yablokov, Y. V., and Ablov, A. V., *Dokl. Akad. Nauk SSSR* **144**, 173 (1962).

722. Yablokov, Y. V., Zelentsov, V. V., Romanenko, L. N., and Allenov, V. M., *Dokl. Akad. Nauk SSSR* **173**, 1136 (1967).

723. Yafaev, N. R., and Garif'yanov, N. S., *Fiz. Tverd. Tela* **5**, 3025 (1963); *Soviet Phys.—Solid State* (*Engl. Transl.*) **5**, 2213 (1964).

724. Yafaev, N. R., Garif'yanov, N. S., and Yablokov, Y. V., *Fiz. Tverd. Tela* **5**, 1673 (1963); *Soviet Phys.—Solid State* (*Engl. Transl.*) **5**, 1216 (1963).

725. Yamaka, E., and Barnes, R. G., *Phys. Rev.* **125**, 1568 (1962).

726. Yarmus, L., Kukk, M., and Sundheim, B. R., *J. Chem. Phys.* **40**, 33 (1964).

727. Zaripov, M. M., and Chirkin, G. K., *Fiz. Tverd. Tela* **7**, 2947 (1965); *Soviet Phys.—Solid State* (*Engl. Transl.*) **7**, 2391 (1966).

728. Zaripov, M. M., Kropotov, V. S., Livanova, L. D., and Stepanov, V. G., *Fiz. Tverd Tela* **9**, 1265 (1967).

729. Zaripov, M. M., Kropotov, V. S., Livanova, L. D., and Stepanov, V. G., *Dokl. Akad. Nauk SSSR* **173**, 1043 (1967).

730. Zdansky, K., Arend, H., and Kubec, F., *Phys. Status Solidi* **20**, 653 (1967).

731. Zefirova, A. K., Tikhomirova, N. N., and Shilov, A. E., *Dokl. Akad. Nauk SSSR* **132**, 1082 (1960); *Dokl. Chem.* (*Engl. Transl.*) **132**, 661 (1960).

732. Zeldes, H., and Livingston, R., *J. Chem. Phys.* **34**, 247 (1961).

733. Zhitomirskii, A. N., and Eliseev, S. S., *Dokl. Akad. Nauk Tadzh. SSR* **10**, 33 (1967).

734. Zvérev, G. M., and Prokhorov, A. M., *Zh. Eksp. Teor. Fiz.* **40**, 1016 (1961) and references therein.

735. Zvérev, G. M., and Prokhorov, A. M., *Zh. Eksp. Teor. Fiz.* **43**, 422 (1962); *Soviet. Phys. JETP* (*Engl. Transl.*) **16**, 303 (1963).